

# **Weak Interactions between a Monoclonal Antibody and Anionic Excipients**

## **Consequences for Protein-Protein Interactions**

### **Dissertation**

zur Erlangung des Doktorgrades der Naturwissenschaften  
(Dr. rer. nat.)

der

Naturwissenschaftlichen Fakultät II  
Chemie, Physik und Mathematik

der Martin-Luther-Universität  
Halle-Wittenberg

vorgelegt von

Frau Katharina Reiche  
geb. am 30.12.1985 in Berlin

Gutachter:

1. Gutachter: Prof. Dr. rer. nat. Alfred Blume
2. Gutachter: Prof. Dr. rer. nat. Patrick Garidel
3. Gutachter: Prof. Dr. rer. nat. Roland Winter

Tag der Verteidigung: 14.12.2020



## Abstract

Monoclonal antibodies are proteins with a high target specificity, which enable their use of treating various diseases, such as cancer and autoimmune disorders. In a liquid antibody solution all solution components such as the antibody, water and salts or buffers, are interacting. The interaction between the antibody and the cosolutes is assumed to affect the protein-protein interactions and thereby influences the stability and the phase behavior of the protein solution.

The aim of the thesis was

- to identify one or more model excipients, which are attractively interacting with the antibody
- to identify approaches to detect and to quantify attractive interactions between excipients and the antibody
- to find a rationale behind the effects of pH, presence and concentration of excipients, ionic strength and temperature on the phase boundaries
- find a rationale behind the effect of pH, presence and concentration of excipients and ionic strength the diffusion of an antibody in solution

Different antibody binding excipients were found. These are citrate, butane-1,2,3,4-tetracarboxylate, benzene-1,2,4,5-tetracarboxylate, benzene-1,2,3,4,5-pentacarboxylate and mellitate. These negatively charged oligovalent ions are assumed to bind to the positively charged antibody by electrostatic interaction.

The interaction between the antibody and the citrate molecules manifested by three experimental approaches:

- Comparison of phase boundaries as a function of pH in the absence and in the presence of citrate
- Mapping of the ion atmosphere after equilibrium dialysis against a mixture of ions competing for the solvation shell

- Accelerated diffusion of the mAb at infinite dilution in the presence of 2 mM and 5 mM citrate, which would not be expected neither based on a two-component nor on a three-component diffusion model

The occurrence of phase separation and the width of the miscibility gap were examined as a function of pH, excipient species and concentration as well as ionic strength and temperature. A rationale was found to explain the phase behaviour and therewith the protein-protein interactions in the solutions of different composition. This rationale is based on the concept that the charge of an antibody increases with increasing distance from pI. In addition to the overall net charge, which induces repulsive electrostatic protein-protein interactions the concept also includes the assumption of an anisotropic charge distribution over the protein surface resulting in attractive protein-protein interaction, which is weakening upon increasing ionic strength. Finally, electrostatic binding between oligovalent ions and the protein resulting in charge neutralization is completing the concept. An upper critical solution temperature was observed for the liquid-liquid phase separation in the presence of citrate, which signifies that the formation of the two liquid phases is exothermic and the entropy decreases upon clustering of the antibodies.

The measurement of diffusion by DLS was giving a deeper understanding into the effects, which are induced by different excipients and excipient concentrations. The simplified two component model of  $k_D$  in the traditional sense was shown to be unsuitable for the charged mAb at low ionic strengths where at least 3 components with varying concentration need to be taken into account. Therefore, the classical interpretation of low  $k_D$  values representing more attractive PPIs and higher  $k_D$  values representing more repulsive interactions is not valid under these circumstances. Instead the theory of coupled protein counterion diffusion was confirmed. This theory is taking into account isotropic electrostatic ion-ion interactions between the antibodies, between the coions as well as between antibodies and coions. As the diffusion of the protein and the counterion is coupled, DLS can reveal information on the counterion diffusion and thereby on the interplay between both, the mAb and the counterion.

## Kurzdarstellung

Monoklonale Antikörper sind Proteine, die mit hoher Spezifität ans pharmakologische Zielprotein binden. Das ermöglicht die Behandlung verschiedener Krankheiten, wie z.B. Krebs oder Autoimmunerkrankungen. In einer flüssigen Antikörperlösung wechselwirken alle Lösungskomponenten, wie das Protein, Wasser und alle weiteren gelösten Stoffe miteinander. Es wird davon ausgegangen, dass die Wechselwirkung zwischen dem Antikörper und den weiteren gelösten Stoffen die Protein-Protein Wechselwirkungen und folglich auch die Stabilität und das Phasenverhalten der Antikörperlösung beeinflussen.

Das Ziel der Arbeit war es:

- Ein oder mehrere Modellhilfsstoffe zu identifizieren, welche eine anziehende Wechselwirkung zum Antikörper aufweisen
- Methoden zur Detektion und zur Quantifizierung anziehender Hilfsstoff-Antikörperwechselwirkungen zu identifizieren
- Begründungen zu finden, welche den Einfluss des pH-Wertes, der Anwesenheit und Konzentration von bestimmten Hilfsstoffen, der Ionenstärke sowie der Temperatur auf die Phasengrenzen beschreiben
- Begründungen zu finden, welche die Auswirkungen des pH-Wertes, der Anwesenheit und Konzentration von Excipients sowie der Ionenstärke auf die Diffusion einer Antikörperlösung beschreiben

Verschiedene Hilfsstoffe konnten identifiziert werden, welche an den Antikörper binden. Diese sind Citrat, Butan-1,2,3,4-tetracarboxylat, Benzol-1,2,4,5-tetracarboxylat, Benzol-1,2,3,4,5-pentacarboxylat und Mellitat. Es ist anzunehmen, dass diese negativ geladenen oligovalenten Ionen durch elektrostatische Wechselwirkung mit dem positiv geladenen Antikörper interagieren.

Die Wechselwirkung zwischen dem Antikörper und den Citratmolekülen zeigte sich mittels drei verschiedener experimenteller Herangehensweisen:

- Vergleich der Phasengrenzen in Abhängigkeit des pH-Wertes in An- und Abwesenheit von Citrat
- Darstellung der Ionenatmosphäre nach Gleichgewichtsdialyse gegen eine Mischung aus verschiedenen Ionen, die um die Solvathülle konkurrieren
- Beschleunigte Diffusion des Antikörpers bei unendlicher Verdünnung in der Anwesenheit von 2 mM und 5 mM Citrat, welche sich weder mittels Zweikomponenten noch mittels Dreikomponenten Diffusionsmodell erklären lässt

Das Auftreten der Phasentrennung und das Ausmaß der Mischungslücke wurden in Abhängigkeit des pH-Wertes, der Hilfsstoffspezies und Hilfsstoffkonzentration sowie der Ionenstärke und der Temperatur untersucht. Es wurden Erklärungen gefunden, die das Phasenverhalten und damit die Protein-Protein Wechselwirkungen in Lösungen unterschiedlicher Zusammensetzung beschreiben können. Diese Erklärungen basieren auf dem Konzept, dass die Ladung des Antikörpers mit steigendem Abstand zum isoelektrischen Punkt ansteigt. Zusätzlich zur Gesamtnettoladung, die abstoßende, elektrostatische Protein-Protein Interaktionen induziert, basiert das Konzept auch auf der Annahme einer anisotropen Ladungsverteilung über der Proteinoberfläche, welche zu anziehenden Protein-Protein Wechselwirkungen führt. Diese anziehenden Wechselwirkungen werden durch Erhöhung der Ionenstärke abgeschwächt. Schließlich wird das Konzept durch elektrostatische Bindungen zwischen oligovalenten Anionen und dem Protein vervollständigt, welche zur Ladungsneutralität des Antikörpers führen können. Für die Flüssig-Flüssigphasentrennung einer Antikörperlösung in Anwesenheit von Citrat wurde eine obere, kritische Lösungstemperatur beobachtet. Dies bedeutet, dass es sich bei der Bildung der zwei flüssigen Phasen um einen exothermen Vorgang handelt und dass die Entropie durch Zusammenlagerung der Antikörpermoleküle sinkt.

Die Messung der Diffusion mittels dynamischer Lichtstreuung vermittelte ein tieferes Verständnis darüber, wie sich verschiedene Hilfsstoffe und Hilfsstoffkonzentrationen auf die Diffusion auswirken. Es wurde gezeigt, dass das herkömmliche, vereinfachende  $k_D$ -Zweikomponentenmodell bei niedriger Ionenstärke ungeeignet für den geladenen

Antikörper ist. Dies lässt sich dadurch begründen, dass für geladene Teilchen bei niedriger Ionenstärke mindestens 3 Komponenten mit sich ändernden Konzentrationen betrachtet werden müssen. Daher ist die herkömmliche Interpretation, nach der niedrige  $k_D$  Werte anziehende Protein-Protein Wechselwirkungen und hohe  $k_D$  Werte abstoßende Wechselwirkungen repräsentieren, unter diesen Bedingungen niedriger Ionenstärken nicht gültig. Stattdessen konnte die Theorie, nach der die Diffusion des Proteins mit der Diffusion des Gegenions gekoppelt ist, bestätigt werden. Diese Theorie berücksichtigt isotrope elektrostatische Ion-Ion Wechselwirkungen zwischen Antikörpern, zwischen Gegenionen, sowie zwischen Antikörpern und Gegenionen. Da die Diffusion des Proteins mit der Diffusion des Gegenions gekoppelt ist, können mittels dynamischer Lichtstreuung Informationen über die Diffusion der Gegenionen und somit über das Wechselspiel zwischen Antikörper und Gegenion erlangt werden.





## Table of Content

1.	Introduction.....	1
2.	Theoretical background .....	7
2.1.	Liquid-Liquid Phase Separation .....	7
2.1.1.	Solution conditions that favor LLPS .....	7
2.1.2.	Definition and properties of complex coacervates .....	7
2.2.	Mapping the ion atmosphere.....	9
2.3.	Diffusion coefficient .....	9
2.3.1.	Factors affecting the diffusion coefficient .....	10
2.3.2.	Measurement of the diffusion coefficient.....	16
2.4.	Net charge of a protein in the presence of ions.....	17
2.4.1.	Bound counterions, freely diffusing protein-related counterions and effective counterions.....	17
2.4.2.	Valence, Debye-Hückel-Henry charge $z_{DHH}$ and effective charge $z_{eff}$ .....	18
2.4.3.	The Gibbs-Donnan equilibrium condition.....	20
3.	Materials and Methods.....	23
3.1.	Materials .....	23
3.1.1.	Consumables.....	24
3.1.2.	Chemicals .....	25
Instrumentation and Software .....		27
3.2.	Methods .....	27
3.2.1.	Analytics .....	27
3.2.2.	Sample preparation – citrate ion removal and NaCl reduction.....	31
3.2.3.	Experimental procedures .....	33
3.2.4.	Determination of anion charges.....	40
3.2.5.	Calculation of diffusion coefficients, $D_0$ and $k_D$ by the model of diffusion in ternary systems .....	43
4.	Results and Discussion .....	45
4.1.	Protein phase behaviour in the presence of oligovalent anions - Dialysis Experiments .....	45

4.1.1.	pH-induced opalescence .....	45
4.1.2.	pH induced LLPS .....	48
4.1.3.	Dependence of the miscibility gap on citrate concentration.....	56
4.1.4.	Dependence of the miscibility gap on ionic strength.....	60
4.1.5.	Dependence of the miscibility gap on the temperature .....	64
4.1.6.	Dependence of phase separation on anion charge .....	71
4.1.7.	Mapping the ion atmosphere .....	74
4.1.8.	Summary and conclusions .....	76
4.2.	Protein phase behavior in the presence of oligovalent Anions - Spiking Experiments .....	78
4.2.1.	Influence of anion charge and anion concentration on phase separation .....	78
4.2.2.	Influence of pH and mellitate concentration on phase behavior .....	90
4.2.3.	Influence of ionic strength on phase separation .....	97
4.2.4.	Influence of the overall protein concentration on phase behaviour.....	101
4.2.5.	Summary and conclusions .....	112
4.3.	Protein diffusion .....	113
4.3.1.	Hydrodynamic diameter of pH-dependent protein solutions.....	113
4.3.2.	$D_0$ and $k_D$ values as a function of buffer species and concentration, pH and salt.....	117
4.3.3.	Summary and conclusions .....	166
5.	Summary, Conclusion and Outlook.....	171
6.	References.....	183
7.	Appendices.....	195
8.	Acknowledgements.....	197
9.	Publications.....	199
10.	Curriculum Vitae .....	200

## Acronyms and Abbreviations

2 (subscript 2)	Relating the parameter to component 2 (protein)
3 (subscript 3)	Relating the parameter to component 3
4 (subscript 4)	Relating the parameter to component 4
<i>I</i> (superscript I)	Relating the parameter to compartment I (protein solution)
<i>II</i> (superscript II)	Relating the parameter to compartment II (outer dialysis medium without protein)
<i>a</i>	Radius of an ideal hard sphere
$B_{22}$	Second virial coefficient of osmotic pressure
BCA	Bicinchoninic acid
BE IC	Measurement of the ion content via ion chromatography subsequent to buffer equilibration
C	Coulomb (unit of electric charge)
<i>c</i>	Weight concentration
$\bar{c}_0$	Average concentration of mellitate adjusted by sample preparation
<i>c'</i>	Molar concentration
$c_c$	Critical concentration (protein concentration at the critical point)
Citric acid	2-Hydroxy-1,2,3-propanetricarboxylic acid
<i>D</i>	Diffusion constant, diffusion coefficient
$D_{22}, D_{23}, D_{33}, D_{32}$	Diffusion coefficients of a ternary system (system consisting of three different components)
$D_0$	Diffusion coefficient at infinite dilution (Brownian diffusion coefficient)
$D_2$	Limiting diffusion coefficient of the protein in ideal solution neglecting influences of protein-protein interactions or coupled protein-counterion diffusion
$D_3$	Limiting diffusion coefficient of the counterion in ideal solution neglecting influences of protein-protein interactions or coupled protein-counterion diffusion
$D_c$	Diffusion coefficient at finite concentration
$D_s$	Self-diffusion coefficient
Da	Dalton (atomic mass unit)
DLS	Dynamic light scattering
DLVO	Derjaguin-Landau-Verwey-Overbeek
DNA	Deoxyribonucleic acid
DSC	Differential scanning calorimetry
<i>e</i>	Elementary charge
equ	Equation
<i>f</i>	Frictional coefficient
$f_0$	Frictional coefficient at infinite dilution
$f_c$	Concentration dependent frictional coefficient

$f-t$	Flow-through
IEF	Isoelectric focusing
$J$	Flux
$K$	Equilibrium constant
$K_c$	Constant: ratio of molar counterion concentration to molar protein concentration
$K_D$	Diffusion interaction parameter (expressed as a function of the volume fraction)
$k$	Boltzmann constant
$k_D$	Diffusion interaction parameter (expressed as a function of the weight concentration)
$k_f$	Parameter which is equal to $k_s$
$k_s$	Parameter obtained by sedimentation velocity experiments
LCST	Lower critical solution temperature
LLPS	Liquid liquid phase separation
LSPS	Liquid solid phase separation
$[M]$	Titrated free citrate concentration of BE IC experiments
$[M_{1/2}]$	Competition constant
Mellitic acid	Benzene-1,2,3,4,5,6-hexacarboxylic acid
$M_w$	Relative molecular mass of the protein
MWCO	Molecular weight cut-off
$N$	Number of associated ions (BE IC experiments)
$N_0$	Number of associated chloride ions at the beginning of buffer equilibration (BE IC experiments)
$N_1$	Number of associated chloride ions at the end of buffer equilibration (BE IC experiments)
$N_A$	Avogadro constant
$n$	Hill coefficient (BE IC experiments)
PALS	Phase analysis light scattering
PDI	Polydispersity index
PEG	Polyethylene glycol
pI	Isoelectric point
$pK_a$	Ionization constant
$R$	Universal gas constant
$r_h$	Stokes radius, hydrodynamic radius
$r_h(0)$	Stokes radius at infinite dilution
$s_0$	Sedimentation coefficient at infinite dilution
$s_c$	Sedimentation coefficient at finite concentration
SI	International system of units
$T$	Temperature in K
$T_c$	Critical temperature (temperature at the critical point)
TCA	Trichloroacetic acid
Trans-aconitic acid	Trans-prop-1-ene-1,2,3-tricarboxylic acid
Tricarballic acid	Propane-1,2,3-tricarboxylic acid
Trimesic acid	Benzene-1,3,5-tricarboxylic acid
UCST	Upper critical solution temperature

UV	Ultraviolet
$w$	Width as defined by equation 38
$x$	Distance
$Z_P$	Valence
$z$	Ionic net charge
$z_{DHH}$	Debye-Hückel-Henry charge
$z_{eff}$	Effective charge
$\hat{\gamma}_2$	Activity coefficient of component 2
$\eta$	Dynamic viscosity
$\psi$	Electrostatic potential
$\Pi$	Osmotic pressure
$\bar{v}$	Partial specific volume of the protein
$v_s$	"Swollen" specific volume
$\phi$	Volume fraction



## 1. INTRODUCTION

Monoclonal antibodies are proteins with a high target specificity, which enable their use of treating various diseases, such as cancer and autoimmune disorders. Their high target specificity is usually accompanied by low unintended side effects (1-4).

The insufficient stability of monoclonal antibodies in the gastrointestinal tract is limiting the route of administration for monoclonal antibodies to parenteral administration, such as intravenous, subcutaneous or intravitreal administration. These types of administration almost exclusively require a liquid formulation which may, in certain cases, be lyophilized in the course of production and reconstituted immediately before administration to achieve an adequate stability.

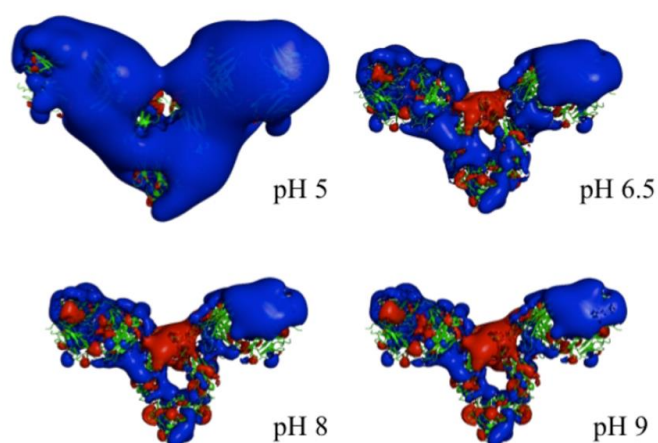


Figure 1: Illustration of the surface charge potential of an antibody. A positive potential is marked in blue and a negative potential is marked in red. The surface charge depends on the pH in solution. The antibody forms an extended Y-like shape (Figure taken from (5))

In a liquid formulation all solution components such as the hydrated protein, water and salts or buffers, are interacting. The physical-chemical properties of the protein and of the cosolutes (salts, buffers and others) may specifically influence the interaction between these different solution components. The interaction between the protein and the cosolutes is assumed to affect the protein-protein interactions and thereby influences the stability and the phase behavior of the protein solution. The latter properties are decisive factors with respect to the suitability of a protein to be used as an active pharmaceutical ingredient.

### *Overall aim of the study*

The classical work of formulation development focuses on selecting an individual formulation for an individual protein molecule to guarantee longterm stability and enable a good processability. There, the focus is the outcome (i.e. a stable and processable formulation) and not as much the mechanism behind stabilization.

The following study focuses on the mechanism behind protein stabilization. Therefore, the thesis statement is formulated as follows:

“The protein-protein interaction potential results from the sum of repulsive and attractive protein-protein interactions. The modification of the protein-protein interaction potential by excipients is caused by interactions between the excipients and the protein.”

Therefore, the aim of the present study is to:

- Identify one or more model excipients, which are attractively interacting with the antibody
- Identify approaches to detect and to quantify attractive interactions between excipients and the antibody
- Find a rationale behind the effects of pH, presence and concentration of excipients, ionic strength and temperature on the phase boundaries of an antibody solution
- Find a rationale behind the effect of pH, presence and concentration of excipients and ionic strength on the diffusion of an antibody in solution

### *Relevance of liquid-liquid phase separation (LLPS)*

Liquid-liquid phase separation (LLPS) due to reversible self-association of antibody molecules is a complex phenomenon already observed by several groups (6-13). The present work focuses on solution conditions that induce LLPS at low ionic strength (< 150 mM) in the absence of polyethylene glycol (PEG) or other molecular crowding substances such as ammonium sulfate. Phase separation observed in the presence of high salt concentrations in the molar range or in the presence of PEG should be regarded separately as these additives induce phase separation via a different mechanism, namely the competition for water of hydration, or salting-out (12, 14, 15).



The importance of LLPS in biotechnology and production ranges from unwanted phase separation during antibody production and storage to a systematic application as membrane-free concentration technique or column-free approaches for protein purification (16, 17). In detail, the purification process ends after the last process step, namely the ultra-/diafiltration step with the aim of conditioning the protein into a specific formulation and/or increase protein concentration. This solution is called bulk drug substance and is often stored in large stainless steel tanks. These tanks are then stored up to few days at 2-8 °C prior to the fill and finish process. During this storage time, the potential occurrence of LLPS may induce a protein concentration gradient in the tank. It is avoided to stir the protein solution in the tank in order to reduce potential protein aggregation induced by mechanical stress. Because of the protein gradient in the tank, fill and finish into e.g. pharmaceutical vials, would induce a batch inhomogeneity with vials having different protein concentrations. This has strictly to be avoided in order to meet batch consistency. This work deals with factors associated with the phenomenon of LLPS (lower temperature, pH close to the isoelectric point (pI), higher valency of counterions and lower salt concentration) and with solution properties such as high turbidity, which precedes LLPS. Medically, certain immunoproliferative and autoimmune diseases such as cryoglobulinemia are associated to reversible precipitation of immunoglobulins upon cooling below 37°C (18, 19). Some types of cataract are associated to opacity of crystallins, a protein class that is performing liquid-liquid phase separation (20-23). In certain cases, LLPS is metastable with respect to crystal formation (24-33). For such cases the exact position of the phase boundary in the phase diagram (excipient concentration vs. protein concentration) can be used to predict and optimize conditions for protein crystallization at specific environmental conditions (33).

### *Relevance of liquid-solid phase separation (LSPS)*

Complexation of proteins by oppositely charged ions may stabilize the protein against dehydration by lyophilization and against elevated temperature (34). The electrostatic interactions between charged proteins and oppositely charged ions can be used for encapsulation and delivery (34-36). Complexation of proteins can also be used for protein separation and purification (37). Several studies indicate proteins immobilized in electrostatic complexes to remain intact and active (37-39).

Electrostatic interactions are of high importance in the purification process of biopharmaceuticals. Negatively charged DNA molecules and negatively charged host-cell proteins may electrostatically interact with the positively charged protein. The findings from this work give insight of how to influence these interactions, e.g. by changing pH or ionic strength. In addition, a column-free fractionated protein precipitation with mellitic acid or mellitate ions could support or replace the cation exchange chromatography step in the purification process of a monoclonal antibody. After the purification step, mellitate could be removed by a diafiltration step at higher ionic strength.

Understanding electrostatic interactions between proteins and excipients as well as between two protein molecules are also of high importance for understanding formulation dependent effects in formulation development. The tendency of a protein to clustering or self-association may be strongly affected by electrostatic interactions. Therefore, physical properties of the protein solution such as its turbidity, its viscosity or the formation of proteinaceous subvisible and visible particles are assumed to be affected by electrostatic interactions. Even though the highly charged anions used in this part of the work are not used in formulation development, there are well suitable to study the effect of negatively charged ions on the solubility of positively charge proteins over a large variety of influencing factors. Understanding protein-excipient interactions may lead to more rational formulation decisions.

### *Relevance of the diffusion coefficient*

Measurement of the diffusion coefficient by Dynamic Light Scattering (DLS) is a commonly used method to determine the hydrodynamic radius of a protein. Size measurement can be used to detect changes in the size distribution of proteins subsequent

to accelerated stress or long-term stability studies (40, 41). In addition to the size, the polydispersity index (PDI) obtained by DLS is a useful parameter to sensitively characterize changes in the size distribution after stressing the protein solution (42, 43). For these types of experiments, the high sensitivity to higher molecular weight species, such as aggregates, is one of the advantages of DLS.

Furthermore, protein concentration dependence of the measured diffusion coefficient and the stability parameter  $k_D$  is assumed to provide information about intermolecular protein interactions. A lower value of  $k_D$  is considered to represent more attractive colloidal interactions, whereas a positive value is connected to repulsive protein-protein interactions. ((5, 44-64))

The stability parameter  $k_D$  has been exhaustively used to study the influence of specific solution conditions on the colloidal stability of monoclonal antibodies. Most of the published data describe the effect of pH and ionic strength on  $k_D$  (5, 44-60). However, certain studies also examined the influence of defined buffers (5, 52), sugars and polyols (54, 63) or cyclodextrins (62) on  $k_D$ . Differences in  $k_D$  of various antibodies or antibody mutants have also been studied (46, 49, 51, 53, 54, 57, 59-61, 64).

Attractive protein-protein interactions in protein solutions lead to higher opalescence (7, 9, 10, 65, 66), higher viscosities (51, 53, 57-61) and enhanced aggregation kinetics of the proteins in solution (53, 54, 67-75).

In previous studies which were measuring  $k_D$ , a pseudobinary system was the basis of data analysis. In this work, the diffusion coefficients will be examined based on the assumption of a three-component system. In particular, the coupled diffusion of the charged protein and its counterions will be pointed out.



## **2. THEORETICAL BACKGROUND**

### **2.1. LIQUID-LIQUID PHASE SEPARATION**

#### **2.1.1. Solution conditions that favor LLPS**

LLPS occurs spontaneously upon changing the solution conditions such as temperature (7-9, 11, 13, 65), pressure (76), pH (7, 8, 11, 65), the presence of cosolutes or their concentration (8, 65). Thereby a homogeneous protein solution separates into a lower phase with high protein concentration and high density and an upper phase with low protein concentration and lower density. Points on the phase boundary, called coexistence curve, describe the concentrations of the two coexisting protein solutions. At temperatures above the maximum of the coexistence curve, termed upper critical point or upper critical solution temperature (UCST), no phase separation takes place and a single phase is formed. The protein concentration at the critical temperature is termed critical concentration. In currently published studies, the critical concentration is similar for most investigated antibodies (approximately 90 mg/ml) (7, 8, 13) whereas the critical temperature strongly depends on the unique antibody and the solution composition. Published data of the critical temperature of monoclonal antibodies vary from  $-3^{\circ}\text{C}$  to  $\geq 25^{\circ}\text{C}$  (7, 8, 13).

Even though not yet systematically described in the literature, it has been shown in several studies that LLPS often occurs at conditions close to the pI (6-11, 65). To my knowledge, up to now just two studies have been published in which LLPS in antibody solutions was also observed more than one pH unit distant from pI at low ionic strength and in the absence of polyethylene glycol (8, 46). In general, LLPS has been shown to be more pronounced at lower temperature (upper critical solution temperature: UCST phase behavior) and lower ionic strength (7-10, 12, 13, 19). A strong correlation between LLPS and opalescence of antibody solutions has been found, probably due to attractive protein-protein interactions which form the basis for both phenomena (7-10).

#### **2.1.2. Definition and properties of complex coacervates**

A well-studied sub-type of LLPS is complex coacervation. Complex coacervation was first mentioned by Tiebackx in 1911, naming a liquid-liquid phase separation as a result of electrical interaction between opposite charges on polyelectrolytes (77, 78). Later, in 1938

Bungenberg de Jong studied the phase behavior of protein solutions (79). Complex coacervation was observed for isolabile globular proteins at the isoelectric point and for biocolloids that interact with oppositely charged ions, such as ferricyanide or picrate (79). These days, complex coacervation is defined as a spontaneous liquid-liquid phase separation that occurs in solution of oppositely charged macromolecules, including both polyelectrolytes and charged colloidal particles (17, 80).

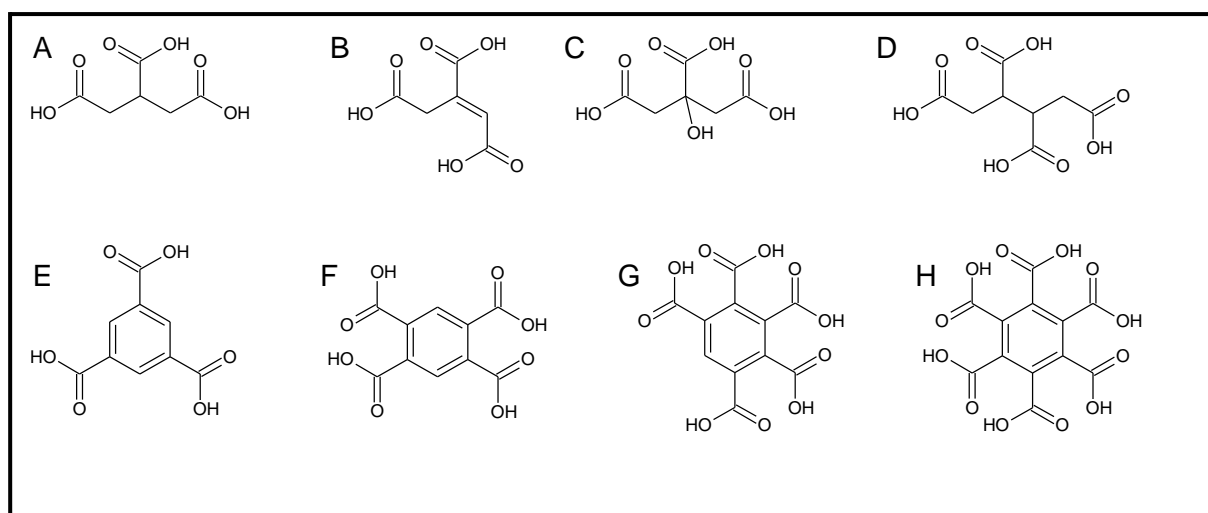


Figure 2: Chemical structures of the oligovalent acids used in this work: A) propane-1,2,3-tricarboxylic acid (tricarballic acid), B) trans-prop-1-ene-1,2,3-tricarboxylic acid (trans-aconitic acid), C) 2-hydroxy-1,2,3-propanetricarboxylic acid (citric acid), D) butane-1,2,3,4-tetracarboxylic acid, E) benzene-1,3,5-tricarboxylic acid (trimesic acid), F) benzene-1,2,4,5-tetracarboxylic acid, G) benzene-1,2,3,4,5-pentacarboxylic acid, and H) benzene-1,2,3,4,5,6-hexacarboxylic acid (mellitic acid)

By current definition (17, 80), the formation of LLPS by an antibody (charged colloidal particle) interacting with oligovalent anions as shown in Figure 2 is not explicitly a complex coacervate, as the interacting ions are not exclusively macromolecules. However, the large number of similarities between complex coacervates and LLPS will be pointed out in the following study.

Complex coacervates have some properties in common: An optimum mixing ratio between the oppositely charged molecules exists, at which the formed complex is electrically neutral and phase separation is most pronounced (17, 77, 79, 81-84). The presence of salt has a dissociating effect on the complex of oppositely charged molecules and coacervation is extenuated or even suppressed (77, 79, 84, 85). Finally, the charge density of the interacting

partners has an influence on the physical appearance of the complex. Weak neutralizing interactions between the involved macromolecules result in liquid-liquid phase separation. When the interacting partners are more densely charged, liquid-solid phase separation (LSPS) i.e. precipitation might occur (77, 86).

Another concept that describes the effect of citrate-varied interactions of the antibodies is the concept of LLPS of effective particles (87, 88). Effective protein-protein interactions are strongly dependent on the presence of other additives in solution, such as salts, buffers, sugars etc. If an additive interacts with the protein, the formed particle is called “effective particle” (88). By changing the solvent composition, effective protein-protein interactions are modified and the phase behavior can thereby be adjusted (88).

## **2.2. MAPPING THE ION ATMOSPHERE**

Binding between anions and monoclonal antibodies (positively charged below pI) has an impact on intermolecular antibody-antibody interactions (52, 89-91). In the mentioned studies (52, 89-91), anion binding was assumed due to differences in the electrophoretic mobility of the antibody in different ion environments. In the following work, a direct quantitative approach is presented to measure the competition of different ions for the composition of the ion atmosphere. The ion atmosphere, i.e. the mobile sheath of ions surrounding the protein, has no discrete structure and interactions between ions and proteins follow complex thermodynamic behaviour, which cannot be described by simple binding isotherms (92, 93). Therefore Bai and co-workers (92) suggest the determination of a competition constant of competing ions rather than a dissociation constant. The method of Bai et al. (92), originally developed for DNA, was adopted in the present study to antibodies by measuring the anion content via ion chromatography subsequent to buffer equilibration (BE IC). The results in the present study confirm that citrate ions preferentially bind to the protein compared to chloride ions.

## **2.3. DIFFUSION COEFFICIENT**

Proteins in solution collide with thermally fluctuating water molecules resulting in random motion of the protein molecules, called Brownian motion. Brownian motion is the origin of diffusion (94).

One-dimensional diffusion is described by Fick's first law of diffusion:

$$J_2 = -D \left( \frac{\partial c_2}{\partial x} \right) \quad (1)$$

The flux  $J_2$  is the rate of mass transport across a surface of unit area of component 2,  $c_2$  is the weight concentration and  $x$  is the distance. The gradient in protein concentration is related to the flux  $J_2$  by the diffusion constant  $D$  (94). The diffusion constant is synonymously termed diffusion coefficient (95). The subscript 2 denotes these quantities to relate to component 2, a dissolved species that diffuses in component 1. In the present study component 1 refers to water, component 2 refers to the (positively charged) antibody molecule and in the following sections component 3 refers to lower molecular weight anions such as chloride, or buffer ions.

### 2.3.1. Factors affecting the diffusion coefficient

#### 2.3.1.1. Binary diffusion model neglecting protein-protein interactions

The diffusion coefficient  $D_0$  describes Brownian motion for an ideal hard sphere of radius  $a$  in a liquid medium of viscosity  $\eta$  at infinite dilution ( $c(c_0) \rightarrow 0$ ):

$$D_0 = \frac{kT}{6\pi\eta a} \quad (2)$$

Here,  $k$  is the Boltzmann constant and  $T$  is the absolute temperature in K.

Hydration and irregular shape of the proteins have damping effects on the random motion of the protein compared to a hard sphere of the same volume (94). The measured diffusion is lower. The Stokes radius or hydrodynamic radius,  $r_h$ , of a non-spherical hydrated protein is defined as the radius of a hard sphere that has the same diffusion coefficient as the protein.

$$D = \frac{kT}{6\pi\eta r_h} \quad (3)$$

#### 2.3.1.2. Binary diffusion model taking into account protein-protein interactions

In real solutions at finite dilution, proteins interact with each other. In this case the mutual diffusion coefficient  $D_c$  is a function of the protein concentration and is defined by (94):

$$D_c = (kT/f_c)[1 + \partial(\ln \gamma_2)/\partial(\ln c_2)] \quad (4)$$



where  $\gamma_2$  is the activity coefficient and  $c_2$  is the weight concentration of the protein. The frictional coefficient  $f_c$  is assumed to be concentration dependent (96):

$$f_c = f_0(1 + k_s c_2) \quad (5)$$

whereby  $k_s$  can be determined by sedimentation velocity experiments (96):

$$s_c = s_0(1 - k_s c_2) \quad (6)$$

Here,  $s_c$  is the sedimentation coefficient at finite concentration and  $s_0$  is the infinite dilution value.

Taking into account the Gibbs-Duhem equation and introducing a relation to osmotic pressure  $\Pi$ , equ (4) can be written as (96):

$$D_c = \frac{RT}{N_A f_c} \left( \frac{Mw(1-\bar{v}c_2)}{RT} \frac{\partial \Pi}{\partial c_2} \right) \quad (7)$$

With the universal gas constant  $R$ , the Avogadro constant  $N_A$ , the relative molecular mass of the protein  $Mw$  and the partial specific volume of the protein  $\bar{v}$  (96).

Inserting the expression for osmotic pressure  $\frac{\partial \Pi}{\partial c_2} = \frac{RT}{M} [1 + 2B_{22}Mw c_2 + \dots]$  with  $B_{22}$  being the second virial coefficient and inserting the expression of the frictional coefficient  $f_c$  from equ (5), the final equation is derived:

$$D_c = \frac{RT}{N_A f_0} \frac{(1-\bar{v}c_2)[1+2B_{22}Mw c_2 + \dots]}{1+k_s c_2} \quad (8)$$

An approximation to equ (8) can be performed by power series expansion of concentration and by neglecting square terms of low values:

$$D_c \approx \frac{RT}{N_A f_0} [1 + c_2(2B_{22}Mw - \bar{v} - k_s)] \quad (9)$$

This approximated expression is in accordance with the empirical equation

$$D_c = D_0(1 + k_D c_2) \quad (10)$$

with

$$D_0 = \frac{RT}{N f_0} \quad (11)$$

and

$$k_D = 2B_{22}MW - \bar{v} - k_s \quad (12).$$

At infinite dilution, the diffusion coefficient  $D_c$  (also called mutual diffusion coefficient), measured by DLS is equivalent to the self-diffusion coefficient,  $D_s$ , and the Brownian diffusion coefficient,  $D_0$  (97).

According to equ (12),  $k_D$  is influenced by thermodynamic contributions ( $B_{22}$ ), i.e. the interaction potential between two proteins as well as hydrodynamic contributions ( $\bar{v}$  and  $k_s$ ) which generally lower  $k_D$ , therefore also termed hydrodynamic drag (98). Hence, a positive  $k_D$  always represents net repulsive interactions between the proteins whereas a largely negative  $k_D$  represents attractive interactions. A slightly negative  $k_D$  could account for attractive as well as repulsive net interactions (98). The  $k_D$  of monoclonal antibodies for vanishing thermodynamic contribution ( $B_{22} = 0$ ) was estimated to  $-5.34 \text{ ml}\cdot\text{g}^{-1}$  (59).

A slightly different form of equ (12) has been reported in the literature (99, 100), which reads as follows:

$$k_D = 2B_{22}MW - 2\bar{v} - k_f \quad (13)$$

$k_f$  in equ (13) corresponds to  $k_s$  in equ (12). The difference between equ (12) and equ (13), i.e. the partial specific volume contributing by a factor of 2 to the hydrodynamic drag can be explained with backflow of solvent, which is only taken into account in equ (13) (101).

The concentration dependence of the diffusion coefficient can be expressed as a function of the weight concentration  $c_2$  (equ (10)) or as a function of the volume fraction  $\phi$  (96):

$$D_c = D_0(1 + K_D\phi) \quad (14)$$

where  $K_D = \frac{k_D}{v_s}$  and  $v_s$  is the ‘swollen’ specific volume, which is the volume of the protein in solution per unit anhydrous mass of the protein, including the volume of solvent associated with the protein (96, 102).

Studies published in the context of colloidal stability of monoclonal antibodies usually use the concentration dependence in terms of mass concentration (46, 49, 51, 53, 54, 57, 59-61, 64). Theoretical studies rather focus on the volume fraction dependence of  $D$ . A study

modeling the diffusion coefficient of hard neutral non-interacting spheres finds a value of 1.45 for the volume fraction dependent parameter  $K_D$  (96).

The relation between  $k_D$ ,  $D_0$  and  $D$  as defined in equ (10) can also be expressed as a relation between  $k_D$  and the protein size in terms of the hydrodynamic radius  $r_h$  of the protein.

By combining equ (10) with equ (3) the following relation is obtained:

$$r_h(c_2) = \frac{r_h(0)}{1+k_D c_2} \quad (15)$$

Here,  $r_h(c_2)$  is the hydrodynamic radius at a defined protein concentration  $c_2$  and  $r_h(0)$  is the hydrodynamic radius obtained by extrapolation of the protein concentration to infinite dilution.  $r_h(0)$  is obtained by converting the diffusion coefficient at infinite dilution  $D_0$  by equ (3).

#### 2.3.1.3. Diffusion model in ternary systems

The theory of  $k_D$  is based on a pseudobinary concept accounting only for interactions between the proteins (component 2) and the surrounding “homogenous” medium (component 1). However, protein solutions often contain buffer salts, additional non-buffering salts, and other cosolutes. Hence, a protein solution is a multicomponent system. However, the two-component model still applies as a pseudobinary model if the concentrations of buffers, salts and various cosolutes stay constant with changing protein concentration and can be defined to be a constant pseudo-homogeneous surrounding medium (component 1).

Charged molecules, such as antibodies, however, are present in solution together with their counterions. At least some of the counterions are not tightly bound to the protein, so they do not belong to component 2. As the concentration of the unbound counterions can change with increasing protein concentration, they are not part of the constant homogeneous surrounding medium and therefore need to be defined as component 3.

A diffusion model for ternary systems includes this dependency. To describe the ternary system an extended form of Fick’s first law of diffusion has been proposed (94, 103-105):

$$J_2 = -D_{22}\nabla c_2 - D_{23}\nabla c_3 \quad (16)$$

$$J_3 = -D_{33}\nabla c_3 - D_{32}\nabla c_2 \quad (17)$$

with the gradient of the protein concentration  $\nabla c_2 = \frac{\partial c_2}{\partial x}$  and the gradient of the counterion concentration  $\nabla c_3 = \frac{\partial c_3}{\partial x}$ . In equ (16) the flux of the protein  $J_2$  is depending on the protein main-term diffusion coefficient  $D_{22}$  which relates the diffusion to the gradient of the protein concentration  $\frac{\partial c_2}{\partial x}$  as well as the crossterm diffusion coefficient  $D_{23}$  which relates the diffusion of the protein to the gradient of the counterion concentration  $\frac{\partial c_3}{\partial x}$  (104, 105). Likewise, the flux of the counterions is described by the main-term diffusion coefficient  $D_{33}$  and the cross-term diffusion coefficient  $D_{32}$  (104, 105).

Electrostatic interactions between the three components are specifically influencing the diffusion in a ternary system. The diffusion of the protein and of its counterions is coupled due to long-range electrostatic forces. This effect, also termed common-ion effect (106), does not vanish at lower protein concentration (94). In many cases the protein in solution is charged and the solution contains a defined number of counter ions. Due to electrostatic forces the diffusion of a protein will impact the diffusion of the counter ions and vice versa. The flux of the protein  $J_2$  and its respective counterion  $J_3$  is not only influenced by thermodynamic forces which occur as a consequence of the protein or counterion concentration gradient, but also by electrostatic forces between proteins and counterions (95).

$$J_2 = -D_2 \left( \nabla c_2 + c'_2 z_2 \frac{eN\nabla\psi}{RT} \right) \quad (18)$$

$$J_3 = -D_3 \left( \nabla c_3 + c'_3 z_3 \frac{eN\nabla\psi}{RT} \right) \quad (19)$$

Here,  $D_2$  is the limiting diffusion coefficient of the protein in ideal solution neglecting influences of protein-protein interactions or protein-counterion coupled diffusion. Likewise,  $D_3$  is the limiting diffusion coefficient of the counterion.  $z$  denotes the ionic net charge of the respective ion,  $e$  is the elementary charge, and  $\psi$  is the electrostatic potential. The concentrations  $c'_2$  and  $c'_3$  are molar concentrations of the protein and the counterions, respectively. In contrast to equ (16) and equ (17), equ (18) and equ (19) do not account for

chemical cross-diffusion, i.e. chemical forces resulting from the concentration gradient of the dissolved species whose flux is not considered. For DLS measurement of charged species the chemical cross-diffusion forces are assumed to be much lower compared to electric forces. The electrostatic potential is stated to be equal in equ (18) and equ (19). This condition is only valid assuming the potential to result from a point charge or spherically symmetric distributed charge quantities. Therefore, the following derived equations only account for ion-ion interactions neglecting dipole-dipole or ion-dipole interactions.

Assuming no macroscopic charge separation the flux of the protein and the flux of the counterion are related by:

$$z_2 J_2 + z_3 J_3 = 0 \quad (20)$$

Additionally assuming the protein concentration gradient and the counterion concentration gradient to be related by:

$$z_2 \nabla c'_2 + z_3 \nabla c'_3 = 0 \quad (21)$$

The flux of the protein can be expressed as follows:

$$J_2 = -D \nabla c'_2 = - \left[ \frac{D_2 D_3 (z_2^2 c'_2 + z_3^2 c'_3)}{D_2 z_2^2 c'_2 + D_3 z_3^2 c'_3} \right] \nabla c'_2 \quad (22)$$

with the diffusion coefficient

$$D = \frac{D_2 D_3 (z_2^2 c'_2 + z_3^2 c'_3)}{D_2 z_2^2 c'_2 + D_3 z_3^2 c'_3} \quad (23)$$

The experimentally measurable diffusion constant  $D$  is thus related to the limiting diffusion constants of the protein  $D_2$  and of the counter ions  $D_3$  (94). The ionic net charge of the protein  $z_2$  corresponds to the Debye-Hückel-Henry charge  $z_{DHH}$  as introduced in section 2.4.2.

A special case of diffusion in a ternary system can be described if the counterion to protein ratio is constant, with  $K_C = \frac{c'_3}{c'_2}$ :

$$D = \frac{D_2 D_3 (z_2^2 + z_3^2 K_C)}{z_2^2 D_2 + z_3^2 K_C D_3} \quad (24)$$

This special case occurs if dilution of the protein solution is performed with water, independent from the initial composition of the protein solution. For this special case the calculated diffusion coefficient is independent of the protein concentration.

Assuming no additional salt to be present in solution, the effective counterions and the protein counterbalance each other ( $z_2 c_2' + z_3 c_3' = 0$ ).

By assuming charge counterbalance between all counterions and the protein and by setting  $z_3 = -I$  for monovalent anions, equ (23) can be simplified to

$$D = \frac{(z_2+1)D_2D_3}{z_2D_2+D_3} \quad (25)$$

The last three equations illustrate that the diffusion coefficient varies with the charge of the protein. As the diffusion of the counter ions  $D_3$  is higher compared to that of the protein  $D_2$ , the experimental measured diffusion of the protein will be faster than expected and the corresponding hydrodynamic radius obtained by Stokes-Einstein relation will be smaller than expected (94).

However, if an excess of low-molecular weight electrolyte is present, the entire electrolyte of right charge acts as effective counter ions. If  $c_3'$  is much higher than  $c_2'$  equ (23) simplifies to  $D \approx D_2$  (94).

Hence, if the ionic strength is sufficiently high, the diffusion and therefore the hydrodynamic radius of the antibody approach values which would be expected from the real spatial properties of the protein (size, shape, hydration) (94).

### 2.3.2. Measurement of the diffusion coefficient

Diffusion can be measured on the microscopic and macroscopic length scale. DLS detects the motions of a protein in a small volume element and thereby measures microscopic fluctuations in the protein concentration (94, 107). To study the net transport over a macroscopic distance, various approaches such as Rayleigh interferometry or Schlieren optics are used (94, 103). A lot of studies examining diffusion of ternary protein systems have been performed on the macroscopic length scale (103-105, 107-110).

Up to now, limited effort has been done on studying diffusion in ternary systems by DLS (104, 106, 107, 111). As far as I know, only one single study examines the effect of coupled diffusion of proteins and counterions on diffusion coefficients measured by DLS (106).

Experimental challenges of free diffusion measurement on the macroscopic length scale are the very slow motion of bigger proteins, as indicated by very low diffusion coefficients. E.g. a monoclonal antibody with a diffusion coefficient of  $46.5 \mu\text{m}^2/\text{s}$  moves on average 2.8 mm in 24 hours (calculated by:  $\langle x^2 \rangle = 2Dt$ , where  $\langle x^2 \rangle$  is the mean square displacement (112)) In addition, potentially occurring thermal gradients will induce convective mixing. Vibrations from thermostatic control devices may also disturb the measurement (94). However, DLS measurements are more affected by high molecular weight impurities due to their higher scattering intensity. Rayleigh interferometry is rather insensitive to these impurities, because high molecular weight aggregates are expected to diffuse very slowly (104). Another advantage of the experimental approaches detecting the net transport over a macroscopic distance is the suitability of determining the whole diffusion coefficient matrix of the multicomponent system as given in equ (16) and equ (17) (107).

The relevance of DLS for measuring protein-protein interactions and protein-counterion interactions in biopharmaceutical development is the short measurement time, a low protein demand and the potential of high throughput screening. In contrast to other techniques for detecting protein-protein interaction or protein interactions with counterions, the system is matrix-free and no additional labeled probes are needed. However, the sensitivity of DLS towards high molecular weight species, limits its application to solutions with a low level of protein aggregates.

## **2.4. NET CHARGE OF A PROTEIN IN THE PRESENCE OF IONS**

### **2.4.1. Bound counterions, freely diffusing protein-related counterions and effective counterions**

To specify the type of charge on a protein, a classification of counterions with different diffusion properties is performed. In solutions of a charged protein (as induced by charged amino acid side chains and terminal charged groups), the same charge concentration of counterions is present in solution for charge counterbalance and electroneutrality. Either

these counterions can bind to the protein or they can freely diffuse in solution. If they are bound to the protein, they move with the protein and thus will diffuse with the same velocity as the protein (113). The counterions which counterbalance the charge of the protein but which are not bound to the protein will be termed “freely diffusing protein-related counterions”. In contrast to bound counterions, the diffusion of freely diffusing protein-related counterions is assumed to be coupled with the diffusion of the protein resulting in accelerated diffusion of the protein and decelerated diffusion of the counterions (94). If additional salt is added to the protein solution, all freely diffusing ions with the opposite charge of the protein will have an impact on protein diffusion. These ions together with the freely diffusing protein-related counterions will be termed “effective counterions” (94). Coions, carrying the same charge sign as the protein, might as well influence the diffusion of the protein, either by direct binding to the protein or by being part of a counterion cloud with a lowered concentration of coion compared to the surrounding medium. However, for the sake of simplicity these ions are neglected in the simple model of protein-ion interaction used in the following work.

The counterions as defined in equ (23) to equ (25) are effective counterions. Bound counterions are not assumed to contribute to the effect described by equ (23) to equ (25) as they are not freely diffusing but move with the protein.

#### **2.4.2. Valence, Debye-Hückel-Henry charge $z_{DHH}$ and effective charge $z_{eff}$**

Two different convertible units systems are generally used to quantify the charge of a protein. The SI (international system of units) unit of electric charge is Coulomb (C). One Coulomb is defined as the charge, which is transported by a constant current of one Ampere in one second. The second quantity of charge, sometimes also termed valence or charge number, is the charge related to the charge of a proton, which is  $1.602 \cdot 10^{-19}$  C. The valence/ charge number is unitless and gives information about the number of charged groups on a protein.

The three types of charges as defined below can be given in both unit systems. In the following work charge will be given in the unitless quantity.



### *Valence*

The valence of a protein is entirely determined by ionizable amino acid side chains as well as amino- and carboxy- terminal groups. The degree of dissociation is assumed to be influenced by equilibrium with free  $H^+$  and  $OH^-$  in solution. Even though potential binding of other charged ions is assumed to have an indirect impact on the valence, binding of charged ions to the protein is not directly considered by the valence. The valence is determined by pH titration in combination with the knowledge of the isoelectric point. The total number of charged groups (with positive and with negative sign) on the protein is higher than the valence. The valence results by summing up all the charged groups of a protein.

Bound counterions (as defined in section 4.2.1) and freely diffusing protein-related counterions counterbalance the valence of the protein. In the following work the term "charge counterbalance" will be used for all counterions which compensate the charge of the protein, independent from a binding event.

### *Debye-Hückel-Henry charge $z_{DHH}$*

The actual net charge of a protein is not only influenced by equilibrium with free  $H^+$  and  $OH^-$  ions but also by binding of other ions, such as sodium, chloride, citrate, carbonate or hydrocarbonate. The Debye-Hückel-Henry charge  $z_{DHH}$  includes bound ions but excludes effects of the solvent ion cloud (113).

The Debye-Hückel-Henry charge is assumed to be counterbalanced by freely diffusing protein-related counterions but not by bound counterions. The charge  $z_2$  as defined in equ (23) to equ (25) is assumed to correspond to the Debye-Hückel-Henry charge  $z_{DHH}$ . In the following work, the term "charge neutralization" will be used, if the counterions bind to the protein and thereby decrease the  $z_{DHH}$  of the protein.

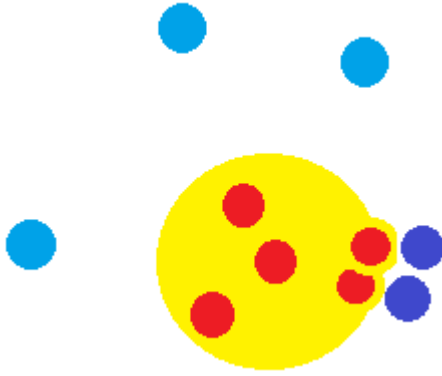


Figure 3: Exemplary depiction of a protein (yellow) with bound counterions (dark blue) and freely diffusing protein-related counterions (light blue). Each circle (red, dark blue, light blue) represents one point charge. The valence of the protein is 5 (5 positive charges on the protein as depicted by red circles). The valence of 5 is counterbalanced by the 5 negatively charged counterions (dark and light blue circles). The  $z_{DHH}$  of the protein is 3, as 2 of the 5 positive charges are neutralized by the two bound counterions. The  $z_{DHH}$  of 3 is counterbalanced by the 3 freely diffusing protein-related counterions (light blue circles).

*Effective charge  $z_{eff}$ :*

A charged particle is interacting with the surrounding medium. An ion cloud or ionic atmosphere forms with an accumulation of oppositely charged ions and a depletion of likely charged ions in the vicinity of the protein. As a result the charge is screened, which means it is lower at a certain distance from the particle surface.  $z_{eff}$  is determined by electrophoretic measurements and represents the charge at the shear plane. It is the ratio between the electrophoretic mobility and the frictional coefficient  $f$ , with  $f = 6\pi\eta r_h$ .  $z_{eff}$  does not differentiate between bound ions and the Debye-Hückel cloud at the shear plane (113).

The theory of the ion cloud and electric double layer is well established for particles of isotropic charge distribution and high charge density. The low net charge of a protein, which is distributed in patches over the large protein surface (thus not isotropic distributed), should be considered if the concept of ion cloud and electric double layer is used to discuss the electrophoretic behavior of a protein.

**2.4.3. The Gibbs-Donnan equilibrium condition**

Dialysis of a charged protein (here: positively charged) against buffers results in higher counterion concentrations (here: molar anion concentration  $c_3^I$ ) and lower coion

concentrations (here: molar cation concentration  $c_4^I$ ) in the protein solution (compartment  $I$ ) compared to molar concentration  $c^{II}$  in the outer dialysis medium (compartment  $II$ ). In the current view, the protein is assumed to be positively charged. The concentration of effective counterions in a protein solution after dialysis is defined by two conditions (114):

The Donnan ratio

$$\frac{c^{II}}{c_3^I} = \frac{c_4^I}{c^{II}} \quad (26)$$

and the principle of electrical neutrality in both compartments

$$c_4^I - c_3^I + z_{DHH}c_2^I = 0 \quad (27)$$

where concentrations of the cation (component 4), the anion (component 3) and the positively charged protein (component 2) are given as molar concentrations. Equ (26) and equ (27) are only valid for a monovalent 1:1 salt. For a salt of higher valence, the equations need to be adjusted as described by Pintauro and Bonta (115).

These relations can be used to calculate the concentration of effective counterions if the Debye-Hückel-Henry charge  $z_{DHH}$  of the protein is known. The total concentration of counterions after dialysis (bound and freely diffusing counterions) will be the sum of bound counterions and effective counterions.



### **3. MATERIALS AND METHODS**

#### **3.1. MATERIALS**

The monoclonal antibody was produced by mammalian cell culture technology (116) by Boehringer Ingelheim Pharma GmbH & Co KG. The antibody has a molecular weight of 145 kDa and a theoretical isoelectric point (pI) of 8.3 (117). The antibody of a concentration of 100 mg/ml was provided in 25 mM citrate buffer pH 6.0 and 115 mM NaCl.

### 3.1.1. Consumables

Table 1: Consumables

Product	Supplier
UV-cuvettes semi-micro, disposable	Brand GmbH & Co KG, Wertheim, Germany
UVette® cuvettes	Eppendorf, Hamburg, Germany
Plastibrand ® micro UV cuvettes, disposable	Brand GmbH & Co KG, Wertheim, Germany
UV-Star Micro plate, 96 well, half area well profile with clear film F-bottom, flat	Greiner Bio-one, Frickenhausen, Germany
optical tape iCycler iQ	BIO-RAD Laboratories Inc. , Hercules, CA, USA
Slide-A-Lyzer™ dialysis cassettes G2, 20.000 Molecular Weight Cut-Off (MWCO), 70 ml nominal volume	Thermo Scientific, Rockford, USA
Sterivex-GV Filter units, sterile	Millipore Corporation, Billerica, USA
Amicon centrifugal filter units, 15 ml nominal volume, 30 kD MWCO	Millipore, Cork, Ireland
regenerated cellulose tubing Spectra Por 7, 25 kDa MWCO, 18 mm flat width,	Spectrumlabs, Inc., Rancho Dominguez, USA
Slide-A-Lyzer dialysis cassettes G2, 10.000 kDa Molecular Weight Cut-Off (MWCO), 30 ml nominal volume	Thermo Scientific, Rockford, USA
Whatman® FP30 / 0.2 Ca-S filter units	GE Healthcare UK Limited, Buckinghamshire, UK
Eppendorf safe-lock tubes, 0.5/1.5/2/5 ml	Eppendorf AG, Hamburg, Germany
Falcon R 15 / 50 ml polystyrene tubes	Corning Inc., Corning, NY, USA
Nalgene R sterile square media bottles	Thermo Scientific, Waltham, MA, USA
EpT.I.P.S.® Reloads	Eppendorf AG, Hamburg, Germany

### 3.1.2. Chemicals

Table 2: Chemicals

Product	Supplier
The BCA <sup>TM</sup> Protein Assay Kit including BCA Reagent A (Cat. 23223) and BCA Reagent B (Cat.23224)	Thermo Scientific (IL, USA)
Trichloroacetic Acid	Sigma-Aldrich, Steinheim, Germany
Sodium sulfate	Sigma-Aldrich, Steinheim, Germany
Urea	GE healthcare
glycerol	GE healthcare
3-[(3-Cholamidopropyl)dimethylammonio]-1-propanesulfonate)	GE healthcare
3.8 % (V/V) Pharmalyte 8 - 10.5 ampholyte solution	GE healthcare
3 % (V/V) servalyt 7 - 9 ampholyte solution	Serva electrophoresis
0.7 % (V/V) servalyte 3 - 10 ampholyte solution (Serva electrophoresis)	Serva electrophoresis
HCl	Carl Roth GmbH & Co. KG, Karlsruhe, Germany
NaOH	Carl Roth GmbH & Co. KG, Karlsruhe, Germany
NaCl	Akzo Nobel GmbH, amsterdam, Netherlands
Na <sub>3</sub> citrate Dihydrate	Jungbunzlauer GmbH, Ladenburg, Germany
Citric Acid Monohydrate	Jungbunzlauer GmbH, Ladenburg, Germany
propane-1,2,3-tricarboxylic acid (tricarballic acid)	Sigma Aldrich (Steinheim, Germany)
trans-prop-1-ene-1,2,3-tricarboxylic acid (trans-aconitic acid)	Sigma Aldrich (Steinheim, Germany)

2-hydroxy-1,2,3-propanetricarboxylic acid monohydrate (citric acid monohydrate)	Sigma Aldrich (Steinheim, Germany)
benzene-1,3,5-tricarboxylic acid (trimesic acid)	Sigma Aldrich (Steinheim, Germany)
butane-1,2,3,4-tetracarboxylic acid	Sigma Aldrich (Steinheim, Germany)
benzene-1,2,4,5-tetracarboxylic acid (pyromellitic acid),	Sigma Aldrich (Steinheim, Germany)
benzene-1,2,3,4,5-pentacarboxylic acid	Sigma Aldrich (Steinheim, Germany)
benzene-1,2,3,4,5,6-hexacarboxylic acid (mellitic acid)	Sigma Aldrich (Steinheim, Germany)
Histidine	S.A. Ajonomoto OmniChem. N.V., Wetteren, Belgium
Histidine hydrochloride monohydrate	S.A. Ajonomoto OmniChem. N.V., Wetteren, Belgium
Sodium acetate trihydrate	Sigma Aldrich (Steinheim, Germany)
Acetic acid, 100 %	Merck KGaA, Darmstadt, Germany
Na <sub>2</sub> succinate hexahydrate	Sigma Aldrich (Steinheim, Germany)
Succinic acid	Sigma Aldrich (Steinheim, Germany)



## Instrumentation and Software

Table 3: Instrumentation and Software

Product	Supplier
UV/Vis Spectrometer, Lambda35	Perkin Elmer, CT, USA
Microman 25 $\mu$ l positive displacement pipette	Gilson S.A.S., Villiers-le-Bel, France
InLab Micro glass electrode	Mettler-Toledo AG, Schwerzenbach, Switzerland
Seven Easy pH voltmeter	Mettler-Toledo AG, Schwerzenbach, Switzerland
ZetaPALS	Brookhaven, NY, USA
Dionex ICS 300 Ion Chromatography system with Dionex IonPac™ AS11-HC, 2 x 250 mm column	Thermo Fisher Scientific, Inc., Sunnyvale, USA
VP-DSC Microcal calorimeter (S/N: 10.02.312)	MicroCal, MA, USA
Phast electrophoresis system	GE Healthcare Life Sciences, NJ, USA
Zetasizer NanoZS ZEN3600	Malvern Instruments Ltd, Worcestershire, UK
Malvern Zetasizer 7.03 software	Malvern Instruments Ltd, Worcestershire, UK
DynaPro® Plate Reader II	Wyatt technology, Santa Barbara, CA, USA
Dynamics 7.1.8	Wyatt technology, Santa Barbara, CA, USA

### 3.2. METHODS

#### 3.2.1. Analytics

##### 3.2.1.1. Determination of the antibody concentration by UV spectroscopy

The antibody concentration was determined by UV absorbance at 280 nm (Perkin Elmer UV/Vis Spectrometer, Lambda35) in plastic disposable UV-cuvettes semi-micro of 1 cm path length (Brand, Wertheim, Germany). According to the manufacturer UV cuvettes made of polyolefines are suitable for measurements in the range from 230 nm to 900 nm. A Microman 25  $\mu$ l positive displacement pipette (Gilson S.A.S., Villiers-le-Bel, France) was used to dilute the protein solution in water. The extinction coefficient at 280 nm of the

antibody was  $1.4 \text{ mL} \cdot \text{mg}^{-1} \cdot \text{cm}^{-1}$ . Dilutions and measurements were performed at room temperature (approximately  $22^\circ\text{C}$ ).

#### 3.2.1.2. Determination of the antibody concentration by using the BCA Assay

25  $\mu\text{l}$  of protein solution or supernatant were mixed with 200  $\mu\text{l}$  of BCA working reagent inside a well of a 96-well microtiter plate. The BCA working reagent was prepared as described by the manufacturer (Thermo Scientific, IL, USA) by mixing 49 parts of BCA Reagent A with 1 part of BCA Reagent B. The BCA working reagent contains sodium carbonate, sodium bicarbonate, bicinchoninic acid ([2,2'-Biquinoline]-4,4'-dicarboxylic acid), sodium tartrate and cupric sulfate in 0.1M sodium hydroxide. A standard series of known concentration of the mAb was prepared and measured simultaneously to align the method in a measuring range between 5  $\mu\text{g}/\text{ml}$  and 150  $\mu\text{g}/\text{ml}$ . After 30 minutes of incubation at  $37^\circ\text{C}$ , the absorption of the BCA-copper-protein complex was measured at 562 nm. Each solution was diluted and measured in duplicate. If the measured absorbance was higher than the calibration range, dilutions with water were performed and the sample preparation and the measurement were repeated. Measurements were performed at room temperature (approximately  $22^\circ\text{C}$ ).

#### 3.2.1.3. pH measurement

pH measurements were performed with an InLab Micro glass electrode (Mettler-Toledo AG, Schwerzenbach, Switzerland) connected to a Seven Easy pH voltmeter (Mettler-Toledo AG, Schwerzenbach, Switzerland), which was calibrated with buffer solutions pH 4.01 and pH 7.00 (Mettler Toledo, Schwerzenbach, Switzerland). Measurements were performed at room temperature (approximately  $22^\circ\text{C}$ ).

#### 3.2.1.4. Opalescence

Opalescence was quantified by measuring the extinction of the sample at 320 nm (Perkin Elmer UV/Vis Spectrometer, Lambda35), in disposable UVette® cuvettes (Eppendorf, Hamburg, Germany) with a path length of 2 mm. According to the manufacturer, UVette® cuvettes are suitable for measurements in the range from 220 nm to 1600 nm (118). Measurements were performed at room temperature (approximately  $22^\circ\text{C}$ ).

#### 3.2.1.5. Zetapotential measurement

Zetapotential measurements were performed with a ZetaPALS (Brookhaven, NY, USA). PALS is an acronym for phase analysis light scattering, measuring the phase shift of scattered light. If available, a protein concentration of 7.5 mg/ml was used for the measurements. In solutions in which phase separation was observed, the supernatant with protein concentrations < 7.5 mg/ml was used. The electrophoretic mobility was measured at 25°C by using the automatic field modus. An emersion electrode with an electrode length of 3.5 mm was used. The applied voltage was between 4V and 8V. The zetapotential was converted from the measured electrophoretic mobility by using the approximation of Smoluchowsky.

#### 3.2.1.6. Citrate and chloride quantification

For citrate and chloride quantification, the protein was separated by precipitation after addition of an equal volume of 50 g/l TCA (trichloroacetic acid). The supernatant was diluted 1:24 (v:v) in Milli Q and finally diluted 1:0.25 (v:v) in 5 mM sodium sulfate as internal standard. 10 µl were injected to a Dionex ICS 300 Ion Chromatography system (Thermo Fisher Scientific, Inc., Sunnyvale, USA), equipped with a Dionex IonPac™ AS11-HC, 2 x 250 mm column (Thermo Fisher Scientific, Inc., Sunnyvale, USA). The method was calibrated for citrate concentrations between 0.25 nM and 50 nM and for chloride concentrations between 1 nM and 1000 nM.

#### 3.2.1.7. Differential Scanning Calorimetry (DSC)

The melting temperature of the protein denaturation was determined using the VP-DSC Microcal calorimeter (S/N: 10.02.312) by MicroCal (MA, USA). The sample with a protein concentration of 2 mg/mL was heated from 13°C to 95°C with a heating rate of 60°C/h. Origin 7.0 software was used to determine the melting temperature. The pH of the citrate free protein solution with reduced salt (see section 3.2.2.2) was adjusted by either adding HCl or NaOH. The reference cell was filled with NaCl solution of the same ionic strength as the sample by considering the ionic strength of the protein and the counterions.

#### 3.2.1.8. Isoelectric focusing (IEF)

IEF was performed using a Phast electrophoresis system (GE Healthcare Life Sciences, NJ, USA). Before usage, the dry gel was hydrated using a solution containing 180 g/l urea, 85 g/l glycerin, 20 g/l CHAPS (3-[(3-Cholamidopropyl)dimethylammonio]-1-propanesulfonate), 3.8 % (V/V) Pharmalyte 8 - 10.5 ampholyte solution (GE healthcare), 3 % (V/V) servalyt 7 - 9 ampholyte solution (Serva electrophoresis) and 0.7 % (V/V) servalyt 3 - 10 ampholyte solution (Serva electrophoresis).

The antibody and an "IEF marker pH 3 - pH 10" (GE Healthcare) were loaded to the gel. The electrophoresis was performed at a temperature of 13°C. The electric voltage was adjusted from 700 V (prefocussing), to 200 V (sample entrance), to 1000 V (isoelectric focusing) to 1500 V (band sharpening). After a total voltage duration of 745 Vh, the electrophoresis was stopped and silver staining was performed.

#### 3.2.1.9. Dynamic light scattering (Zetasizer NanoZS ZEN3600)

DLS measurements were performed using the Zetasizer NanoZS ZEN3600 (Malvern Instruments Ltd, Worcestershire, UK). The solutions were measured in disposable micro UV cuvettes (Plastibrand ®Brand GmbH & Co KG, Wertheim, Germany). Scattered light of 633 nm wavelength was detected at an angle of 173° at 20 °C. Three measurements of 10 cycles lasting 10 seconds each were performed. Malvern Zetasizer 7.03 software was used to determine the *z*-average hydrodynamic particle diameter by cumulant method. Hydrodynamic diameters were calculated with equ (3) by setting the viscosity constant to 1.002 mPas (viscosity of water at 20°C (119)), neglecting slight increases in viscosity induced by the proteins in solution.

#### 3.2.1.10. Dynamic light scattering (DynaPro® Plate Reader II)

For the determination of the interaction parameter  $k_D$  the DynaPro® Plate Reader II (Wyatt technology, Santa Barbara, CA, USA) was used. Measurements were performed in a UV-Star Micro plate, 96 well, half area well profile with clear film F-bottom, flat (Greiner Bio-one, Frickenhausen, Germany) which was covered with an optical tape iCycler iQ (BIO-RAD Laboratories Inc. , Hercules, CA, USA). Each well was measured 20 times with an acquisition time of 3 s. Three wells were filled with each of the samples to be tested.

Scattered light of 589 nm wavelength was detected at 158° at 25°C. Data analysis was conducted with Dynamics 7.1.8 (Wyatt technology, Santa Barbara, CA, USA) providing z-average and PDI by cumulant fit.

### **3.2.2. Sample preparation – citrate ion removal and NaCl reduction**

#### **3.2.2.1. Citrate ion removal and NaCl reduction near the proteins' isoelectric point (pI)**

To remove citrate ions from the antibody solution, the antibody was dialyzed against 300 mM NaCl. Three dialysis steps were performed, each step provided a volume excess of NaCl solution of 100 and was lasting 24 hours. The dialysis was carried out in Slide-A-Lyzer™ dialysis cassettes G2 (Thermo Scientific, Rockford, USA), 20.000 Molecular Weight Cut-Off (MWCO), 70 ml nominal volume. After dialysis into 300 mM NaCl the solutions' pH was adjusted to pH 8.7 with 1 M NaOH and the antibody was dialyzed against 10 µM NaOH under nitrogen atmosphere (Figure 4). All dialysis steps were performed at room temperature. 6 Dialysis steps lasting 24 hours each were performed with a volume excess of 100 times each. The solution was filtered through sterile Sterivex-GV Filter units (Millipore Corporation, Billerica, USA) and stored at 4°C. The final protein concentration was about 46 mg/ml and the pH of the solution was 8.5.

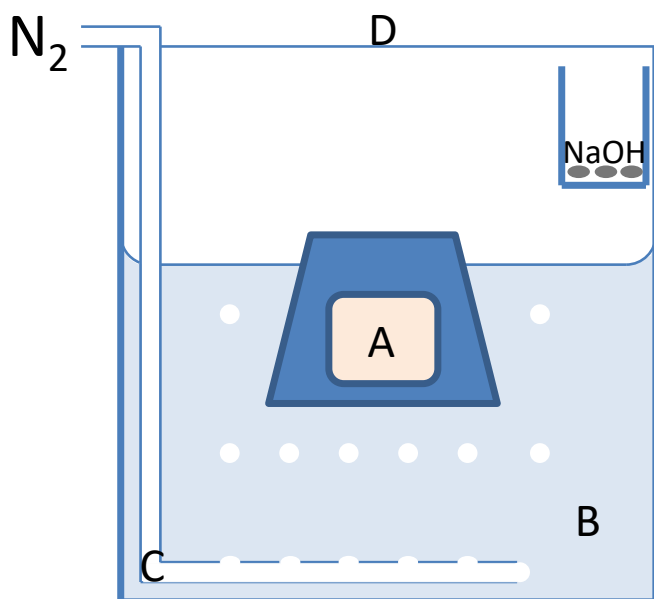


Figure 4: Citrate ion removal and NaCl reduction near the isoelectric point: The protein solution at pH 8.7 (A) was dialyzed against 10  $\mu$ M NaOH (B). A constant nitrogen stream (C) was supplied to keep carbon dioxide out of solution. Sodium hydroxide pellets (NaOH) were provided at the top of the beaker to bind carbon dioxide. The dialysis beaker was sealed with Parafilm® (D) and was stored under nitrogen atmosphere in a box. The figure is not drawn to scale.

#### 3.2.2.2. Citrate ion removal and NaCl reduction at pH 6.0

To remove the citrate ions from the antibody solution, dialyses against 300 mM NaCl was performed. Three dialysis steps were performed, each step provided a volume excess of NaCl solution of 100 and was lasting 24 hours. The dialysis was carried out in Slide-A-Lyzer dialysis cassettes G2 (Thermo Scientific, Rockford, USA), 20.000 Molecular Weight Cut-Off (MWCO), 70 ml nominal volume. Afterwards the same dialysis cassette with the protein was dialysed 6 times against water, for 24 hours each. All dialysis steps were performed at room temperature. The solution was filtered through sterile Sterivex-GV Filter units (Millipore Corporation, Billerica, USA) and stored at 4°C. The final solution had a protein concentration of 25 mg/ml ( $\pm$  3 mg/ml) and a pH of 5.9 ( $\pm$  0.1). In the following work this solution will be termed citrate free antibody solution.

### 3.2.3. Experimental procedures

#### 3.2.3.1. Valence determination

Valence titration is based on a concept as described by Filoti et al. (113) and Tanford et al. (120) and applied by Xia et al (23). A titration curve of the antibody at a final mAb concentration of 13 mg/ml was generated by adding either HCl or NaOH standard solutions (Sigma-Aldrich, Steinheim, Germany) to the citrate-free antibody solution (obtained as described in 3.2.2.2). Each system was mixed and pH as well as protein concentration were measured immediately. At pH 5.8 (corresponding to the initial pH:  $pH_0$ ) the citrate free antibody solution that had been exhaustively dialyzed against MilliQ water contained 18 (+/-1) chloride ions per antibody ( $n_0(Cl^-)/n_0(mAb)$ ) for charge counterbalance as measured by ion chromatography (3.2.1.6). Taking a mAb valence of +18 at pH 5.8 the added amount of NaOH ( $n(NaOH)$ ) or HCl ( $n(HCl)$ ) was assumed to be needed for (de-)protonation of the antibody ( $n(mAb)$ ) and  $pH$  adjustment of the surrounding water. The valence of the protein  $Z_P$  can then be calculated using the following equations:

$$Z_P = \frac{n_0(Cl^-)}{n_0(mAb)} + \frac{n(HCl) - (10^{-pH} - 10^{-pH_0}) \cdot V}{n(mAb)} \quad (28)$$

$$Z_P = \frac{n_0(Cl^-)}{n_0(mAb)} - \frac{n(NaOH) - (10^{pH-14} - 10^{pH_0-14}) \cdot V}{n(mAb)} \quad (29)$$

where  $V$  corresponds to the final volume of the solution.

It is assumed that the valence of the protein is entirely determined by ionizable amino acid side chains as well as amino- and carboxy- terminal groups. The degree of dissociation is assumed to be exclusively influenced by equilibrium with free  $H^+$  and  $OH^-$  in solution and binding of other charged ions is not considered. Hence, the valence determined by pH titration can be different to the actual Debye-Hückel Henry charge  $z_{DHH}$  that takes into account binding of ions such as sodium, chloride, citrate, carbonate or hydrocarbonate (113) (see section 2.4.2).

In addition,  $pK_a$  values of ionizable groups and therefore also titration data depend on the ionic strength. With increasing ionic strength the pH titration curve is getting steeper (120). Hence, the obtained results are only applicable for a given ionic strength.

### 3.2.3.2. pH dependent opalescence and LLPS

Citrate free antibody solutions (obtained as described in 3.2.2.2) were concentrated to a final concentration of approximately 100 mg/ml with Amicon centrifugal filter units (Millipore, Cork, Ireland) of 15 ml nominal volume and 30 kD MWCO. Thereafter, they were titrated to defined pH values using HCl or NaOH standard solutions and aliquots were taken to examine protein concentration, opalescence and the occurrence of phase separation after a storage time of 7 days at 5°C (phase behavior via visual inspection). Another aliquot of the pH adjusted solution was dialyzed against 1 mM citrate solution of the same pH. Dialysis was performed 5 times with a 200-fold volume excess each in pre-treated regenerated cellulose tubing (Spectra Por 7, 25 kDa MWCO, 18 mm flat width, Spectrumlabs, Inc., Rancho Dominguez, USA). Each dialysis step took at least 24 hours at room temperature. After dialysis the sample was (temporarily) homogenized by slightly mixing the protein solution in the dialysis tube and immediately thereafter it was analyzed regarding the protein concentration, pH, opalescence (apparent absorbance at 320 nm, 2 mm path length). The phase behavior after a storage time of 7 days at 0°C, 5°C, 10°C, 15°C and room temperature (22°C) was visually observed and if phase separation occurred, the concentration of the dilute upper phase and the concentrated lower phase were determined by UV spectroscopy.

### 3.2.3.3. Phase behaviour in variable citrate and NaCl concentrations

The influence of the citrate concentration and of the NaCl concentration on the phase behavior was also examined. 200 µl of the lower concentrated phase from the experiment described above (1 mM citrate, varying pH, and 5 °C) were mixed with either 150 µl buffer of different citrate concentrations (0 – 10 mM) adjusted to the corresponding pH, or 150 µl of various (0, 5 mM and 20 mM) NaCl solutions. The solution obtained thereby was homogenized and stored at 5 °C for 7 days to allow a new phase equilibrium to adjust. The protein concentration in the upper dilute phase and the denser lower phase were analyzed.

### 3.2.3.4. Impact of anion charge on phase separation

The following acids purchased from Sigma Aldrich (Steinheim, Germany) were diluted to 1 mM: propane-1,2,3-tricarboxylic acid (tricarballic acid), trans-prop-1-ene-1,2,3-tricarboxylic acid (trans-aconitic acid), 2-hydroxy-1,2,3-propanetricarboxylic acid



monohydrate (citric acid monohydrate), benzene-1,3,5-tricarboxylic acid (trimesic acid), butane-1,2,3,4-tetracarboxylic acid, benzene-1,2,4,5-tetracarboxylic acid (pyromellitic acid), benzene-1,2,3,4,5-pentacarboxylic acid, and benzene-1,2,3,4,5,6-hexacarboxylic acid (mellitic acid). The solution was adjusted to pH 7.0 by using NaOH solution. The added amount of NaOH was utilized to estimate the protonation state and thereby the charge of the corresponding anion at pH 7.0. At pH 7.0 the main part of the acid is assumed to exist in its anionic states and therefore the excipients will be termed by their anionic form in the following work. Citrate free antibody solution with a concentration of 100 mg/mL (obtained as described in section 3.2.2.2, thereafter concentrated to a concentration of 100 mg/mL) was dialyzed against the above mentioned buffers, with 100-fold volume excess of the buffer. Three dialysis steps at room temperature were performed, each of them lasting 24 hours. Dialysis was conducted with pre-treated regenerated cellulose tubing (Spectra Por 7, 25 kD MWCO, 18 mm flat width, Spectrumlabs, Inc., Rancho Dominguez, USA)

#### 3.2.3.5. Mapping the ion atmosphere

Amicon centrifugal filter units (Millipore, Cork, Ireland) of 15 ml nominal volume and 30 kDa MWCO were used to adjust an ion equilibrium around the antibody of the two competing ions citrate and chloride. 4 ml of citrate free antibody solution (obtained as described in section 3.2.2.2) were mixed with 6 ml buffer pH 6.0 with varying citrate concentrations from 0 to 2 mM, and a constant chloride concentration of 4 mM. After centrifugation at 5000 x g from a volume of 10 ml to a volume of approximately 4 ml, the process was repeated another 5 – 7 times to obtain a protein solution equilibrated with the desired buffer. The last centrifugation step was completed when a retentate volume of 1 ml was reached, corresponding to a protein concentration of about 100 mg/ml. The last flow-through was collected representing the bulk solution. The centrifugation was performed at room temperature.

After equilibration, the protein concentration  $c_{protein}$ , ion concentration ( $c_{ion}$ ) and pH of the protein sample and the flow-through ( $f-t$ ) were measured. The number  $N$  of anions associated with the protein was calculated as follows (92):

$$N_{\#ion/protein} = \frac{c_{ion}^{protein} - c_{ion}^{f-t}}{c_{protein}} \quad (30)$$

Associated anions consist of specifically bound ions, unspecifically bound ions and freely diffusing protein-related counterions.

The number of associated ions,  $N$ , was plotted against the titrated free citrate concentration  $[M]$  in the bulk solution and the data were fitted as proposed by Bai et al., (92).

$$N = N_1 + \frac{N_0 - N_1}{1 + \left(\frac{[M]}{[M_{1/2}]}\right)^n} \quad (31)$$

Here,  $N_0$  and  $N_1$  correspond to the number of associated chloride ions at the beginning and at the end of the buffer equilibration, respectively. Two parameters are derived from the fit, namely the competition constant  $[M_{1/2}]$  and the Hill coefficient  $n$ . The competition constant is the midpoint of chloride association, i.e. it is the free citrate concentration at which half of the number of associated chloride ions are displaced by citrate. The Hill coefficient is a measure of the steepness of the competition curve. The underlying fitting function is used to phenomenologically describe the curve. No physical model of ion association is represented by this function (92).

Intermolecular protein-protein self-association of the antibodies is not assumed to critically affect protein-ion association. By calculating the number of associated ions (equ (30)), the exact excluded volume of the protein is not considered. Carbonate and hydrocarbonate could not be detected by ion chromatography and were therefore not considered. The only competing ions considered in this study are chloride and citrate. The valence is assumed constant over the course of experiment, as the pH was measured and shown to be constant.

#### 3.2.3.6. Phase separation determined by adjusting the concentration of oligovalent anions by spiking

750  $\mu$ l of pH-adjusted citrate-free antibody solution were mixed with 750  $\mu$ l of pH adjusted solution of the respective acid. The different parameters, which were examined, are depicted in Table 4. If not otherwise stated, the standard protein concentration was 15 mg/ml before mixing. Phase separations were noted if they were taking place. The resulting system was first mixed and was then stored at room temperature for 30 minutes. Thereafter

the system was centrifuged at 10.000 rpm for 15 minutes. Independently from the occurrence of phase separation, the protein concentration at the top of the tube was determined. After mixing, the pH was measured again. The measured pH was used for charge calculations. Due to the absorbing properties of the aromatic moiety of the tested carboxylates at 280 nm, the protein concentration was not determined by UV spectroscopy but by a different approach, the BCA assay as described in section 3.2.1.2.

Table 4: Table of the investigated parameters and conditions. The mellitate concentration (or oligovalent anion concentration) was a parameter which was additionally tested for all the listed conditions. The NaCl was added as part of the mellitate spiking solution. For the dependence of phase separation on protein concentration, the mellitate concentration was adjusted for each protein concentrations to keep the molar ratio of both binding partners constant. In this case, the protein concentrations adjusted after mixing were between 2.5 mg/ml and 22.5 mg/ml.

	Investigated parameters and conditions				
Oligovalent anion	Pyromellitate		Benzene Pentacarboxylate		Mellitate
pH	pH 2.9	pH 3.8	pH 5.3	pH 7.6	pH 9.3
NaCl concentration	0 mM		10 mM	30 mM	50 mM
n(Mellitate)/n(mAb)	1.9		9.7	97	290

### 3.2.3.7. Dynamic light scattering of protein solutions at different pH values

The pH of the citrate-free protein solution (obtained as described in section 3.2.2.1) was adjusted to values between pH 4 and pH 8.5 with 0.1 M HCl. Afterwards the solutions were diluted to a final concentration of 25 mg/ml ( $\pm 3$  mg/ml). Thereafter, the pH was measured again.

DLS measurements were performed using the Zetasizer NanoZS ZEN3600 (section 3.2.1.9)

### 3.2.3.8. Determination of $k_D$ of different antibody formulations

The interaction parameter  $k_D$  was determined for the formulations listed in Table 5. To examine the pH dependence in buffer-free formulations (as indicated by the notation H<sub>2</sub>O), the citrate-free antibody solution (obtained as described in 3.2.2.2) was titrated to pH 3.2, pH 5.5, pH 6.5 and 7.0 by adding either 0.1 M NaOH or 0.1 M HCl. For the NaCl dependence in buffer-free formulations, the citrate-free antibody solution (obtained as

described in 3.2.2.2) was mixed with NaCl stock solutions to receive protein solutions with a protein concentration of 20 mg/ml and sodium concentrations as indicated. All other formulations were obtained by dialysis of the citrate-free antibody solution (obtained as described in 3.2.2.2) against the respective buffer. Three dialysis steps were performed, each providing a volume excess of 100 and lasting 24 hours at room temperature. The dialysis was carried out in Slide-A-Lyzer dialysis cassettes G2 (Thermo Scientific, Rockford, USA), 10.000 kDa Molecular Weight Cut-Off (MWCO), 30 ml nominal volume. All solutions were filtered through Whatman® FP30 / 0.2 Ca-S filter units (GE Healthcare UK Limited, Buckinghamshire, UK). The solutions were diluted with appropriate buffer, NaCl solution or water to final concentrations of 20 mg/ml, 15 mg/ ml, 10 mg/ml, 7.5 mg/ml, 5 mg/ml and 2.5 mg/ml.

Table 5: Scheme of the investigated protein formulations using Dynamic Light Scattering (DynaPro® Plate Reader II). The notation H<sub>2</sub>O indicates that the formulation is buffer-free and contains a minimal amount of chloride (and sodium at pH 6.5 and pH 7.0), which was added upon pH adjustment.

	Investigated parameters and conditions								
pH (buffer-free)	H <sub>2</sub> O pH 3.2		H <sub>2</sub> O pH 5.5		H <sub>2</sub> O pH 6.0		H <sub>2</sub> O pH 6.5		H <sub>2</sub> O pH 7.0
NaCl concentration (buffer-free, pH 6.0)	+ 0 mM NaCl	+ 1 mM NaCl	+ 2 mM NaCl	+ 5 mM NaCl	+ 10 mM NaCl	+ 50 mM NaCl	+ 100 mM NaCl	+ 150 mM NaCl	
pH in 10 mM histidine	pH 5.0		pH 6.0		pH 6.5		pH 7.0		pH 7.5
pH in 10 mM citrate	pH 5.0		pH 5.5		pH 6.0		pH 6.5		pH 7.5
NaCl concentration in 10 mM citrate	+ 0 mM NaCl		+ 10 mM NaCl		+ 50 mM NaCl		+ 100 mM NaCl		+ 150 mM NaCl
citrate concentration at pH 6.0	2 mM		5 mM		10 mM		25 mM		40 mM
buffer species at pH 6.0	H <sub>2</sub> O pH 6.0		10 mM acetate,		10 mM histidine		10 mM succinate		10 mM citrate

For the determination of the diffusion constant the DynaPro® Plate Reader II was used (section 3.2.1.10).  $k_D$  and  $D_0$  were determined by linear regression of diffusion coefficients plotted against the protein concentration of values up to 10 mg/ml (equ (10)). The linear fit was limited to a maximal protein concentration of 10 mg/ml as in certain cases a deviation from linearity was observed for higher protein concentrations. Hydrodynamic diameters were calculated with equ (3) by setting the viscosity to 0.890 mPas (viscosity of water at 25°C (119)), neglecting slight increases in viscosity induced by the proteins in solution.

### 3.2.4. Determination of anion charges

#### 3.2.4.1. Anion charge determined by titration

The experimental charge of the anions used in this work was determined by titration with NaOH solution. The charge was calculated by dividing the molar amount of NaOH required to reach a specific pH by the molar amount of oligovalent acid dissolved in solution.

#### 3.2.4.2. Anion charge determined using theoretical $pK_a$ values

##### 3.2.4.2.1. Pyromellitic acid, benzene pentacarboxylic acid and mellitic acid

Dissociation of benzene-1,2,4,5-tetracarboxylic acid (pyromellitic acid), benzene-1,2,3,4,5-pentacarboxylic acid (benzene pentacarboxylic acid) and benzene-1,2,3,4,5,6-hexacarboxylic acid (mellitic acid) occurs over a broad pH range between ~ pH 2.0 and the  $pK_a$  of the last dissociation step (121-123). The titration curves show a smooth almost straight line without any distinct steps indicating the different  $pK_a$ -values (121-123). The  $pK_a$  values of these acids were taken from Maxwell (124) and are listed in Table 6.

Table 6:  $pK_a$  values taken from Maxwell (124) determined at a temperature of 25°C and an ionic strength of 30 mM.

	Benzene-1,2,4,5-tetracarboxylic acid	Benzene-1,2,3,4,5-pentacarboxylic acid	Mellitic acid
$pK_{a1}$	1.92	1.80	1.40
$pK_{a2}$	2.87	2.73	2.19
$pK_{a3}$	4.49	3.97	3.31
$pK_{a4}$	5.63	5.25	4.78
$pK_{a5}$		6.46	5.69
$pK_{a6}$			6.96

For the calculation of the anion charge based on published  $pK_a$  values, Henderson Hasselbalchs equation was used:

$$pH = pK_a + \log_{10} \left( \frac{[A^-]}{[HA]} \right) \quad (32)$$

Here  $[A^-]$  is the concentration of conjugate base and  $[HA]$  is the concentration of conjugate acid of an individual protonation step. For each dissociation step, a degree of dissociation  $\alpha$  can be calculated:

$$\alpha = \frac{[A^-]}{[A^-]+[HA]} \quad (33)$$

The negative charge of the anion resulting from an individual protonation step corresponds to the degree of dissociation  $\alpha$ . Therefore, the charge resulting from a specific dissociation step can be calculated as follows:

$$z_C(\text{weak acid}) = -\frac{10^{pH-pK_a}}{1+10^{pH-pK_a}} \quad (34)$$

To calculate the total charge of the anion, not only for a specific dissociation step, the following procedure was performed. The  $pK_a$  value of the carboxylic group most proximate to the pH was used in combination with equ (34). The remaining carboxylic groups of lower or higher  $pK_a$  were assumed to be completely dissociated or protonated, respectively. The negative charges resulting from completely dissociated carboxylic groups were added to the charge calculated by equ (34).

#### 3.2.4.2.2. Citric acid, succinic acid, acetic acid and histidine hydrochloride

The  $pK_a$  values of citric acid, succinic acid, acetic acid and histidine hydrochloride were taken from Lide (119) and are listed in Table 7.

Table 7:  $pK_a$  values taken from Lide (119) determined at a temperature of 25°C

	Citric acid	Succinic acid	Acetic acid	Histidine*HCl
$pK_{a1}$	3.13	4.21	4.756	1.80
$pK_{a2}$	4.76	5.64		6.04
$pK_{a3}$	6.40			9.33

The charge of the corresponding anions  $z_C$  as a function of pH was determined by the Henderson Hasselbalch equation and the degree of dissociation. For the acetate buffer the net charge was calculated with equ (34).

For citrate and succinate buffer, the  $pK_a$  value of the carboxylic group most proximate to the pH (here pH 6.0) was used in combination with equ (34). The remaining carboxylic groups of lower  $pK_a$  were assumed to be completely dissociated. The negative charges resulting were added to the charge calculated by equ (34).

In histidine - histidine hydrochloride buffer, chloride ions with a charge of -1 were acting as counterions to the protein. The average positive charge of the histidine molecule was calculated by:

$$z (\text{weak base}) = \frac{1}{1 + 10^{pH - pK_a}} \quad (35)$$

The dissociation step of the imidazole side chain with a  $pK_a$  of 6.04 (119) was the only protonation equilibrium considered for the calculation. The concentration of chloride ions in histidine buffer was calculated as the product of the histidine charge as determined in equ (35) and the total histidine concentration.

$pK_a$  values were corrected for effects of ionic strength using a relation derived from the Debye Hückel theory which is valid for ionic strengths < 100 mM (117, 125)

$$pK'_a = pK_a - \frac{0.51z_a^2\sqrt{I}}{1 + \sqrt{I}} \quad (36)$$

Here,  $z_a$  is the charge of the acidic form of the buffer of the considered dissociation step,  $I$  is the ionic strength in solution and  $pK'_a$  is the corrected  $pK_a$  value. The ionic strength  $I$  was calculated by (125):

$$I = \frac{1}{2} \sum_{i=1}^n c_i z_i^2 \quad (37)$$

Here,  $i$  is the ionic species number,  $n$  is the total number of different ions and  $c$  is the molar concentration of each ion species(125).  $z$  is the charge of the buffer or chloride ion which was calculated as mentioned above. As the ionic strength is itself influenced by the dissociation of the buffer, three iterative cycles were performed to gain the corrected  $pK'_a$  value. The ionic strength of the protein solutions was not calculated due to the unknown actual charge  $z_{DHH}$  of the protein at specific conditions.



### 3.2.5. Calculation of diffusion coefficients, $D_0$ and $k_D$ by the model of diffusion in ternary systems

Diffusion coefficients were calculated using equ (23) to equ (25). These equations account for electrostatic Coulomb interactions between proteins and their counterions as well as protein-protein interactions and counterion-counterion interactions. The model is not accounting for the extended irregular shape of the protein and the uneven charge distribution on the protein.

The charge of the counterion  $z_C$  as a function of pH was determined as described above in section 3.2.4.2.2.

Influences of the Donnan potential and the electrical neutrality condition as described in 2.4.3 were disregarded for the calculation of the effective counterion concentration. Due to the lower protein concentration and the lower  $z_{DHH}$ , differences between the anion concentration in the dialysis buffer and the anion concentration in the protein compartment were considered to be minimal.

$D_0$  and  $k_D$  were derived from the calculated data of diffusion coefficients for protein concentrations between 2.5 and 10 mg/ml by linear regression to equ (10). This protein concentration range was selected to allow for comparison with experimental values, which were also fitted between 2.5 mg/ml and 10 mg/ml.



## **4. RESULTS AND DISCUSSION**

In a first part, the phase behaviour of a protein solution in the presence of oligovalent anions, whose concentration was adjusted by dialysis, will be described. This first part of the work is focused on the influence of citrate on macroscopic phase separation in a protein solution. In the second part of this work the phase behaviour in the presence of oligovalent anions, whose concentration was adjusted by spiking these ions to the protein solution, will be considered. The focus in this part will be on phase separation in the presence of mellitate. The last part of this work describes the diffusion of the monoclonal antibody in different buffer-free and buffered solutions of varying composition. A comparison between measured diffusion coefficients and calculated diffusion coefficients will be made using a diffusion model, which is taking into account ternary interactions between water, the protein and counterions.

### **4.1. PROTEIN PHASE BEHAVIOUR IN THE PRESENCE OF OLIGOVALENT ANIONS - DIALYSIS EXPERIMENTS**

#### **4.1.1. pH-induced opalescence**

Protein-protein interactions depend on the net charge of the proteins (126, 127). The net charge is pH dependent, as the pH determines the number of amino acid side chains that are ionized. In the current study, a pH titration was performed to determine the valence of the antibody in solution (Figure 5).

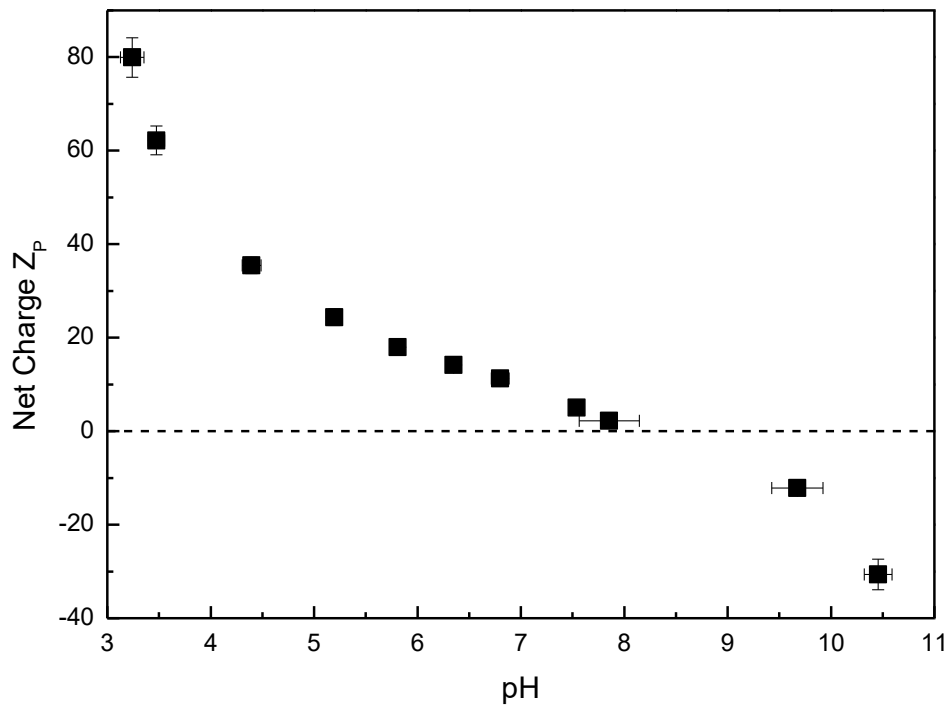


Figure 5: Valence  $Z_P$  of the antibody determined by titration with HCl or NaOH calculated using equ (28) or equ (29) as described in section 3.2.3.1. The theoretical pI of the antibody is 8.3. The protein concentration was kept constant at 13 mg/mL.

The antibody was positively charged up to pH 8. Above pH 9 negative charges dominated over the entire protein. The X-axis intercept of the titration curve agrees with the theoretical isoelectric point at pH 8.3 (Figure 5).

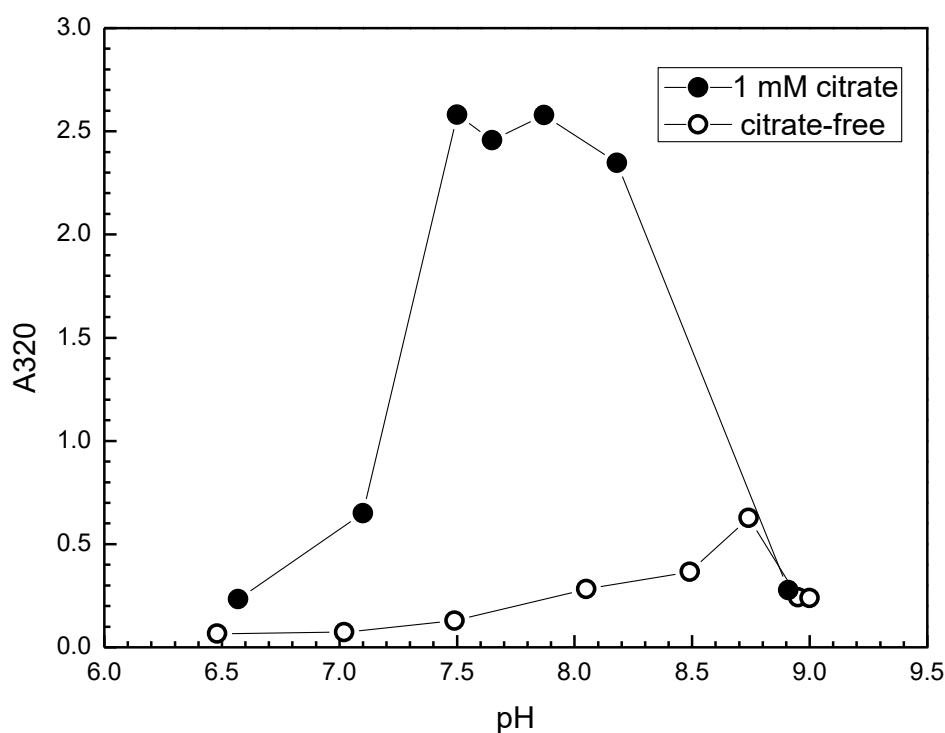


Figure 6: Opalescence (apparent absorbance at 320 nm) of antibody solutions at 22 °C. Citrate-free solutions (open symbols) and those dialysed against 1 mM citrate (filled symbols). The maximum in opalescence of citrate-free solutions was observed around pH 8.7. The presence of citrate induced higher opalescent solutions from pH 7.0 to pH 8.7 probably due to neutralizing the positive charges of the protein and thus increasing protein-protein interactions. The protein concentration of the citrate-free samples was between 90 mg/mL and 102 mg/mL (exception: protein concentration of 28 mg/mL at pH 8.7). The protein concentration of the samples dialysed against 1 mM citrate was between 74 mg/mL and 98 mg/mL.

To study the opalescence and the phase behavior of the “citrate-free” antibody solution, it was titrated to different pH values and opalescence and potential phase separation after a storage time of seven days at 5°C were observed. The experimental procedure is described in detail in section 3.2.3.2. As can be seen from Figure 6, with increasing pH, the opalescence of the protein solution increased. It had a maximum at pH 8.7 and with further addition of NaOH it decreased again (Figure 6). Consequently, the high opalescence at pH 8.7 was reversible. The maximum opalescence observed at pH 8.7 indicates the experimental isoelectric point.

A high opalescence in protein solutions at the respective isoelectric point is a common observation (7, 10, 49, 128-133). Approaching the pI of a protein in solution its net charge decreases and electrostatic protein-protein repulsion forces due to likely charges are reduced (52, 128, 134, 135). Attractive protein-protein interactions such as hydrophobic interaction or electrostatic di- and multipolar interactions may then dominate and an “assembly” of protein molecules can take place. The high opalescence can either indicate the formation of particles (associates, aggregates or precipitates) or the formation of liquid-liquid phase separation. The connection between opalescence and onset of phase separation is commonly used in cloud point experiments (22, 136). The nature of high opalescence observed in this experiment will be discussed later.

A deviation between the isoelectric point determined by pH titration (Figure 5) and opalescence titration (Figure 6) can be explained with the starting point of pH titration. The positive charge of the antibody at the starting point of pH titration was assumed to be completely counterbalanced by chloride ions. However, other ions such as carbonate and hydrocarbonate might have been present in the sample and were not detected. An actual experimental pI of the antibody of 8.7 is in good agreement with data from isoelectric focusing (data shown in Appendix 1). pH titration revealed a net charge of about minus four (-4) at pH 8.7 (Figure 5). Therefore it may be concluded, that the pH titration curve shown in Figure 5 is shifted on the y-axis by minus four charges.

After dialyses against 1 mM citrate, solutions of pH values between pH 7.0 and pH 8.8 showed a significant opalescence (Figure 6), which was not observed for the citrate-free solution. Negatively charged citrate molecules might interact with the positively charged protein and form neutral protein-citrate complexes. Due to a lack of net charge of the complex, the protein-citrate solution might show similar opalescence as the pure protein solution at its isoelectric point.

#### **4.1.2. pH induced LLPS**

After a storage time of 7 days at 5 °C, the potential occurrence of phase separation was visually observed and protein concentrations in upper and lower phase were measured. The results are shown in Figure 7.

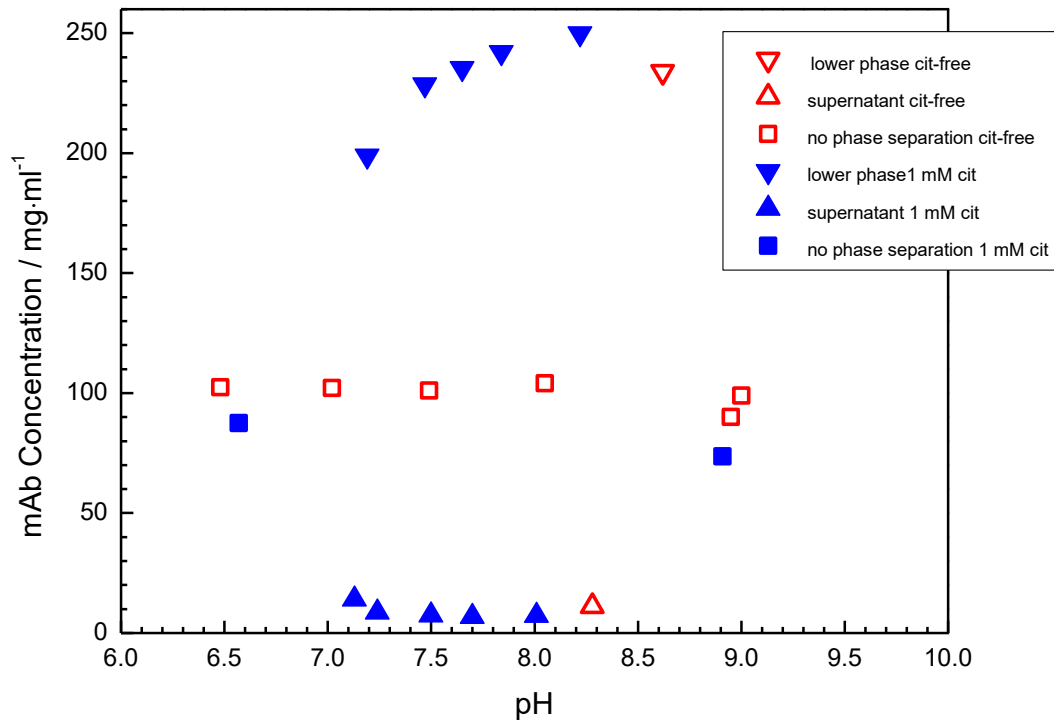


Figure 7: Protein concentration of antibody solutions at 5°C undergoing no phase separation (squares) and those undergoing phase separation into lower phase with high protein concentration (triangles pointing downwards) and upper protein-depleted phase (triangles pointing upwards). “Citrate-free” solutions are represented by red open symbols and solutions which were dialyzed against 1 mM citrate (cit) are represented by blue filled symbols. The phenomenon of phase separation occurred for initially opalescent solutions. The pH of the supernatant of the citrate-free protein solution at pH 8.5 was shifted to a lower pH of 8.3, whereas the pH of the lower phase was shifted to a pH of 8.6.

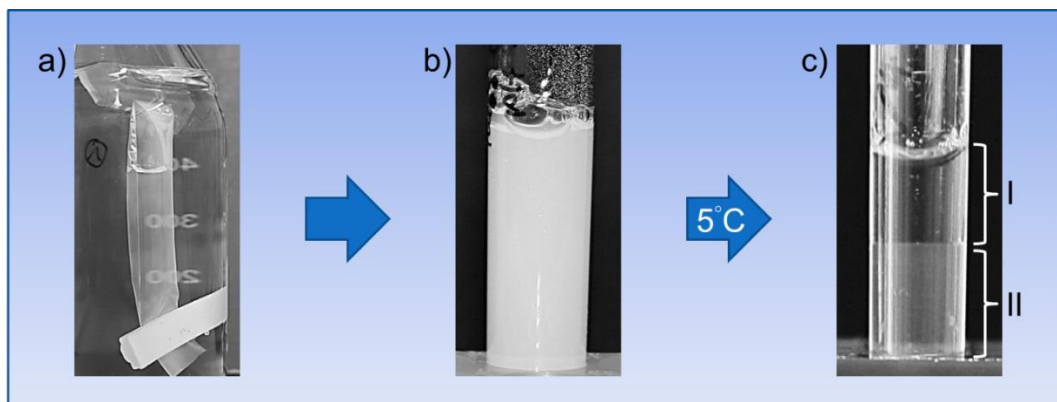


Figure 8: a) Dialysis of antibody solution (100 mg/ml) against 1 mM citrate buffer. b) Opalescence of the antibody solution after dialysis against 1 mM citrate pH 7.2 and c) liquid-liquid phase separation after 7 days at 5°C, with I: protein-depleted upper phase and II: protein-enriched lower phase.

After a storage time of 7 days at 5 °C, the citrate-free antibody solution with an initial concentration of 100 mg/ml showed the phenomenon of liquid-liquid phase separation close to the isoelectric point of the protein at pH 8.5 (Figure 7). A protein-rich phase with 234 mg/ml and a dilute phase with 11 mg/ml were formed. In the presence of citrate, these solutions of high opalescence between pH 7.0 and pH 8.8 underwent a liquid-liquid phase separation at 5°C (Figure 7 and Figure 8). The lower dense phases had protein concentrations between 200 mg/ml and 250 mg/ml and the upper phases consisted of protein solutions with 6 mg/ml - 14 mg/ml. The high opalescence was thus indicating that formation of two liquid phases would occur.

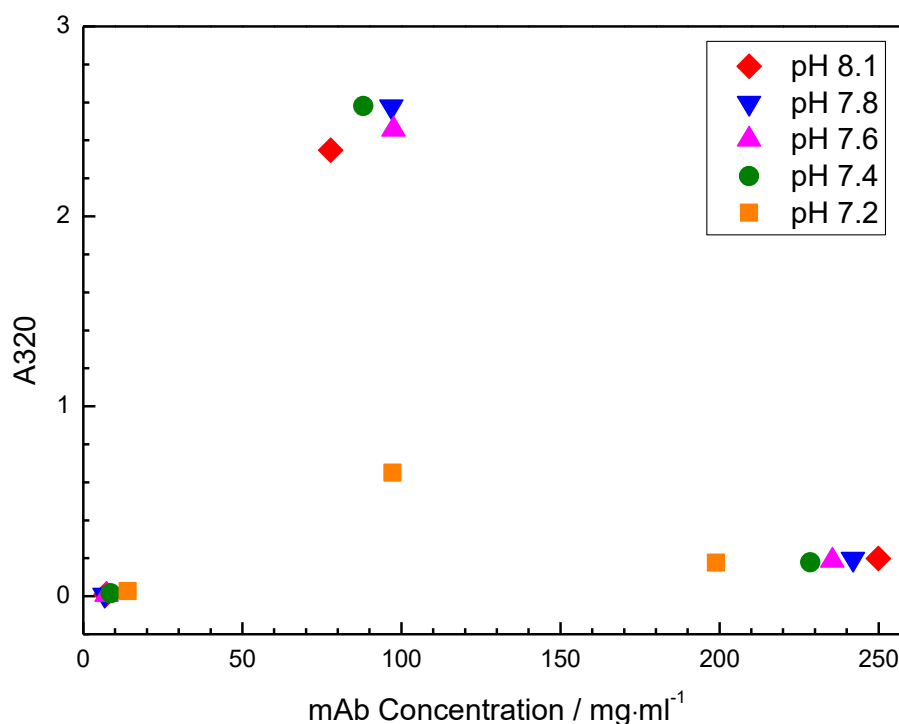


Figure 9: Opalescence (apparent absorbance at 320 nm) of antibody solutions in 1 mM citrate at pH 7.2 (orange squares), pH 7.4 (green circles), pH 7.6 (magenta triangles pointing upwards), pH 7.8 (blue triangles pointing downwards), and pH 8.1 (red rhombs). The protein solution showed higher opalescence close to the critical concentration of about 90 mg/ml compared to the opalescence at higher (> 200 mg/ml) or lower (< 20 mg/ml) protein concentrations.



After demixing the two separated liquid phases with low and high protein concentration showed lower opalescence compared to the original mixed antibody solution of intermediate (approximately 90 mg/ml) protein concentration (Figure 8 and Figure 9). Close to the critical point, the system is unstable with respect to the formation of the two coexisting liquid phases and large scale fluctuations occur (137). These fluctuations of the antibody concentration lead to an increase in light scattering, a phenomenon termed critical opalescence. Thus, opalescence is not necessarily indicating the formation of protein particles or aggregates but can be considered as precursor for liquid-liquid phase separation (7, 9, 66).

Liquid-liquid phase separation observed at the isoelectric point in the absence of citrate is to be expected, as most of the studies reported on LLPS at low ionic strength in the absence of PEG or ammonium sulfate were conducted at conditions close to the pI (6-11, 65). According to Bungenberg de Jong (79) proteins can be classified concerning the phase behavior at the isoelectric point into isostable and isolabile. Solutions of isolabile proteins undergo liquid-liquid phase separation or liquid-solid phase separation at the isoelectric point. Solutions of isostable proteins do not phase separate at the pI (79).

The overall protein-protein interaction is an interplay between attractive and repulsive interactions. A theoretical description of the interaction potential between colloids was first given by Derjaguin-Landau-Verwey-Overbeek DLVO theory (138-140) which takes into account attractive van der Waals' interaction and repulsive electrostatic interactions. Depending on the net charge of the particle, electrostatic repulsion is to some extent predominating attractive interactions. For proteins, the attractive interactions close the isoelectric point are besides van der Waals interactions electrostatic di- and multipolar interactions, as well as non-fundamental forces such as hydration-related interactions. A schematic protein-protein interaction potential in the absence and in the presence of citrate (1mM adjusted by dialysis) can be derived from the data presented in Figure 7 and is depicted in Figure 10.

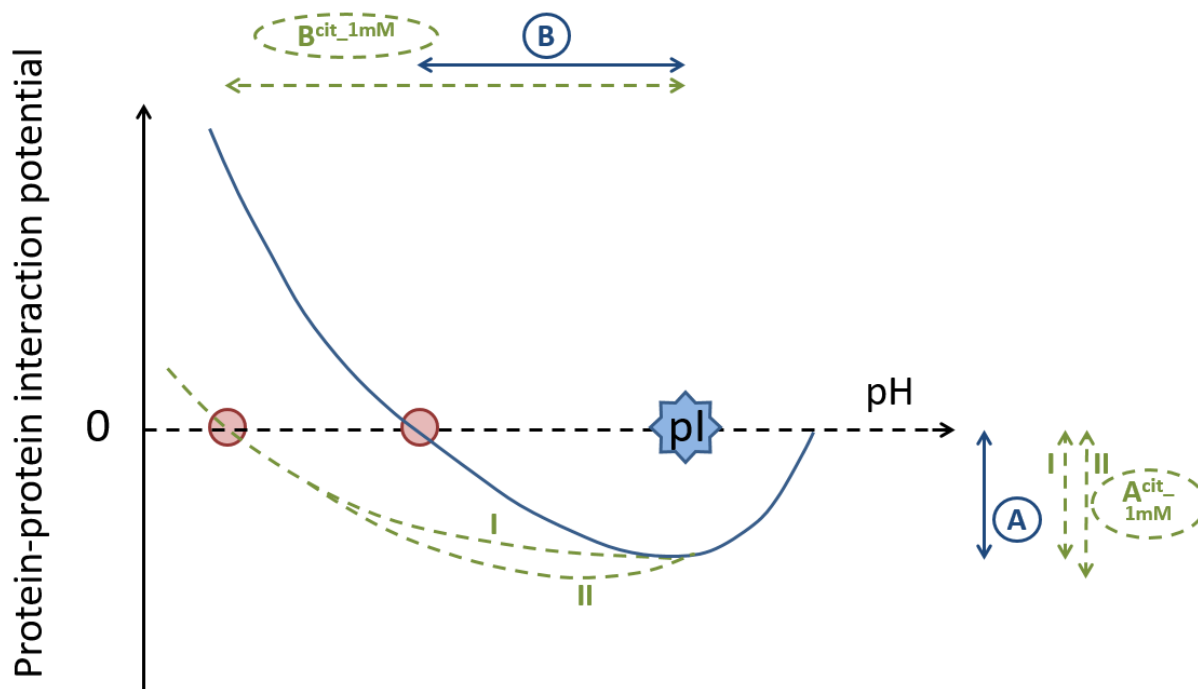


Figure 10: Schematic presentation of the protein-protein interaction potential as a function of pH. The position of the pI of the mAb is depicted by a blue star. The blue solid line represents the protein-protein interaction potential of the mAb in the absence of any excipients (except counterions) as a function of pH. The two green dashed lines represent two possible protein-protein interaction potentials as a function of pH in the presence of citrate (1 mM adjusted by dialysis). The extent of maximal attractive net interactions in the absence of citrate is depicted by a blue arrow of size A. Maximal net attraction in the absence of citrate (or other binding excipients) is by theory expected at the pI. The size of A is assumed to either stay constant (case I) or to increase (case II) in the presence of citrate (1 mM adjusted by dialysis), as depicted by the green dashed arrows  $A^{cit_{1mM}}$ . Experimental data (presented in Figure 7) do not clearly indicate, which case applies, as no data are available exactly at the isoelectric point in the absence of citrate (discussion below in the text). Case I would apply if citrate only neutralizes the net charge of the antibody neglecting an impact of citrate on the protein surface charge distribution or citrate induced protein-protein cross-linking. Case II would apply if either citrate mediated protein-protein cross-linking takes place or citrate introduces a disturbance of the protein hydration or a higher charge anisotropy to the protein. The pH at which repulsive balance attractive PPIs (neutral protein-protein interaction potential) is marked by a red circle. The distance between this specific pH and the pI in the absence of any excipients (except counterions) is depicted by the blue arrow of length B. The presence of citrate (1 mM adjusted by dialysis) leads to a larger distance between the pH of neutral protein-protein interaction potential and pI as depicted by a longer arrow  $B^{cit_{1mM}}$  compared to B. The sizes A and B are assumed to be protein specific values. The figure is a schematic presentation of the protein-protein interaction potential as a function of pH and the presence of citrate.

In addition to the loss in repulsive Coulomb interaction at the pI, reversible conformational changes could potentially induce LLPS. Larger conformational changes would appear in differences in DSC (differential scanning calorimetry) curves. The DSC curves of the antibody are similar over the pH range from pH 6.5 to pH 8.5 with a first transition peak

between 69 °C and 71 °C and a second transition peak between 78 °C and 81 °C (data shown in Appendix 2). It can be concluded, that changes in the protein charge in the observed pH range are not accompanied by significant conformational changes that could be detected by calorimetry.

As LLPS for monoclonal antibodies has often been observed near the isoelectric point (6-11, 65), most antibodies are assumed to be least stable with respect to phase separation at the isoelectric point. However, not all antibodies are assumed to undergo macroscopic LLPS at the isoelectric point. Some antibodies might stay in a homogeneous liquid solution in the observed temperature range (data not shown) whereas other antibody solutions might undergo reversible or irreversible liquid solid phase separation (i.e. association or aggregation) or undergo gelation close to the isoelectric point (Boehringer Ingelheim internal communication, data not shown). The differences in phase behavior are attributed to differences in the charge distribution of the protein (different dipole moments), differences in the overall hydrophobicity of the protein, as well as differences in specific local patchiness.

Phase separation occurring between pH 7.0 and pH 8.8 can be explained with a complex formation between negatively charged citrate and positively charged protein. This observation is consistent to statements made by Bungenberg de Jong and Kruyt in 1929 (79, 141) who observed coacervation by mixing positively charged gelatin with  $K_4Fe(CN)_6$ , a salt made up of an inorganic oligovalent anion and a monovalent cation. Bungenberg de Jong proposed a classification of complex coacervation (79). If only one biocolloid takes part in complex coacervation (instead of two biocolloids) the system was called auto-complex coacervate. Auto-complex coacervate systems were again divided into two groups: The first one including isolabile proteins at their isoelectric point. The second group includes systems of one biocolloid interacting with oppositely charged ions. Phase separation in citrate buffer at pH values distant from pI can therefore be classified into the second group of auto-complex systems (79).

According to the results of this study and to the theory postulated by Bungenberg de Jong (79) it should be sufficient to neutralize the protein, either by citrate binding or by (de-)protonation, to induce LLPS. However, certain studies propose a cross-linking mechanism between antibodies mediated by citrate molecules (52, 142-144) resulting in

mAb self-assembly. The occurrence of LLPS in the absence of citrate at the isoelectric point demonstrates that no cross-linking additive is required to induce LLPS. However, the width of the miscibility gap at 5°C was larger in citrate solutions at pH 8.1 compared to the width of the miscibility gap at 5°C in the absence of citrate at pH 8.5. The latter experiment was not performed exactly at the isoelectric point of the antibody. This possibly results in a smaller miscibility gap which was expected for conditions exactly at the isoelectric point. Therefore, a cross-linking mechanism is claimed to be a possible but not a mandatory mechanism.

Citrate-binding can not only neutralize the protein net charge but might introduce a disturbance of protein hydration or a higher charge anisotropy. Attractive protein-protein interactions are generally believed to result from charge anisotropy resulting in attractive dipole-dipole interactions (46, 58). The dipole moment, a measure of the overall charge anisotropy, can be measured by dielectric relaxation spectroscopy. It has been shown to moderately correlate with colloidal stability parameters (46, 58). Smaller local regions or patches on the protein surface are assumed to specifically be important in protein-protein interactions as well (87, 145, 146). E.g. oppositely charged patches on different proteins could induce attractive protein-protein interactions. The resulting so called patchy interactions could also be modified by citrate-binding. However, no direct measurement technique currently exists that can measure these specific interactions (147). For theoretical considerations, detailed knowledge about the protein surface would be necessary (147). Roosen-Runge et al. (87) propose a model to account for attractive patchy interactions as induced by ion bridging between proteins. However, in the present thesis LLPS also occurred in the absence of oppositely charged ions at the isoelectric point. Therefore, the model proposed by Roosen-Runge et al., (87) does not go far enough to account for all the effects observed here. Patches in the studied system might not only result from ion-bridging but also from the intrinsic positively and negatively charged regions of the protein due to charged amino acid side chains.

The phase diagram (Figure 7) does not provide the width of the miscibility gap in the absence and in the presence of citrate exactly at the isoelectric point. Therefore, it cannot be clarified if the extent of maximal net attractive interactions (size A in Figure 10) is the same in the absence and in the presence of citrate (1mM adjusted by dialysis). If the width

of the miscibility gap in the absence of citrate at the isoelectric point would be equal to the maximal width of the miscibility gap in the presence of citrate at any pH, case I would apply (as depicted in Figure 10). If the width of the miscibility gap in the absence of citrate at the pI would be smaller than the maximal width of the miscibility gap in the presence of citrate at any pH, case II would apply (as depicted in Figure 10). As the data are not available, all the above-mentioned citrate-specific mechanism (citrate-mediated cross-linking, impact on protein hydration and anisotropy and induction of patchy interactions) are possible but not mandatorily taking place.

At pH 6.5 and pH 9 no phase separation was observed (Figure 7). At pH 6.5 the positive charge of the protein has increased and the citrate concentration or the citrate-protein interaction strength might not be sufficient to completely neutralize the protein. Additionally, citric acid has its third  $pK_a$  value of 6.4 (52), which means that the negative charge of the citrate molecule decreases with decreasing pH from -3 to -2 at pH 6.4. Therefore the protein-citrate interaction is likely to be reduced. At pH 9, the protein bears a negative net charge, which cannot be neutralized by citrate binding. Apparently, sodium ions in the solution do not seem to be binding to the protein and thereby fully neutralizing the net charge of the protein.

Fukuda et al. (6) observed LLPS of an antibody in citrate buffer at pH 6 whose pI was 6.6 indicating binding between the positively charged antibody and citrate. However, solutions of another antibody which was formulated more closely to its pI (5.7) in citrate but which was negatively charged at pH 6 did not show LLPS, but only opalescent appearance. Hence, LLPS has been induced by citrate at pH values lower than the pI but not at pH values above the pI of a protein. This observation is consistent with the pH dependence examined here.

It is not clear if citrate is generally inducing LLPS of antibody solutions. However, two studies have been reported in which LLPS was observed in citrate formulated antibody solutions (6, 46). In addition, citrate has been shown to reduce the protein-protein interaction parameter  $k_D$  and therefore induce attractive protein-protein interactions (52). Hence, citrate in suitable concentrations might enhance the probability of an antibody solution to undergo LLPS but not all antibodies will form two liquid phases upon citrate addition. In general, trivalent ions might have the potential to trigger LLPS in protein

solutions, if they are oppositely charged to the respective protein. This thesis is supported by results of Zhang et al. (148), who studied the phase behavior of one positively and 4 negatively charged proteins upon addition of trivalent ions. Phase separation was observed if the ions were oppositely charged to the protein (148).

#### **4.1.3. Dependence of the miscibility gap on citrate concentration**

The influence of the citrate concentration on the width of the miscibility gap at 5°C was studied by replacing the original upper phase with low protein concentration by water or citrate buffers of various buffer concentrations (see section 3.2.3.3). The thereby obtained solution was homogenized and stored at 5 °C for 7 days to allow for adjustment of the new phase equilibrium. It should be noted that the added citrate concentration is different compared to the total citrate concentration in the sample, which is the average of the citrate concentration of the dense highly concentrated phase (approximately 5 mM – 7 mM) and the citrate concentration of the added buffer. However, this experimental setup is suitable to demonstrate the overall trend of the citrate dependence of the LLPS.

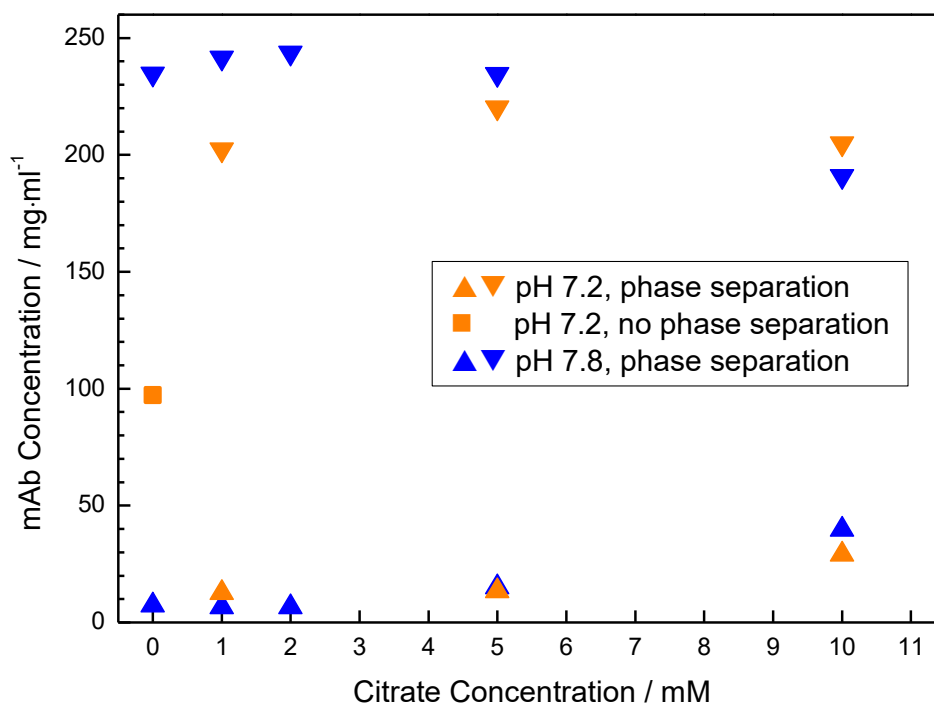


Figure 11: The upper protein-depleted phase of low protein concentration was replaced by water and citrate solutions of various concentrations at pH 7.2 (orange symbols) and pH 7.8 (blue symbols). Protein concentrations are depicted of antibody solutions undergoing no phase separation (square) at 5°C and those leading to phase separation after 7 days at 5°C: concentration in the protein rich lower phase (triangles pointing downwards) and upper protein-depleted phase (triangles pointing upwards).

The influence of citrate concentration on liquid-liquid phase separation was dependent on the pH (Figure 11). By replacing the upper phase of an antibody solution at pH 7.2 in 1 mM citrate by water, no phase separation occurred after 7 days at 5°C. According to the preparation procedure of the sample, a (charge) equivalent amount of citrate to protein is assumed to be present, as the sample arises from the lower, protein-rich phase which is stated to consist of a protein-citrate complex. Apparently, not all the present citrate molecules were necessarily binding to the antibody. The binding strength might have been not high enough. This observation is consistent with a dissociation constant around 1 mM for citrate to antibody binding (142, 149). By increasing the citrate concentration to 5 mM

the formation of an antibody-citrate complex was assumed to be enhanced and more and more antibody molecules were assumed to be neutralized by citrate binding.

Table 8: Calculated molar concentration of positive charges in the antibody solution resulting from the net charge of the antibody at pH 7.2 and pH 7.8. The valence was obtained by pH titration. The titrated value obtained at pH 7.2 and 7.8 was corrected by adding a value of 4 to the experimental value (for explanation please refer to section 4.1.1)

	Antibody concentration / mM	Corrected valence	Molar concentration of positive charges / mM	Calculated citrate concentration to counterbalance charge of the antibody/ mM
pH 7.2	0.79	12	9.6	3.2
pH 7.8	0.95	7	6.9	2.3

LLPS at pH 7.2 showed a maximal miscibility gap at 5°C if 5 mM citrate were added to the lower protein-rich phase. However, at pH 7.8 the optimal citrate concentration was lower with 2 mM citrate. The protein bears a higher positive net charge at pH 7.2 compared to pH 7.8 (Table 8). Therefore a higher citrate concentration (about 3.2 mM – assuming all citrate molecules are binding) is necessary to neutralize the positive charges at pH 7.2. With higher citrate concentrations, i.e. 10 mM, the miscibility gap at 5°C narrowed indicating decreasing attractive forces acting between the proteins (136). This could be due to either charge reversal of the protein-citrate complex or due to an increase in ionic strength. As the effect was more pronounced at pH 7.8 and it turned up with lower citrate concentrations at pH 7.8 compared to pH 7.2, charge reversal is the more probable explanation.

The width of the miscibility gap at 5°C was highest for pH 7.8 with 2 mM citrate added. This extent of separation was not obtained at pH 7.2 by adding any of the citrate concentrations. It may be deduced from these results that the ionic strength, which is increasing concomitantly with citrate concentration, weakens the attractive forces between the antibody-citrate complexes as discussed later.



Summing up, the interplay between three factors influences the extent of liquid-liquid phase separation:

- the ratio between oppositely charged species ideally leading to charge neutralization.
- the degree of binding between the interacting partners.
- ionic strength concomitantly increasing with increasing ion and protein concentration. Increasing the ionic strength leads to a reduction of the electrostatic interactions between citrate and the antibody.

Several studies suggest the optimal proportion between oppositely charged species to be a typical property of complex coacervates, indicating a similarity between the antibody-citrate system and complex coacervation (17, 77, 79, 81-84, 150).

A nonlinear dependence between anion concentration and critical temperature  $T_c$  of LLPS has been reported by Mason et al., in 2010 (8). In mAb solutions at pH values below the pI of 7.2, the critical temperature was reported to decrease with decreasing pH. However, addition of KSCN led to an initial increase of the critical temperature with an optimal KSCN concentration. The optimal KSCN concentration was pH dependent and increased with decreasing pH (8). This behavior is similar to the citrate dependence observed here. However, a difference to the present work is the higher optimal concentration of KSCN of up to 100 mM (8).

When the citrate concentration increased to 10 mM at pH 7.2 or 5 mM at pH 7.8 negatively charged protein-citrate complexes may have formed. However as described in the literature, measurements of zeta-potential have not yet detected a clear charge reversal from positive to negative values for antibodies in citrate buffers (52, 90). Merely, a reduction of the zeta-potential from higher to lower positive values or to zero has been reported (52, 90). The missing results for charge reversal by citrate could indicate that charge reversal does not take place or it could indicate that the charge reversal is not detectable by the measuring principle of zeta-potential measurement. The binding interaction between the antibody and the citrate molecules could have been broken by the applied voltage during the measurement. Likewise, complex coacervate droplets are known to perform disintegration if electric current is applied (151).

The optimum citrate concentration observed at pH 7.2 and pH 7.8 can be interpreted in terms of reentrant condensation. Reentrant condensation, i.e., enhanced phase separation by slightly increasing the ion concentration and redissolution on further increasing the ion concentration, has been observed for negatively charged proteins upon addition of trivalent cations (33, 148). According to Zhang et al., (33, 148) the phenomenon is due to an effective charge inversion which is induced by binding of these cations to the negatively charged proteins. However, the present study deals with organic trivalent anions. These anions bear a much lower charge density than trivalent metal ions. Therefore, the interaction between the protein and the anion might be weaker compared to the interaction between proteins and trivalent cations. Hence, a charge inversion is not necessarily occurring here.

Esue et al., already observed the assembly of monoclonal antibodies by citrate phenomenologically resulting in gelation (149). No answer was found to the question if the citrate-protein interaction was due to neutralizing charges or if citrate interacts with a specific binding site on the protein as observed for calmodulin (152) potentially involving a conformational change of the antibody (142). In the specific case in the present thesis, the assembly of antibody molecules is most probably due to the neutralizing effect of citrate binding. However, conformational changes of the antibody cannot entirely be excluded.

#### **4.1.4. Dependence of the miscibility gap on ionic strength**

The effect of increasing ionic strength was examined at pH 7.8 by replacing the original dilute upper phase by NaCl solutions of increasing concentrations between 0 to 20 mM (see section 3.2.3.3).

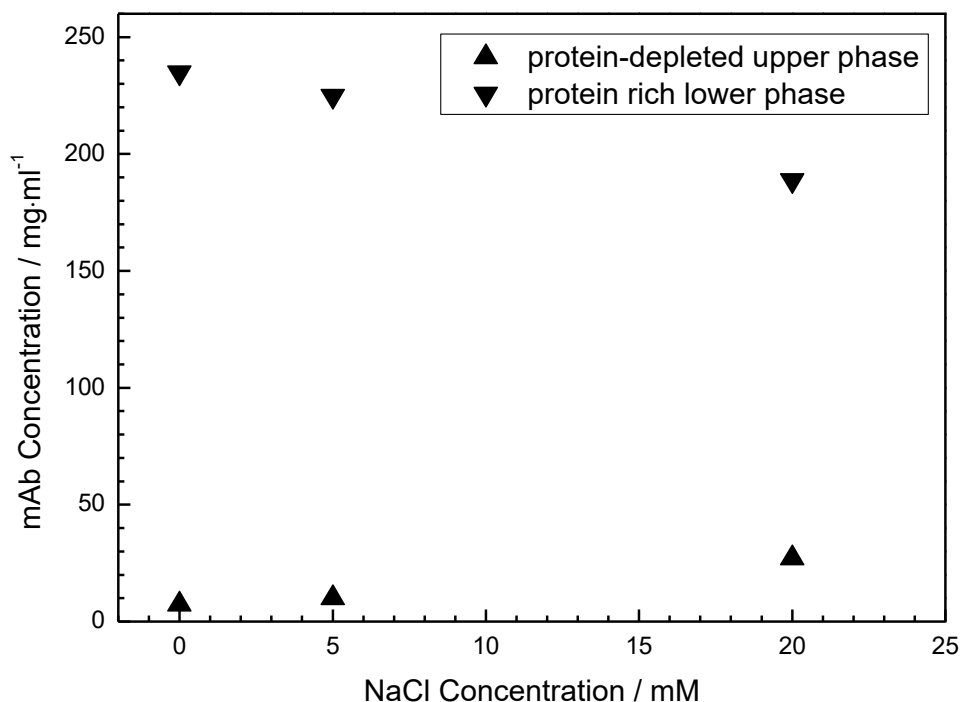


Figure 12: The original protein-depleted upper phase of the antibody solution at pH 7.8 was replaced by NaCl solution of various concentrations. The protein concentration of the coexisting phases was measured after 7 days storage at 5°C. Concentrations in the lower protein rich phase are represented by triangles pointing downwards and concentrations in the dilute upper phase are represented by triangles pointing upwards. The miscibility gap was narrowing with increasing ionic strength.

A decreasing width of the miscibility gap at 5°C was observed with increasing ionic strength (Figure 12). This result indicates that overall attractive antibody-antibody interactions were reduced (136). The electrostatic attraction between citrate and the antibody might be reduced due to charge screening effects resulting in a higher actual charge (Debye-Hückel Henry valence  $z_{DHH}$ ) of the antibody (113) and higher intermolecular electric double layer repulsion between the antibodies. In addition, attractive antibody-antibody interactions, dominant close to pI, e.g. charge-dipole or electrostatic di- and multipolar interactions, might also be screened and thus reduced (10). By considering the overall trend of the miscibility gap as a function of ionic strength, LLPS is assumed to vanish at higher salt concentration in the range of 100 mM NaCl. The dissociative effect of ionic strength on LLPS of antibodies has been reported before (8, 9, 19). Furthermore, complex coacervates typically dissolve by increasing ionic strength (77, 79, 84, 85). A

closely related phenomenon is “salting-in”, i.e. an increase in solubility of a protein upon addition of salt concentrations  $< 500$  mM (126). However, the effects of salts in the millimolar range on protein-protein interactions seem to be depending on the pH related to the pI (126, 153), on the intrinsic properties of the protein (126, 154) and on specific additional cosolutes such as buffers or oligovalent ions present in solution (65, 155). Sule et al.,(153) claim self-association to be reduced by increasing ionic strength close to the pI but to be enhanced by increasing ionic strength away from pI as schematically depicted in Figure 13. This theory is strengthened by the results of the present thesis as reduced self-association was observed by increasing ionic strength close to the pI.

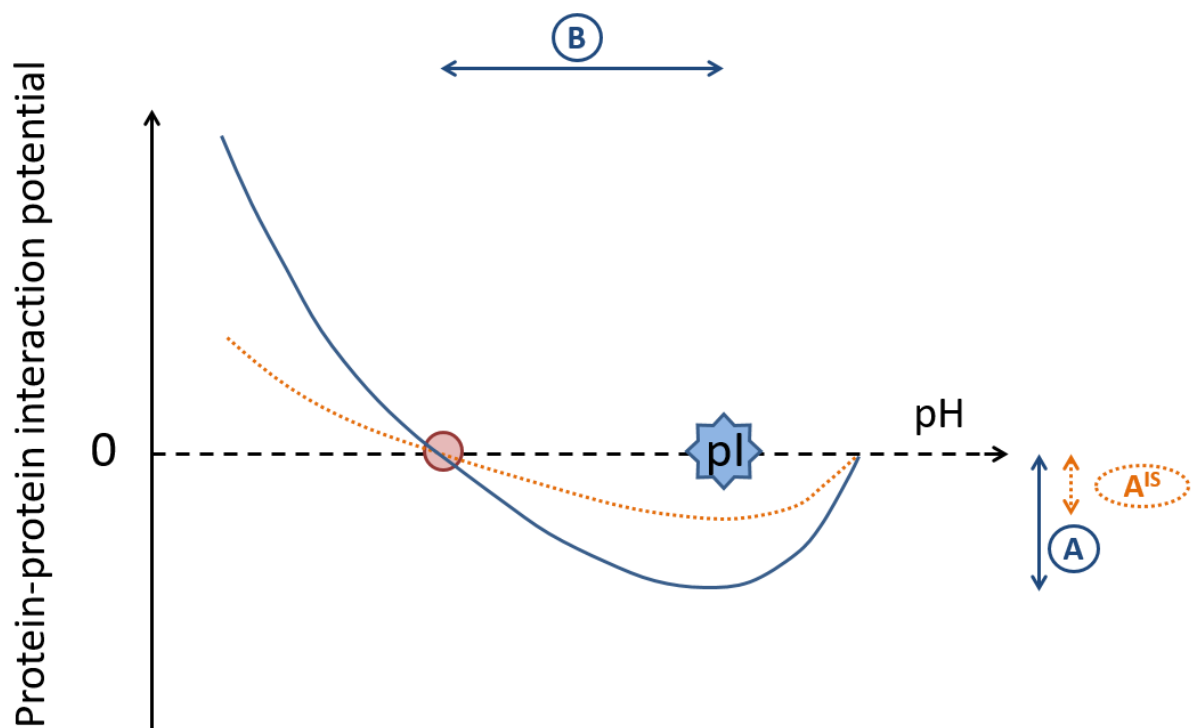


Figure 13: Schematic presentation of the influence of ionic strength on the protein-protein interaction potential as a function of pH. The position of the pI of the mAb is depicted by a blue star. The blue solid line represents the protein-protein interaction potential of the mAb in the absence of any excipients (except counterions) as a function of pH. The orange dotted line represents the protein-protein interaction potential at elevated (but moderate) ionic strength (Theory taken from Sule et al., (153)). The extent of maximal attractive net interactions in the absence of citrate is depicted by a blue arrow of size A. Maximal net attraction is by theory expected at the pI. A is assumed to decrease with increasing ionic strength as shown by the shorter orange arrow  $A^{IS}$  (153). The pH at which repulsive balance attractive PPIs (neutral protein-protein interaction potential) is marked by a red circle. The distance between this specific pH and the pI is depicted by a blue arrow of size B. The size of B at higher ionic strength ( $B^{IS}$ ) is not necessarily equal to the size of B, but it was not more precisely plotted here (insufficient data situation). The sizes A and B are assumed to be protein specific values. The figure is a schematic presentation of the protein-protein interaction potential as a function of pH and ionic strength.

According to Dumetz (154) the intrinsic property of a protein typically related to salting-in behavior is a high dipole moment. As the antibody studied in the present work undergoes LLPS at the isoelectric point it likely exhibits a certain charge inhomogeneity and therefore possibly a high dipole moment. Raut and Kalonia (65) observed different effects for a dual variable domain immunoglobulin protein ( $pI = 7.5$ ) upon increasing the ionic strength. Depending on the buffer (histidine or phosphate buffer) the cloud temperature representing the onset of LLPS, was shifted to different directions (65). At pH 6.1 in histidine buffer, the cloud temperature was increased from 10.3 °C to 16.8 °C by adding NaCl to a final ionic strength of 50 mM. However, at pH 6.5 in phosphate buffer, the cloud point was decreasing from  $\geq 37$  °C to 24.5 °C with increasing ionic strength to 50 mM (65). Thus, attractive protein-protein interactions were enhanced upon NaCl addition in histidine buffer, but reduced in phosphate buffer. In this work (65), specific binding between histidine and the protein e.g. via cation- $\pi$  interaction is proposed. This would result in a higher positive net charge of the protein resulting in lowered attractive protein-protein interactions and thus lowered cloud temperature (65). Increasing ionic strength in histidine buffered solutions could reduce protein-histidine interactions and therefore lead to an increase of cloud temperature and stronger protein-protein interaction.

Jordan et al. (155), studied the phase behavior of negatively charged human serum albumin (HSA), in the presence of yttrium chloride ( $YCl_3$ ) and NaCl. In this particular case, the impact of NaCl on the protein concentration in the supernatant was depending on the concentration of  $YCl_3$ . For lower  $YCl_3$  concentrations, increasing the NaCl concentration was resulting in higher protein concentration in the supernatant and thus reduced propensity to LLPS. For higher  $YCl_3$  concentrations, opposite effects were observed. This can be explained with a shift in the optimum  $YCl_3$  concentration upon addition of NaCl to higher  $YCl_3$  concentration. NaCl might weaken the interaction of  $Y^{3+}$  with HSA so that higher concentrations of  $Y^{3+}$  are required to enter the turbid regime but also to exit this regime again. However, this study was performed with HSA, an isostable protein. In addition, the trivalent cation  $Y^{3+}$  has a higher charge density compared to citrate<sup>3-</sup> and is probably stronger interacting with the protein. It is not clear however, if this phenomenon is only observed for trivalent cations of high charge density or if the results are transferable to citrate induced LLPS, too.

#### 4.1.5. Dependence of the miscibility gap on the temperature

The antibody solution in 1 mM citrate pH 7.2, pH 7.4 and pH 8.1 was stored for 7 days at 0°C, 5°C, 10°C, 15°C, and at room temperature (22°C) (see section 3.2.3.2). For samples stored at 22°C, no phase separation was observed at pH 7.2 (Figure 14 a). At this pH, phase separation occurred for samples stored at 15°C and below and the width of the miscibility gap increased with decreasing temperature (Figure 14 a). To compare the coexistence curve with published data of  $\gamma_{II}$ -crystallin, lysozyme and two different monoclonal antibody, the data points near the critical point were fitted using the following equation proposed by Thomson (22) and Wang (13) derived from mean-field theory

$$[(c - c_c)/c_c]^2 = w(T_c - T)/T_c \quad (38)$$

where  $c$  is the concentration of the protein at a given temperature  $T$  in the upper dilute phase and in the lower concentrated phase, respectively,  $w$  is a parameter determining the width of the miscibility gap, and  $c_c$  and  $T_c$  correspond to the critical concentration and the critical temperature, respectively. If data for  $c_c$  and  $T_c$  were given in the literature, only the width  $w$  was fitted. The fitting results for the coexistence curves of data published by Thomson (22), Taratuta (156), Mason(8), Wang (13) and own data of the mAb at pH 7.2 are shown in Table 9. To visually compare different coexistence curves, data of concentration and temperature were scaled relative to their critical parameters (Figure 14 b).

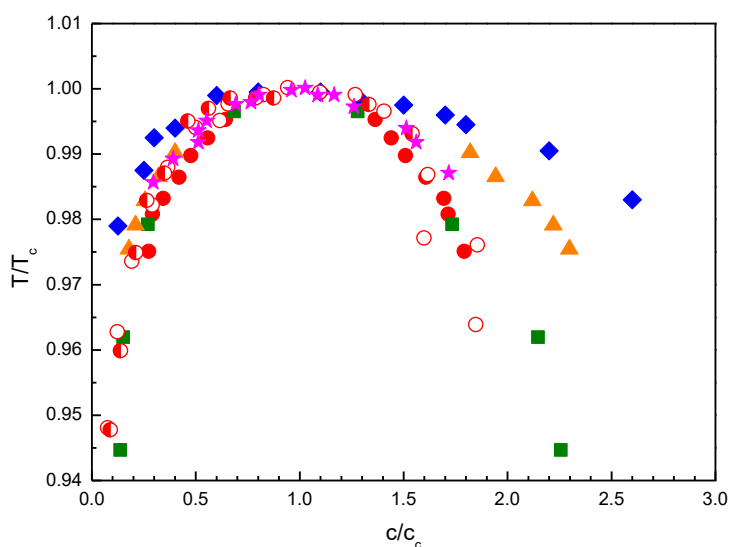
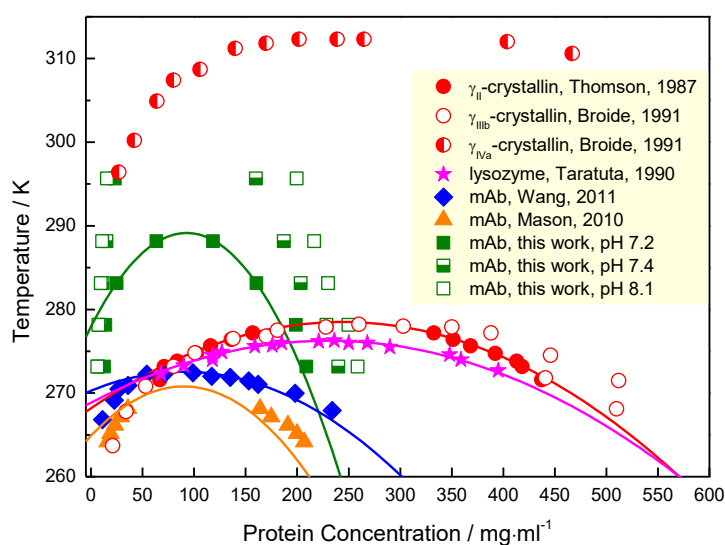


Figure 14 a): Concentration of coexisting protein solutions as a function of temperature. Monoclonal antibody examined in this work (green squares), in 1 mM citrate at pH 7.2 (filled), at pH 7.4 (half-filled) and pH 8.1 (open), monoclonal antibody examined by Wang et al.,(13)(blue rhombs), monoclonal antibody examined by Mason et al.,(8) (orange triangle),  $\gamma$ II-crystallin examined by Thomson et al.,(22) (red filled circles),  $\gamma$ IIIb-crystallin (open red circles) and  $\gamma$ IVa-crystallin (half-filled red circles) both examined by Broide et al.,(20) and lysozyme (magenta stars) examined by Taratuta et al.,(156). The width  $w$  was fitted according to equ (38). The lines refer to the fitted function with parameters as depicted in Table 9. Fitting was not performed with equ (38) for  $\gamma$ IIIb-crystallin and  $\gamma$ IVa-crystallin as another exponent would be necessary according to Broide et al.(20).

b): Normalized depiction of coexisting protein solutions. Fitting and normalization was not performed for the mAb examined in this work at pH 7.4 and pH 8.1 due to insufficient data close to the critical point.

Table 9: Comparison of the coexistence curve of different proteins concerning their position and shape.

	Critical concentration $c_c$ / mg/ml	Critical temperature $T_c$ / K	Width $w$ (as described by equ (38))	Asymmetry
$\gamma_{II}$ -crystallin (22)	244	279	27	(?)
Lysozyme (156)	230	276	37	(?)
mAb (13), Wang	90	273	120	++
mAb (8), Mason	90	271	46	++
mAb this work	93	289	26	+

The coexistence curve of the antibody in 1 mM citrate pH 7.2 shows the following properties: i) an upper critical solution temperature (Figure 14); ii) a critical concentration of 93 mg/ml, a critical temperature of 289 K (16 °C), a width  $w$  (defined by equ 38) of 26 (Table 9) and iii) an asymmetry with respect to  $c = c_c$  (Figure 14). The coexistence curve is steeper on the low concentration side than on the high concentration side.



Table 10: Four cases of thermodynamic parameters potentially resulting in clustering (clust) of the protein. The only case (case 4) for which phase separation is observed and the reaction is endothermic ( $\Delta H^{\text{clust}}$  pos.  $\rightarrow$  fourth case) shows LCST phase behavior. Hence, if UCST phase behavior is observed, the third case applies and  $\Delta H^{\text{clust}}$  is negative, hence the reaction is exothermic. (Boundary condition:  $\Delta H^{\text{clust}}$  and  $\Delta S^{\text{clust}}$  are independent from the temperature)

Case		Phase separation	UCST / LCST	Explanation
1	$\Delta H^{\text{clust}} > 0, \Delta S^{\text{clust}} < 0$	no		$\Delta G^{\text{clust}}$ pos.
2	$\Delta H^{\text{clust}} < 0, \Delta S^{\text{clust}} > 0$	yes	insoluble in all proportions	$\Delta G^{\text{clust}}$ neg.
3	$\Delta H^{\text{clust}} < 0, \Delta S^{\text{clust}} < 0$	possible <sup>1</sup>	UCST (if phase separation is temperature dependent <sup>1</sup> )	With <b>decreasing</b> temperature clustering is <ul style="list-style-type: none"> <li>• enthalpically favored (as <math>\Delta H^{\text{clust}} &lt; 0</math>)</li> <li>• entropically favored (as <math>-T\Delta S^{\text{clust}} &gt; 0</math>)</li> </ul>
4	$\Delta H^{\text{clust}} > 0, \Delta S^{\text{clust}} > 0$	possible	LCST (if phase separation is temperature dependent)	With <b>increasing</b> temperature clustering is <ul style="list-style-type: none"> <li>• enthalpically favored (as <math>\Delta H^{\text{clust}} &gt; 0</math>)</li> <li>• entropically favored (as <math>-T\Delta S^{\text{clust}} &lt; 0</math>)</li> </ul>

<sup>1</sup> the occurrence of phase separation as a function  $|\Delta H^{\text{clust}}|, |-T\Delta S^{\text{clust}}|$  and the temperature is described in Table 11.

An upper critical solution temperature transition signifies that clustering or agglomeration of the proteins to form the lower concentrated phase is exothermic (Table 10) (157, 158). All reported studies of antibody solutions undergoing LLPS and most of the proteins studied show UCST phase behavior (7-10, 12, 13). Exceptions are hemoglobin, resilin, tropoelastin and certain polypeptides which show lower critical solution temperature transition (LCST) (52, 159-161).

Table 11: Three cases of  $|\Delta H^{\text{clust}}|$  in relation to  $|-T\Delta S^{\text{clust}}|$  and their impact on the occurrence of phase separation as well as their impact on a potential temperature dependence of phase separation. The present table only applies to case 3 as described in Table 10 ( $\Delta H^{\text{clust}} < 0$ ,  $\Delta S^{\text{clust}} < 0$ ). (Boundary condition:  $\Delta H^{\text{clust}}$  and  $\Delta S^{\text{clust}}$  are independent from the temperature)

Case		Phase separation	Explanation
1	$ \Delta H^{\text{clust}}  \gg  -T\Delta S^{\text{clust}} $	Yes  (Protein insoluble over the whole temperature range)	$\Delta G^{\text{clust}}$ neg.
2	$ \Delta H^{\text{clust}}  \ll  -T\Delta S^{\text{clust}} $	No  (Protein soluble over the whole temperature range)	$\Delta G^{\text{clust}}$ pos.
3	$ \Delta H^{\text{clust}}  \approx  -T\Delta S^{\text{clust}} $	Possible, depending on the temperature  (Phase separation only at lower temperature)	At higher temperature: $\Delta G^{\text{clust}}$ pos.  At lower temperature: $\Delta G^{\text{clust}}$ neg.

Phase separation was not observed at higher but at lower temperature. This indicates that case 3 of Table 10 applies. However, the occurrence of phase separation is possible but not mandatory if  $\Delta H^{\text{clust}} < 0$  and  $\Delta S^{\text{clust}} < 0$  (Case 3 in Table 10). As clustering in case 3 (Table 10) is accompanied with a loss in entropy, clustering does not take place if the entropy term ( $-T\Delta S^{\text{clust}}$ ) strongly dominates over the enthalpy term ( $\Delta H^{\text{clust}}$ ) (case 2 in Table 11). If, however, the enthalpy term ( $\Delta H^{\text{clust}}$ ) strongly dominates the entropy term ( $-T\Delta S^{\text{clust}}$ ), phase separation would take place independent from the temperature (case 1 in Table 11). Conclusively, the temperature dependent occurrence of phase separation indicates that case 3 applies to the observed clustering reaction (Table 11). At higher temperature, the entropy term ( $-T\Delta S^{\text{clust}}$ ) dominates over the enthalpy term ( $\Delta H^{\text{clust}}$ ) and clustering does not take place. At lower temperature, the entropy term ( $-T\Delta S^{\text{clust}}$ ) decreases and the enthalpy dominates, resulting in clustering. Thus, for the observed clustering reaction  $|\Delta H^{\text{clust}}|$  and  $|-T\Delta S^{\text{clust}}|$  are of similar size.

The critical concentration of 93 mg/ml found for the antibody in this study is similar to values reported for other monoclonal antibodies (molecular weight of approximately 150 kDa) which range from 87.4 mg/ml (7) to 90.1 mg/ml (8). Smaller proteins like  $\gamma$ -crystallins

showed higher critical concentrations, e.g. bovine  $\gamma_{II}$ -crystallin (molecular weight of approximately 21 kDa) showed a critical concentration of 244 mg/ml (22) and lysozyme (molecular weight of 14.4 kDa) showed a critical concentration of 230 mg/ml (156). Converting these data into volume fractions, by using a partial specific volume of 0.728 mL/g (9), the critical volume fraction is about 6.8 %, 17.8 % and 16.7 % for antibody in the present work,  $\gamma_{II}$ -crystallin and lysozyme, respectively.

According to Bianchi et al. (162), the critical volume fraction is a function of "sticky" sites on the protein surface. Grand-canonical Monte Carlo (GCMC) simulations revealed the critical packing fraction to shift to lower values on decreasing the number of "sticky" spots. If the range of interaction decreases for spherically symmetric attraction, larger critical packing fractions do result (162). Hence, a small critical volume fraction can either be due to an increase in the range of isotropic attraction or due to a decrease in the number of "sticky" sites(162). Which model applies depends on the strength of the interactions (163). For weak patchy interactions the fluid behaves rather like an isotropically short-ranged attractive fluid, whereas stronger patchy interactions result in patchy hard sphere fluids (163).

Based on the data in the present work, the model of patchy interactions is proposed to better fit to this protein system than a model assuming only isotropic attractions. The critical volume fraction of 6.8 % observed for the antibody in the present work is lower than the van der Waals limit of the critical volume fraction of 8.3 % (164). Therefore, attractions present between antibody molecules cannot be solely isotropical. Anisotropic interactions, such as ion-dipole interactions, which belong to the category of patchy interactions, need to be taken into account. According to Bianchi et al. (162), the critical volume fraction of 6.8 % results from particles with approximately 3 patches. Due to the Y-like shape of the antibody, the three patches could arise from the two Fab regions and one Fc region. Studies published by the group of Benedek also claim that the low critical volume fraction observed for antibodies result from their extended Y-like shape (13, 165).

The critical temperature was pH-dependent (Figure 14 a). At pH 7.2, the critical temperature of 16°C was lower compared to pH 7.4 or pH 8.1 with critical temperatures  $\geq$  22°C. The coexisting points at pH 7.4 and 8.1 were not fitted due to missing data nearby

the critical concentration. An increasing critical temperature indicates enhanced attractive protein-protein interactions (136). A correlation between the critical temperature and the width of the miscibility gap at 5°C exists, which signifies that the width of the miscibility gap is an indicator of attractive protein-protein interactions as well. The critical temperature of proteins is known to be strongly dependent on the solution conditions such as pH, ionic strength and presence of various ionic species and their concentration (9, 65, 156).

The width  $w$  of the coexistence curve of the examined antibody as obtained by fitting with equ (38) is 26 (Table 9). This value is much lower than the width  $w$  of 120 observed for a monoclonal antibody by Wang et al. (13) and slightly lower than the width  $w$  of 46 observed for a monoclonal antibody by Mason et al. (8) (Figure 14 b). It is similar to the width  $w$  of 17 of bovine  $\gamma_{II}$ -crystallin (22) but it is larger than the theoretical width  $w$  of 6.15 calculated for spherical particles using mean field theory of attraction and Carnahan-Starling expression for entropy (13).

Data of bovine  $\gamma_{II}$ -crystallin were generated similar to the approach used in the present work by macroscopic phase separation also termed temperature-quench method (22). However, data presented by Wang et al., (13) were obtained by cloud point measurements. Thereby, the opalescence of a protein solution at a given protein concentration is measured while first lowering and later raising the temperature. Differences in the width of 120 reported for a monoclonal antibody by Wang et al., (13) and data of the present work could be due to the differences in the measuring principle and possibly due to the lower absolute value in  $T_c$ . For the temperature-quench method, phase separation was observed after conditioning the samples by various methods, e.g., centrifugation at different speeds and different durations. Therefore the width  $w$  obtained for the different samples is not comparable. The larger width observed for bovine  $\gamma_{II}$ -crystallin and the monoclonal antibody in the present study, compared to the theoretical value of 6.15, reveals the theory to be insufficient (165). Additional interparticle interactions such as electrostatic or hydrophobic interaction not considered by mean field theory can influence the interaction potential. Anisotropy in the interaction potential can have an impact on the width of the coexistence curve as well (165).

The asymmetry of the coexistence curve observed for the antibody solutions in the present study is less pronounced compared to the asymmetry of the curve reported by Wang et al. (13) and Mason et al.(8) (Figure 14 b). The coexistence curve of bovine  $\gamma_{II}$ -crystallin is not asymmetric at first glance. However, this curve ranges over a smaller temperature interval at which asymmetry is not observed in the present study either. Asymmetry can be explained with the nonspherical shape of the antibody and with its high flexibility (13, 166). However, even spherically symmetric particles may have an asymmetric phase diagram (167). The real cause of asymmetry is unknown.

#### **4.1.6. Dependence of phase separation on anion charge**

Different oligovalent anions (Figure 2) were tested with regards to their effects on the induction of phase separation and in order to evaluate, whether induced phase separation is a citrate specific phenomenon or if other charged species are able to induce phase separation as well. Therefore, a dialysis of the citrate free antibody solution with a concentration of approximately 100 mg/ml into buffers of the anions with a concentration of 1 mM and pH 7.0 was performed (see section 3.2.3.4).

Table 12: Phase behaviour of a 100 mg/ml antibody solution dialyzed against 1 mM buffer, pH 7.0 of the oligovalent anions at room temperature. The anion charge was calculated from titration data as described in section 3.2.4.1.

	Anion Charge at pH 7.0	Appearance
tricarallylitate	-2.8	opalescent solution
<i>trans</i> -aconitate	-2.9	opalescent solution
citrate	-2.9	opalescent solution
trimesitate	-3.0	opalescent solution
butane-1,2,3,4-tetracarboxylate	-3.5	two liquid phases
benzene-1,2,4,5-tetracarboxylate	-3.9	two liquid phases
benzene-1,2,3,4,5-pentacarboxylate	-4.0	two liquid phases
mellitate	-5.2	flocculent white precipitate

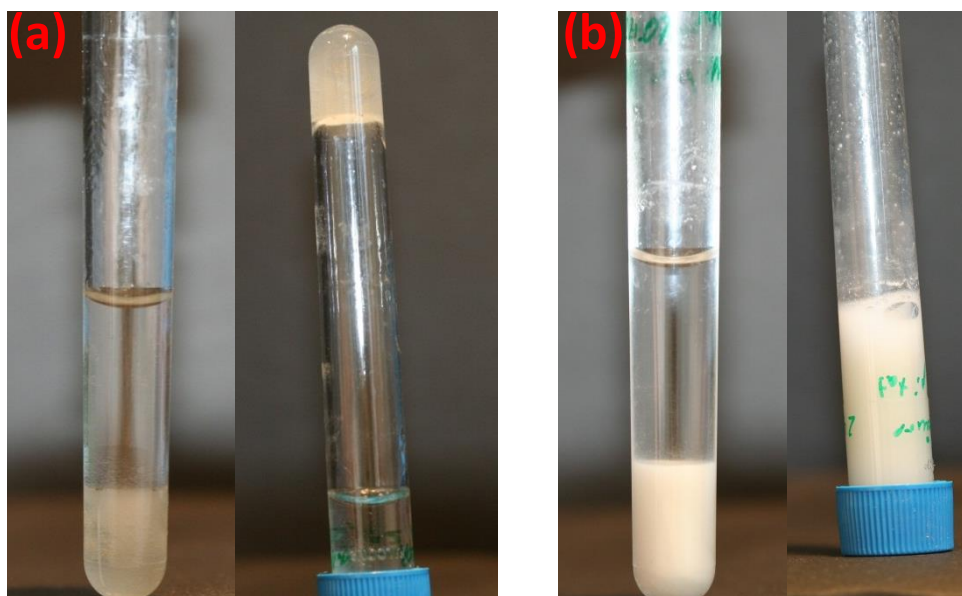


Figure 15: Macroscopic appearance of LLPS (a) and LSPS (b). In the case of LLPS a highly viscous lower phase is formed whereas for LSPS the lower phase is a fluffy suspension.

Those anions, carrying a net negative charge of -3 or less (e.g. -2, -1) did not induce phase separation at pH 7.0. Only opalescent solutions at room temperature were observed (Table 12). If the charge of the anion was between -3.5 and -4.0 LLPS was observed (Table 12 and Figure 15 a). The anion of mellitic acid (mellitate) with a net charge of -5.2 induced liquid-solid phase separation (precipitation) (Table 12 and Figure 15 b). The precipitate could be dissolved again in 400 mM sodium chloride solution.

The effective charge of the anion has a strong impact on the phase behaviour of the antibody solution. For charged anions up to a charge of -3, soluble complexes may form, as indicated by the opalescent appearance of the solutions. If the charge of the anion increases, interaction between the positively charged antibody and the anion gets stronger and charge neutralization leads to LLPS. Mellitate even induced a protein precipitate, indicating a cross-linking between the antibody molecules as observed before when oppositely charged polyelectrolytes were mixed (168).

The spatial arrangement of the carboxyl groups seemed to play a minor role compared to the number of actual charges. However, as the number of charges of the molecules increases, the charge density is concomitantly increasing. Results of Zhang et al.(148) imply the charge density to play a more significant role than the actual net charge of oppositely charged ions.

Even though the interaction partners here are oligovalent anions and proteins, similar properties to polyelectrolyte-protein complexes as summarized by Cooper et al. (86) can be seen. Depending on the stoichiometry and on the interaction strength, three phenomenological degrees of solvation were deduced: highly hydrated soluble complexes, less hydrated complexes leading to coexisting liquid phases, and poorly hydrated precipitates (86). The main differences between the complexes described by Cooper and those observed by us, is the total charge of the anion compared to the charge of the protein and the general size of the oligovalent anions compared to polyelectrolytes. Chain-like polyelectrolytes bear a total charge usually much higher than the protein. The monomeric oligovalent anions of the here presented experiments have much lower charge numbers than the protein, but the phenomenological behaviour is similar.

If LLPS or LSPS occurs, the interaction between the protein molecules themselves is predominating over the interaction between protein and water. Therefore, these states are claimed to be less hydrated. First of all, this is a phenomenological observation, which does not provide direct information about the mechanism and cause of phase separation. Conclusively, the less hydrated states (i.e. the lower phase observed in a system undergoing LLPS and the precipitate in a system undergoing LSPS) can either result from enhanced protein-protein interactions and/ or can result from reduced interaction of the protein with water, if oligovalent anions are present. Enhanced protein-protein interaction could be due to reduced electrostatic repulsion if the net charge decreases caused by protein-anion interaction and possibly from anion induced protein cross-linking. Reduced interaction of the protein with water induced by oligovalent anions could also result from protein-anion interaction if the formed complex is less hydrophilic. Both proposed mechanism might go hand in hand and are not mutually exclusive. In the next section the experimental proof of protein-anion interaction will be given to verify the first part of the proposed mechanisms.

#### **4.1.7. Mapping the ion atmosphere**

To directly test and prove that citrate binds to the antibody, an experimental approach reported by Bai and coworkers (92) was adapted to antibody solutions. The antibody solution was equilibrated with solutions containing citrate buffer of varying concentration at pH 6.0 together with sodium chloride of a constant concentration of 4 mM (arbitrarily chosen). NaCl was used as a background salt as it is assumed to not specifically interact with proteins and simply act as a screening salt (52). The final concentration of anions was detected via ion chromatography and the number of associated citrate and chloride ions was calculated by equ (30) and is reported in Figure 16. Associated ions are counterions and those binding more specifically, both constituting the ion atmosphere (93).



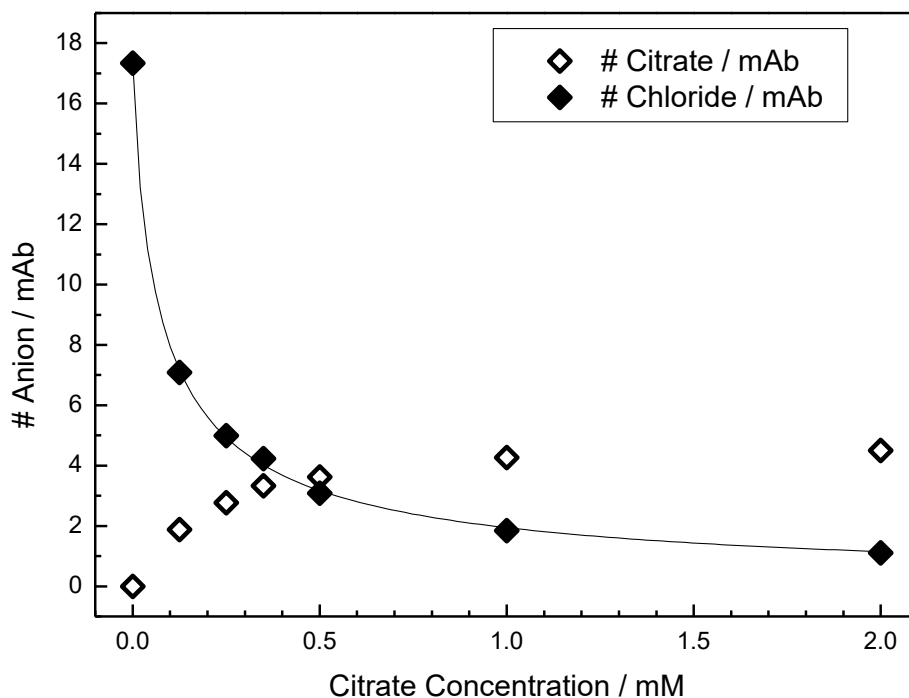


Figure 16: Number of associated ions per antibody as a function of the free citrate concentration at a constant NaCl concentration of 4 mM, at pH 6.0 and an antibody concentration of approximately 100 mg/ml (conditions arbitrarily chosen). The number of associated chloride ions is represented by filled symbols and the number of associated citrate ions is represented by open symbols. Data were fitted with equ (31) (see section 3.2.3.5).

The number of chloride ions associated to the protein in the absence of citrate was 17.3 ( $\pm 1$ ) (Figure 16). With increasing citrate concentration and a constant chloride concentration of 4 mM, the chloride ions were displaced by citrate ions. The competition constant was obtained by fitting data of associated chloride ions to equ (31).  $A_0$  and  $A_1$  were set constant to values of 17.3 and zero, respectively. A competition constant of  $82 \mu\text{M} \pm 3 \mu\text{M}$  and a Hill coefficient of  $0.83 \pm 0.03$  were derived from the fit.

A citrate concentration of  $82 \mu\text{M}$  was needed to replace half of the chloride ions from the protein at a protein concentration of 100 mg/ml and a background chloride ion concentration of 4 mM. In competition with chloride ions citrate ions associated preferentially with the protein. E.g., with an excess of chloride ions (4 mM) over citrate

ions (1 mM) in the bulk solution the ion atmosphere still had twice the amount of citrate (4 ions associated) compared to chloride (2 ions associated). When the citrate concentration reached a concentration of 2 mM, together with 4 mM chloride, only 1 chloride ion remained associated to the antibody (Figure 16).

Preferential association of citrate over chloride can be expected due to the total charge of citrate of - 2.8 at pH 7.0. A higher ionic charge leads to stronger Coulomb interactions with the protein. A smaller number of citrate ions compared to chloride ions is required to neutralize the positive charges of the protein. Therefore, the loss in entropy is smaller for binding of citrate compared to anions having only one negative charge (92, 169).

The approach presented here has the potential to sensitively detect differences in the interaction between various ions with antibodies. Therefore, it is a useful complementary tool to explain phenomenological differences in physicochemical properties of antibodies in different solution conditions. Furthermore, it can be used to screen for specific ion association potentially occurring during ultrafiltration and diafiltration in biopharmaceutical production (170, 171).

The results suggest that LLPS is induced by binding of the anion to the protein. However, not all cosolutes which are binding to the protein are necessarily inducing LLPS. The overall solubility of the formed complex is of critical importance. Histidine or human serum albumin, possibly binding to monoclonal antibodies, have been shown to diminish or prevent LLPS (13, 65). In each case it would be necessary to directly prove binding between the cosolute and the antibody.

#### **4.1.8. Summary and conclusions**

In this part of the work the solution conditions which favour LLPS in monoclonal antibody solutions were investigated. First of all, LLPS was observed at the isoelectric point of the mAb. Secondly, LLPS did occur at pH below the pI if citrate or other oligovalent anions, such as butane-1,2,3,4-tetracarboxylate, benzene-1,2,4,5-tetracarboxylate or benzene-1,2,3,4,5-pentacarboxylate were present. These oligovalent anions are proposed to bind to the positively charged protein and thereby neutralize the protein in a limited pH region, resulting in LLPS. A non-monotonic dependence of the width of the miscibility gap at 5°C

on the citrate concentration was observed. Therefore an optimal citrate concentration is proposed to exist, at which charge neutralization is reached. In addition to that, ionic strength attenuated phase separation. Furthermore, the extent of phase separation was shown to increase with anion charge. Depending on the anion charge, different states of hydration of the antibody-anion complex have been deduced. The coexistence curve of the antibody in 1 mM citrate pH 7.2 showed the following properties: i) an upper critical solution temperature ii) a critical protein concentration of 93 mg/ml, a critical temperature of 289 K (16 °C) and a width  $w$  of 26 (Table 9) (obtained by fitting with equ 38) and iii) an asymmetry with respect to  $c = c_c$  (Figure 14). The coexistence curve was steeper on the low concentration side than on the high concentration side. The critical temperature in 1 mM citrate buffer was pH-dependent with a higher critical temperature observed at pH 7.4 and pH 8.1 compared to pH 7.2. The effects observed here and conclusions made for one single antibody might also occur and apply for other protein classes or other antibody molecules (87, 148). A new approach was introduced to measure weak binding between ions and antibodies. The identified characteristics for the solution conditions inducing LLPS in antibody solutions, together with this new approach, may enable us to rationally modify the use of ionic excipients and their concentration, to either reduce opalescence or to induce or avoid phase separation.

Summing up, a rationale can be found to explain the phase behaviour and therewith the protein-protein interactions in the protein solution as a function of pH, excipient species and concentration, as well as ionic strengths. This rationale is based on the concept, that the charge of an antibody increases with increasing distance from pI. In addition to the overall net charge, which induces repulsive protein-protein interactions, the concept also includes the assumption of an anisotropic charge distribution over the protein surface resulting in attractive protein-protein interactions, which become weaker with increasing ionic strength. Finally, electrostatic binding between oligovalent ions and the protein, resulting in charge neutralization, is completing the concept.

## **4.2. PROTEIN PHASE BEHAVIOR IN THE PRESENCE OF OLIGOVALENT ANIONS - SPIKING EXPERIMENTS**

As described in section 4.1.6, a protein solution containing oligovalent anions showed the phenomenon of liquid-liquid or liquid-solid phase separation at specific conditions, i.e. in 1 mM oligovalent anion solution, pH 7.0. The occurrence and the type of phase separation were depending on the charge of the oligovalent anion.

In further experiments the effect of pH, anion charge, anion concentration and protein concentration as well as ionic strength will be examined. In contrast to the experiment described in section 4.1.6, in this part of the work, the concentration of anions (of 1,2,4,5-tetracarboxylate, benzene-1,2,3,4,5-pentacarboxylate, and mellitate) was adjusted by spiking and not by dialysis. This experimental procedure has the advantage that the concentration of the anions can be adjusted more precisely and is well known after spiking. A disadvantage of the spiking procedure is the presence of additional chloride ions in the solution which would be removed during dialysis. The chloride ions may weaken the effects of protein-anion interaction and the resulting phase separation phenomena.

### **4.2.1. Influence of anion charge and anion concentration on phase separation**

The influence of the anion concentration on phase separation was investigated for protein solutions containing benzene-1,2,4,5-tetracarboxylate (pyromellitate), benzene-1,2,3,4,5-pentacarboxylate (benzene pentacarboxylate) and benzene-1,2,3,4,5,6-hexacarboxylate (mellitate). The concentration of the oligovalent benzene carboxylates, ranging from 0.05 mM to 15 mM was adjusted by spiking (see section 3.2.3.6). The results are listed in Table 13 and displayed in Figure 17. The pH dependent net charge of the oligovalent anion as given in Table 13 was estimated from titration data (see section 3.2.4.1). The net charge was also calculated on the basis of the Henderson Hasselbalch equation using  $pK_a$  values published by Maxwell (124) (see section 3.2.4.2.1).

Table 13: Influence of anion charge and anion concentration on phase separation. The concentration values in the first row ( $C_{\text{End}}$ ) correspond to the excipient concentration after mixing both solutions. The protein concentrations measured in the mixed solution or in the supernatant, if phase separation occurred, are listed in the cells in units of mg/ml. The cells colored in grey indicate that no phase separation was observed after mixing. The cells colored green indicate that the solution showed turbidity after mixing but no macroscopic phase separation was observed. The cells colored yellow indicate that liquid-solid phase separation was observed and the cells colored purple indicate that liquid-liquid phase separation was observed. After mixing, the solution's pH was 5.3 ( $\pm 0.3$ ). The charge of the anions was either determined by titration (at a concentration of 1 mM of additive) or by calculation (calc.) on the basis of the Henderson Hasselbalch equation using  $pK_a$  values as published by Maxwell (124).

Additive	Charge at pH 5.3 (titration)	Charge at pH 5.3 (calc.)	$C_{\text{End}}$ (additive) / mM									
			0.05	0.1	0.2	0.35	0.5	0.75	1.0	2.0	5.0	15.0
Pyromellitate	-3.0	-3.3	7.35	7.29	6.91	7.86	8.07	7.25	7.48	6.89	6.75	6.95
Benzene pentacarboxylate	-3.0	-3.5	7.52	7.43	7.39	3.03	0.75	0.30	0.31	0.51	1.58	6.78
Mellitate	-3.8	-4.3	7.64	7.53	3.36	0.02	0.01	0.03	0.04	0.11	0.79	7.01

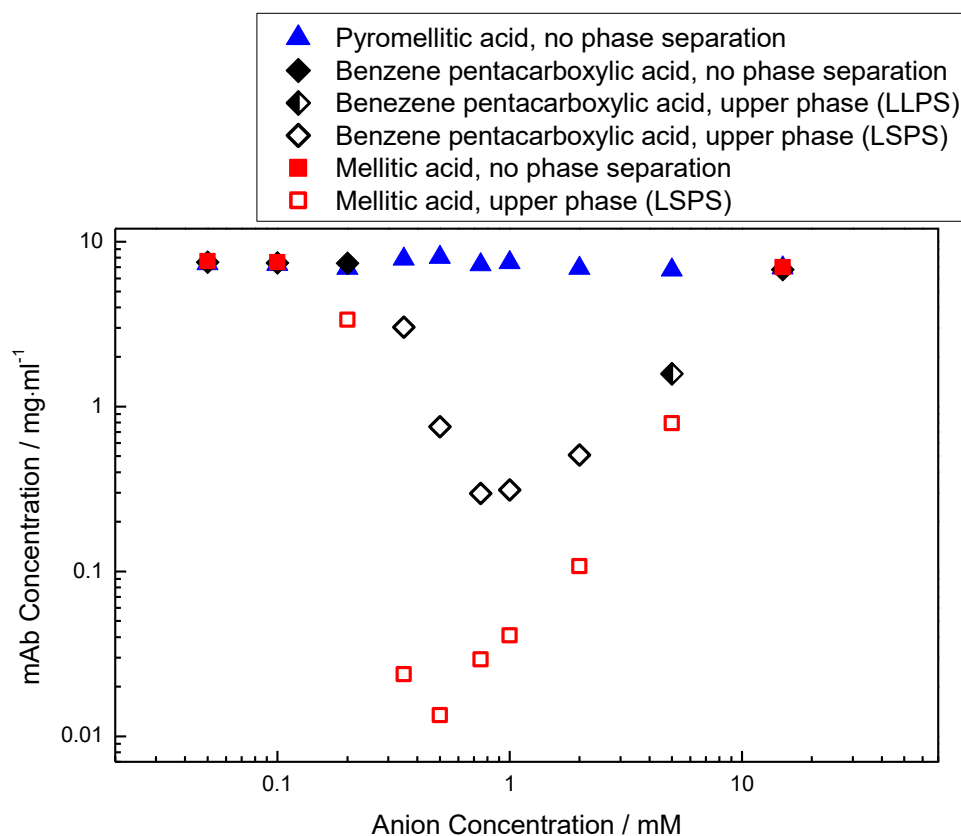


Figure 17: Influence of anion concentration on phase separation at pH 5.3 ( $\pm 0.3$ ). The concentration on the X-axis corresponds to the excipient concentration after mixing both solutions. The protein concentrations measured in the mixed solution or in the supernatant, if phase separation occurred, is plotted on the Y-axis. The addition of pyromellitate (blue triangle) did not induce phase separation. The addition of benzene pentacarboxylate (black rhomb) resulted in LSPS (empty symbols) between 0.35 mM and 2 mM and resulted in LLPS (half-filled symbols) at a concentration of 5 mM. The addition of mellitate induced LSPS (empty red squares) at concentrations between 0.2 mM and 5 mM.

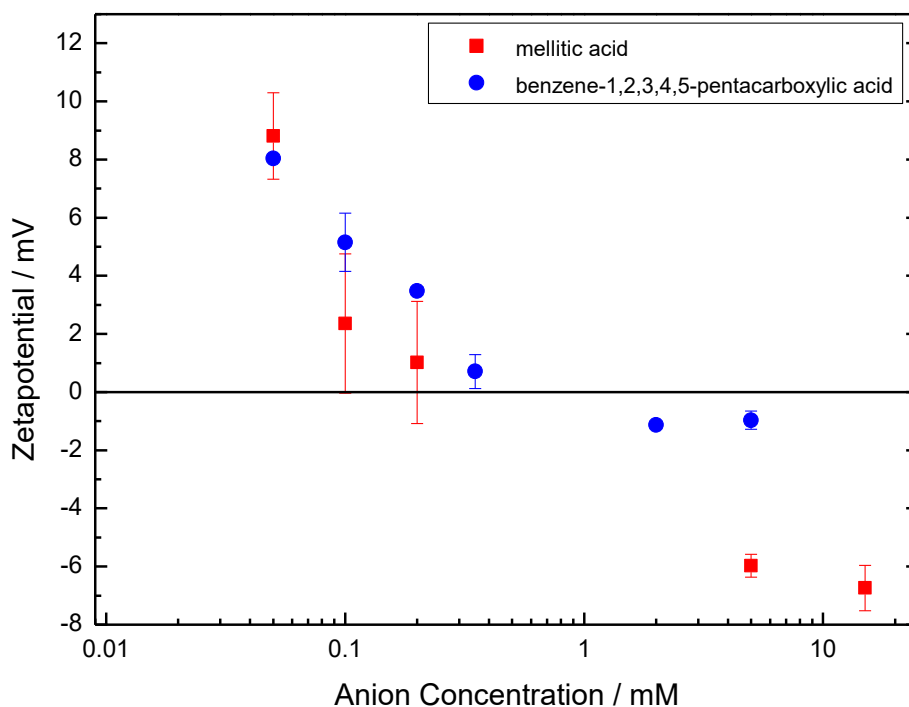


Figure 18: The zetapotential of protein solutions containing mellitate (red squares) and benzene pentacarboxylate (blue circles) as a function of anion concentration at pH 5.3. The concentration on the X-axis corresponds to the anion concentration after mixing both solutions.

Phase separation was induced in systems containing benzene pentacarboxylate and mellitate. It was not induced under these conditions in the presence of pyromellitate. However, turbidity was observed in solutions containing 0.35 mM to 0.75 mM of pyromellitate indicating microscopic phase separation (172). For systems containing mellitate and benzene pentacarboxylate a non-monotonic trend was observed for the protein concentration in the supernatant as a function of excipient concentration. By increasing the mellitate concentrations between 0.1 mM and 0.5 mM the protein concentration in the supernatant was decreasing, whereas it was increasing at mellitate concentrations above 0.5 mM up to 15 mM. In the presence of benzene pentacarboxylate, the trend was the same, however higher concentrations of benzene pentacarboxylate were required to induce phase separation and the minimal protein concentration was observed at a slightly higher excipient concentration of 0.75 mM. The curve shows an asymmetry with a steeper

decrease of protein concentration at lower anion concentrations compared to the increase of protein concentration at higher anion concentrations (Figure 17).

A benzene pentacarboxylate concentration of 5 mM was inducing the formation of LLPS instead of LSPS, in contrast to all other examined benzene pentacarboxylate concentrations and to phase separations induced by mellitate.

The protein concentration in the upper phase was lower in solutions containing mellitate, compared to those systems containing benzene pentacarboxylate, independent of the concentration of benzene carboxylates.

The zeta potential was positive at lower anion concentrations up to 0.2 mM for mellitate and up to 0.35 mM for benzene pentacarboxylate. At higher anion concentrations the zetapotential was negative (Figure 18). Charge reversal was estimated by interpolation to occur at 0.3 mM ( $\pm 0.2$  mM) mellitate and 0.6 mM ( $\pm 0.2$  mM) benzene pentacarboxylate.

#### *Charge of the different ions*

The number of carboxylic groups and the maximal possible charge of the three tested excipients increases in the following order: pyromellitate < benzene pentacarboxylate < mellitate. The experimentally determined charge of the oligovalent anions at pH 5.3 is listed in Table 13. The experimentally determined negative charge is lower than the charge that would be expected based on  $pK_a$  values published by Maxwell (124). The negative charge was calculated on the basis of Henderson Hasselbalchs equation.  $pK_a$  values reported by Maxwell are listed for an ionic strength of 30 mM.  $pK_a$  values of the dissociation steps are influenced by the ionic strength in solution (equ (36)). This influence is enhanced if the charged species bears a higher number of charges as found for benzene oligocarboxylates (equ (36)). Differences in  $pK_a$  values will result in differences in the calculated charge of the benzene carboxylate ions. The experimentally derived charge of pyromellitate and benzene pentacarboxylate were the same. This may be caused by the measuring uncertainty of about 0.2 pH units. The charge of benzene pentacarboxylate is probably slightly higher.



### *Comparison of phase separation in the presence of the three tested oligocarboxylates*

The capacity of inducing phase separation increased with increasing charge of the added anion (Figure 17, Table 13).

The macroscopic formation of a protein precipitate could be explained with the microscopic formation of a protein network. One oligovalent anion could bind to positively charged regions of two or more proteins and thereby act as a cross-linking agent. If the protein has more than one potential binding site for the oligovalent anions and if these binding sites are pointing into different directions, the formation of a protein-protein-anion network via cross-linking may occur. A higher negative charge leads to stronger binding to the protein and a higher propensity for cross-linking. Assuming cross-linking to take place, the network is assumed to be stronger if protein-excipient binding is stronger.

Enhanced propensity of phase separation in mellitate is most easily explained with enhanced protein cross-linking. However, another scenario may contribute as well. As described before in section 4.1 phase separation could also result from charge neutralization of the protein. Assuming mellitate to bind stronger to the protein compared to benzene pentacarboxylate, the concentration of the free anions is assumed to be lower in systems containing mellitate compared to systems with benzene pentacarboxylates at constant degree of charge neutralization of the protein. The presence of free anions is increasing the ionic strength. As calculated and listed in Table 15, the ionic strength in systems containing benzene pentacarboxylate is higher compared to mellitate at the condition of charge neutralization of the protein. Assuming ionic strength to weaken the intermolecular attractive protein-protein interactions (induced for example by multipolar electrostatic interactions), the lower propensity of phase separation in benzene pentacarboxylate could also be due to the higher ionic strength in that system at constant protein net charge. However, from a steric point of view, anion induced protein cross-linking is strongly expected, due to the negative charges on the oligovalent anions pointing in different directions. Therefore, both effects may contribute to the different extent of phase separation observed for solutions containing either mellitate or benzene pentacarboxylate.

In a previous section (section 4.1.6) phase separation was observed for the same anions as examined here. Previous experiments in section 4.1.6 were performed at pH 7.0 using

dialysis instead of spiking sample preparation and the only excipient concentration tested was 1 mM. In opposite to the observations in this section, in the previous experiments, LLPS was observed for pyromellitate at a concentration of 1 mM. The reasons that could explain, that phase separation was not observed in the spiking experiments are the different experimental procedure with chloride ions remaining in the sample, the different pH-value and therefore different charges on the protein and the benzene oligocarboxylate and the lower protein concentration. It is possible that the miscibility gap under these conditions is narrow and phase separation would only be detected at higher protein concentrations.

*Non-monotonic dependence of the protein concentration in the supernatant as a function of the anion concentration*

Higher concentrations of benzene pentacarboxylate are required compared to mellitate to induce phase separation and reach the excipient concentration at which the protein concentration in the supernatant is minimal. This could be due to the lower negative charge of benzene pentacarboxylate. For stoichiometric reasons, charge neutralization is expected to occur at higher anion concentration for lower charged anions. In addition, the degree of binding between the positively charged protein and the negatively charged anion is assumed to be stronger for higher charged binding partners. Therefore, charge neutralization is also expected to occur at lower concentrations of mellitate compared to benzene pentacarboxylate.

Table 14: Calculation of the theoretical anion concentration required to counterbalance the net charge of the mAb. The anion charge was determined from titration data at an anion concentration of 1 mM. The mAb charge was estimated from valence titration in combination with the knowledge of the experimental isoelectric point. Calculations are based on a mAb concentration of 7.5 mg/mL (0.052 mM) and a molecular weight  $M_w$  of 145,000 g/mol.

	Experimental anion charge at pH 5.3 for an anion concentration of 1 mM	mAb charge (valence) at pH 5.3	Calculated anion concentration required to counterbalance positive charge of mAb (based on experimental charge) / mM	Minimal anion concentration at which separation observed / mM	Anion concentration at which protein supernatant is minimal / mM
Pyromellitate	- 3.0	+26	0.45	-	-
Benzene pentacarboxylate	- 3.0	+26	0.45	0.35	0.75
Mellitate	- 3.8	+ 26	0.35	0.2	0.5

Table 15: Calculation of the ionic strength for the anion concentration at which the protein concentration in the supernatant is minimal. The ionic strength was calculated with equ (37). The net charge of the protein is assumed to be completely neutralized at the anion concentration of minimal protein concentration in the supernatant. The anion concentration of minimal protein concentration in the supernatant and the calculated anion concentration required to counterbalance the positive charge of the mAb. Chloride ion concentrations which were introduced into the sample together with the protein are equal for both anion types. The chloride concentration in the mixed solution is calculated to be  $26 \times 0.052 \text{ mM} = 1.34 \text{ mM}$ .

	Experimental anion charge at pH 5.3 for an anion concentration of 1 mM	Calculated anion concentration required to counterbalance positive charge of mAb (based on experimental charge) / mM	Anion concentration at which protein concentration in the supernatant is minimal / mM	Concentration of the anion fraction which is not binding to the protein / mM	Sodium concentration	Ionic strength at the anion concentration where the protein concentration in the supernatant is minimal / mM
Benzene pentacarboxylate	-3.0	0.45	0.75	0.3	$3 \times 0.75 \text{ mM} = 2.25 \text{ mM}$	3.1
Mellitate	-3.8	0.35	0.5	0.15	$3.8 \times 0.5 \text{ mM} = 1.9 \text{ mM}$	2.7

By determining the charges of the oligovalent anions (see section 3.2.4.1) and of the polyvalent positively charged protein from titration data (see section 3.2.3.1), the ratio which is assumed to induce charge counterbalance can be estimated (Table 14). The calculated anion concentration which is expected to induce charge counterbalance is 0.45 mM for benzene pentacarboxylate and 0.35 mM for mellitate.

These calculated anion concentrations are higher than the minimal anion concentration at which phase separation was observed (0.35 mM for benzene pentacarboxylate and 0.2 mM for mellitate) but lower than the anion concentration at which the minimal protein concentration in the supernatant was observed (0.75 mM for benzene pentacarboxylate and 0.5 mM for mellitate).

The proximity of the calculated and experimental values confirms the theory of charge neutralization induced by oligovalent anions and potential charge reversal at higher anion concentrations.

The lowest anion concentration where phase separation occurs can be interpreted as the anion concentration where a defined degree of binding and therefore also a defined degree of protein charge neutralization occurs. The protein concentration at the lowest anion concentration where phase separation occurs is rather high with values of 3.03 mg/ml and 3.36 mg/ml compared to the minimum values of 0.3 mg/ml and 0.01 mg/ml at higher anion concentrations for benzene pentacarboxylate and mellitate, respectively. These higher protein concentrations indicate that charge neutralization is not completely achieved and the proteins net charge is still positive.

The calculated anion concentrations required for charge counterbalance are lower than the anion concentrations at which the protein concentration in the supernatant is minimal. This could be due to an adapted charge of the benzene carboxylate ion and/or the protein, or due to incomplete binding or due to enhanced protein cross-linking at anion concentrations higher than those at which charge neutralization occurs.

Estimating the charges of the benzene carboxylate ion and the protein in the mixture to be different to the assumptions in Table 14, the lower calculated anion concentration compared to the actual anion concentration of minimal protein concentration in the supernatant could

either be due to a lower negative charge of the respective anion or a higher valence of the protein. The valence of the protein could be expected to be modified by the binding of the anions. As a result, the  $z_{DHH}$  of the protein is assumed to decrease, however the valence of the protein may increase as a consequence of introducing negative charges by mellitate and benzene pentacarboxylate and thereby changing  $pK_a$  values of specific amino acid residues. This phenomenon has been described earlier and was termed induced charging (34) or charge regulation (173).

Incomplete binding could contribute to the difference between the calculated anion concentration required for charge counterbalance and the anion concentration at which the protein concentration in the supernatant is minimal. This would be expected if the interaction between both binding partners is weak and therefore the concentration of free anion is in the order of magnitude as the concentration of the protein anion complex. A higher total anion concentration would be required for charge neutralization as part of the anions would not be binding to the protein.

Finally, cross-linking may be enhanced at anion concentrations higher than those at which charge neutralization occurs, as cross-linking may not only be affected by the overall charge of the protein but also by the availability of potential binding sites. The number of positive patches and structural location on the protein surface representing potential binding sites for the oligovalent benzene carboxylates is assumed to be larger than the overall positive net charge of the antibody. The net charge (valence) of an antibody is resulting from the composition of acidic and basic amino acids and the pH of the surrounding solution. The net charge (valence) results by summing up all the charged groups of a protein. In most cases, the total number of charged groups with positive and with negative sign of the protein is higher than the valence. In contrast to the proteins net charge, the surface charge distribution is defined by the position of the acidic and basic amino acids on the protein surface and on the pH. The charged groups can either be evenly distributed over the surface of the protein or an accumulation of likely charged groups can form charged patches (44, 174). Even if mellitate binding results in charge neutralization or charge reversal of the protein-mellitate complex, some positive patches may remain on the protein surface, which are potential binding sites for mellitate. Therefore cross-linking could be enhanced at higher mellitate concentrations, independently from the actual charge of the protein-

mellitate complex, as long as sufficient positive patches are present on the surface of the antibody.

Zetapotential measurements also confirm the theory of charge neutralization and charge reversal induced by oligovalent anion binding (Figure 18). Charge reversal was observed by zetapotential measurements at 0.3 mM ( $\pm 0.2$  mM) mellitate and 0.6 mM ( $\pm 0.2$  mM) benzene pentacarboxylate. These concentrations are similar to the calculated anion concentration required for charge counterbalance as well as the anion concentration of minimal protein concentration in the supernatant as listed in Table 14. The poor precision and the high uncertainty of the zetapotential measurement make it impossible to clarify if charge neutralization occurs at the calculated anion concentration required for charge counterbalance or at the anion concentration of the lowest protein concentration in the supernatant. The knowledge about the experimental anion concentration where the protein is neutral could clarify the reasons behind the deviation between the theoretical anion concentration of charge counterbalance and the anion concentration of minimal protein concentration in the supernatant.

The onset of phase separation and the anion concentration of minimal protein concentration were observed at lower mellitate concentrations compared to benzene pentacarboxylate concentration (Figure 17). This shift was not clearly observed for the second part of the curve, where the protein concentrations in the supernatant increase upon increasing the anion concentration. The missing shift of the second part of the curve could indicate that charge reversal does not take place at higher mellitate concentration, or that the general enhanced propensity of phase separation in mellitate levels out the effect. The second explanation is the more likely explanation, as the zeta potential in protein solutions containing mellitate has been shown to become negative at mellitate concentrations higher than approximately 0.3 mM (Figure 18).

The values in Figure 17 show an asymmetry with a steeper decrease of protein concentration at lower anion concentrations compared to the increase of protein concentration at higher anion concentrations. This may be due to the different net charges of the protein in both anion regions. The degree of binding of oligovalent anions to the protein is higher at a higher positive net charge of the protein, i.e. lower anion concentration.

The non-monotonic trend of the protein concentration in the supernatant has been observed before in protein solutions containing citrate (see section 4.1.3). The decrease of the protein concentration in the supernatant with increasing anion concentration at low anion concentrations was explained with decreasing net charge of the protein upon citrate binding resulting in protein self-association. The increase of the protein concentration in the supernatant at higher anion concentration was explained with weakening of the protein-citrate complex and weakening attractive protein-protein interactions by higher ionic strength and potential charge reversal upon citrate binding. The effect of charge reversal is assumed to play a minor role for the non-monotonic trend in citrate but it may play a larger role in systems containing anions of higher valence such as benzene pentacarboxylate or mellitate.

A direct comparison of effective anion concentrations where LLPS was observed in citrate solutions as depicted in section 4.1.3 is not allowed due to the different procedure of sample preparation, i.e. dialysis vs. spiking experiment.

#### **4.2.2. Influence of pH and mellitate concentration on phase behavior**

The influence of the pH on phase separation was investigated for protein solutions containing mellitate (as described in detail in section 3.2.3.6). The examined anion concentrations were varied depending on the pH tested. The results are listed in Table 16 and displayed in Figure 19.



Table 16: Influence of pH and anion concentration on phase separation. The concentration values shown in the first row correspond to the excipient concentration after mixing both solutions. The protein concentrations measured in the mixed solution or in the supernatant, if phase separation occurred, are listed in the cells in units of mg/ml. The cells colored in grey indicate that no phase separation was observed after mixing. The cells colored yellow indicate that liquid-solid phase separation was observed and the cells colored purple indicate that liquid-liquid phase separation was observed. The pH was measured after mixing. Empty cells indicate that no mixing experiment was performed for this experimental condition. The superscripts are defined as follows: <sup>a</sup>: The precipitate separated from the supernatant was soluble in 300 mM NaCl. <sup>b</sup>: The precipitate separated from the supernatant was not soluble in 300 mM NaCl but in 500 mM NaCl. <sup>c</sup>: The precipitate separated from the supernatant was neither soluble in 300 mM nor in 500 mM, but it was soluble in 1000 mM NaCl.

c(mel- litate) / mM	0.01	0.03	0.05	0.1	0.2	0.35	0.5	0.75	1	2	5	15	50	2000
pH 2.8- 3.0			7.96	8.09	7.57	7.21	7.37	7.10	7.12	4.2 <sup>a</sup>	<0.01 <sup>b</sup>	<0.01 <sup>c</sup>	<0.01 <sup>c</sup>	<0.01
pH 3.6- 3.9			7.87	7.83	7.70	7.44	7.44	4.35	3.17	0.24	<0.01	0.01	0.02	
pH 5.0- 5.6			7.64	7.53	3.36	0.02	0.01	0.03	0.04	0.11	0.79.	7.01		
pH 7.4- 7.8	7.69	6.00	3.27	0.19	0.31	0.56	1.15	2.69	3.94	7.75	7.61	7.65		
pH 9.0- 9.5			7.68	7.47	7.80	7.50	7.54	7.50	7.53	7.66	7.40	7.88		

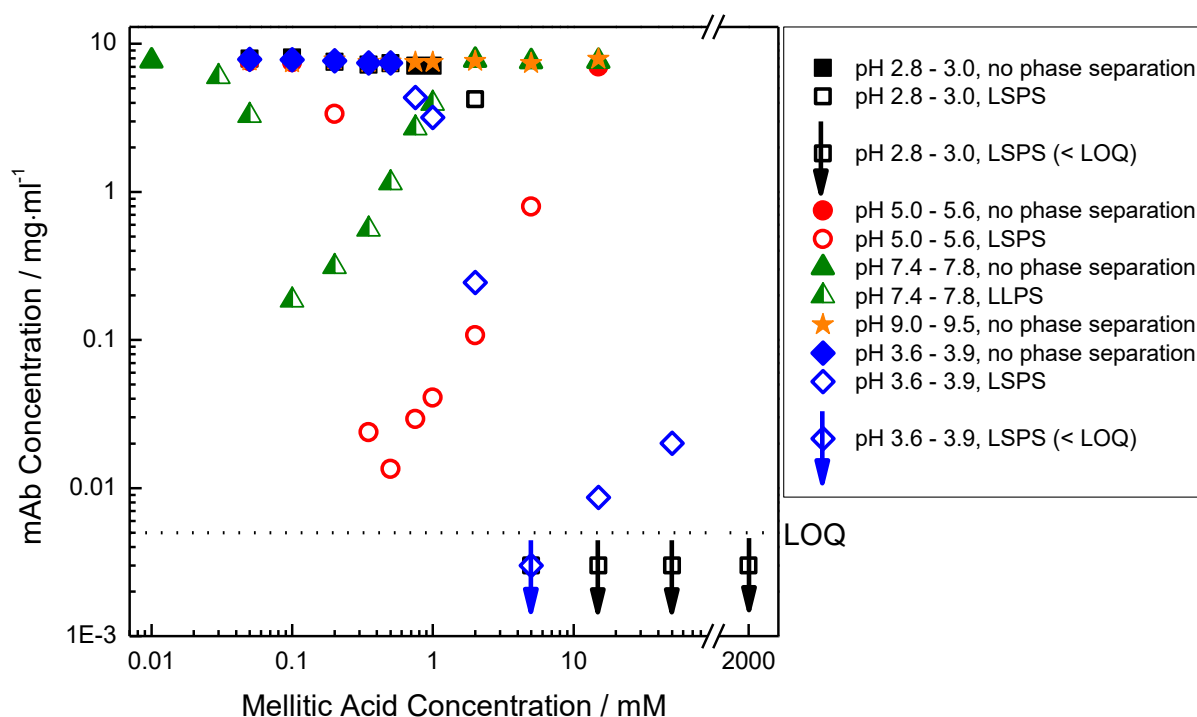


Figure 19: Influence of pH and mellitate concentration on phase separation. The concentration on the X-axis corresponds to the excipient concentration after mixing both solutions. The protein concentrations measured in the mixed solution or in the supernatant, if phase separation occurred, is plotted on the Y-axis. If the protein concentration in the supernatant was below the limit of quantification (LOQ) of 0.005 mg/ml an arrow was inserted into arbitrarily positioned squares. The limit of quantification is depicted by a dotted line. The symbols are defined as follows: black squares: pH 2.8 – pH 3.0, blue rhoms: pH 3.6 – pH 3.9, red circles: pH 5.0 – pH 5.6, green triangles: pH 7.4 – pH 7.8, orange stars: pH 9.0 – pH 9.5. Filled symbols represents that no phase separation was observed. Empty symbols represent that LSPS was observed and half-filled symbols represent that LLPS was observed. The pH was measured after mixing.

LSPS was observed in solutions containing protein and mellitate with pH values between pH 2.9 and pH 5.3 in a limited anion concentration range. LLPS was observed at pH 7.6 between 0.03 mM and 1.0 mM mellitate. No phase separation was observed at pH 9.3 in an anion concentration range between 0.05 mM and 15 mM. If phase separation occurred, the minimal anion concentration at which phase separation occurred was increasing with decreasing pH. The same trend was observed for the anion concentration where the protein concentration in the supernatant had its minimal value (apparent only between pH 3.8 and pH 7.6) and the maximal anion concentration at which phase separation was observed

(apparent only at pH 5.3 and 7.6). Despite difficulties in determining the protein concentrations in the supernatant at pH 2.9 and pH 3.8 due to the limit of quantification (LOQ) of the BCA assay, it seems that the protein concentrations in the supernatant were generally lower in solutions of lower pH. On the linear scale, the anion concentration range at which phase separation was observed is wider with decreasing pH. At pH 2.9 the phenomenon of LSPS was observed up to a mellitate concentration of 2000 mM. Between pH 3.8 and pH 7.6 a non-monotonic trend of protein concentration in the supernatant as a function of anion concentration was observed. The asymmetry at pH 5.3, mentioned already in the previous section (section 4.2.1), was also observed at pH 7.6. No sufficient data were collected to determine the possible asymmetry at pH 2.9 and pH 3.8.

The precipitate of certain samples (pH 2.8 - 3.0: 2 mM - 50 mM mellitate) was examined with regards to reversibility, by first removing the supernatant and then adding NaCl solution of different concentrations. The higher the mellitate concentration (except 2000 mM, which was not examined here), the higher was the NaCl concentration needed to dissolve the precipitate. The influence of ionic strength on phase separation and explanations will be discussed in more detail in the following section (0).

#### *pH dependence of phase separation*

No phase separation was observed at pH 9.3 for anion concentrations between 0.05 mM and 15 mM. At pH 9.3 the protein with an experimental isoelectric point of 8.7 is negatively charged (see section 4.1.1 and Appendix 1). Therefore electrostatic interactions between the protein and the anions are repulsive. Remaining positive patches on the protein surface may be present and could result in binding of the oligovalent anion to the protein. However, protein-anion interaction seems to be not strong enough to induce protein-protein cross-linking resulting in phase separation at the given conditions.

Phase separation was enhanced at lower pH. This can be seen in the formation of LSPS instead of LLPS at pH 5.3 and lower, the generally lower protein concentrations in the supernatant at lower pH, and the wider anion concentration range at which phase separation was observed. The lower protein concentrations in the supernatant indicate an increase in the width of the miscibility gap at lower pH, indicating enhanced attractive protein-protein interactions induced by mellitate. At lower pH the positive net charge of the protein

increases whereas the negative charge of the oligovalent anion mellitate decreases. The increasing positive net charge of the protein could result in enhanced protein-mellitate interaction resulting in enhanced protein-protein cross-linking and therefore in enhanced phase separation. Higher charges of the interacting binding partners in a protein-polyelectrolyte complex are related to enhanced phase separation (86). The decreasing net charge of mellitate with decreasing pH would be expected to result in reduced protein-mellitate interaction and therefore reduced phase separation. The experimental results indicate that the increase in protein net charge has a stronger impact on phase separation compared to the decreasing negative charge of mellitate.

Different possible reasons can be found for this experimental result: First, the changes in net charge resulting from a pH change are higher for the antibody (a difference of 54 charge units between pH 3.8 and pH 9.3) compared to mellitate (a difference of 3.2 charge units between pH 3.8 and pH 9.3). Second, even though induced charging (see section 4.2.1) may occur for both binding partners (mellitate and the protein), cross-linking may be stronger influenced by induced charging of mellitate compared to the protein. This could be due to the lower spatial expansion of the mellitate ion. Induced charging is assumed to occur in the immediate vicinity of the charged group which is involved in binding. The carboxylic groups (potential negative charges) of the mellitate ion are close together whereas the basic amino acids side chains (potential positive charges) of the protein are widely distributed over the protein. Induced charging may therefore be enhanced for mellitate. In addition, the precondition for mellitate induced protein cross-linking is the presence of positive charges pointing into different directions of the protein. However, induced charging of a protein may rather take place close to the positive patch where the mellitate binds. Therefore, even if it occurs, it may not enhance the formation of positive patches on the protein distant from the positive patch where binding occurs.

The pH-dependent charges of the protein and of the mellitate ion (determined as described in section 3.2.3.1 and 3.2.4.1) can be used to calculate the anion concentration required for charge counterbalance. The results are listed in Table 17.

Table 17: Calculation of the theoretical anion concentration required to counterbalance the net charge of the mAb. The anion charge was determined from titration data at an anion concentration of 1 mM. The mAb charge was estimated from valence titration in combination with the knowledge of the experimental isoelectric point of 8.7. Calculations are based on a mAb concentration of 7.5 mg/mL (0.052 mM) and a molecular weight of  $M_w = 145.000$  g/mol. The abbreviation n.d. stands for not determined.

	Experi- mental anion charge	Calculated anion charge (Maxwell (124))	mAb charge	Anion concentration required to counterba- lance mAb (calculated using the experimental charge) / mM	Minimal anion concentrat ion at which phase separation is observed / mM	Anion concentration at which protein concentration in the supernatant is minimal / mM
pH 2.9	- 2.3	- 2.3	n.d.		2	
pH 3.8	- 2.7	- 2.8	+ 48	0.92	0.75	5
pH 5.3	- 3.8	- 4.3	+ 26	0.35	0.2	0.5
pH 7.6	- 5.8	- 5.8	+ 8	0.07	0.03	0.1
pH 9.3	n.d.	- 6.0	- 6	-	-	-

The calculated anion concentration required to counterbalance the positive charge of the protein and the experimental anion concentration of minimal protein concentration in the supernatant follow the same trend. They are increasing with decreasing pH. Similar to the results in section 4.2.1, the calculated anion concentration required for charge counterbalance is higher than the minimal anion concentration at which phase separation was observed but lower than the anion concentration at which the protein concentration in the supernatant was minimal. The protein concentration in the supernatant at minimal anion concentrations where phase separation was observed is again rather high (between 3.36 mg/ml and 6 mg/ml, see Table 16). One can therefore deduce that charge neutralization is not fully achieved at these anion concentrations.

The deviation between the calculated anion concentration required for charge neutralization and the anion concentration of minimal protein concentration in the supernatant is maximal at pH 3.8. The potential reasons for these deviations were discussed in detail in section 4.2.1.

As shown in section 4.2.1, solutions containing pyromellitate were not undergoing phase separation at pH 5.3. This was explained with the lower negative charge of pyromellitate (calculated: -3.3, experimental: -3.0). The results presented as a function of pH show a different trend where phase separation was even enhanced in solutions of lower anion charge, with phase separation still occurring at an experimentally determined anion charge of only -2.7 or -2.3 at pH 3.8 or pH 2.9. The negative charge of the oligovalent anion which is assumed to be affected by protein-binding (induced charging see section 4.2.1), can reach higher values for anions of higher maximum possible charge. This indicates a high impact of the **maximum** possible charge of an anion on phase separation. However, by comparing these two experiments one should keep in mind that the pH does not only affect the charge of the mellitate but of the protein as well. A higher positive net charge of the protein could enhance the effect of induced charging of the oligovalent anion, with a stronger effect on phase separation if the oligovalent anion bears a high number of carboxylic groups.

At first glance, enhanced phase separation in mellitate solutions at lower pH could also be due to enhanced hydrophobic interactions or pronounced “salting-out”. Conformational changes could occur at lower pH caused by repulsive intramolecular interactions. These conformational changes could result in enhanced exposure of hydrophobic patches to the surrounding hydrophilic medium, which could enhance phase separation by introducing additional attractive hydrophobic protein-protein interactions. The antibody’s melting temperature of the first transition peak ( $T_{m1}$ ) determined by DSC is increasing from 54.1°C to 69.3°C by increasing the pH from 3.5 to 6.5 indicating a lower conformational stability at lower pH (see Appendix 2).

Hydrophobic interactions and “salting-out” should be enhanced at higher ionic strength. However, the solid phase which was resulting from precipitation at pH 2.9 and mellitate concentrations of 2 mM - 50 mM was observed to be soluble in NaCl solution. If the attractive protein-protein interactions were mainly caused by hydrophobic interactions or salting-out, the precipitate would not dissolve in NaCl solution. Therefore, precipitation in mellitate may not mainly be driven by hydrophobic interaction but by electrostatic attractive protein-protein interactions induced by mellitate.

However, no experiments on dissolution in NaCl solution were performed with the precipitate formed in 2000 mM mellitate at pH 2.9. Therefore, the mechanism behind precipitation under these conditions could be “salting-out”. At higher salt concentrations the solubility of the positively charged model protein lysozyme has been reported to decrease with decreasing pH (175). Salting-out could therefore be enhanced at lower pH.

In contrast to the pH dependence of phase separation observed here, the maximal width of the miscibility gap at 5°C in citrate buffer (LLPS) was decreasing with decreasing pH (section 4.1.3). This can be explained with the higher maximum negative charge of mellitate, which may enable enhanced cross-linking at lower pH. Binding between the protein and mellitate is supposed to result in higher valences of the mellitate ion. This phenomenon of induced charging may be enhanced at lower pH, where the net charge of the protein increases.

#### 4.2.3. Influence of ionic strength on phase separation

The influence of the ionic strength on phase separation was investigated for protein solutions with mellitate concentrations of 0.2 mM, 0.5 mM and 2 mM. Ionic strength was adjusted by NaCl which was added as part of the mellitate spike solution (see section 3.2.3.6). The results are listed in Table 18 and displayed in Figure 20.

Table 18: Influence of ionic strength (NaCl) on phase separation at pH 5.3. The mellitate and NaCl concentrations correspond to the concentrations after mixing both solutions. The protein concentrations measured in the mixed solution or in the supernatant, if phase separation occurred, are listed in the cells in units of mg/ml. The cells colored in grey indicate that no phase separation was observed after mixing. The cells colored yellow indicate that liquid-solid phase separation was observed and the cell colored purple indicate that liquid-liquid phase separation was observed. The protein concentration was measured using the BCA assay.

c(mellitate) / mM	0.2	0.5	2
0 mM NaCl	3.72	0.01	0.09
10 mM NaCl	7.90	0.34	0.30
30 mM NaCl	7.75	6.91	1.80
50 mM NaCl	7.90	7.68	8.00

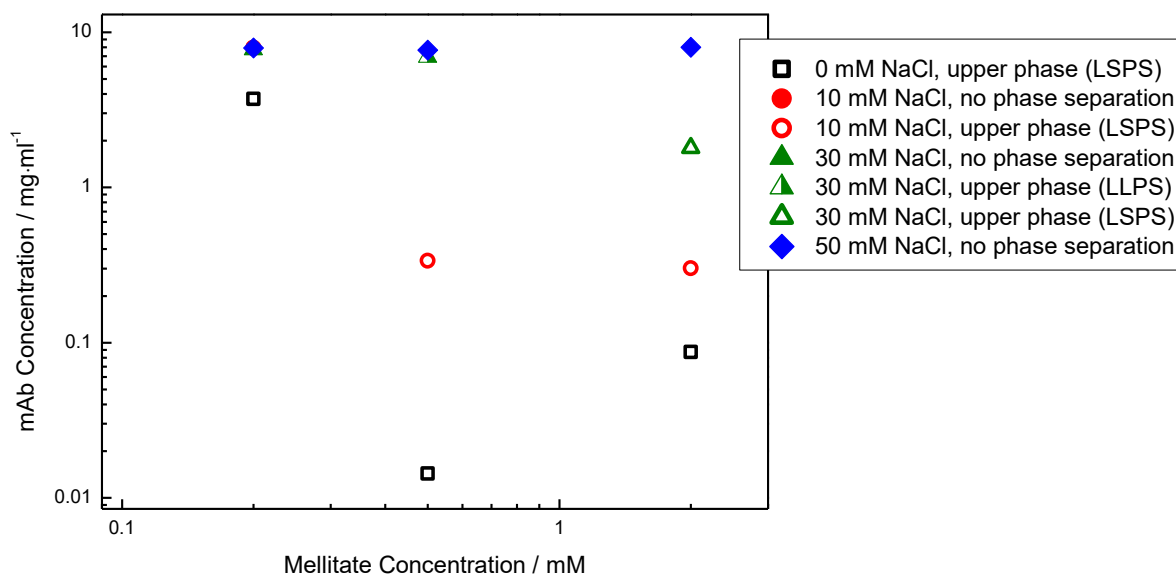


Figure 20: Influence of NaCl and mellitate concentration on phase separation at pH 5.3. The concentration on the X-axis corresponds to the mellitate concentration after mixing both solutions. The protein concentrations measured in the mixed solution or in the supernatant, if phase separation occurred, is plotted on the Y-axis. The symbols are defined as follows: black square: 0 mM NaCl, red circle: 10 mM NaCl, green triangle: 30 mM NaCl, blue rhomb: 50 mM NaCl. Filled symbols represent that no phase separation was observed. Empty symbols represent that LSPS was observed and half-filled symbols represent that LLPS was observed.

In mixed solutions containing 0.2 mM, 0.5 mM and 2 mM mellitate, LSPS was observed. The lowest protein concentration was measured in the supernatant of the solution containing 0.5 mM mellitate.

At a concentration of 0.2 mM mellitate, the addition of 10 mM NaCl lead to a homogeneous solution. The same concentration of NaCl leads to LSPS in the presence of 0.5 mM and 2 mM mellitate. At a concentration of 0.5 mM mellitate, two liquid phases were observed upon addition of 30 mM NaCl. The same concentration of NaCl resulted in LSPS in the presence of 2 mM mellitate. Upon addition of 50 mM NaCl, phase separation was no more observed in any of the 3 tested mellitate concentrations.



The lower the concentration of mellitate, the lower was the NaCl concentration which led to a homogeneous solution. The influence of the mellitate concentration on phase separation was depending on the presence of NaCl. In the absence of NaCl, the protein concentration in the supernatant was increasing upon increasing the mellitate concentration from 0.5 mM to 2 mM. However, in the presence of 30 mM NaCl, the protein concentration in the supernatant was decreasing upon increasing the mellitate concentration from 0.5 mM to 2 mM.

*Higher tendency to homogeneous solution upon increasing ionic strength at lower mellitate concentration*

The lower the concentration of mellitate, the lower was the NaCl concentration leading to a homogenous solution. Applying the model of charge neutralization up to mellitate concentrations of 0.5 mM and charge reversal at higher mellitate concentrations, the protein-protein-mellitate complex would be expected to be most stable at 0.5 mM mellitate with the highest resistance against dissolution caused by ionic strength (150). However, the results indicate the protein-protein mellitate network to be more stable against NaCl addition at 2 mM mellitiate.

According to the theory in the present thesis, mellitate binding to the protein has two opposite effects: at lower anion concentrations it forms the protein-protein-mellitate precipitate whereas at higher anion concentrations precipitation does not occur due to charge reversal and the formation of negatively charged soluble protein-mellitate complexes. NaCl is assumed to weaken mellitate binding to the protein by specific and unspecific effects. Specific effects are the competition for anion binding sites on the protein surface whereas unspecific effects are weakening of the electrostatic interaction through enhanced ionic strength.

In solutions containing 0.5 mM mellitate, protein-mellitate interaction is enhancing network formation by two effects: the charge of the protein is neutralized resulting in decreasing repulsive protein-protein interactions and cross-linking is enhanced. In solutions containing 2 mM mellitate, protein-mellitate interaction has two opposite effects on network formation: charge reversal is taking place thereby increasing repulsive protein-protein interaction and cross-linking is probably enhanced. The addition of NaCl is

weakening the protein-mellitate interaction. Therefore, at 0.5 mM mellitate, the two effects which are enhancing the protein-protein mellitate network are weakened upon NaCl addition. At 2 mM mellitate, charge reversal is reduced and mellitate induced protein-protein cross-linking is reduced upon NaCl addition. The first event is assumed to consolidate the protein-protein-mellitate network whereas the second event is assumed to weaken the protein-protein- mellitate network. The experimental results indicate the second event to dominate as the protein concentration in the supernatant increases upon increasing ionic strength. However, the first event seems to contribute as well, as the effect of increasing protein concentrations in the supernatant by increasing ionic strength is less pronounced at a mellitate concentration of 2 mM compared to 0.5 mM.

#### *Influence of mellitate concentration on phase separation*

This mechanism can also explain the increase and the decrease of the protein concentration in the supernatant as a function of the mellitate concentration ( $\geq 0.5$  mM) in the absence and in the presence of 30 mM NaCl, respectively. In the absence of NaCl the protein network is destabilized at mellitate concentrations higher than 0.5 mM due to charge reversal resulting in repulsive protein-protein interactions. In the presence of 30 mM sodium chloride mellitate binding to the protein is reduced at 0.5 mM and at 2 mM mellitate. However, at a concentration of 0.5 mM mellitate and lower the reduced binding only results in weakening of the protein-protein-mellitate-network. At a concentration of 2 mM mellitate the reduced protein-mellitate binding is assumed to result in weakening of the network and weakening of repulsive protein-protein interactions which are resulting from charge reversal. The reduced repulsive protein-protein interactions may result in lower protein concentrations in the supernatant at higher mellitate concentration (2 mM).

In the field of empirical pharmaceutical formulation development, it is sometimes observed that excipients can have different effects on a defined parameter, such as turbidity or viscosity. The effect of one excipient is depending on the excipients and concentration of excipients which are additionally part of the formulation. One potential reason for such an observation is described here.

#### 4.2.4. Influence of the overall protein concentration on phase behaviour

The influence of the overall protein concentration on phase separation was investigated for mixtures of protein and mellitate. The results are listed in Table 19 and displayed in Figure 21.

Table 19: Influence of the overall protein concentration on phase separation at pH 5.3. The mellitate concentration was adjusted for each protein concentration to keep the molar ratio of mellitate to protein constant. The concentrations of mellitate in the dark blue cells correspond to the concentrations after mixing both solutions. The protein concentrations measured in the mixed solution or in the supernatant, if phase separation occurred, are listed in the cells in units of mg/ml. The cells colored in grey indicate that no phase separation was observed after mixing. The cells colored yellow indicate that liquid-solid phase separation was observed and the cells colored purple indicate that liquid-liquid phase separation was observed. The acronym n.d. indicates that no mixing experiment was performed for this experimental condition. The protein concentration of 26.3 mg/mL measured for a molar ratio of mellitate to protein of 1.9 and a mAb concentration of 22.5 mg/mL may result from a large measurement uncertainty of the BCA assay.

Molar ratio of mellitate to protein	1.9	9.7	97	290
c(mellitate) / mM	0.03	0.17		5
c(mAb) = 2.5 mg/ml	2.54	0.02	n.d.	0.56
c(mellitate) / mM	0.1	0.5	5	15
c(mAb) = 7.5 mg/ml	7.54	0.02	0.79	7.27
c(mellitate) / mM	0.3	1.5	15	45
c(mAb) = 22.5 mg/ml	26.3	0.15	11.8	23.0

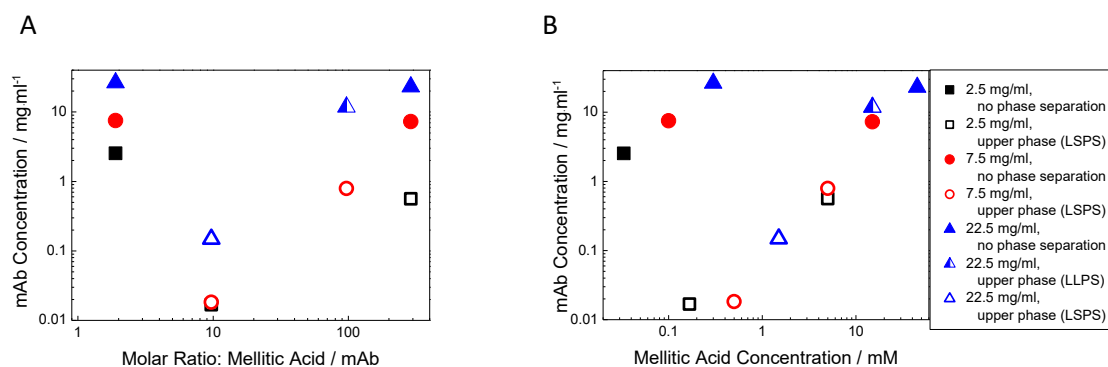


Figure 21: Influence of the overall protein concentration and mellitate concentration on phase separation at pH 5.3. The concentration on the X-axis corresponds to the molar ratio of mellitate to antibody (A) or the mellitate concentration (B) after mixing both solutions. The protein concentrations measured in the mixed solution or in the supernatant, if phase separation occurred, is plotted on the Y-axis. The symbols are defined as follows: black square:  $c(\text{mAb}) = 2.5 \text{ mg/ml}$  after mixing, red circle:  $c(\text{mAb}) = 7.5 \text{ mg/ml}$  after mixing, blue triangle:  $c(\text{mAb}) = 22.5 \text{ mg/ml}$  after mixing. Filled symbols indicate that no phase separation was observed. Empty symbols indicate that LSPS was observed and half-filled symbols indicate that LLPS was observed.

Phase separation was not observed for mixed solutions containing a molar ratio of mellitate to protein of 1.9. In contrast, liquid solid phase separation was observed for all solutions containing a molar ratio of mellitate to protein of 9.7. At a higher ratio of mellitate to mAb, the occurrence of phase separation and the protein concentration in the supernatant was not depending on that ratio but on the absolute mellitate concentration. The similar protein concentrations in the supernatant of 0.56 mg/ml and 0.79 mg/ml in solutions containing 5 mM mellitate and either 2.5 mg/ml or 7.5 mg/ml monoclonal antibody are underlining the dependence of the protein concentration in the supernatant on the total and not the relative mellitate concentration at higher mellitate concentrations.

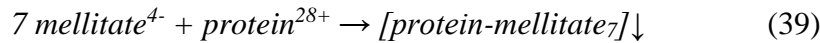
*Theory of the dependence of phase separation on the ratio of mellitate to protein and on the total mellitate concentration*

In a previous section, the protein concentration in the supernatant as a function of the mellitate concentration was discussed. The decrease in the protein concentration at lower anion concentrations was steeper than the increase in protein concentration at higher mellitate concentrations. It was concluded, that this asymmetry was due to stronger anion

binding to the protein at lower anion concentrations. At higher anion concentration the binding to the protein becomes weaker because of charge reversal.

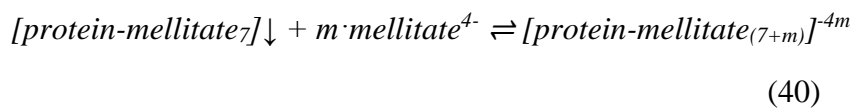
This assumption can also explain the two different mellitate concentration dependencies here.

At lower anion concentration, strong protein-mellitate binding leading to phase separation is assumed. This can be formally written as:



The higher the initial total protein concentration, the higher is the mellitate concentration required for reaching charge neutrality. The occurrence of phase separation at lower mellitate concentrations which is assumed to depend on the degree of protein neutralization would therefore depend on the ratio of mellitate to protein.

The absence of phase separation at higher mellitate concentrations is stated to result from charge reversal. Even though not directly observed by the experimental procedure in this part, the precipitate is assumed to dissolve upon further mellitate addition. For higher anion concentrations, mellitate binding to the protein is assumed to become weaker and the dissolution of the precipitated complex  $[\text{protein-mellitate}_7]\downarrow$  can be described by the following equilibrium:



Here  $m$  is the number of mellitate ions required to provide sufficient negative charge to the protein-mellitate complex  $[\text{protein-mellitate}_{(7+m)}]^{-4m}$  to dissolve one protein molecule from the neutral precipitate complex on a molecular level.

Law of mass action of the equilibrium yields:

$$K = \frac{c([\text{protein-mellitate}_{(7+m)}]^{-4m})}{c^m(\text{mellitate}^{4-}) \cdot c([\text{protein-mellitate}_7])} \quad (41)$$

Based on that equation, a strong dependence of the concentration of the soluble complex  $[\text{protein-mellitate}_{(7+m)}]^{-4m}$  on the free mellitate concentration would be assumed, if  $m$  is assumed to be significantly higher than 1.

The concentration of the precipitate as a solid phase is by convention a constant. This leads to equ (42):

$$K' = \frac{c([\text{protein-mellitate}_{(7+m)}]^{-4m})}{c^m(\text{mellitate}^{4-})} \quad (42)$$

Consequently, the concentration of the soluble species in the supernatant  $[\text{protein-mellitate}_{(7+m)}]^{-4m}$  only depends on the free mellitate concentration in the supernatant and the constant  $K'$ .

The total average concentration of mellitate  $\bar{c}_0$  which is adjusted by sample preparation is the sum of all species formed by mellitate:

$$\bar{c}_0 = 7 \cdot \bar{c}([\text{protein} - \text{mellitate}_7] \downarrow) + \bar{c}(\text{mellitate}^{4-}) + m \cdot \bar{c}([\text{protein} - \text{mellitate}_{(7+m)}]^{-4m}) \quad (43)$$

The concentrations listed here are average concentrations over the total volume of 1.5 ml, without considering that local concentrations in individual phases may be higher or lower.  $7 \cdot \bar{c}([\text{protein} - \text{mellitate}_7] \downarrow)$  is by definition the amount of mellitate in the neutral precipitated complex at that total mellitate concentration ( $\bar{c}_0$ ) where mellitate binding is resulting in a neutral protein-mellitate complex (condition of charge neutralization) and not the amount of mellitate in the complex in equilibrium when part of the insoluble complex has already been disappeared by charge reversal.

The following calculations are based on the assumption that the amount of mellitate as part of the precipitate reaches its maximum at a total mellitate concentration where the protein concentration of the supernatant is minimal. In addition, it is assumed that the amount of mellitate as part of the precipitate is lower or equal to the total amount of mellitate added. Under these assumptions, experimental values of the total mellitate concentrations where the protein concentration in the supernatant is minimal can be used to estimate the maximal mellitate amount bound in the precipitated complex. The actual mellitate amount bound in the neutral complex may be slightly lower assuming charge neutralization to occur at slightly lower mellitate concentrations (see section 4.2.1) and assuming a small part of

mellitate to be soluble in the supernatant and not bound in the precipitate. The minimal protein concentration in the supernatant at pH 5.3 was observed between mellitate concentrations of 0.17 mM and 1.5 mM for protein concentrations between 2.5 mg/ml and 22.5 mg/ml (Table 17). These mellitate concentrations (0.17 mM – 1.5 mM), corresponding to the maximal mellitate amounts in the neutral complex, are low compared to the total concentration of mellitate required to obtain a homogeneous solution without phase separation. The total anion concentration required to increase the protein concentration in the supernatant above 7.5 mg/ml (0.052 mM) is about 15 mM for the protein concentrations of 7.5 mg/ml and 22.5 mg/ml. For higher total mellitate concentrations where the precipitate is about to disappear, the mellitate amounts bound in the neutral complex can therefore be neglected.

Equ (43) then simplifies:

$$\bar{c}_0 \approx \bar{c}(\text{mellitate}^{4-}) + m \cdot \bar{c} \left( [\text{protein} - \text{mellitate}_{(7+m)}]^{-4m} \right) \quad (44)$$

The maximal volume of the precipitate can be estimated by the maximal volume of precipitated protein. Assuming the partial specific volume of the protein (0.728 ml/g, see section 4.1.5) to remain approximately constant upon precipitation and assuming the protein to contribute much stronger to the precipitated volume than the mellitate, the maximal volume fraction of the precipitate is 1.64 % ( $0.728 \text{ ml}_{\text{protein/g}} \times 22.5 \text{ g/l}_{\text{total}} = 16.4 \text{ ml}_{\text{protein/l}_{\text{total}}}$ ). Therefore, the average concentrations  $\bar{c}(\text{mellitate}^{4-})$  and  $\bar{c} \left( [\text{protein} - \text{mellitate}_{(7+m)}]^{-4m} \right)$  are almost equal to the concentrations  $c(\text{mellitate}^{4-})$  and  $c \left( [\text{protein} - \text{mellitate}_{(7+m)}]^{-4m} \right)$  in the supernatant.

Therefore, inserting equ (42) into equ (44) yields:

$$\bar{c}_0 \approx \sqrt[m]{\frac{c([\text{protein} - \text{mellitate}_{(7+m)}]^{-4m})}{K'}} + m \cdot c \left( [\text{protein} - \text{mellitate}_{(7+m)}]^{-4m} \right) \quad (45)$$

Consequently, the concentration of the soluble protein-mellitate complex  $[protein-mellitate_{(7+m)}]^{-4m}$  is only dependent on the total concentration of mellitate. At anion concentrations higher than the anion concentration of minimal protein concentration in the supernatant, the protein concentration measured in the supernatant is supposed to be mainly composed of the soluble overcharged protein-mellitate complex  $[protein-mellitate_{(7+m)}]^{-4m}$ . Under the given assumptions and for sufficiently high anion concentrations, these calculations can explain why the protein concentration in the supernatant and likewise the width of the miscibility gap depends on the total mellitate concentration but not on the total protein concentration as experimentally observed.

The occurrence of phase separation as a function of protein concentration depends on the width of the miscibility gap but just as well on the position of the total protein concentration in relation to the width of the miscibility gap. Therefore, phase separation can be observed for an overall protein concentration of 22.5 mg/ml for a mellitate concentration of 15 mM, which would not be detectable for an overall protein concentration of 7.5 mg/ml (Table 19). As the concentration of the protein in the supernatant was measured, one can distinguish between an effect of the total protein concentration on the miscibility gap and an effect of the total protein concentration on the relative position to the miscibility gap. The results as listed in Table 19 indicate the occurrence of phase separation at higher anion concentrations to be mainly depending on the overall protein concentration due to the different positions related to the position of the miscibility gap and to a lesser extent due a change of the width of the miscibility gap.

#### *Calculation of the variable constants $m$ and $K'$*

For the calculation of  $K'$  equ (42) and equ (43) are combined using the total mellitate concentration of minimal protein concentration in the supernatant  $c(mellitate - prec)$  instead of  $7 \cdot c([protein - mellitate_7] \downarrow)$  for estimating the amount of mellitate bound in the precipitate at the condition of charge neutralization. In addition, as derived above, the average total concentrations of the individual soluble species are again assumed to be approximately equal to the concentrations of the individual soluble species in the supernatant.



$$K' = \frac{c([protein-mellitate_{(7+m)}]^{-4m})}{(\bar{c}_0 - c(mellitate-prec) - mc([protein-mellitate_{(7+m)}]^{-4m}))^m} \quad (46)$$

The protein concentration in the supernatant corresponding to  $c([protein-mellitate_{(7+m)}]^{-4m})$  is a function of the known total mellitate concentration  $\bar{c}_0$  and the estimated mellitate concentration bound in the neutral complex  $c(mellitate-prec)$ . Therefore, an equation with the two unknown variables  $K'$  and  $m$  is resulting. Assuming  $K'$  and  $m$  to be constant for a higher range of anion and overall protein concentrations, more than one equation with two unknown variables can be developed and  $K'$  and  $m$  can be determined.

The values underlying the calculation of  $K'$  and  $m$  are listed in Table 20.

Table 20: Concentrations of different species formed by mellitate required for calculating  $K'$  and  $m$ .  $\bar{c}(mellitate - prec)$  corresponds to the mellitate concentration complexed in the neutral protein-mellitate complex at that total mellitate concentration  $\bar{c}_0$ , where mellitate binding is resulting in a neutral protein-mellitate complex. This value was estimated from the mellitate concentration  $\bar{c}_0$ , where the protein concentration in the supernatant is minimal.  $\bar{c}_0$  corresponds to the total mellitate concentration in the whole system. The concentration of the soluble protein-mellitate complex  $[protein-mellitate_{(7+m)}]^{-4m}$  corresponds to the measured protein concentration in the supernatant. The soluble protein-mellitate complex is assumed to dissolve from the insoluble complex at a defined but unknown value of  $m$ .

		$\bar{c}$ (mellitate- prec)	$\bar{c}_0 - \bar{c}$ (mellitate- prec)	$c([protein-mel-litate_{(7+m)}]^{-4m})$
1)	5 mM mellitate, c(mAb) = 2.5 mg/ml	0.17 mM	4.83 mM	0.004 mM
2)	5 mM mellitate, c(mAb) = 7.5 mg/ml	0.5 mM	4.5 mM	0.005 mM
3)	15 mM mellitate, c(mAb) = 22.5 mg/ml	1.5 mM	13.5 mM	0.081 mM

$m$  was determined by equating  $K'$  from equ (46) for two experimental data sets. The experimental data set 1 and 3 as well as 2 and 3 were combined. The experimental data sets

1 and 2 were not combined due to the similarity of their values.  $m$  was then calculated using a numerical approach provided in the internet (176). The algorithm behind the numerical approach is an extension of the Newton's approach for the approximation of roots of various dimensions (176). Finally,  $K'$  was calculated from equ (46). The results of  $m$  and  $K'$  are listed in Table 21.

Table 21: Results of  $m$  and  $K'$  as defined by equ (46), calculated with values as listed in Table 20.

	$m$	$K'$
1) + 3) (from Table 20)	3.0	$37 \text{ M}^{-2.0}$
2) + 3) (from Table 20)	2.5	$3.8 \text{ M}^{-1.5}$

The number of binding mellitate ions  $m$  required to dissolve the negatively charged complex  $[\text{protein-mellitate}_{(7+m)}]^{-4m}$  out of the neutral protein-mellitate precipitate is similar for both combinations, with values between 2.5 and 3.0. The values of  $K'$  strongly deviate between  $3.8 \text{ M}^{-1.5}$  and  $37 \text{ M}^{-2.0}$ . The differences could occur due to the influence of  $m$  on  $K'$ . Smaller measurement errors in the determination of  $\bar{c}$  (*mellitate-prec*) or  $c([\text{protein-mellitate}_{(7+m)}]^{-4m})$  could result in high differences in  $K'$ . In addition the deviation could be due to a simplified model. As mentioned in section 4.2.1 the mellitate concentration where the lowest protein concentration in the supernatant is measured may not precisely correspond to the mellitate concentration where the insoluble complex is neutral, as cross-linking may affect the protein concentration in the supernatant. Finally, the effect of ionic strength which increases with the overall protein concentrations is not covered by the theory.

In equilibrium, the mellitate is assumed to be distributed in different species: As part of the solid complex, as part of the soluble complex  $[\text{protein-mellitate}_x]^{-y}$  and free and uncomplexed. Three mellitate ions are assumed to be needed to dissolve a negatively charged protein-mellitate complex from the neutral precipitated complex. The neutral precipitated complex may contain about 9.7 mellitate ions per protein. Therefore, in sum, the soluble protein-mellitate complex  $[\text{protein-mellitate}_x]^{-y}$  may contain  $3 + 9.7 = 12.7$  mellitate ions per protein. However, the actual charge of this complex is not known. Assuming three mellitate ions to be binding to the protein as part of the neutral protein-

mellitate precipitate resulting in dissolution ( $m = 3$ ), the three species would be distributed as listed in Table 22.

Table 22: Calculated equilibrium of species containing mellitate in the mellitate concentration region, where the occurrence of phase separation is not depending on the ratio but on the absolute mellitate concentration. Mellitate is assumed to occur in the remaining precipitated complex, in the soluble negatively charged complex  $[protein-mellitate_x]^y$  and as part of the unbound free mellitate. For the calculations it is assumed that the negatively charged complex dissolves from the insoluble neutral protein-mellitate complex if three mellitate ions are binding to a protein of the neutral protein-mellitate complex. The mellitate concentration remaining in the precipitated complex was calculated as product of  $\bar{c}$  (mellitate-prec) and the protein fraction which is remaining in the precipitated complex ( $1-c(mab-supernatant)/c(mab-total)$ ). The concentration of mellitate in the complex  $[protein-mellitate_x]^y$  is calculated as the sum of the mellitate binding to the neutral protein-mellitate complex ( $3 \times c(mab-supernatant)$ ) and the fraction of mellitate as part of the neutral protein-mellitate complex which has dissolved ( $c(mab-supernatant) \times \bar{c} (mellitate-prec)/c(mab-total)$ ). The free mellitate was calculated as the difference between the total mellitate concentration and the mellitate as part of soluble and precipitated protein-mellitate complexes.

	$c(mAb-supernatant)$	$c(mellitate)$ in the soluble complex $[protein-mellitate_x]^y$	$\bar{c}$ (mellitate) remaining in the precipitated complex	$c(mellitate)$ - free
5 mM mellitate, $c(mAb-total) = 2.5$ mg/ml	0.004 mM (0.56 mg/ml)	0.05 mM	0.13 mM	4.82 mM
5 mM mellitate, $c(mAb-total) = 7.5$ mg/ml	0.005 mM (0.79 mg/ml)	0.07 mM	0.45 mM	4.48 mM
15 mM mellitate, $c(mAb-total) = 22.5$ mg/ml	0.081 mM (11.8 mg/ml)	1.03 mM	0.71 mM	13.26 mM

The amount of free mellitate in equilibrium is much higher than the amount of mellitate complexed in the soluble negatively charged protein-mellitate complexes. Hence, high amounts of free mellitate are required to dissolve part of the protein from the precipitated complex.

*Calculation of the mellitate concentration required to dissolve the complex*

The total mellitate concentration required to increase the protein concentration in the supernatant above 2.5 mg/ml, 7.5 mg/ml or 22.5 mg/ml can be calculated using equ (46). A numeric solution of equ (46) was found by using a free website (176). Thus, the mellitate concentration required for forming a homogeneous solution without phase separation in a protein solution containing 2.5 mg/ml, 7.5 mg/ml or 22.5 mg/ml protein can be calculated. The calculated values are listed in Table 23.

Table 23: Calculated (equ (46)) maximal mellitate concentrations at which precipitation would be expected. Values of  $K'$  and  $m$  were taken as presented in Table 21.

		Maximal calculated mellitate concentration at which phase separation is expected / mM	Experimentally determined mellitate concentration at which phase separation disappears
2.5 mg/ml = 0.017 mM	1) + 3) $K' = 37 \text{ M}^{-2.0}$ $m = 3.0$	8.24	> 5 mM
7.5 mg/ml = 0.052 mM		12.1	> 5 mM; < 15 mM
22.5 mg/ml = 0.155 mM		18.1	> 15 mM; < 45 mM
2.5 mg/ml = 0.017 mM	2) + 3) $K' = 3.8 \text{ M}^{-1.5}$ $m = 2.5$	7.37	> 5 mM
7.5 mg/ml = 0.052 mM		11.6	> 5 mM; < 15 mM
22.5 mg/ml = 0.155 mM		18.7	> 15 mM; < 45 mM

All the calculated mellitate concentrations confirm with the experimentally determined phase boundaries. However, the large intervals in the tested mellitate concentration of the experimentally determined phase boundaries prevent more accurate conclusions.

Instead of large differences in  $K'$  for both approaches, the calculated mellitate concentration which is required to dissolve the lower phase is similar for both fittings. Higher values of  $K'$  indicate enhanced binding between mellitate and the neutral complex  $[Protein-mellitate]_{\downarrow}$ , resulting in enhanced dissolution of the precipitate and higher protein concentrations in the supernatant. The first approach with higher  $K'$  and higher  $m$  values seems to reveal in similar mellitate concentrations, required to dissolve the precipitate as the approach with lower  $K'$  and lower values of  $m$ . If a higher negative charge, related to the value of the variable  $m$ , is required to dissolve the precipitate, a higher binding constant  $K'$  is required to result in dissolution under the same conditions.

#### *Estimating the influence of ionic strength on phase separation*

A protein solution with proteins of either positive or negative net charge with higher overall protein concentration is generally assumed to have a higher ionic strength. The experimental design of spiking instead of dialysis additionally results in higher concentrations of counterions and therefore enhanced ionic strength in protein solutions of higher overall protein concentration, even if all of the proteins are neutralized by mellitate binding and would therefore not themselves contribute to ionic strength. As shown in section 0 increasing ionic strength is resulting in dissolution of the precipitate.

By considering these results the protein concentrations in the supernatant would be expected to increase with increasing overall protein concentration. A higher protein concentration of 0.15 mg/ml in the supernatant of the sample containing 22.5 mg/ml compared to the lower protein concentration of 0.02 mg/ml in the supernatant of samples containing 2.5 and 7.5 mg/ml protein was observed. This difference could be due to the higher ionic strength in mixed systems of higher protein concentrations.

#### 4.2.5. Summary and conclusions

The occurrence of phase separation in antibody solutions upon addition of oligovalent anions depends on the charge of the added anion, the pH, ionic strength, the concentration of the oligovalent anion and the overall protein concentration.

The maximum possible charge of the oligovalent anion (charge after complete dissociation) seems to have a stronger influence on phase separation than the charge that would be expected at a given pH (incomplete dissociation of the weak acid). Phase separation in the presence of mellitate was enhanced at lower pH where the protein net charge increases. Ionic strength had a dissolving effect on the precipitate. Phase separation followed a non-monotonic trend upon increasing the anion concentration. The protein concentration in the supernatant first decreased with increasing anion concentration but increased with increasing anion concentration at larger anion concentrations. At anion concentrations lower than the anion concentration of minimal protein concentration in the supernatant, a dependence of the occurrence of phase separation on the ratio between anion and protein was observed. At anion concentrations higher than the concentration of minimal protein concentration in the supernatant, the protein concentration in the supernatant was observed to depend on the total anion concentration and not on the protein concentration. A theoretical model was applied and the number of mellitate ions required to dissolve the neutral protein-mellitate precipitate  $m$  as well as the equilibrium constant  $K'$  for mellitate binding were calculated. The experimental results indicate that dissolution of individual proteins from the neutral protein-mellitate precipitate occurs upon binding of additional 2.5 – 3 mellitate ions.

The non-monotonic trend of the protein concentration in the supernatant as a function of anion concentration was observed before in section 4.1 for antibody solutions upon citrate addition. In addition to the difference of the state of the lower phase, i.e. LLPS in citrate instead of LSPS predominating in mellitate, two major differences between phase separation induced by either citrate or mellitate were seen: First, phase separation was enhanced at lower pH in the presence of mellitate whereas it was reduced at lower pH in the presence of citrate. Second, the disappearance of LLPS in the presence of higher concentrations of citrate may be mainly caused by concomitantly increasing ionic strength,

whereas the disappearance of LSPS in the presence of higher concentrations of mellitate is assumed to be mainly induced by protein charge reversal, resulting from binding of mellitate to the protein.

### **4.3. PROTEIN DIFFUSION**

Measurements of the diffusion of proteins in pure water by DLS have been shown to result in much higher diffusion coefficients for the protein than would be expected from the size of the protein (48, 103). In the following section this effect will be investigated at different pH values and therefore with differently charged proteins. A theoretical explanation is presented for comparison.

#### **4.3.1. Hydrodynamic diameter of pH-dependent protein solutions**

In the following part the influence of the protein net charge on its diffusion coefficient and its hydrodynamic diameter is described. The net charge of a protein is pH dependent. The protein solution was first dialyzed against a NaCl solution and later against water to first remove electrostatically interacting ions such as citrate from the protein solution and later remove NaCl. (See section 3.2.2.1). The procedure was performed at pH 8.5 near the experimental isoelectric point of the protein ( $pI \sim 8.7$ ) (determined as described in section 4.1.1, results shown in Appendix 1). At pH 8.5 the positive net charge of the protein is low and therefore the amount of negatively charged counterions remaining in solution is reduced compared to a dialysis at e.g. pH 6.0. The pH of the solution was then adjusted to values between pH 8.5 and pH 4.1 using hydrochloric acid. The protons added by adjusting the pH were partly binding to the protein and partly changing the pH. The major part of the protons is assumed to be binding to the protein resulting in a higher valence of the protein. The chloride ions added concomitantly were acting as counterions but they could, to some extent, also bind to the protein and thereby reduce the actual charge (Debye-Hückel-Henry charge  $z_{DHH}$  as defined by Filoti et al. (113)) of the protein. The valence of the antibody at the respective pH was derived from pH titration data as reported elsewhere (23, 113, 177) (see section 4.1.1). If some of the chloride ions bind to the protein, the valence determined by pH-titration is higher than the actual Debye-Hückel-Henry charge as defined by Filoti et al. (113) and described in detail in section 2.4.2.

The diffusion coefficient of the protein of pH-adjusted solutions was determined by DLS (see section 3.2.1.9). Measured diffusion coefficients were converted to apparent diameters by equ (3). The results are depicted in Figure 22. The theoretical curve as calculated from equ (25) is depicted in Figure 22 as well. The curve describes the theoretical size of the protein which is expected due to coupled diffusion between the protein and its counterions assuming only proteins and counterions without additional salt to be present and excluding attractive protein-protein interactions. For the calculation the hydrodynamic diameter of the protein was assumed to be 10.6 nm, corresponding to a diffusion coefficient  $D_2$  of 40.4  $\mu\text{m}^2/\text{s}$  at 20°C. This value was estimated from measurements of the protein at different concentration and an extrapolation to infinite dilution in 10 mM citrate buffer pH 6.0 at various ionic strengths (see section 4.3.2.3.1, as the value did not change with ionic strength, it was regarded to be mainly independent from the solution conditions and therefore suitable to be used as a molecule specific value). The value shall account for size, shape and hydration of the protein at pH 6.0 but it does not account for interactions between proteins or interactions between the protein and its counterions.

The diffusion coefficient  $D_3$  of the chloride ion was reported at 25°C ( $D_3 = 2032 \mu\text{m}^2/\text{s}$  at 25°C) (119). Therefore a conversion was performed to the measurement temperature of 20°C by correcting for viscosity and temperature effects as described in (94) resulting in  $D_3$  of 1775  $\mu\text{m}^2/\text{s}$  at 20°C. For the conversion the viscosity of water instead of the viscosity of the protein solutions was taken, neglecting slight increases in viscosity induced by the proteins in solution (1.002 mPas at 20°C and 0.890 mPas at 25°C) (119).



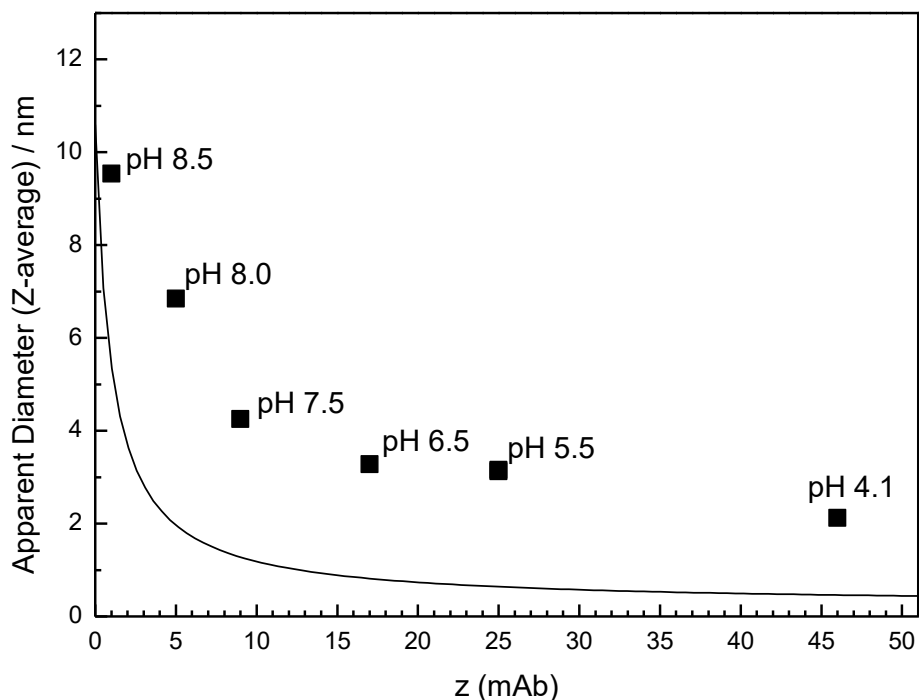


Figure 22: Calculated (solid line) and experimental (squares) diameters of a monoclonal antibody with chloride counterions in water depending on the net charge,  $z_2$ , of the antibody. The diffusion coefficient  $D$  was calculated by equ (25) taking  $D_2 = 4.04 \cdot 10^{-11} \text{ m}^2/\text{s}$  and  $D_3 = 1.775 \cdot 10^{-9} \text{ m}^2/\text{s}$  as parameters. The calculated diameter was derived from the apparent diffusion coefficient  $D$  by the Stokes-Einstein equation (equ (3)). Experimental data correspond to the value of the z-average at different pH values for an antibody concentration of 25 mg/ml at 20°C (Malvern Zetasizer NanoZS ZEN3600).

The experimental apparent diameter of the protein decreased from 9.5 nm at pH 8.5 to 2.1 nm at pH 4.1. The observed trend is consistent with the calculated diameter obtained by equ (25). The calculated curve describes the theoretical size which is expected due to coupled diffusion of the protein and its counterions. According to equ (25), the apparent size of the protein is assumed to be independent of the protein concentration. However, actual experimental values were higher than the calculated diameters depicted by the solid curve in Figure 22. This could be due to attractive protein-protein interactions which are assumed to decrease the experimental diffusion coefficient  $D$  with increasing protein concentration. Attractive protein-protein interactions are not considered by equ (25). In addition, deviations in solution viscosity induced by the proteins not considered here could result in lower diffusion and thus larger apparent protein diameters. Furthermore, the value

of  $D_2$  corresponding to a hydrodynamic diameter of 10.6 nm which should account for the protein size, shape and hydration could not appropriately wrongly chosen not accounting for the overall hydrodynamic drag. In addition, cross-term diffusion caused by chemical gradients influencing the diffusion of the oppositely charged species may take place. Besides this, impurities such as aggregates, foreign particles or traces of NaCl could result in larger values of z-average. This hypothesis is supported by PDI values in the range between 0.17 and 0.37 indicating midrange polydispersity (178). And finally, if part of the chloride counterions are not freely diffusing but binding to the protein, the actual charge  $z_{DHH}$  might be lower compared to the charge determined by pH valence titration. This would also result in higher experimental diameters than expected by equ (25). Factors affecting the apparent diameter of a protein are summarized in Table 24. Thus, quite a few factors are potentially increasing the apparent diameter of a protein, but explicit reasons for lower apparent diameters are limited to repulsive Coulomb protein-protein interactions and the phenomenon of mutual electrostatic interaction and resulting coupled diffusion between counterions and the protein. Both effects which would result in lower apparent diameters are covered by equ (25). To further elucidate the latter phenomenon, the following experiments were conducted at different protein concentrations and diffusion coefficients were extrapolated to zero concentration. Thereby effects occurring due to additional attractive protein-protein interactions which are assumed to vanish at infinite dilution can be excluded with greater confidence.

Table 24: Factors that influence the apparent diameter measured by DLS of a protein of constant size.

Factors affecting the hydrodynamic diameter to larger values than expected	Factors affecting the hydrodynamic diameter to lower values than expected
Attractive protein-protein interactions (equ (10))	Repulsive protein-protein interactions (equ (23) and equ (25))
Viscosity of the protein solution (if changes are not considered)	Coupled diffusion of freely diffusing counterions and the protein at low concentration of effective counterions (equ (23) and equ (25))
Hydration	
Deviation in shape from a sphere	
Impurities of larger particles in solution	
Hard-sphere crowding (179)	

### 4.3.2. $D_0$ and $k_D$ values as a function of buffer species and concentration, pH and salt

In the following section diffusion coefficients are examined in the absence of buffer and in the presence of different buffers. The influence of the pH, the presence of salt and the buffer concentration on diffusion coefficients is investigated.

#### 4.3.2.1. Diffusion coefficients in the absence of buffer

##### 4.3.2.1.1. Dependence of the diffusion coefficient on the pH in the absence of buffer

#### Experimental data

Assuming small amounts of buffers to strongly influence the colloidal interactions of proteins in solution, the diffusion of the antibody in buffer-free conditions was first examined. Through the concept of  $k_D$ , the diffusion is assumed to be strongly related to colloidal interactions of the proteins (equ (8) - equ (10)). The citrate-free protein solution at pH 6.0 with a protein concentration of  $25 (\pm 2)$  mg/ml was titrated with HCl and NaOH to pH 3.2, pH 5.5, pH 6.5 and pH 7.0. Dilutions to protein concentrations between 2.5 and 20 mg/ml were performed with MilliQ water. The pH was assumed to stay approximately constant upon dilution due to the buffer capacity of the protein (117). The results of DLS measurements performed as described in section 3.2.1.10 are displayed in Figure 23.

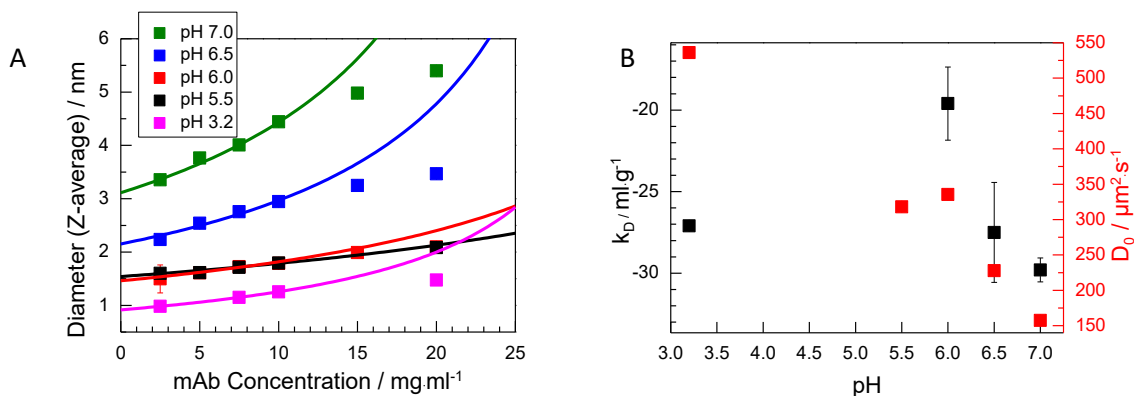


Figure 23: Influence of the pH on the hydrodynamic diameter, the  $k_D$  and on  $D_0$  of the mAb diluted with pure water as measured by DLS (Wyatt, Plate Reader, 25°C). The hydrodynamic diameters shown in Figure 23A were converted from the measured diffusion coefficients with equ (3).  $k_D$  and  $D_0$  were obtained as described in section 3.2.3.8 by fitting data of the diffusion coefficient to equ (10) (plot not shown here). The solid lines in Figure 23A show the results of the curve fitting converted to diameters by equ (3) and equ (15) as described in section 2.3.1.2.  $k_D$  and  $D_0$  values as a function of pH are separately depicted in Figure 23B. The linear fit was limited to data between 2.5 and 10 mg/mL. For higher protein concentrations a deviation from linearity (plot of the diffusion coefficient vs mAb concentration, not shown here) was often observed. In the presented figure (plot of apparent diameter vs mAb concentration), this deviation appears in the deviation between the fitted curve and the measured values.

The hydrodynamic diameter extrapolated to zero concentration increased with increasing pH from 0.9 nm at pH 3.2 to 3.1 nm at pH 7.0. The apparent inverse trend of the protein solutions at pH 5.5 and pH 6.0 is within the range of the measuring uncertainty. The  $k_D$  as defined by equ (10) was negative in all cases, with values ranging from -29.8 ml/g to -13.8 ml/g. Excluding the value of -27.1 ml/g at pH 3.2, the  $k_D$  was decreasing with increasing pH.

#### *Infinite-dilution diameters*

Assuming the protein to form a compact sphere without hydration shell the minimal radius can be calculated as follows (94):

$$r = \sqrt[3]{\frac{3M\bar{v}}{4\pi N_A}} \quad (47)$$

Here  $M$  is the molecular weight of the protein,  $\bar{v}$  is the partial specific volume of the protein and  $N_A$  is Avogadro's number (94). Supposing a partial specific volume of 0.728 cm<sup>3</sup>.g<sup>-1</sup> (9) and a molecular weight of 145,000 Da, the minimal diameter of the antibody is 6.9 nm.

Lower values as determined here are most likely not due to the actual physical size of the particle itself as fragmentation upon dialysis against water or 300 mM NaCl is very unlikely. Repulsive protein-protein interactions may result in lower diameters. Even at very low protein concentrations these interactions may influence diffusion due to the long range of electrostatic interactions at very low ionic strength. In combination with repulsive protein-protein interactions electrostatic coupled diffusion between the charged protein and its counterions is proposed to be the origin of these low values for the radius. Electrostatic interaction between the protein and its counterions is assumed to depend on the actual charge  $z_{DHH}$  of the protein as well as the effective counterion concentration (94).

The charge of the antibody increases with decreasing pH as the experimental pI of the protein is 8.7 (as shown in section 4.1.1). This assumption is in accordance with the observation of decreasing values of infinite-dilution diameter with decreasing pH (Figure 23). However, data obtained by titrating the protein solution with NaOH to more basic pH values (pH 6.5 and pH 7.0) should be considered with some caution as small amounts of NaCl (0.5 mM at pH 6.5 and 1 mM at pH 7.0 at 20 mg/ml as calculated from titration data) were formed by neutralizing the protein solution with NaOH. The observation of increasing infinite-dilution diameter values with increasing pH between pH 6.0 and 7.0 might be due to the reduced charge of the protein and due to the presence of NaCl in solution at higher pH.

The infinite-dilution diameter reported here are much lower than the experimental diameters of monoclonal antibodies reported in the literature with values ranging from 9.7 nm to 11.8 nm (49, 180). Experimental smaller diameters than expected have been determined for several proteins at very low ionic strength. For BSA (Mw = 66 kDa (181)) with an estimated hydrodynamic diameter of 10.2 nm (value is the infinite dilution diameter at pH 3.65 and various ionic strengths (10 mM - 200 mM)), a diameter of 5.2 nm has been reported at 10 mM ionic strength at pH 3.1 (182). Lysozyme (Mw = 14.3 kDa (181)) with a hydrodynamic diameter of 4.1 nm at 150 mM ionic strength was apparently 4-times smaller (0.9 nm) at 0 mM ionic strength (and a protein concentration of 0.45 % for both values, pH 3.3 – 3.6) (103). For a dual-variable domain immunoglobulin (Mw = 200 kDa (183)) a hydrodynamic diameter of 13.1 nm was reported, which significantly decreased to values smaller than 3.3 nm in water at protein concentrations > 2 mg/ml (48). The latter

study suggests that the unrealistically small diameters vanish at protein concentration below 2 mg/ml (48). In the present study, no measurements were performed to examine the diffusion in this concentration regime, due to bad data quality, as the scattering density of the protein decreased.

#### *k<sub>D</sub> values*

The diffusion coefficient decreased with increasing protein concentration for all tested pH values and the protein diameters converted by using equ (3) were therefore increasing with increasing protein concentration. The  $k_D$  as defined by equ (10) was negative in all cases, with values ranging from -29.8 ml/g to -13.8 ml/g. Excluding the value of -27.1 ml/g at pH 3.2, the  $k_D$  was decreasing with increasing pH. This trend is to be expected assuming the positive net charge of the protein to decrease with increasing pH up to the isoelectric point of pH 8.7 where the net charge becomes zero. A decreasing net charge is accompanied by decreasing Coulomb repulsive interactions. The unexpected low  $k_D$  at pH 3.2 could be due to unfolding or structural changes which are more likely at extreme pH values. Structural changes could result in different protein-protein interactions.

However, for this experimental setup, the surrounding medium, composed of water and chloride counterions or even additional NaCl at pH 6.5 and pH 7.0, changes its composition by diluting the protein solution with water. Therefore, a pseudobinary concept, as the concept of  $k_D$  should be interpreted with caution.

#### Calculating diffusion coefficients in a three-component system on the basis of valence data

For more accurate statements, equ (23) was used to calculate diffusion coefficients assuming a three-component system. The results are shown in Figure 24. The charge was taken from valence titration data and a differentiation between bound and freely diffusing counterions was neglected. All counterions were considered to be freely diffusing. The counterion and coion concentration required for calculating using equ (23), were estimated from titration data as presented before in chapter 4.1.1. The calculated diameter of the antibody increases from 0.37 nm at pH 3.2 (in the absence of NaCl) to 1.59 nm at pH 7.0 (in the presence of small amounts of NaCl: 0.5 mM at pH 6.5 and 1 mM at pH 7.0, both at 20 mg/ml). The diameter does not change with the antibody concentration. At pH 3.2, pH

5.5 and pH 6.0 the chloride ions are exclusively protein-related counterions assumed to be freely diffusing. Therefore, in principle equ (25) could also be used, in which  $D$  is independent of the protein concentration. According to the model described in section 2.3.1.3, the diameter is not depending on the protein concentration if no additional excipients except component 2 and protein related counterions are present.

*Effects of NaCl in the protein solution on the calculated diffusion coefficients*

At pH 6.5 and pH 7.0, where the pH was adjusted by titration with NaOH, the formed NaCl diluted with decreasing protein concentration as the dilution was performed with MilliQ and not with NaCl solution. The consequence of the dilution with water is a constant ratio of effective counterions (here chloride) to protein over the range of the protein concentrations, assuming the charge of the protein to be not affected by dilution. Therefore, equ (24) applies and the calculated diameter does not depend on the protein concentration.

The NaCl formed by neutralization does not affect the slope of the calculated diffusion coefficient as a function of protein concentration but it does affect the magnitude of the calculated diffusion coefficient and the resulting diameter (Figure 24). The actual value of the calculated diameter is increased compared to the calculated diameter expected in the absence of NaCl. For example, at pH 7.0 the calculated diameter in the absence of additional salt is 1.25 nm whereas the NaCl that formed by pH titration increases the calculated diameter to 1.94 nm (Figure 24).

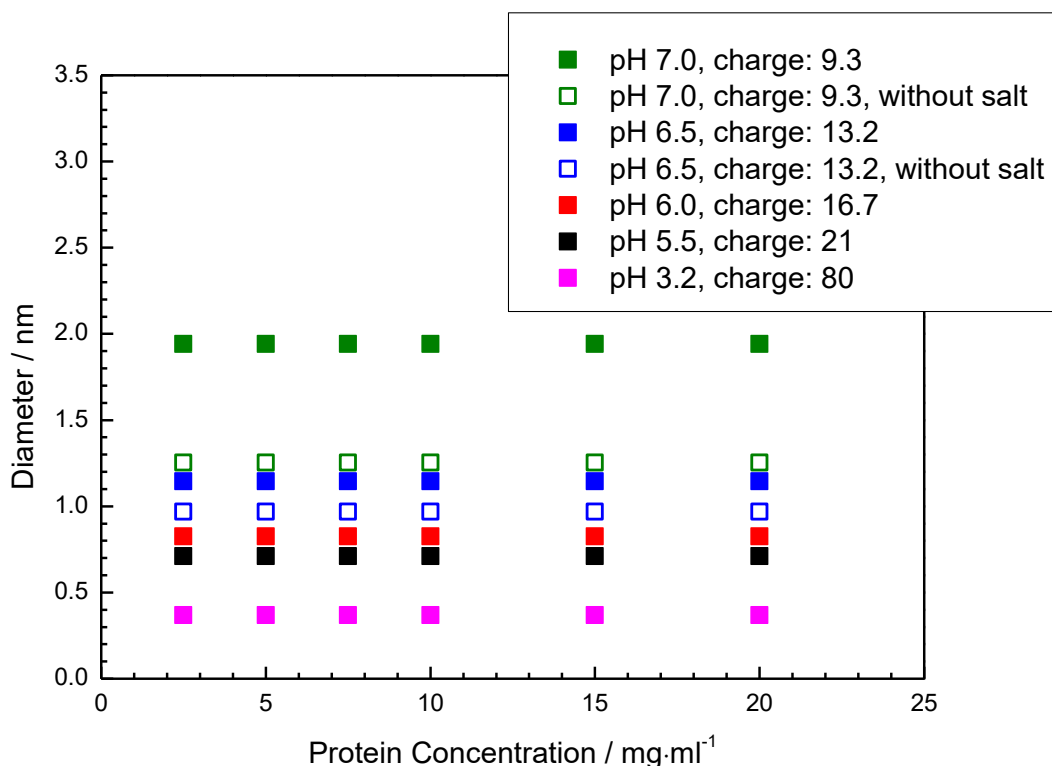


Figure 24: Calculation of hydrodynamic diameters of the mAb of defined charge using equ (23) and equ (3). Assumption of a three-component system consisting of water, charged mAbs and counterions with coupled protein counterion diffusion. All ions in solution are assumed to be freely diffusing but their diffusion is assumed to be coupled. Attractive interactions between the antibodies are not covered by this model. Titration to pH 6.5 and pH 7.0 was performed with NaOH, resulting in small amounts of NaCl formed (1 mM at pH 7.0 and 0.5 mM at pH 6.5, both at 20 mg/ml). The dilution of NaCl formed at pH 6.5 and pH 7.0 upon protein dilution with MilliQ was covered by the model. For comparison, the hypothetical diameter in protein solutions without formed NaCl were also calculated (without additional salt, only chloride counterions, open symbols).

### Comparison of calculated with experimental data

#### *Apparent diameter at infinite dilution*

The experimental diameter at infinite dilution is larger than expected by the model of three-component effects. Possible explanations for this discrepancy are a lower actual charge of the protein, a certain degree of polydispersity of the sample, sodium or other additional ions in the protein solution, an incorrect estimate of the diffusion coefficient of the protein  $D_2$  or transient and local charge separations which invalidate equ (20).



The charge of the protein used for calculating diffusion coefficients was derived from valence pH-titration and does not account for ion binding which could reduce the actual charge  $z_{DHH}$  of the protein. The experimental diffusion coefficient at infinite dilution could therefore be used to calculate the actual charge  $z_{DHH}$  by neglecting effects of polydispersity and transient and local charge separations and assuming a correct estimate of  $D_2$ . For estimating  $z_2$ ,  $D_0$  determined for each pH condition was taken for  $D$  in equ (24) and in equ (25) to exclude effects of potential protein-protein interactions on  $D$ . The total amount of counterions (bound and effective counterions) is known from valence data and sample preparation. The counterion concentration  $c_3$  however, is defined as the amount of effective counterions. As the counterion concentration  $c_3$  is not a priori known, as some of the counterions are assumed to be binding to the protein, an iterative approach was used to receive values for  $z_2$ . For the approach the whole amount of counterions present in solution (bound and effective counterions) was first used to calculate a first starting value for  $z_2$ . Using this first value for  $z_2$ , the amount of bound counterions was calculated and subtracted from the total amount of counterions. This procedure was repeated and after 10 of these iterative cycles the values converged. The resulting values of  $z_2$  are shown in Table 25.

Table 25: Estimation of  $z_2$  from infinite dilution diffusion coefficients. The valence was determined by pH titration (177),  $z_2$  was calculated either by equ (25) or by equ (24) using an iterative approach. The total amount of chloride ions was derived from valence data and the sample preparation procedure. The ratio of chloride ions  $\#_{Cl^-}$  in relation to the number of proteins  $\#_P$  in solution is displayed for different species of counterions.

	Valence	$z_2$ (equ (25))	$z_2$ (equ (24)) iterative approx. (10 cycles)	$\#_{Cl^-} / \#_P$ sum of all chloride ions	$\#_{Cl^-} / \#_P$ bound chloride ions	$\#_{Cl^-} / \#_P$ freely diffusing protein- related chloride ions	$\#_{Cl^-} / \#_P$ effective counterions	Ratio of bound freely diffusing protein- related chloride ions
pH 3.2	80.0	14.3	14.3	80.0	65.7	14.3	14.3	4.6
pH 5.5	21.0	6.9	7.0	21.0	14	7.0	7.0	2.0
pH 6.0	16.7	7.4	7.4	16.7	9.3	7.4	7.4	1.2
pH 6.5	7.4		6.7	16.7	6.5	6.8	10.2	1.0
pH 7.0			5.9	16.7	3.3	5.9	13.4	0.6

The results obtained by either applying equ (25) or equ (24) coincide for all samples prepared by addition of HCl. Consequently, the iterative approach is suited to estimate the actual net charge of the protein. In the presence of additional NaCl, which may occur if the pH is adjusted by using NaOH, the iterative approach is the only suitable way to calculate the actual net charge  $z_{DHH}$  as equ (25) is not accounting for additional salt. The results shown in Table 25 are only valid for a protein concentration extrapolated to  $c = 0$ . At higher protein concentration the equilibrium between freely diffusing and bound counterions might readjust. As shown in Table 25, the ratio of bound counterions to freely diffusing protein-related counterions is decreasing with increasing pH. Hence a higher net charge of the protein seems to result in a higher affinity of counterions binding to the protein.

#### *Dependence of $D$ on protein concentration*

Experimental data of diffusion coefficients decreased with increasing protein concentration. According to the three-component model, diffusion coefficients should be constant with varying protein concentration, if the effective counterion concentration was proportional to the protein concentration, the net charge was constant and no attractive protein-protein interactions would occur. Therefore, the decrease in diffusion coefficient could be either due to a relative (with regards to the protein concentration) decrease in net charge with increasing protein concentration or due to attractive protein-protein interactions.

Excluding values at pH 3.2, the effect of decreasing diffusion coefficients with increasing protein concentrations was enhanced at elevated pH as indicated by the decreasing trend of  $k_D$  with increasing pH (Figure 23). Even though the pseudobinary model of  $k_D$  does not apply under the given experimental setup, values of  $k_D$  are reflecting the slope of the diffusion coefficient as a function of protein concentration and will therefore be discussed here. The experimental  $k_D$  values can be compared with those values that would be expected by calculation with equ (23) as depicted in Figure 24.

#### *Analysis of causes of negative $k_D$*

The negative  $k_D$  could either be due to a decreasing net charge with increasing protein concentration or due to attractive protein-protein interactions. It is not possible to

theoretically estimate the trend of the net charge with increasing protein concentration as a function of pH.

However, attractive protein-protein interactions that may be induced by ion-dipole and dipole-dipole interactions are assumed to increase at pH values approaching the pI as the dipole moment of the protein is assumed to increase in the vicinity of the pI (5). To differentiate between the two possible causes of decreasing diffusion coefficients with increasing protein concentration, alternative techniques to DLS could be used.

Attractive protein-protein interactions could be measured by self-interaction chromatography (as described by LeBrun et al. (75)), even though accelerated diffusion, as induced by electrostatic interaction of the mAb with counterions, could influence the retention time as well. Another alternative approach is the measurement of the activity of the counterions by ion selective electrodes. The dependence of the chloride activity as a function of protein concentration could render information about the activity of effective counterions at various protein concentrations. The determination of diffusion coefficients of individual ions by conductivity measurements is another alternative approach (119). However, the electric field applied for the measurement, could influence the actual charge of the protein by either influencing the valence of the protein or by modifying the number of bound ions and thereby the Debye-Hückel-Henry charge  $z_{DHH}$ . To measure the dipole moment of the protein as a function of pH or as a function of the protein concentration dielectric spectroscopy could be used. Hence, measuring attractive protein-protein interactions independent from coupled protein counterion diffusion may be difficult to measure and boundary conditions always have to be taken into account.

Hence, attractive protein-protein interactions might additionally influence the diffusion of the proteins. However, the interpretation of exact  $k_D$  values as a function of pH in the absence of buffer is not reliable as the assumption of a two-component system does not apply. In particular, the  $k_D$  of zero in this experimental setup is stated to correspond to repulsive protein-protein interactions as the model behind the present calculation includes repulsive ion-ion interactions. This is due to electrostatic interactions between the diffusion of charged protein and counterions. The interactions do not vanish at infinite dilution, phenomenological appearing by larger values of  $D_0$ , as described before.

#### 4.3.2.1.2. Dependence of the diffusion coefficient on the NaCl concentration in the absence of buffer

The protein solution obtained by dialysis against water (prepared as described in section 3.2.2.2,  $c(\text{Protein}) = 23.6 \text{ mg/ml}$ ) was adjusted to a protein concentration of 20 mg/ml by adding NaCl stock solutions or water. The sodium concentration of the resulting solution was adjusted as indicated between 0 mM and 150 mM. The chloride concentration in the protein solutions was higher than indicated, due to chloride counterions already present in the protein solution before mixing with the NaCl stock solution. The solution with a protein concentration of 20 mg/ml was diluted with NaCl solution as indicated. The results of DLS measurements performed as described in section 3.2.1.10 are displayed in Figure 25.

#### Experimental data

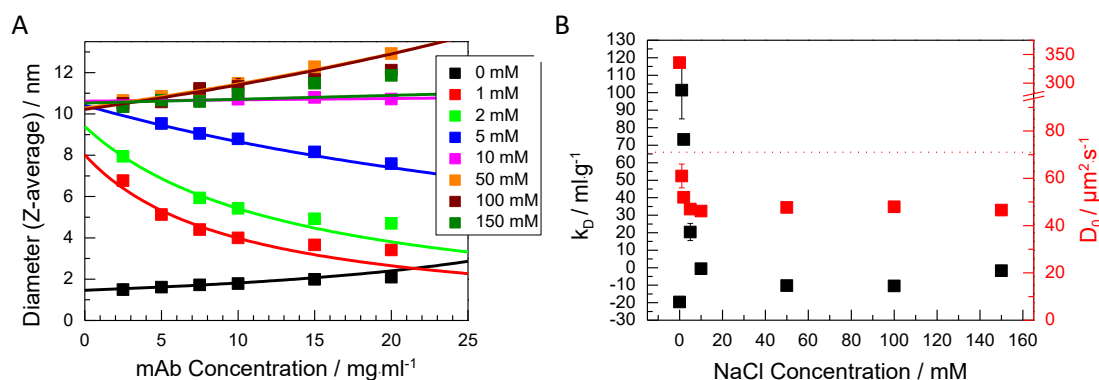


Figure 25: Influence of the NaCl concentration on the hydrodynamic diameter, the  $k_D$  and on  $D_0$  of the mAb in pure water as measured by DLS (Wyatt, Plate Reader, 25°C). The hydrodynamic diameters shown in Figure 25A were converted from the measured diffusion coefficients with equ (3).  $k_D$  and  $D_0$  were obtained as described in section 3.2.3.8 by fitting data of the diffusion coefficient to equ (10) (plot not shown here). The solid lines in Figure 25A show the results of the curve fitting converted to diameters by equ (3) and equ (15) as described in section 2.3.1.2.  $k_D$  and  $D_0$  values as a function of the NaCl concentration are separately depicted in Figure 25B. Diffusion coefficients larger than  $71 \mu\text{m}^2/\text{s}$  (as depicted by the dotted red line in Figure 25B) correspond to diameters lower than 6.9 nm (equ 3). This diameter is considered to be the minimal real diameter of the mAb as described in section 4.3.2.1.1.

#### Apparent diameter at infinite dilution

The apparent diameter of the antibody at infinite dilution in pure water was 1.5 nm. It was increasing with increasing NaCl concentration from 8.0 nm at 1 mM NaCl to 10.4 nm at 5

mM NaCl. A further increase in NaCl concentration to 150 mM did not significantly affect the apparent diameter at infinite dilution. Between 5 mM NaCl and 150 mM NaCl the infinite dilution diameter was between 10.3 nm and 10.6 nm.

Taking the model of coupled protein counterion diffusion, the increase of the infinite-dilution diameter could either be due to a decrease in actual net charge and/or due to the increasing amount of effective counterions.

It is obvious, that the increasing NaCl concentration results in an increasing amount of effective counterions. The effect of NaCl on the actual net charge is difficult to estimate, as an increase in ionic strength would result in a higher net charge whereas the higher concentration of available chloride ions might result in enhanced protein-chloride binding and thus a lower net charge. The problem will be discussed below, by comparison of calculated data with experimental data.

#### *Dependence of $D$ on protein concentration*

In the absence of  $\text{Na}^+$  the diffusion coefficient of the antibody was decreasing with increasing protein concentration indicating a negative  $k_D$ . The  $k_D$  was positive between 1 mM and 5 mM NaCl, it decreased to a relative minimum roughly between 50 mM and 100 mM  $\text{Na}^+$  and then slightly increased in the presence of 150 mM NaCl, still with slightly negative values.

The preparation of the samples resulted in a changing chloride to protein ratio upon protein dilution. The chloride ions as introduced into solution as protein-related counterions were proportionally decreasing with decreasing protein concentration. The chloride ions as introduced into solution by diluting with solutions containing a constant NaCl concentration were not changing with protein concentration. Therefore, the chloride to protein ratio was increasing upon dilution. The effect was most pronounced at lower NaCl concentrations. However, it did not occur, if the dilution was performed with water. Due to the changing chloride to protein ratio, the effect of coupled protein counterion diffusion is assumed to be smaller at lower protein concentration and to be enhanced at higher protein concentration.

Due to the changing composition of the surrounding medium an interpretation of  $k_D$  values should again be considered with caution. The sign of  $k_D$  does not necessarily point out the transition between protein-protein attraction and repulsion.

### Calculation of hydrodynamic diameters on the basis of valence data and estimated charge data

The theoretical diameter of the protein was calculated applying equ (23) and equ (3) by either using the valence of the antibody at pH 6.0 of 16.7 (see section 4.1.1) or using the  $z_{DHH}$  of 7.4 which was estimated by extrapolating diffusion coefficients in the absence of salt to a protein concentration of zero (see chapter 4.3.2.1.1). The results are displayed in Figure 26.

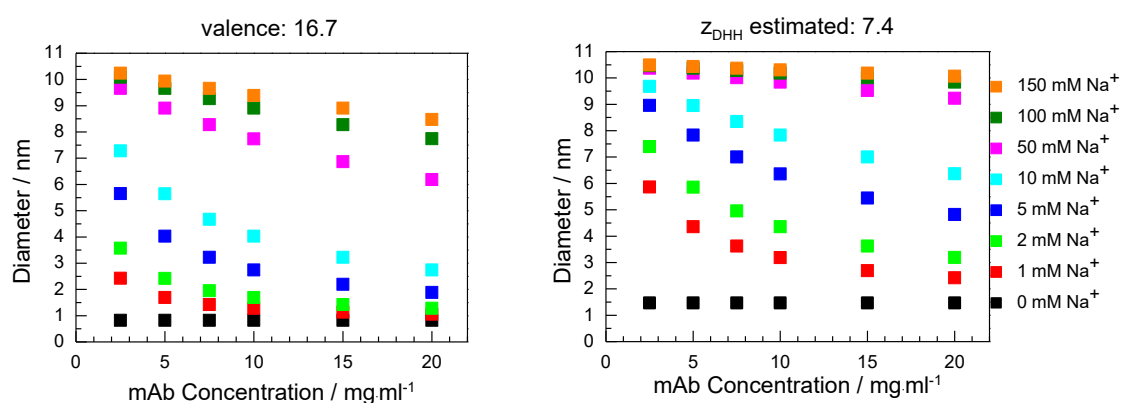


Figure 26: Calculation of hydrodynamic diameters as determined by equ (23) and equ (3). Assumption of three-component system consisting of water, charged mAbs and counterions with coupled protein counterion diffusion. Attractive interactions between the antibodies are not covered by this model. The chloride concentration in the solutions is assumed to be slightly higher than the declared Na<sup>+</sup> concentration (by:  $c(\text{mAb}) \cdot \text{Mw}(\text{mAb})^{-1} \cdot z(\text{mAb})$ ) due to protein-related counterions additionally present in the solution. The valence  $z$  of the antibody is assumed to be 16.7 as measured by valence titration (4.1.1). The  $z_{DHH}$  of 7.4 is estimated from the experimental  $D_0$  of the antibody in water and equ (25), assuming the actual charge to solely influence the diffusion coefficient of the protein at infinite dilution (and not protein-protein interactions or protein aggregates) (see 4.3.2.1.1).

The accelerating effect on the diffusion coefficient of coupled protein counterion diffusion is enhanced at higher protein concentrations compared to lower protein concentrations. This phenomenon is most pronounced in an intermediate NaCl range which varies with the net charge of the protein. At very low NaCl concentrations this dependence is not very pronounced in the protein concentration range between 2.5 and 20 mg/ml. However, in this NaCl region the linearity of the diameter as a function of protein concentration is rather

low. The dependence of coupled protein counterion diffusion on protein concentration is shifted to lower protein concentrations ( $< 2.5$  mg/ml), which are not depicted in Figure 26. The dependence of the effect of coupled protein counterion diffusion on the protein concentration can be explained with the lower effective counterion to protein ratio present at higher protein concentrations. Therefore a slope in  $D$ , equal to a positive  $k_D$ , is estimated. The effect is more pronounced by estimating a higher net charge of the antibody of 16.7 compared to the lower charge of 7.4. The latter charge was assumed to result from protein-chloride binding resulting in partial charge neutralization. The exact value of 7.4 was derived from equ (25) by taking  $D = D_0$  in water at pH 6.0 =  $336 \mu\text{m}^2/\text{s}$ ,  $D_{mAb} = 46.5 \mu\text{m}^2/\text{s}$  and  $D_{chloride} = 2032 \mu\text{m}^2/\text{s}$ .

Even though the calculated slope of diffusion coefficient as a function of protein concentration is positive at lower NaCl concentrations whereas it is zero in the absence of NaCl in water, this does not indicate the repulsive protein-protein interactions to be enhanced in NaCl. As the system is multicomponent the interpretation of the pseudobinary model behind  $k_D$  is not suitable. The positive slope can be explained with a lower counterion to protein ratio and thereby enhanced coupled protein counterion diffusion at higher protein concentrations. Coupled protein counterion diffusion is including repulsive protein-protein interactions, repulsive counterion counterion interactions and attractive protein-counterion interactions.

Hence, for experimental data, the size of  $k_D$  does not necessarily quantify the magnitude of protein-protein interactions. However, the comparison between calculated data and experimental data could render information about the magnitude of attractive protein-protein interactions.

#### Comparison of calculated data with experimental data

Comparison of theoretical values with experimental data reveals information about the origin of positive  $k_D$  values. Therefore  $D_0$  and  $k_D$  were derived from the calculated data presented in Figure 26 for protein concentrations between 2.5 and 10 mg/ml. This protein concentration range was selected to allow for comparison with experimental values, which were also fitted between 2.5 mg/ml and 10 mg/ml. The results are listed in Table 26.



Table 26: Results of calculated  $D_0$  and  $k_D$  values for protein solutions in pure water and in NaCl solutions with different concentrations. The values were obtained as described in section 3.2.5. Data were derived from calculations of diffusion coefficients by using equ (23). Calculations were performed with  $D_{2(\text{mAb})} = 46.5 \mu\text{m}^2/\text{s}$  and  $D_{3(\text{chloride})} = 2032 \mu\text{m}^2/\text{s}$ . Experimental data are displayed for comparison.

	Calculated data, with an estimated charge of +16.7		Calculated data, with an estimated charge of +7.4		Experimental data		Difference in $k_D$ between experim. data and calcul. data (charge: +7.4)
	$D_0$ [ $\mu\text{m}^2/\text{s}$ ]	$k_D$ [ml/g]	$D_0$ [ $\mu\text{m}^2/\text{s}$ ]	$k_D$ [ml/g]	$D_0$ [ $\mu\text{m}^2/\text{s}$ ]	$k_D$ [ml/g]	
0 mM NaCl	595	0	336	0	336	-20	-20
1 mM NaCl	156	154	63	149	61	101	-48
2 mM NaCl	94	216	52	119	52	73	-46
5 mM NaCl	58	211	48	63	47	20	-43
10 mM NaCl	50	145	47	35	46	-1	-36
50 mM NaCl	47	36	47	7	48	-10	-17
100 mM NaCl	47	18	47	4	48	-10	-14
150 mM NaCl	47	12	47	3	47	-2	-5

#### *D<sub>0</sub> at infinite dilution*

Comparison of  $D_0$  values of calculated with experimentally derived data (Figure 25, Figure 26 and Table 26), shows larger differences if a charge of 16.7 is estimated than a charge of 7.4. The similar values of  $D_0$  of either calculated (charge of 7.4) or experimental origin, confirm the validity of the theory of coupled protein counterion diffusion as given in equ (23). In addition, the measurement of diffusion coefficients as a function of protein concentration and NaCl could therefore be used to measure the actual charge ( $z_{DHH}$ ) of a protein at low ionic strength, taking into account binding of ions.

The matching values of  $D_0$  for calculated data in the presence of NaCl also indicate the net charge of 7.4 to be approximately constant between 0 mM and 2 mM NaCl. At higher NaCl concentrations the net charge has a vanishing impact on the diffusion as the effective counterion concentration dominates the influence on the diffusion coefficient. At higher NaCl concentrations estimates of the protein net charge through  $D_0$  are not possible.

#### *Dependence of $D$ on protein concentration*

The trend and value of  $k_D$  of calculated data is depending on the assumed net charge. Assuming a net charge of 16.7,  $k_D$  has a maximum at 2 mM ionic NaCl with a value of 216 ml/g. The maximum in  $k_D$  occurs at lower NaCl concentration of 1 mM if a net charge of 7.4 is presumed. The maximum seems to be lower (149 ml/g) compared to the maximum of  $k_D$  of 16.7 net charge. For smaller NaCl concentrations than 1 mM and a net charge of 7.4 the  $k_D$  for protein concentrations ranging from 2.5 mg/ml to 10 mg/ml does not exceed the value of 150 ml/g (calculated data not shown).

As  $D_0$  values of calculated data, assuming an actual charge of 7.4, and experimental data of  $D_0$  values correspond well, a comparison between  $k_D$  values can render information on additional protein-protein interactions which are not considered by the model of coupled protein counterion diffusion. For all NaCl concentrations observed, the experimental  $k_D$  is smaller than the  $k_D$  derived from the calculations. This indicates attractive protein-protein interactions to additionally occur at pH 6.0. Another indication for attractive protein-protein interactions at pH 6.0 is the negative experimental value at 0 mM NaCl. According to the calculations, the diffusion coefficient would be expected to be independent from the protein concentration, if only ion-ion three component interactions and no attractive protein-protein interactions would occur.

However, lower experimentally derived  $k_D$  values compared to calculated  $k_D$  values could also be due to the hydrodynamic drag, i.e. the partial specific volume  $\bar{v}$  and the concentration dependence of the frictional coefficient  $k_s$  as given in equ (11) and equ (12). For all NaCl concentrations up to 100 mM the difference in  $k_D$  is much higher than 5.34 ml/g, which should account for the hydrodynamic drag (59). Therefore attractive protein-protein interactions can still be assumed to influence the diffusion of the protein.

The overall interaction between the proteins is the sum of all attractive and repulsive interactions. Attractive interactions can be estimated by the difference between calculated and experimental  $k_D$  values. Repulsive interactions cannot be determined as easily. Especially at very low NaCl concentrations the calculated and experimental  $k_D$  is rather low even though strong repulsion would be expected under these conditions.

Attractive protein-protein interactions could be hydrophobic interactions, van-der-Waals interactions and / or di- and multipolar electrostatic interactions. The protein-protein attraction (as presented by the difference between experimental  $k_D$  and calculated  $k_D$ ) seems to decrease with increasing NaCl concentration (excluding the value in the absence of NaCl). Hence, the attraction between the antibody molecules seems to be screened by increasing the ionic strength. Therefore, in addition to potential hydrophobic interactions, van-der-Waals and di- and multipolar electrostatic interactions might contribute to the overall protein-protein interaction profile.

The impact of coupled protein counterion diffusion reaches over a broader range of NaCl concentrations regarding the  $k_D$  compared to the value of  $D_0$ . That means a “correct” or realistic value of  $D_0$  (which does not change by increasing the NaCl or effective counterion concentration) does not mean that data are not influenced by the effect of coupled protein counterion diffusion. An impact of the effect on  $k_D$  needs to be considered over a wider NaCl or counterion concentration range.

Another two buffer systems were tested to examine the effect of coupled protein counterion diffusion as a function of pH in different conditions. In addition to pH adjustment, buffers are known to interact with the protein and thereby modify molecular and macroscopic properties of the protein solution (184, 185).

#### 4.3.2.2. Dependence of the diffusion coefficient on the pH in 10 mM histidine buffer

The pH dependence of  $D_0$  and  $k_D$  on the pH was determined in histidine buffer, with a histidine concentration of 10 mM and pH values between pH 5.0 and pH 7.5. The samples were obtained by dialysis and subsequent dilution with histidine buffer of respective pH. Histidine has a buffering effect due to the partial protonated imidazole side chain in a pH

range between pH 5.0 and pH 7.0 with a  $pK_a$  of 6.04 (119). The results of DLS measurements performed as described in section 3.2.1.10 are displayed in Figure 27.

### Experimental data

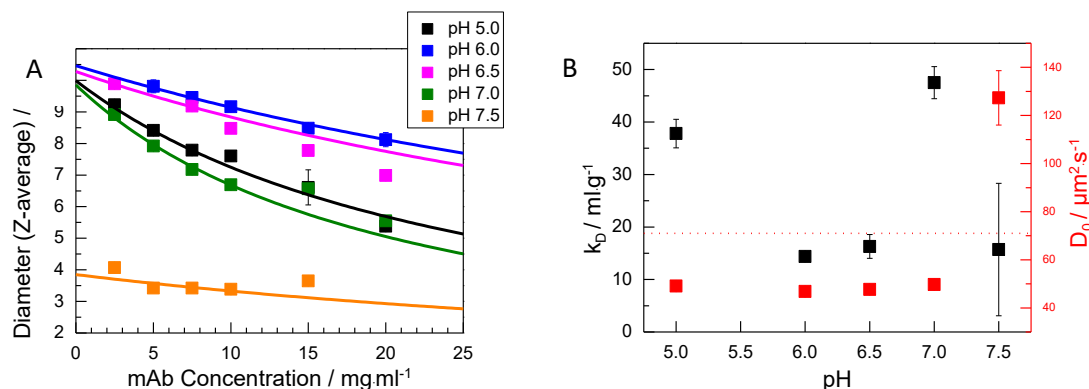


Figure 27: Influence of the pH on the hydrodynamic diameter, the  $k_D$  and on  $D_0$  of the mAb in 10 mM histidine buffer as measured by DLS (Wyatt, Plate Reader, 25°C). The hydrodynamic diameters shown in Figure 27A were converted from the measured diffusion coefficients with equ (3).  $k_D$  and  $D_0$  were obtained as described in section 3.2.3.8 by fitting data of the diffusion coefficient to equ (10) (plot not shown here). The solid lines in Figure 27A show the results of the curve fitting converted to diameters by equ (3) and equ (15) as described in section 2.3.1.2.  $k_D$  and  $D_0$  values as a function of pH are separately depicted in Figure 27B. Diffusion coefficients larger than  $71 \mu\text{m}^2/\text{s}$  (as depicted by the dotted red line in Figure 27B) correspond to diameters lower than 6.9 nm (equ 3). This diameter is considered to be the minimal real diameter of the mAb as described in section 4.3.2.1.1.

### Experimentally determined diameter at infinite dilution of the protein in 10 mM histidine buffer between pH 5.0 and pH 7.5

The experimental diameter of the protein at infinite dilution varied between 9.5 nm and 10.5 nm in the pH range between pH 5.0 and pH 7.0 (Figure 27). It was much smaller at pH 7.5 with a value of 3.9 nm. Histidine is an amino acid with an imidazole side chain with a  $pK_a$  of 6.04 (119). At pH 7.5 only 3 % of the histidine molecules are positively charged, whereas 97 % are neutral (zwitterionic) (calculated as described in section 3.2.4.2.2). At lower pH values a larger fraction of the histidine is positively charged and counterions (here: chloride ions) will therefore be present at higher concentrations as well. The chloride ions can act as effective counterions to the protein. The low apparent diameter at infinite dilution at pH 7.5 is probably due to the very small amount of chloride counterions (calculated concentration of 0.3 mM, calculated as described in section 3.2.4.2.2). From pH 5.0 to pH

7.0 the net charge of the protein is assumed to be higher, but the chloride ions in solution from the histidine buffer may be sufficient to prevent the effect of coupled protein counterion diffusion at infinite dilution.

These data point out the huge impact of effective counterions on the effect of coupled protein counterion diffusion compared to the impact of the protein net charge. The smallest diameter was observed at pH 7.5 which is closest to the isoelectric point. At these conditions, repulsive electrostatic protein-protein interactions are supposed to be minimal but the effect of coupled protein-counterion diffusion seems to be maximal.

#### *Dependence of $D$ on protein concentration*

The diffusion coefficient increased with increasing protein concentration for all pH values tested which is synonymous with a positive  $k_D$ . The value of  $k_D$  was highest for pH 5.0 and pH 7.0. The  $k_D$  at pH 7.5 bears a great uncertainty due to poor data quality and should therefore not be compared with other data. The positive  $k_D$  in histidine buffer could be due to repulsive protein-protein interactions and due to the decreasing chloride to protein ratio with increasing protein concentration. The highest values of  $k_D$  at pH 5.0 and pH 7.0 could be due to the increasing net charge of the protein at pH 5.0 and the decreasing chloride concentration of the histidine buffer at pH 7.0. Therefore, the effect of coupled protein counterion diffusion could be enhanced at these conditions.

#### *Comparison of the curve progression of the diffusion coefficient in histidine buffer with buffer-free conditions*

By preparing the protein solution in histidine buffer by dialysis, an unknown amount of chloride ions was introduced into the sample. This amount depends on the ratio of histidine hydrochloride to histidine in the buffer, which is well known, but it also depends on the charge of the antibody. The higher the net charge of the antibody and the higher the protein concentration, the more counterions were accumulated in the samples and the more coions were depleted from the sample (dialysis procedure described in section 3.2.3.8. Theoretical background on ion distribution after dialysis: 2.4.3). The sum of accumulated counterions and depleted coions guarantees electrical neutrality in solution (114). By diluting the solution obtained by dialysis with respective buffer, the chloride concentrations in the

protein solution and in the buffer mixed. Therefore, the concentration of chloride was not constant in solutions at specific pH. Similar to the conditions in NaCl-dependent buffer-free solutions, the anion to protein ratio is assumed to decrease with increasing protein concentration.

The protein solution containing 10 mM histidine buffer at pH 6.0 may be compared with the buffer-free protein solution in 5 mM NaCl pH 6.0 assuming a similar protein charge and a similar chloride concentration. For the histidine buffered solutions a chloride concentration of 6.2 mM is calculated (as described in section 3.2.4.2.2). The data are selectively displayed in Figure 28.

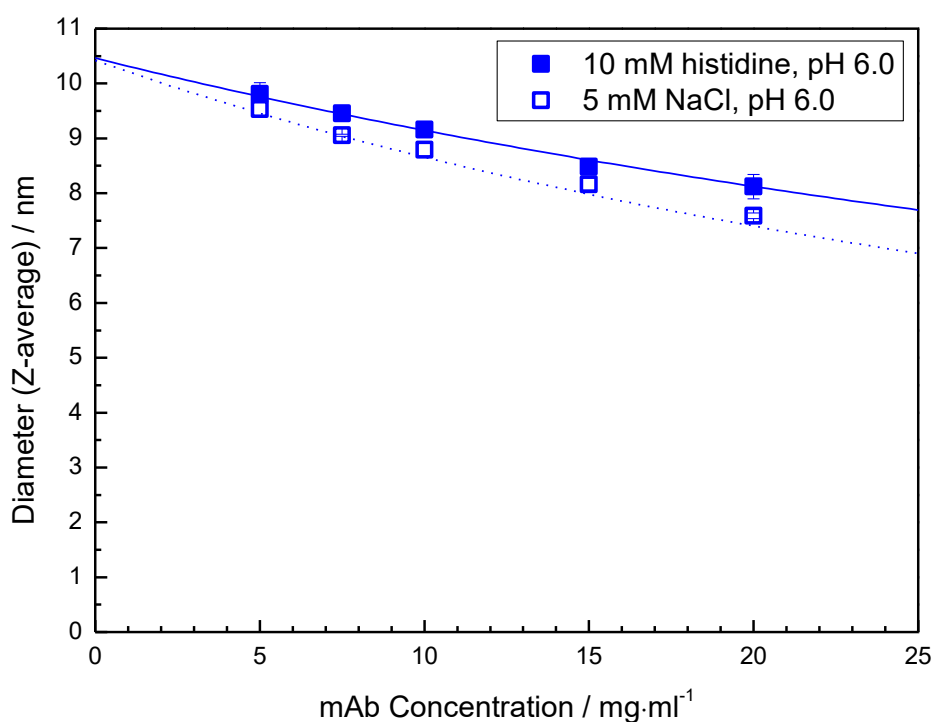


Figure 28: Comparison of measured mAb diameters in 10 mM histidine, pH 6.0 and 5 mM NaCl, pH 6.0 (Wyatt, Plate Reader, 25°C). The hydrodynamic diameters were converted from the measured diffusion coefficients with equ (3).  $k_D$  and  $D_0$  were obtained as described in section 3.2.3.8 by fitting data of the diffusion coefficient to equ (10) (plot not shown here). The solid line (10 mM histidine, pH 6.0) and the dotted line (5 mM NaCl, pH 6.0) show the results of the curve fitting converted to diameters by equ (3) and equ (15) as described in section 2.3.1.2.

A similar curve progression was observed for the protein in 5 mM NaCl solution, pH 6.0 and the protein in 10 mM histidine buffer, pH 6.0. The infinite-diffusion coefficient was

equal for both cases; the  $k_D$  was slightly larger in 5 mM NaCl solution, pH 6.0. Either attractive protein-protein interactions are enhanced in 10 mM histidine buffer or the effect of coupled protein counterion diffusion is enhanced in 5 mM NaCl solution. Enhanced coupled protein counterion diffusion in 5 mM NaCl solution could be due to the slightly lower chloride concentration in 5 mM NaCl solution compared to the calculated chloride concentration of 6.2 mM in the histidine buffer and due to the difference in sample preparation. The histidine buffered protein solution was prepared by dialysis whereas the protein solution containing NaCl was prepared by spiking a NaCl stock solution to a “salt-free” protein solution. The dialysis procedure enables anions and cations to permeate through the semipermeable dialysis membrane and the charge of the protein is counterbalanced by accumulated counterions (here chloride) and depleted coions (here positively charged histidine ions) (see section 2.4.3). By spiking a NaCl stock solution to the “salt-free” protein solution, the charge is counterbalanced exclusively by accumulated counterions. Therefore the counterion concentration in the protein solutions of like protein charge is higher for the solution prepared by spiking than a solution prepared by dialysis. This means the difference in the counterion to protein ratio as a function of protein concentration is higher for the protein solutions containing NaCl which was prepared by spiking. This is a second reason to expect enhanced coupled protein counterion diffusion as a function of the protein concentration in the solution containing NaCl.

Summing up, the similar curve progression of diffusion coefficients in 10 mM histidine buffer pH 6.0 and 5 mM NaCl solution indicates the diffusion of the protein in 10 mM histidine buffer, with an estimated chloride concentration of 6.2 mM to be similar to the diffusion of the protein in 5 mM NaCl solution. The coupled protein counterion diffusion which was observed in a protein solution containing 5 mM NaCl also seems to influence the diffusion of the protein in 10 mM histidine buffer. The lower anion to protein ratio at higher protein concentration is a suitable explanation for increasing diffusion coefficients with increasing protein concentration.

No calculations were performed for the histidine buffered protein solutions as the exact amount of chloride in solution was not measured and cannot exactly be deduced from the sample preparation. The concentration of chloride ions in the protein solution after dialysis

against 10 mM histidine buffer may be affected by the pH and the positive net charge of the protein.

#### 4.3.2.3. Diffusion coefficients in citrate buffer

##### 4.3.2.3.1. Dependence of the diffusion coefficient on the NaCl concentration in 10 mM citrate buffer pH 6.0

The diffusion coefficients of the antibody dissolved in 10 mM citrate buffer pH 6.0 with varying NaCl concentration were measured using DLS as described in section 3.2.1.10. The protein solutions were obtained by dialysis and subsequent dilution with respective buffer. The results are displayed in Figure 29.

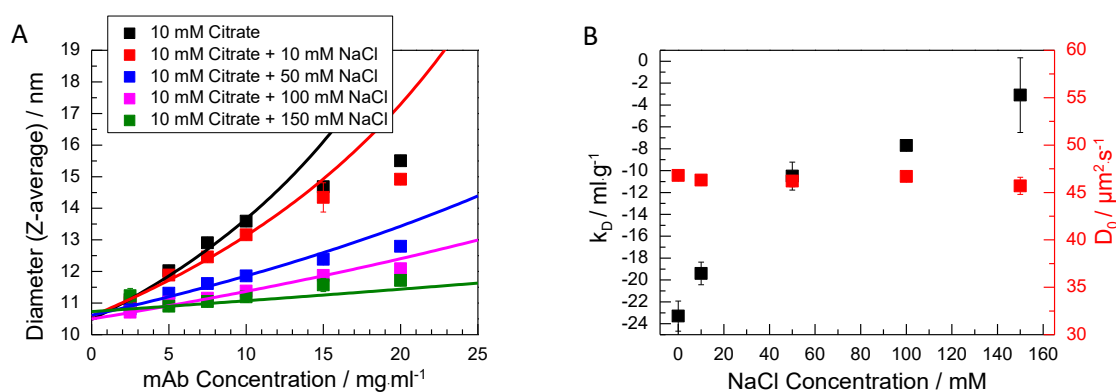


Figure 29: Influence of the NaCl concentration on the hydrodynamic diameter, the  $k_D$  and on  $D_0$  of the mAb in 10 mM citrate buffer as measured by DLS (Wyatt, Plate Reader, 25°C). The hydrodynamic diameters shown in Figure 29A were converted from the measured diffusion coefficients with equ (3).  $k_D$  and  $D_0$  were obtained as described in section 3.2.3.8 by fitting data of the diffusion coefficient to equ (10) (plot not shown here). The solid lines in Figure 29A show the results of the curve fitting converted to diameters by equ (3) and equ (15) as described in section 2.3.1.2.  $k_D$  and  $D_0$  values as a function of the NaCl concentration are separately depicted in Figure 29B.

#### *Apparent diameter at infinite dilution*

The diffusion coefficients at infinite dilution and the apparent diameters at infinite dilution (Figure 29) were almost constant over the entire range of ionic strengths investigated. Extrapolated diameters were between 10.5 nm and 10.7 nm.

Most probably the citrate concentration of 10 mM at pH 6.0 is sufficient to mask the effect of coupled protein counterion diffusion at infinite dilution. The citrate ion may either neutralize the actual net charge of the protein or the effective counterion concentration of



10 mM citrate buffer is sufficient to overrule the effect of coupled protein counterion diffusion on the apparent diameter at infinite dilution. In the absence of citrate buffer, a NaCl concentration of 5 mM was sufficient to mask the effect of coupled protein counterion diffusion on the infinite dilution diameter (Figure 25). As the citrate buffer concentration of 10 mM in this section is higher than 5 mM the constant apparent diameters at infinite dilution would be expected. The diameters extrapolated to zero protein concentration in solutions containing 5 mM – 150 mM NaCl in the absence of citrate buffer were 10.3 nm – 10.6 nm (4.3.2.1.2). They agree well with the diameters of 10.5 nm - 10.7 nm obtained in the presence of 10 mM citrate buffer and various ionic strengths.

#### *Dependence of $k_D$ on protein concentration*

The  $k_D$  was negative for all examined formulations. The lowest value of  $k_D$  of  $-23.3 \text{ ml}\cdot\text{g}^{-1}$  was observed for the antibody in 10 mM citrate buffer pH 6.0 in the absence of NaCl. Upon addition of NaCl,  $k_D$  was monotonically increasing to a value of  $-3.1 \text{ ml}\cdot\text{g}^{-1}$  in the presence of 150 mM NaCl (Figure 29).

Arzensek et al. (44), examined the influence of ionic strength on  $k_D$  values between 15 mM ionic strength and 175 mM ionic strength. The ionic strength of 15 mM was adjusted with different buffers and the higher ionic strengths up to 175 mM were adjusted by adding NaCl to the buffer. They observed increasing  $k_D$  values with increasing ionic strength at pH values more than one pH unit away from pI (44). This observation supports the data obtained here.

As will be shown in section 4.3.2.3.2 the strongly negative value of  $k_D$  in 10 mM citrate buffer pH 6.0 is expected to mainly result from attractive protein-protein interactions. The increase in  $k_D$  as induced by NaCl might indicate lowered attractive protein-protein interactions with increasing NaCl concentration. This could be due to screening of attractive protein-protein interactions such as dipole-dipole, ion-dipole or electrostatic multipolar interactions. This trend of reduced attractive interactions with increasing ionic strength is typically termed “salting-in”. As discussed in detail in section 4.1.4 the occurrence of salting-in depends on the difference between pH and isoelectric point (126, 153), on the intrinsic properties of the protein (126, 154), and on specific additional cosolutes, such as buffers or oligovalent ions present in solution (65, 155).

In addition to potential screening of attractive protein-protein interactions by NaCl, chloride counterions could also influence protein-citrate binding which is assumed to induce attractive protein-protein interactions e.g. via cross-linking. The electrostatic protein-citrate binding could be reduced due to screening caused by the higher ionic strength or due to competition between citrate and chloride ions for the potential binding sites.

In section 4.1.4 the occurrence of liquid-liquid phase separation was examined in different solution compositions at pH 7.8 for the same antibody in the presence of citrate buffer. NaCl was narrowing the width of the miscibility gap at 5°C, also indicating decreasing attractive protein-protein interactions.

*Comparison of the NaCl dependence of  $k_D$  in citrate buffer with buffer-free conditions*

A comparison of  $k_D$  values obtained for citrate-free and 10 mM citrate buffered protein solutions is only meaningful for NaCl concentrations of at least 10 mM NaCl. Values of  $k_D$  for solutions in buffer-free NaCl solutions decreased from  $-0.6 \text{ ml}\cdot\text{g}^{-1}$  in 10 mM NaCl to  $-10.4 \text{ ml}\cdot\text{g}^{-1}$  in 100 mM NaCl solution and then increased to  $-1.7 \text{ ml}\cdot\text{g}^{-1}$  in 150 mM NaCl solution (4.3.2.1.2).

As shown before in section 4.3.2.1.2, the  $k_D$  obtained for buffer-free solutions was strongly influenced by the effect of coupled protein counterion diffusion and the decreasing chloride to protein ratio with increasing protein concentration. The difference between the experimental  $k_D$  values and the calculated values accounting for the effect induced by coupled protein counterion diffusion (for an estimated net charge of 7.4) was negative for all NaCl concentrations and its extent was decreasing with increasing NaCl concentrations in a NaCl concentration range from 1 mM to 150 mM (Table 26). Hence, the trend of reduced protein-protein attraction with increasing NaCl concentration can also be concluded in a buffer-free system. However, a quantitative comparison is not allowed as the system is multicomponent (94).

Event though reduced protein-protein attraction with increasing NaCl can be deduced in the presence and in the absence of 10 mM citrate, the absolute  $k_D$  values strongly differ for both conditions. In the absence of citrate, the  $k_D$  is between  $-10.4 \text{ ml}\cdot\text{g}^{-1}$  and  $-0.6 \text{ ml}\cdot\text{g}^{-1}$  following a non monotonic trend with increasing NaCl concentration, whereas in the presence of 10 mM citrate, the  $k_D$  is between  $-23.3 \text{ ml}\cdot\text{g}^{-1}$  and  $-3.1 \text{ ml}\cdot\text{g}^{-1}$  and is

monotonically increasing with increasing NaCl concentration. The positive contribution on  $k_D$  (as specified in section 4.3.2.1.2) which is resulting from the effect of coupled protein counterion diffusion seems to be missing in the presence of 10 mM citrate. As mentioned before, this could be due to the different limiting diffusion coefficient of the citrate molecule compared to the chloride ion. In addition, this could be due to differences in protein-counterion interaction resulting from a modified net charge of the protein or from the higher valence of the citrate counterion. Finally, it could be due to differences in attractive protein-protein interaction.

Regarding absolute values of diffusion coefficients,  $k_D$  was inversely affected by NaCl comparing the buffer-free system in a NaCl concentration range from 10 mM – 100 mM and the system buffered by 10 mM citrate in the NaCl concentration range from 10 – 150 mM. The decreasing trend in  $k_D$  in buffer-free conditions is assumed to result from a reduced effect of coupled protein counterion diffusion at higher NaCl concentration as the ratio between protein and counterion is less affected by the protein concentration at higher NaCl concentration. In 10 mM citrate buffer, this effect is assumed to be reduced and the protein-protein interactions are assumed to be more attractive. A similar trend in two different buffer systems has been reported by Raut and Kalonia (65). They observed the phase behavior of a dual variable domain immunoglobulin. The phenomenon observed, i.e. the phenomenon of liquid-liquid phase separation is assumed to be related to lowered diffusion of the protein. In histidine buffer at pH 6.1, the cloud temperature increased from 10.3°C to 16.8°C by adding NaCl to a final ionic strength of 50 mM. This increase in cloud temperature is simultaneous to lowered diffusion upon NaCl addition. In phosphate buffer at pH 6.5, the cloud point was decreasing from  $\geq 37$  °C to 24.5 °C with increasing ionic strength to 50 mM. This trend is synonymous for an increase in diffusion in of the antibodies in solution. As shown before in section 4.2.2, the histidine buffered protein solutions show similar diffusion coefficients as systems containing NaCl, most probably due to the same type of counterion, i.e. chloride. The phosphate buffer may be comparable to the citrate buffer due to its higher number of protonation sites and the higher molecular weight (which is related to the limiting diffusion coefficient) compared to chloride. The lowered diffusion upon NaCl addition observed in the histidine buffer by Raut and Kalonia (65) could be due to weakening of the effect of coupled protein counterion diffusion upon

increasing the effective counterion concentration as expected for histidine buffered protein solutions (4.3.2.2).

#### 4.3.2.3.2. Dependence of the diffusion coefficient on the pH-profile in 10 mM citrate buffer

The pH dependence of  $D_0$  and  $k_D$  was determined in 10 mM citrate buffer between pH 5.0 and pH 7.0. The samples were obtained by dialysis and subsequent dilution with citrate buffer of respective pH. A citrate solution has a buffering effect due to the three carboxylic groups with  $pK_{a1} = 3.13$ ,  $pK_{a2} = 4.76$  and  $pK_{a3} = 6.40$  at 25°C (119). The results of DLS measurements performed as described in section 3.2.1.10 are displayed in Figure 30.

#### Experimental data

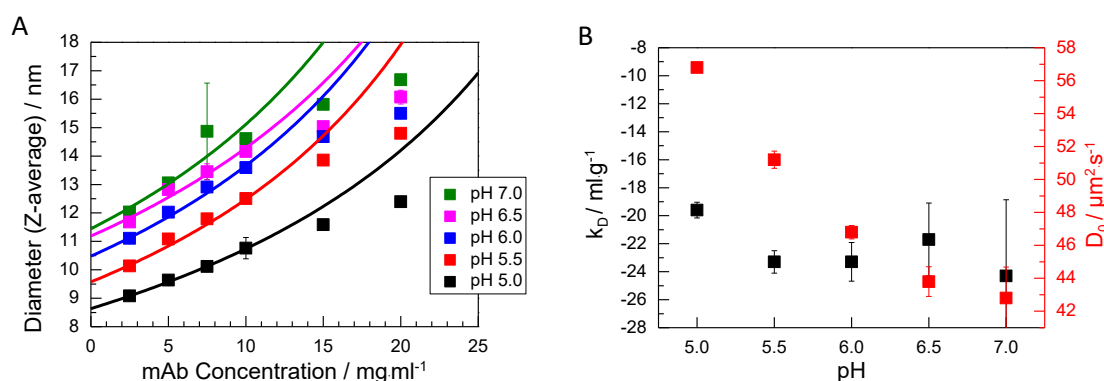


Figure 30: Influence of the pH on the hydrodynamic diameter, the  $k_D$  and on  $D_0$  of the mAb in 10 mM citrate buffer as measured by DLS (Wyatt, Plate Reader, 25°C). The hydrodynamic diameters shown in Figure 30A were converted from the measured diffusion coefficients with equ (3).  $k_D$  and  $D_0$  were obtained as described in section 3.2.3.8 by fitting data of the diffusion coefficient to equ (10) (plot not shown here). The solid lines in Figure 30A show the results of the curve fitting converted to diameters by equ (3) and equ (15) as described in section 2.3.1.2.  $k_D$  and  $D_0$  values as a function of pH are separately depicted in Figure 30B.

#### Apparent diameter at infinite dilution

The apparent diameter at infinite dilution increased with increasing pH from 8.6 nm at pH 5.0 to 11.5 nm at pH 7.0. The higher net charge at lower pH could result in an enhanced effect of coupled protein counterion diffusion and thereby lower diameters. If the pH had an effect on the protein structure and the extended three-dimensional shape, a reverse trend

would be expected as a higher protein net charge would result in intramolecular charge-charge repulsion and therefore (partial) unfolding and a less compact protein structure. An effect of the pH on the protein structure cannot be excluded but the results of increasing diameters with increasing pH indicate the effect of coupled protein counterion diffusion to be dominating over the effect of the pH on the three-dimensional structure of the protein.

#### *Dependence of $D$ on protein concentration*

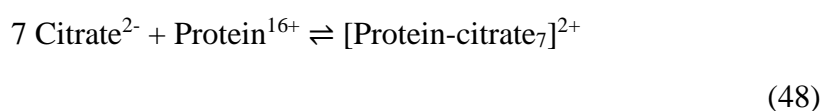
The diffusion coefficient decreased with increasing protein concentration for all pH values tested which is synonymous with a negative  $k_D$ . The  $k_D$  was approximately constant with values of  $-23.0 \text{ ml}\cdot\text{g}^{-1}$  ( $\pm 1.3 \text{ ml}\cdot\text{g}^{-1}$ ) between pH 5.5 and pH 7.0 with a slightly higher value at pH 5.0 of  $-19.6 \text{ ml}\cdot\text{g}^{-1}$ .

A negative  $k_D$  indicates attractive protein-protein interactions. The effect of coupled protein counterion diffusion could also contribute to the value of  $k_D$ . Negative values could result if the actual net charge of the protein decreases with increasing protein concentration or if the counterion to protein ratio is lower at smaller protein concentration.

According to the sample preparation, the counterion to protein ratio is assumed to be higher at lower protein concentration. This fact would rather result in positive  $k_D$  values as observed for the protein dissolved in solutions containing NaCl or histidine.

The actual net charge of the protein is assumed to depend on the equilibrium between freely diffusing and bound citrate molecules.

The reversible reaction of citrate antibody binding may be exemplarily written as follows:



Considering the law of mass action:

$$K = \frac{c([\text{Protein-citrate}_7]^{2+})}{c(\text{Citrate}^{2-})^7 c(\text{Protein}^{16+})} \quad (49)$$

with  $K$  being constant, the dependence of the net charge on the protein concentration as influenced by citrate binding can be deduced.

The citrate concentration of the initial sample ( $c = 23 \text{ mg/mL}$ ) was adjusted by dialysis against 10 mM citrate. The dilutions to lower protein concentrations were performed with 10 mM citrate. The absolute citrate concentration in the initial protein sample is assumed to be higher than 10 mM if citrate binding is assumed. However, the concentration  $c(\text{Citrate}^{2-})$  in equ (23) is defined by the effective citrate concentration, i.e. the concentration of freely diffusing citrate molecules. This concentration is assumed to be slightly higher than 10 mM, if the protein bears a positive net charge  $z_{DHH}$ , as the requirement of electrical neutrality results in an accumulation of counterions (citrate) and a depletion of co-ions ( $\text{Na}^+$ ) (see section 2.4.3). This effect is more pronounced for a higher protein actual charge,  $z_{DHH}$ . By diluting the protein solution with 10 mM citrate buffer, the concentration of freely diffusing citrate is lowered.

In citrate buffer, the actual charge  $z_{DHH}$  is expected to be reduced due to citrate binding. Consequently, the effect of decreasing citrate concentration with decreasing protein concentration may be negligible. Assuming the free citrate buffer concentration  $c(\text{Citrate}^{2-})$  to be constant over the range of protein concentrations, the  $\text{Protein}^{16+}$  to  $[\text{Protein-citrate}_7]^{2+}$  ratio is constant. Hence, the net charge of the protein is unaffected by the protein concentration, if the effective citrate concentration is constant.

The effective citrate concentration however might have a strong influence on the binding equilibrium if the net charge  $z_{DHH}$  of the protein is positive and the effective citrate concentration is decreasing with decreasing protein concentration. In this case, the equilibrium is strongly influenced by the effective citrate concentrations and small changes in the citrate concentration could strongly influence the  $[\text{Protein-citrate}_7]^{2+}$  to  $\text{Protein}^{16+}$  ratio and therefore the net charge of the protein. Assuming the effective citrate concentration to increase with the protein concentration, the  $[\text{Protein-citrate}_7]^{2+}$  to  $\text{Protein}^{16+}$  ratio is assumed to increase with increasing protein concentration. Consequently the net charge is assumed to decrease with increasing protein concentration. A lower net charge would result in lower diffusion coefficients and the phenomenon could influence  $k_D$  with a negative contribution.

In general, if coupled protein counterion diffusion takes place, the diffusion coefficients of the proteins will always be larger than diffusion coefficients of proteins whose diffusion is

not affected by coupled protein counterion diffusion. The converted diameters will be smaller than expected in the absence of coupled protein counterion diffusion. The effect on  $k_D$ , i.e. the dependence of coupled protein counterion diffusion on the protein concentration can in theory be either positive or negative, if the counterion to protein ratio or if the protein net charge  $z_{DHH}$  depends on the protein concentration (Table 27).

Table 27: Effects that potentially influence  $k_D$

	Positive contribution to $k_D$	Negative contribution to $k_D$
Protein-protein interaction	repulsive	attractive
Effective counterion to protein ratio, if it changes with the protein concentration	The ratio decreases with increasing protein concentration	
$z_{DHH}$ of the protein, if it changes with the protein concentration		The charge decreases with increasing protein concentration (only for binding excipients)

The data presented in Figure 30 show that the experimental diameters at pH 6.0 for all protein concentrations were larger than the infinite-dilution value of 10.6 nm. As shown in section 4.3.2.3.1 the apparent diameter at infinite dilution was constant (10.6 nm) independently from the NaCl concentration in addition to the background buffer of 10 mM citrate, pH 6.0 (Figure 29). Consequently, the larger experimental diameters in 10 mM citrate, pH 6.0 were not occurring due to coupled protein counterion diffusion but due to attractive protein-protein interactions. However, the effects explained above and listed in Table 27 may still have an impact on  $k_D$ , even if attractive protein-protein interactions are dominant.

At pH 5.0 the experimental diameters were lower than 10.6 nm for protein concentrations between 2.5 mg/ml and 7.5 mg/ml and larger than 10.6 nm for protein concentrations of 15 mg/ml and 20 mg/ml. As no estimate can be made on the size of the protein which would be expected in the absence of coupled protein counterion diffusion, but which may be

affected by the larger net charge at pH 5.0 compared to pH 6.0, the negative  $k_D$  may be either due to attractive protein-protein interactions or due to a decreasing net charge with increasing protein concentration.

At pH 6.5 and pH 7.0 all experimental diameters were larger than 10.6 nm and the diameter in the absence of coupled protein counterion diffusion is assumed to be approximately 10.6 nm or smaller. The larger diameters indicate the negative  $k_D$  to result from attractive protein-protein interaction rather than from a decreasing net charge with increasing protein concentration.

The pH dependence of  $k_D$  showed a plateau of  $-23.0 \text{ ml}\cdot\text{g}^{-1}$  ( $\pm 1.3 \text{ ml}\cdot\text{g}^{-1}$ ) between pH 5.5 and pH 7.0 and a slightly higher value of  $-19.6 \text{ ml}\cdot\text{g}^{-1}$  at pH 5.0.

The pH-dependence of attractive protein-protein interactions is not easily predictable as citrate is assumed to bind to the protein resulting in potential neutralization or even reversal of the protein net charge or potential cross-linking of various antibody molecules. The remaining net charge might depend on the pH but the pH dependency is not predictable. However, as an effect of pH on the apparent diameter at infinite dilution was observed, a remaining net charge is expected at least for the protein formulated in citrate buffer at pH 5.0 and pH 5.5.

The impact of pH on coupled protein counterion diffusion cannot simply be estimated as the net charge of the citrate molecule and the net charge of the protein are both contributing to the effect. In general, the lower the pH, the higher the net charge of the protein. However, citrate binding might influence the actual net charge and the extent of citrate binding as a function of pH is not predictable. In addition, the citrate molecule bears a lower net charge at lower pH. The influence of the net charge of the counterion on the effect of coupled protein-counterion diffusion will be discussed in the next section.

Hence, effects of attractive protein-protein interaction and effects of coupled protein counterion diffusion might superimpose and the influence of pH on these two effects is unpredictable. Summing up, the negative  $k_D$  might indicate a strong impact of attractive protein-protein interactions. Smaller contributions to  $k_D$  might be due to a decreasing net



charge with increasing protein concentration resulting from citrate binding or due a decreasing counterion to protein ratio with increasing protein concentration.

*Comparison of hydrodynamic diameters in citrate buffer with diameters in 50 mM NaCl solution*

The 10 mM citrate buffer at pH 6.0 has an ionic strength of 44 mM. A NaCl concentration of 44 mM has the same ionic strength. As no measurements were performed with a NaCl concentration of 44 mM, the most proximate NaCl concentration of 50 mM was used for comparison (Figure 31).

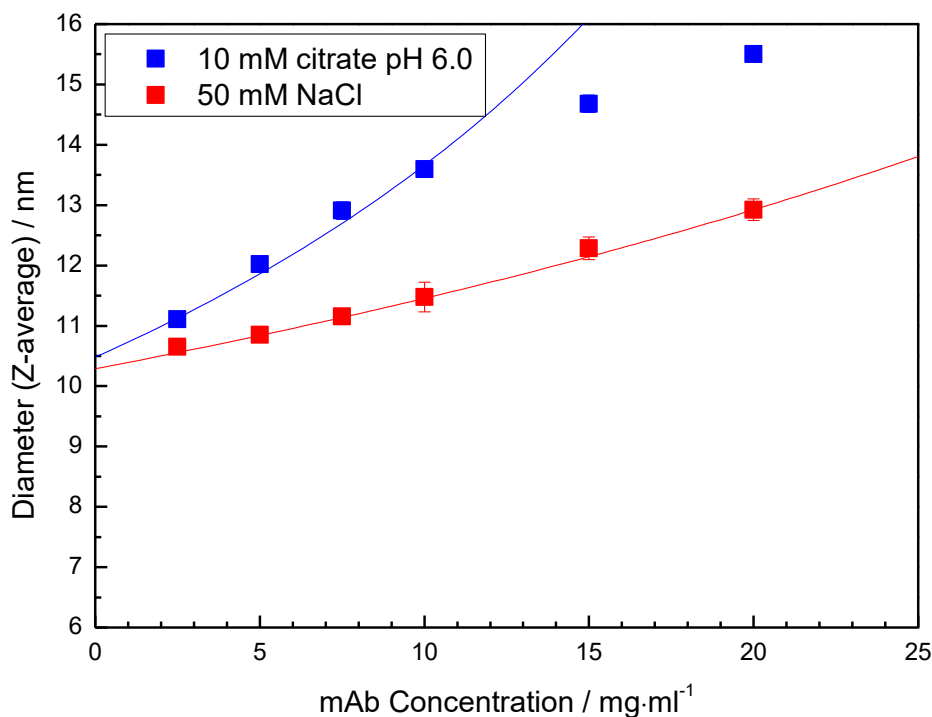


Figure 31: Hydrodynamic diameters of the antibody dissolved in 10 mM citrate buffer pH 6.0 and in 50 mM NaCl solution without buffer as measured by DLS (Wyatt, Plate Reader, 25°C). The hydrodynamic diameters were converted from the measured diffusion coefficients with equ (3).  $k_D$  and  $D_0$  were obtained as described in section 3.2.3.8 by fitting data of the diffusion coefficient to equ (10) (plot not shown here). The solid lines show the results of the curve fitting converted to diameters by equ (3) and equ (15) as described in section 2.3.1.2.

The apparent diameter at infinite dilution was 10.5 nm in 10 mM citrate buffer and 10.3 nm in 50 mM NaCl solution. The difference may be due to measuring uncertainties. The  $k_D$  value was negative for both cases. However, the value was more negative in 10 mM citrate buffer, pH 6.0 with a  $k_D$  of  $-23.3 \text{ ml}\cdot\text{g}^{-1}$  compared to the value of  $-10.2 \text{ ml}\cdot\text{g}^{-1}$  in 50 mM NaCl solution. For all NaCl concentrations examined, the  $k_D$  did not decrease below  $-10.4 \text{ ml}\cdot\text{g}^{-1}$  (Table 26).

The difference between  $k_D$  values in 10 mM citrate buffer and 50 mM NaCl solution can be explained with a different limiting diffusion coefficient of the citrate molecule, or with differences in coupled protein counterion diffusion either due to different actual net charges of the protein or due to the higher valence of the citrate counterion, or with differences in protein-protein interaction.

As the limiting diffusion coefficient of citrate has been published (119), the influence of the limiting diffusion coefficient in combination with the higher valence of the citrate ion compared to chloride ion on the diffusion coefficients and the resulting hydrodynamic diameter can be calculated by equ (23). The results are displayed in Figure 32.

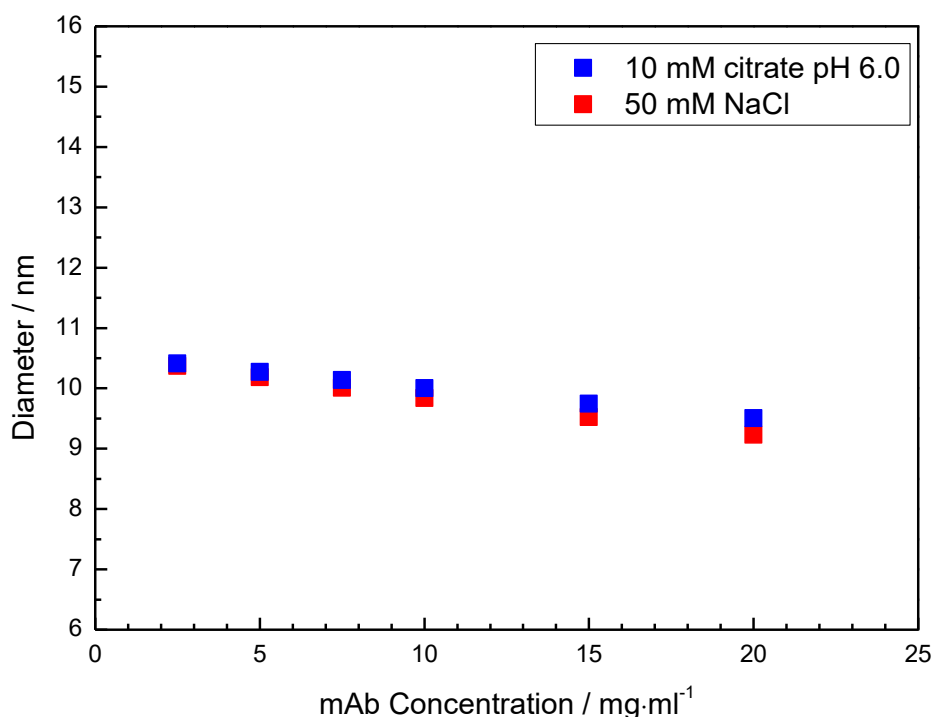


Figure 32: Calculated diameters of the protein in 10 mM citrate buffer, pH 6.0 and in buffer-free solutions containing 50 mM NaCl. The underlying parameters for the calculation with equ (23) are:  $z_{DHH2} = 7.4$ ,  $z_3$  (chloride) = -1,  $z_3$  (citrate) = -2.5,  $pK_{a3}'$  (citrate at an ionic strength of 44 mM) = 6.01,  $D_3$  (chloride) =  $2.032 \cdot 10^{-9} \text{ m}^2 \text{ s}^{-1}$ ,  $D_3$  (citrate) =  $0.623 \cdot 10^{-5} \text{ cm}^2 \text{ s}^{-1}$ ,  $D_2$  (mAb) =  $46.5 \text{ } \mu\text{m}^2/\text{s}$ ,  $c_3$  (Citrate) = 10 mM. The values of  $D_3$  were taken from (119). The chloride concentration in the solutions containing NaCl is assumed to be slightly higher than the declared NaCl concentration (by:  $c(\text{mAb}) \cdot M_w(\text{mAb})^{-1} \cdot z(\text{mAb})$ ) due to protein-related counterions additionally present in the protein solutions.

The net charge of +7.4 as obtained in section 4.3.2.1.1 is only estimated for the conditions here. In 10 mM citrate buffer or in 50 mM NaCl solution, the net charge may differ. However, the correct net charge is assumed to be lower than +7.4 as citrate anions are stronger binding to the antibody than chloride ions (see section 4.1.7). A concentration of 50 mM NaCl is most probably saturating more positive charges than the lower chloride concentration used for the experiments described in section 4.3.2.1.1.

The calculated  $k_D$  is slightly positive for both conditions with values of 7 ml/g in 50 mM NaCl solution and 6 ml/g in 10 mM citrate buffer, pH 6.0.

The similar value of  $k_D$  for both conditions occurring in spite of the different counterion concentration is not directly due to the similar ionic strength but due to the higher valence of the citrate molecule and to a much lower contribution due to the lower limiting diffusion coefficient of the citrate molecule (equ (23)).

Experimental  $k_D$  values were negative with a value of -23.3 ml/g for the protein solutions containing citrate and a value of -10.2 ml/g for the protein solutions containing NaCl. The negative values are most probably not resulting from the effect of coupled protein counterion diffusion as the effect always results in smaller diameters than expected for the uncharged protein. Therefore, the negative  $k_D$  indicates attractive protein-protein interactions in both solution conditions.

The difference between the experimental  $k_D$  of the protein in citrate buffer and the  $k_D$  of the protein in NaCl solution could be due to enhanced protein-protein attraction in the citrate bufferd formulation or due to a missing or reduced positive contribution of coupled protein counterion diffusion on  $k_D$  due to a lower net charge of the protein in citrate buffer. For the calculation of the values displayed in Figure 32, the same net charge was assumed. However, as shown before, by using the approach of buffer equilibration (4.1.7), the citrate ion is assumed to bind more strongly to the antibody compared to chloride. Therefore the positive net charge of the protein is assumed to be lower comparing the two counterion systems with the same concentration of counterion. However, no data are available enabling a comparison of the actual net charge  $z_{DHH}$  of protein in 10 mM citrate buffer pH 6.0 or in 50 mM NaCl solution. If the net charge is lower in 10 mM citrate buffer, the difference in  $k_D$  between 10 mM citrate buffer and 50 mM NaCl solution could be (partly) due to the effect of coupled protein counterion diffusion. The actual extent of this effect is difficult to estimate due to the large uncertainty in protein net charge at higher counterion concentrations.

In addition to the potential of charge neutralization, the citrate ion could potentially crosslink two antibody molecules (52, 142-144) or it could introduce a higher charge anisotropy to the protein thereby enhancing attractive protein-protein interactions (5, 46, 58).

Similar to the results shown here, various studies in the literature report about attractive protein-protein interactions in citrate buffer (52, 149, 186). The attractive interactions were either detected by  $k_D$  measurements (52, 186) or by mechanical rheometry (149).

According to previous results of this thesis, attractive protein-protein interactions of the antibody in citrate buffer are to be expected as the molecule showed the phenomenon of LLPS at higher pH ( $\text{pH} > 7$ ) in 1 mM citrate buffer (see section 4.1.2). However, the absence of LLPS at pH 7.0 in the presence of chloride counterions could also be due to the accelerating effect of coupled protein counterion diffusion which may be more pronounced in the presence of chloride compared to citrate.

The effect of coupled protein counterion diffusion should be considered for all experiments at lower ionic strength which are influenced by the diffusion of the protein. These are phase equilibrium experiments or all types of light scattering experiments, such as turbidity measurements or electrophoretic light scattering experiments (113, 187).

#### 4.3.2.3.3. Dependence of the diffusion coefficient on the citrate buffer concentration at pH 6.0

The citrate concentration dependence of  $D_0$  and  $k_D$  was determined citrate buffer pH 6.0 for citrate concentrations ranging between 0 and 40 mM. The samples were obtained by dialysis and subsequent dilution with citrate buffer of respective concentration. The results of the DLS measurements performed as described in section 3.2.1.10 are displayed in Figure 33.

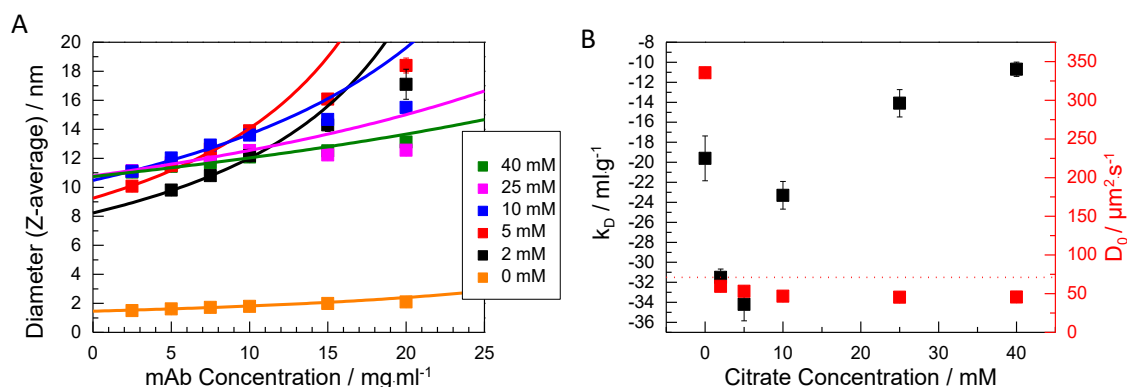


Figure 33: Influence of the citrate buffer concentration on the hydrodynamic diameter, the  $k_D$  and on  $D_0$  of the mAb as measured by DLS (Wyatt, Plate Reader, 25°C). The hydrodynamic diameters shown in Figure 33A were converted from the measured diffusion coefficients with equ (3).  $k_D$  and  $D_0$  were obtained as described in section 3.2.3.8 by fitting data of the diffusion coefficient to equ (10) (plot not shown here). The solid lines in Figure 33A show the results of the curve fitting converted to diameters by equ (3) and equ (15) as described in section 2.3.1.2.  $k_D$  and  $D_0$  values as a function of pH are separately depicted in Figure 33B. Diffusion coefficients larger than  $71 \mu\text{m}^2/\text{s}$  (as depicted by the dotted red line in Figure 33B) correspond to diameters lower than 6.9 nm (equ (3)). This diameter is considered to be the minimal real diameter of the mAb as described in section 4.3.2.1.1.

#### *Apparent diameter at infinite dilution*

The apparent diameter at infinite dilution was 1.5 nm in the absence of citrate buffer. It increased with increasing citrate concentration from 8.2 nm in 2 mM citrate to 10.5 nm in 10 mM citrate buffer. Between 10 mM and 40 mM citrate buffer, the apparent diameter at infinite dilution was approximately constant (10.5 – 10.8 nm).

The effect of coupled protein counterion diffusion might result in lower hydrodynamic diameters between 0 mM and 5 mM citrate buffer. At a citrate buffer concentration of 10 mM the effect of coupled protein counterion diffusion disappears. This could either be due to citrate-protein binding and thereby decreasing the actual net charge or due to the higher effective counterion concentration.

In the absence of buffer, a NaCl concentration of 5 mM was sufficient to abolish the effect of coupled protein counterion diffusion (Figure 25). Therefore, for both types of anions the impact of coupled protein counterion diffusion on infinite dilution diameters disappears at a similar concentration.

The diameters extrapolated to zero protein concentrations obtained in 5 mM – 150 mM NaCl solutions in the absence of buffer of 10.3 nm – 10.6 nm (see section 4.3.2.1.2) were slightly lower than the infinite dilution diameters of 10.5 nm – 10.8 nm between 10 mM and 40 mM citrate buffer. However, this difference is assumed to be not significant.

The infinite dilution diameters of 10.5 nm – 10.7 nm obtained in the presence of 10 mM citrate buffer and various NaCl concentrations (see section 4.3.2.3.1) agree well with diameters of 10.5 nm – 10.8 nm between 10 mM citrate buffer and 40 mM citrate buffer.

The agreement between values for the apparent diameter at infinite dilution obtained under various experimental conditions at a minimum citrate concentration of 10 mM and a minimum NaCl concentration of 5 mM allows us to calculate the limiting diffusion coefficient of the protein. For a diameter of 10.6 nm the limiting diffusion coefficient is  $46.5 \mu\text{m}^2/\text{s}$  at  $25^\circ\text{C}$ .

#### *Dependence of $D$ on protein concentration*

$k_D$  decreased from  $-19.6 \text{ ml}\cdot\text{g}^{-1}$  to  $-34.2 \text{ ml}\cdot\text{g}^{-1}$  by increasing the citrate buffer concentration from 0 mM to 5 mM and then increased again to a value of  $-10.7 \text{ ml}\cdot\text{g}^{-1}$  at a citrate buffer concentration of 40 mM.

The less negative values of  $k_D$  in the solutions of 0 mM and 2 mM citrate buffer compared to the value at 5 mM citrate buffer may be due to coupled protein counterion diffusion and the varying counterion to protein ratio with increasing protein concentration. With increasing citrate buffer concentration this effect is assumed to vanish and attractive protein-protein interactions may superimpose the effect of protein-counterion diffusion interaction on  $k_D$ . As shown before in section 4.3.2.1.2 and section 4.3.2.3.1, attractive protein-protein interactions are assumed to be lowered with increasing ionic strength. Therefore, the  $k_D$  may increase with increasing citrate buffer concentration for citrate buffer concentrations larger than 5 mM.

Another possible explanation for the non-monotonic trend of  $k_D$  as a function of citrate concentration could be a charge reversal of the protein at higher citrate buffer concentrations. A citrate buffer concentration of 5 mM could neutralize the protein by protein-citrate binding. The missing net charge would result in minimal electrostatic

repulsion. Larger citrate buffer concentrations of  $> 5$  mM could result in charge reversal of the protein-citrate complex to a negative net charge and therefore enhanced repulsive Coulomb interactions and reduced attractive interactions due to reduced charge anisotropy of the protein. The missing effect of the negative net charge on the diffusion coefficient  $D_0$  could be due to the larger concentration of effective counterions.

#### *The dependence of $k_D$ on ionic strength*

In Figure 34  $k_D$  -values are plotted as a function of ionic strength adjusted by citrate or NaCl in the presence of 10 mM citrate.

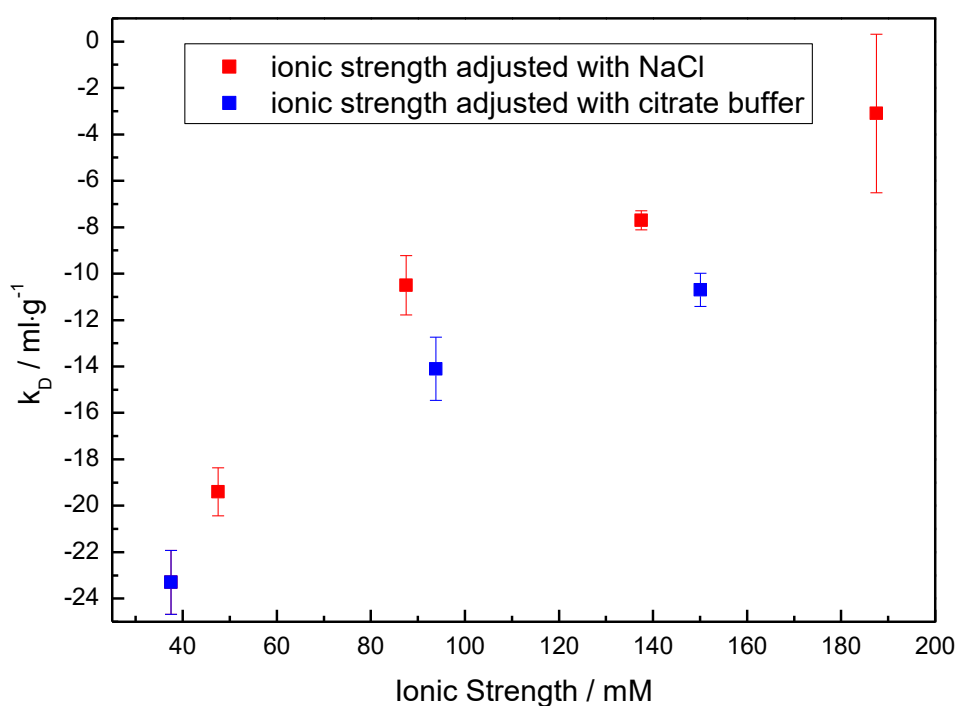


Figure 34: Comparison of  $k_D$  values as a function of ionic strength. The minimal ionic strength of 38 mM arose from the citrate buffer concentration of 10 mM. Ionic strength was either adjusted by increasing the citrate buffer concentration or by adding NaCl.

$k_D$  values in citrate buffer were approximately  $4 \text{ ml}\cdot\text{g}^{-1}$  lower than in solutions adjusted with NaCl to the given ionic strength. Due to the lower number of measurements, the difference may not be significant.



Screening attractive protein-protein interactions is supposed to depend on the ionic strength and not on the effective counterion concentration. If screening was the only effect appearing here, NaCl and citrate buffer should have the same effect on  $k_D$ . However, in addition to screening, specific effects of the citrate molecule, such as protein net charge neutralization or protein-protein cross-linking could take place. Protein-citrate binding could therefore result in enhanced protein-protein attraction.

If the increasing values of  $k_D$  as a function of citrate buffer concentration for concentrations  $> 5$  mM (Figure 33) would be due to charge reversal at higher citrate buffer concentrations, the addition of NaCl would be expected to electrostatically screen the protein-citrate interaction and thereby increase the charge anisotropy as well as decrease the protein net charge. Therefore, the  $k_D$  should be lower if ionic strength is adjusted with NaCl compared to adjustment with citrate buffer (Table 28). The results obtained as shown in Figure 34 with higher  $k_D$  values for NaCl compared to citrate buffer do not support the scenario of charge reversal by citrate buffer concentrations  $> 5$  mM. Therefore, the increasing values of  $k_D$  with increasing citrate buffer concentration are most probably due to screening of electrostatic multipolar attractive interactions, which are slightly influenced by citrate-specific effects.

Table 28: Verification table of a potential charge reversal by citrate: Expectations for the dependence of additional NaCl or citrate buffer on dipole-dipole interactions or ion-ion interactions assuming an initial protein solution containing 10 mM citrate buffer pH 6.0 where citrate-induced charge reversal occurs. Factors with an increasing effect on  $k_D$  are labelled in blue, factors with a decreasing effect on  $k_D$  are labelled in red. An increasing net charge is assumed to result in a lowered dipole moment (5).

		Citrate	NaCl
Dipole-dipole	Citrate binding	Citrate-binding is enhanced → Dipole moment decreases Reduced attractive interactions	Citrate-binding is reduced → dipole moment increases Enhanced attractive interactions
	Unspecific screening	Dipole-dipole interactions are screened	Dipole-dipole interactions are screened
Ion-Ion	Citrate-binding	Citrate-binding is enhanced → Protein net charge increases Ion-Ion repulsion increases	Citrate-binding is reduced → Protein net charge decreases Ion-ion repulsion decreases
	Unspecific screening	Ion-ion repulsion is screened	Ion-ion repulsion is screened

*Comparison of the citrate buffer concentration dependence on  $k_D$  with the buffer-free NaCl dependence*

A non-monotonic change in  $k_D$  as a function of anion concentration was observed after addition of NaCl or citrate. The  $k_D$  was decreasing to a minimum of -10.4 ml/g in 100 mM NaCl, whereas the minimal  $k_D$  -value was much lower (-34.2 ml/g) in 5 mM citrate. The decrease in  $k_D$  at low anion concentrations seems to be influenced by the effect of coupled protein counterion interaction, which is decreasing with increasing effective counterion concentration. Likewise, the electrostatic protein-protein repulsions are screened and thereby decreasing with increasing ionic strength. The second part of the curve is assumed to be dominated by attractive protein-protein interactions of dipole-dipole or ion-dipole nature which are decreasing with increasing ionic strength, leading to an increase in  $k_D$ .

This scenario can only apply if dipolar and multipolar attractions are considered to be less shielded than electrostatic ion-ion repulsion. Several studies indicate the validity of this

assumption (188, 189). The specific excipient concentration at the minimum of  $k_D$  marks the point where attractive protein-protein interactions decrease stronger with increasing ionic strength than repulsive protein-protein interactions increase. In such buffers that induce enhanced protein-protein attraction, such as citrate buffer, the minimal  $k_D$  is expected to occur at a lower excipient concentration.

Another theory postulated by Paunov et al.(190), claims the second part of the curve to be dominated by non-DLVO repulsion, also termed hydration repulsion. At higher salt concentrations an exchange of  $H^+$  against  $Na^+$  on the hydroxylate groups of the protein is postulated. These sodium ions are supposed to form the Stern layer. According to Paunov et al., non-DLVO repulsion is caused by these overlapping Stern layers (190).

As shown in section 4.1.3 LLPS of the same antibody also shows a non-monotonic dependence on the citrate buffer concentration. The maximal width of the miscibility gap at 5°C was observed at 5 mM citrate buffer at pH 7.2 and at 2 mM citrate buffer at pH 7.8. The maximal width of the miscibility gap indicates overall protein-protein interactions to be most attractive. The mechanism behind the maximum may be the same as the mechanism behind the lowest  $k_D$  values at a specific citrate buffer concentration.

#### 4.3.2.4. Dependence of the diffusion coefficient of the antibody on the buffer species with a buffer concentration of 10 mM at pH 6.0

The diffusion coefficients of the monoclonal antibody buffered in acetate, histidine, citrate or succinate at a buffer concentration of 10 mM and pH 6.0 were measured between protein concentrations of 2.5 mg/mL and 20 mg/mL. The results of DLS measurements performed as described in section 3.2.1.10 are displayed in Figure 35. For comparison, data of the protein in water at pH 6.0 are also displayed.

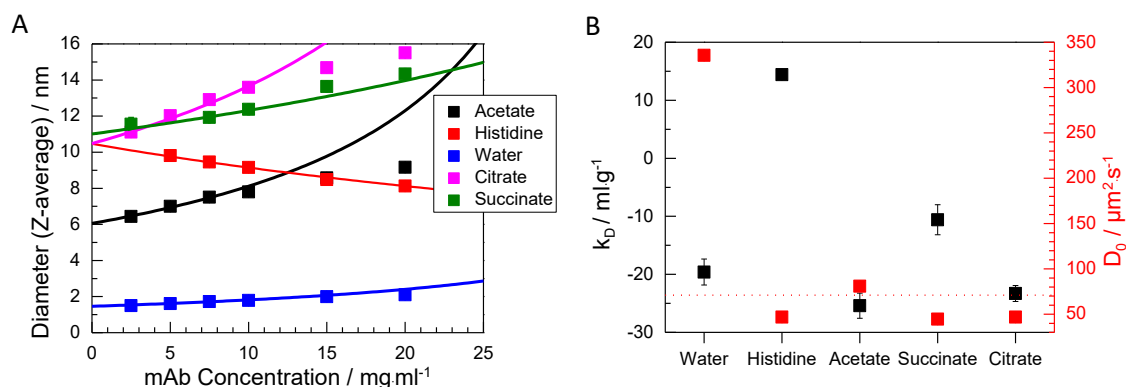


Figure 35: Influence of the buffer species on the hydrodynamic diameter, the  $k_D$  and on  $D_0$  of the mAb as measured by DLS (Wyatt, Plate Reader, 25°C). The hydrodynamic diameters shown in Figure 35A were converted from the measured diffusion coefficients with equ (3).  $k_D$  and  $D_0$  were obtained as described in section 3.2.3.8 by fitting data of the diffusion coefficient to equ (10) (plot not shown here). The solid lines in Figure 35A show the results of the curve fitting converted to diameters by equ (3) and equ (15) as described in section 2.3.1.2.  $k_D$  and  $D_0$  values as a function of pH are separately depicted in Figure 35B. Diffusion coefficients larger than  $71 \mu\text{m}^2/\text{s}$  (as depicted by the dotted red line in Figure 35B) correspond to diameters lower than 6.9 nm (equ 3). This diameter is considered to be the minimal real diameter of the mAb as described in section 4.3.2.1.1.

At infinite dilution, the lowest value for the protein apparent diameter with 1.5 nm was observed for the antibody dissolved in water. The respective values for the infinite dilution diameter for the antibody dissolved in buffers were: 6.1 nm in 10 mM acetate buffer pH 6.0, 10.5 nm in 10 mM citrate buffer and 10 mM histidine buffer pH 6.0 and 11.0 nm in 10 mM succinate buffer pH 6.0

For the antibody dissolved in acetate buffer the diameter was smaller than 6.9 nm, which is the minimal diameter of the protein expected to form a compact sphere (see section 4.3.2.1.1). The low diameter is assumed to result from coupled protein counterion diffusion and repulsive Coulomb protein-protein interactions. The infinite-dilution diameter found for the protein in 10 mM histidine seems to be less affected by the two effects compared to acetate buffer. However, the positive  $k_D$  observed in histidine buffer, which likely results from the effect of coupled protein counterion diffusion and a varying effective counterion to protein ratio, was not observed in 10 mM acetate buffer.

The effective counterion concentration was lower in 10 mM histidine buffer, compared to 10 mM acetate buffer (Table 29). Therefore, the effects of coupled protein counterion diffusion should be more pronounced in 10 mM histidine buffer. However, the effect of

coupled protein counterion diffusion does not solely depend on the effective counterion concentration, but on the actual protein charge and limiting diffusion coefficients of the counterions. Therefore, a calculation based on equ (23) will be performed to quantify these effects. The occurrence of the lower infinite dilution diameter in 10 mM acetate will be discussed in section 4.3.2.5.

The  $k_D$  was negative in all buffer systems except histidine. The  $k_D$  of the antibody in succinate ( $-10.6 \text{ ml}\cdot\text{g}^{-1}$ ) was less negative compared to the  $k_D$  of the antibody in acetate buffer ( $-25.4 \text{ ml}\cdot\text{g}^{-1}$ ) or citrate buffer ( $-23.3 \text{ ml}\cdot\text{g}^{-1}$ ). No explanation is found for this observation.

Table 29: Effective counterion concentration and ionic strength of the buffers of a concentration of 10 mM

	Charge of the counterion at pH 6.0	Counterion of the antibody	Effective counterion concentration	Calculated ionic strength of the buffer/ mM
Histidine	+0.5	chloride	5 mM	4
Acetate	-0.9	acetate	9 mM	9
Succinate	-1.7	succinate	10 mM	23
Citrate	-2.3	citrate	10 mM	38

#### Comparison of calculated and experimental data

The influence of the different limiting diffusion coefficients and the higher valence of some of the counterions on diffusion coefficients and resulting hydrodynamic diameters of the mAb can be calculated by equ (23). The results are displayed in Figure 36 and are listed in Table 30 and Table 31.

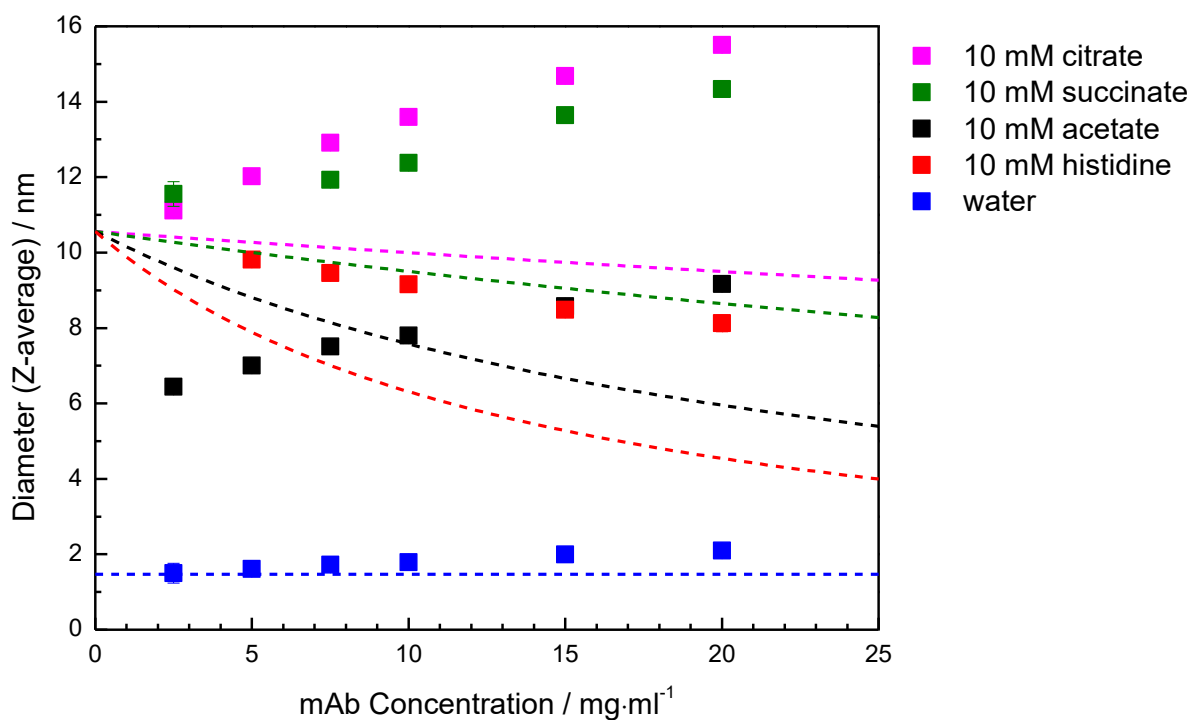


Figure 36: Comparison of calculated diffusion coefficients (dashed lines) with experimental values (squares). The parameters for the calculation using equ (23) are  $z_{DHH2} = 7.4$ ,  $D_2$  (mAb) =  $46.5 \mu\text{m}^2/\text{s}$ ,  $z_3$  (10 mM citrate) =  $-2.5$ ,  $pK_{a3}'$  (10 mM citrate) =  $6.01$ ,  $D_3$  (citrate) =  $0.623 \cdot 10^{-5} \text{ cm}^2 \text{ s}^{-1}$ ,  $z_3$  (10 mM succinate) =  $-1.78$ ,  $pK_{a2}'$  (10 mM succinate) =  $5.45$ ,  $D_3$  (succinate) =  $0.783 \cdot 10^{-5} \text{ cm}^2 \text{ s}^{-1}$ ,  $z_3$  (10 mM acetate) =  $-0.95$ ,  $pK_{a1}'$  (10 mM acetate) =  $4.71$ ,  $D_3$  (acetate) =  $1.089 \cdot 10^{-5} \text{ cm}^2 \text{ s}^{-1}$ ,  $z_3$  (10 mM histidine) =  $0.54$ ,  $pK_{a1}'$  (10 mM histidine) =  $6.07$ ,  $z_3$  (chloride) =  $-1$ ,  $D_3$  (chloride) =  $2.032 \cdot 10^{-9} \text{ m}^2 \text{ s}^{-1}$ . The values of  $D_3$  were taken from (119). Accumulation of counterions and depletion of coions according to the Donnan theory were not considered for the calculation (except for data in water).

Table 30: Comparison of calculated infinite-dilution diameters with experimental values. The calculated infinite-dilution diffusion coefficients were obtained as described in section 3.2.5, using parameters as presented in the description of Figure 36. The infinite-dilution diffusion coefficients were converted to infinite-dilution diameters by equ (3).

Buffer	Concentration / mM	Protein charge (unitless)	Calculated diameter $d_0$ / nm	Experimental diameter $d_0$ / nm
citrate	10	+7.4	10.5	10.5
acetate	10	+7.4	10.5	6.1
		+16.7	10.0	
histidine	10	+7.4	10.5	10.5
succinate	10	+7.4	10.5	11.0
water	0	+7.4	1.5	1.5

Table 31: Comparison of calculated  $k_D$  values with experimental values. The calculated  $k_D$  values were obtained as described in section 3.2.5, using parameters as presented in the description of Figure 36.

Buffer	Concentration / mM	Protein charge (unitless)	Calculated $k_D$ / ml·g <sup>-1</sup>	Experimental $k_D$ / ml·g <sup>-1</sup>
citrate	10	+7.4	5.6	-23.3
acetate	10	+7.4	39.1	-25.4
		+16.7	174.3	
histidine	10	+7.4	66.9	14.4
succinate	10	+7.4	11.1	-10.6
water	0	+7.4	0	-19.6

The majority of calculated diameters at infinite dilution are well fitting to the experimental data. The only value which does not coincide at all is the infinite-dilution diameter in acetate buffer.

A variation of the calculations with a net charge of 16.7 instead of 7.4 was performed to test whether the low experimental diameter of 6.1 nm in 10 mM acetate could be due to a higher actual protein net charge. The valence of 16.7 would account for the protonation

state of the antibody without considering bound counterions. However, calculations assuming a net charge of 16.7 would result in an infinite-dilution diameter of 10.0 nm. Therefore, a higher net charge is most probably not a suitable explanation for the low experimental infinite-dilution diameter of 6.1 nm in acetate buffer. The dependence of diffusion coefficients on the protein concentration in 10 mM acetate has some similarity with values in 2 mM citrate buffer pH 6.0. This similarity will be discussed in detail in section 4.3.2.5.

All experimental  $k_D$  values were lower than the calculated data. The only positive  $k_D$  value was measured in histidine buffer. Calculated  $k_D$  data were all positive due to the decreasing counterion to protein ratio with increasing protein concentration which results in decreasing coupled protein counterion diffusion with increasing protein concentration.

The lower experimental  $k_D$  values may be due to attractive protein-protein interactions which may occur independently from the used formulation. Attractive protein-protein interactions could be due to a large dipole moment of the antibody and resulting di- and multipolar interactions or due to hydrophobic patches resulting in hydrophobic interactions. These interactions are not considered by the model described by eq. 22.

A negative contribution to  $k_D$  of the phenomenon of coupled protein counterion diffusion is possible if the counterions are only weakly binding to the protein (see section 4.3.2.3.2). This effect was not considered by eq. (23).

Even though the results of calculations do not well coincide with experimental results, the trend of diffusion coefficients of the different buffers is the same at protein concentrations  $\geq 15$  mg/ml. In this concentration range, the ranking of calculated and experimental diffusion coefficients is: water  $\geq$  histidine-chloride  $\geq$  acetate  $\geq$  succinate  $\geq$  citrate. This ranking is also the inverse trend of ionic strengths of the buffers (Table 29).

At lower protein concentrations ( $c \leq 10$  mg/ml), the diffusion coefficient of the antibody in acetate buffer was larger than the diffusion coefficient of the antibody in histidine. Similar to the unexpected low experimental diameter at infinite dilution, the experimental diameters were lower in acetate buffer compared to histidine buffer at protein concentrations up to 10 mg/ml.



The ranking at protein concentrations  $\geq 15$  mg/ml could have two reasons which go hand in hand. First, repulsive Coulomb protein-protein interactions are assumed to be screened with increasing ionic strength. This would result in lower diffusion coefficients and larger protein diameters at higher ionic strengths. Second, the effect of coupled protein counterion diffusion is assumed to be weakened at higher effective counterion concentration and higher valence of the counterions. Therefore, higher diffusion coefficients and lower protein diameters are expected for the protein in water and histidine buffer due to their lower effective counterion concentration. Oppositely lower diffusion coefficients and larger protein diameters are expected for the antibody buffered in succinate and citrate, due to their higher valence. Equ (23) accounts for both effects. The analogy in ranking between experimental and calculated data underlines the significance of simple electrostatic effects in solutions of complex biomolecules.

#### 4.3.2.5. Comparison of protein diffusion coefficients in aqueous solutions containing 2 mM citrate buffer, 10 mM acetate buffer or 2 mM NaCl

As described in detail in section 4.3.2.4 in 10 mM acetate buffer pH 6.0 the proteins experimental infinite-dilution diameter and diameters of the protein at protein concentrations up to 10 mg/ml showed lower values than expected in comparison to experimental diameters of the protein in other buffer systems. The diameters of the protein as a function of the protein concentration in 10 mM acetate pH 6.0 were similar to the experimental protein diameters in 2 mM citrate buffer pH 6.0 (see section 4.3.2.3.3). In both buffer systems the infinite-dilution diameter of the protein was lower than 9 nm and the proteins  $k_D$  was negative. To further examine the effect, the diameters of the protein in 10 mM acetate pH 6.0, 2 mM citrate buffer pH 6.0 and 2 mM NaCl solution are plotted as a function of protein concentration. The results are displayed in Figure 37 and are listed in Table 32 and Table 33.

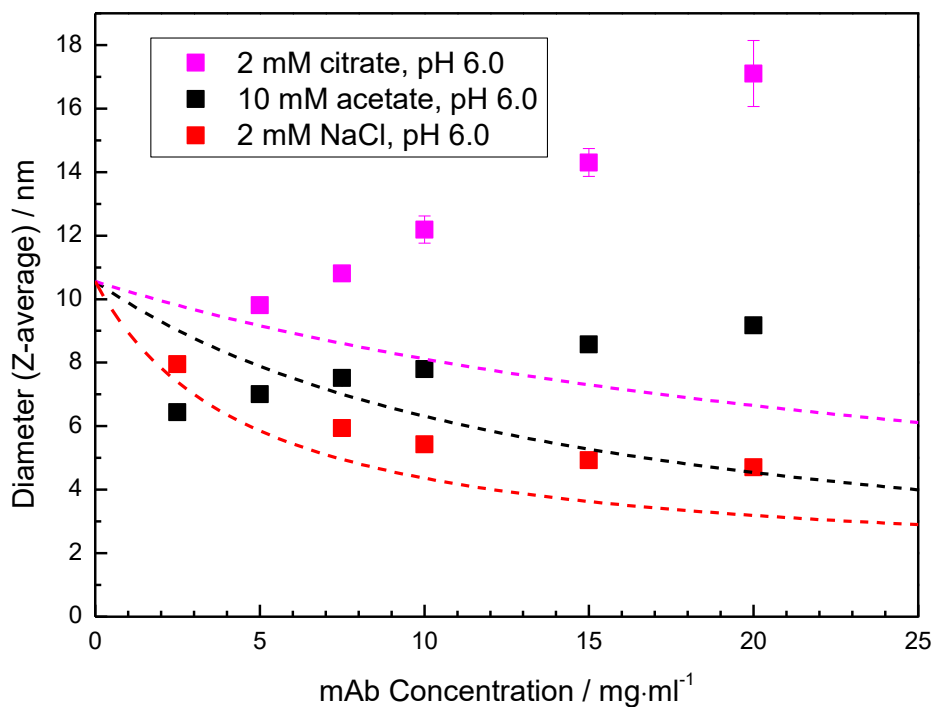


Figure 37: Comparison of calculated diffusion coefficients (dashed lines) with experimental values (squares). The parameters for the calculations using equ (23) are  $z_{DHH2} = 7.4$ ,  $D_2$  (mAb) =  $46.5 \mu\text{m}^2/\text{s}$ ,  $z_3$  (2 mM citrate) =  $-2.38$ ,  $pK_{a3'}$  (2 mM citrate) =  $6.20$ ,  $D_3$  (citrate) =  $0.623 \cdot 10^{-5} \text{ cm}^2 \text{ s}^{-1}$ ,  $z_3$  (10 mM acetate) =  $-0.95$ ,  $pK_{a'}$  (10 mM acetate) =  $4.71$ ,  $D_3$  (acetate) =  $1.089 \cdot 10^{-5} \text{ cm}^2 \text{ s}^{-1}$ ,  $z_3$  (chloride) =  $-1$ ,  $D_3$  (chloride) =  $2.032 \cdot 10^{-9} \text{ m}^2 \text{ s}^{-1}$ . The values of  $D_3$  were taken from (119). Accumulation of counterions and depletion of coions according to the Donnan theory were not considered for the calculation (except for data in 2 mM NaCl solution).

Table 32: Comparison of calculated infinite-dilution diameters with experimental values. The calculated infinite-dilution diffusion coefficients were obtained as described in section 3.2.5, using parameters as presented in the description of Figure 37. The infinite-dilution diffusion coefficients were converted to infinite-dilution diameters by equ (3).

Buffer	Concentration / mM	Protein charge (unitless)	Calculated diameter $d_0$ / nm	Experimental diameter $d_0$ / nm
Citrate	2	+7.4	10.5	8.2
		+16.7	10.0	
Acetate	10	+7.4	10.5	6.1
		+16.7	10.0	
NaCl	2	+7.4	9.4	9.4
		+16.7	5.2	

Table 33: Comparison of calculated  $k_D$  values with experimental values. The calculated  $k_D$  values were obtained as described in section 3.2.5, using parameters as presented in the description of Figure 37.

Buffer	Concentration / mM	Protein charge (unitless)	Calculated $k_D$ / ml·g <sup>-1</sup>	Experimental $k_D$ / ml·g <sup>-1</sup>
Citrate	2	+7.4	29.9	-31.5
		+16.7	128.6	
Acetate	10	+7.4	39.1	-25.4
		+16.7	174.3	
NaCl	2	+7.4	118.2	73.3
		+16.7	215.6	

The experimental diameter at infinite dilution of the protein dissolved in the three formulations was increasing with the following ranking: acetate < citrate < NaCl. Comparison of the infinite-dilution diameter of the protein in 2 mM citrate buffer and in 2 mM NaCl solution leads one to expect a higher protein diameter in citrate buffer, due to the higher valence of the citrate ion. The infinite dilution diameter in 10 mM acetate would be expected to be higher than the diameter in NaCl solution, due to the similar charge of the counterion but the higher counterion concentration in acetate. Hence, in both organic

buffers the infinite dilution diameter of the protein is smaller than expected by using the theory of coupled protein counterion diffusion. However, for proteins dissolved in water and in NaCl solution, this theory is valid (see section 4.3.2.1).

The lower diameter could result from a higher net charge of the protein. However, an increase in net charge from 7.4 to 16.7 (corresponding to the valence of the protein at pH 6.0) results in a calculated infinite-dilution diameter of 10.0 nm. This increase in net charge is not sufficient to result in diameters as small as experimentally obtained. However, an even higher increase is not very probable. Comparison of  $k_D$  values of experimental and calculated data indicates that the smaller diameter of the protein dissolved in acetate and citrate buffer is not due to a higher net charge. Experimental  $k_D$  values of the protein dissolved in 10 mM acetate and 2 mM citrate buffer were relatively low. An increasing net charge should result in very high  $k_D$  values (Table 33). A higher net charge would enhance Coulomb protein-protein repulsion and coupled protein counterion diffusion and should thereby increase the value of  $k_D$ .

The theory resulting in equ (23) seems not to be correct to explain the low diameters in 2 mM citrate buffer and 10 mM acetate. A potential theory to explain this deviation is an enhanced coupling between counterions and the protein if the interactions between both species are attractive but binding does not yet occur. These results would then indicate in another manner an attractive interaction between the organic anions (citrate and acetate) and the protein.

Summing up, more specific protein excipient interactions may take place in the organic buffer systems whereas the diffusion in the presence of chloride counterions is mainly predictable by equ (23) taking into account simple electrostatics. This observation is in accordance with assumption that chloride ions do not specifically interact with the protein but simply act by electrostatic screening (52).

### **4.3.3. Summary and conclusions**

The model introduced here which relates diffusion coefficients for charged proteins in aqueous solutions to the charge of the protein is well suited to calculate the Debye-Hückel-Henry charge of a protein in protein solutions by using the diffusion coefficient at infinite

dilution in the absence of additional salt. The apparent diameter of the protein at infinite dilution as a function of NaCl concentration could be predicted by the established model. Experimental  $k_D$  values were generally lower than calculated  $k_D$  values probably due to attractive protein-protein interactions not considered by the model. These attractive interactions can therefore be quantitatively estimated by taking the difference between experimental and calculated  $k_D$  values. The diffusion coefficients of the antibody in various buffer systems at pH 6.0 were markedly different. In histidine buffer, the diffusion coefficients were comparable to those observed in unbuffered NaCl solution. For the antibody in citrate buffer low  $k_D$  values were observed, probably caused by strong attractive interactions. These were weakened with increasing ionic strength, either by addition of NaCl or additional citrate. The protein diffusion coefficients in succinate buffer were similar to the diffusion coefficients measured using citrate buffer, even though  $k_D$  values were less negative. In acetate buffer at pH 6.0, up to a protein concentration of 15 mg/ml, the diffusion coefficient was higher than expected with a concomitant much lower apparent diameter at infinite dilution. A similar observation was made for the protein diffusion coefficient in 2 mM citrate buffer at pH 6.0.

The diffusion behavior of the protein is well described by equ (23) in the case when the counterions are chloride ions. However, if the solution contains organic counterions (acetate and citrate) at low ionic strength, equ (23) fails. This failure could be due to attractive interactions between the organic counterions and the protein resulting in enhanced coupling of the diffusion of both interacting partners. Even though further experiments would be needed to confirm this theory the measurement of diffusion by DLS could be used as an additional method to detect and quantify protein-excipient interaction.

As shown with equ (23), a  $k_D$  of zero was calculated for a protein-counterion solution, if only Coulomb interactions between the proteins, between the counterions and between the proteins and the counterions are taking place. In the classical concept of  $k_D$  a large repulsion and therefore a positive  $k_D$  would be expected for such a scenario. Furthermore, a largely positive  $k_D$  was observed and determined by equ (23) in solutions containing small, constant amounts of NaCl, but varying protein concentrations. It was shown, that this largely positive  $k_D$  was resulting from the decreasing ratio of counterions to protein with

increasing protein concentration and therefore enhanced coupled protein counterion diffusion with increasing protein concentration and not directly from repulsive PPIs.

Conclusively, the simplified model of  $k_D$  of a two component system in the traditional sense was shown not to be applicable for the charged mAb at low ionic strengths where at least 3 components with varying concentration need to be taken into account. Therefore, the classical interpretation of low  $k_D$  values representing more attractive PPIs and higher  $k_D$  values representing more repulsive interactions is not valid under these circumstances. Even though a correlation between the  $k_D$  and the protein-protein interaction potential is not given, a number of experimental studies have found empirical correlations between the  $k_D$  and the opalescence (10, 65), the viscosity (51, 53, 57-61) and the aggregation kinetics (53, 54, 70, 74) of a protein solution. Although the protein-protein interaction potential is not the origin of the sign and size of  $k_D$ , a non-causal correlation might exist. This correlation could be limited to a defined range of pH or excipient concentration or ionic strength. At very low ionic strength, where the calculated  $k_D$  (by the three component model as described in section 3.2.5) is zero and the diffusion coefficient at infinite dilution is larger than expected from the real size of the protein, large protein-protein repulsions would be expected and a correlation between the  $k_D$  and the protein-protein interaction potential does likely not exist. However, at higher ionic strengths, where the diffusion coefficient at infinite dilution approaches values, which stay constant upon further increase of ionic strength, a (non-causal) correlation between the  $k_D$  and the protein-protein interaction potential might exist. Further experimental and theoretical work is necessary, to elucidate a potential non-causal correlation with statistical significance and to define the valid range.

DLS measurements for size determinations should be interpreted with care, as the measured size is strongly depending on the solution composition. However, a comparison in the protein size and size distribution is meaningful, if the formulation of the protein solution is the same. This could be used for example for accelerated stress tests, where a non-stressed and a stressed solution (of the same formulation) are measured.

Implications of the observed effects of protein-counterion diffusion interaction do not only cover DLS measurements but all methods affected by the diffusion of a protein. Different studies report about apparently lower measured molecular weights by SLS at very low ionic

strength (191) or lower turbidities (187, 191). Electrophoretic light scattering has been reported to be challenging at salt concentrations below 10 mM – 20 mM (113). Diffusion also influences the Sorret coefficient measured by thermophoresis and should therefore be taken into account (192). And finally, the phenomenon of LLPS is closely related to diffusion (193).





## 5. SUMMARY, CONCLUSION AND OUTLOOK

### Summary

In the first part of the work, the phenomenon of LLPS of an antibody solution in the presence of citrate was examined in detail. In the second part of the work, the focus was LSPS induced by oligovalent anions such as mellitate. And the last part of the work dealt with protein diffusion measured by DLS in solutions with different compositions.

In part I and part II, solution conditions which (dis-)favour LLPS or LSPS in monoclonal antibody solutions were investigated. These are:

1. pH
2. (maximum) charge of the added anion
3. ionic strength
4. concentration of the oligovalent anion
5. overall protein concentration
6. temperature

#### 1: pH

LLPS was observed at the isoelectric point of the mAb in the absence of excipients. LLPS or LSPS were observed at pH below the pI if citrate or other oligovalent anions, such as butane-1,2,3,4-tetracarboxylate, benzene-1,2,4,5-tetracarboxylate, benzene-1,2,3,4,5-pentacarboxylate or benzene-1,2,3,4,5,6-hexacarboxylate were present.

These oligovalent anions are proposed to bind to the positively charged protein and thereby neutralize the protein in a limited pH region, resulting in LLPS. An additional cross-linking mechanism may strengthen the attractive protein-protein interactions resulting in LSPS as observed for benzene-1,2,3,4,5-pentacarboxylate or benzene-1,2,3,4,5,6-hexacarboxylate.

Regarding the pH range below the pI, phase separation was enhanced at lower pH in the presence of mellitate whereas it was reduced at lower pH in the presence of citrate. At lower pH the protein net charge increases and the negative charge of citrate and mellitate decreases. The remaining net charge of the citrate ion might not be sufficient to neutralize

the net charge of the mAb at sufficiently low ionic strengths. In contrast, the remaining net charge of the mellitate ion seems to be sufficient to neutralize the positive net charge of the mAb and cross-linking might even be enhanced caused by the higher positive charge of the mAb.

## 2: (Maximum) charge of the added anion

The extent of phase separation was shown to increase with anion charge. Depending on the anion charge, different states of hydration of the antibody-anion complex were deduced. At lower anion charge, turbid solutions were observed (highly hydrated antibody molecules), at intermediate anion charge, LLPS was observed (medium hydrated antibody molecules) and at higher anion charge, LSPS was observed (least hydrated antibody molecules). Depending on the experimental parameters (pH, ionic strengths) LLPS was observed for citrate, butane-1,2,3,4-tetracarboxylate, benzene-1,2,4,5-tetracarboxylate, benzene-1,2,3,4,5-pentacarboxylate and mellitate as anions. In contrast LSPS was only observed for benzene-1,2,3,4,5-pentacarboxylate and benzene-1,2,3,4,5,6-hexacarboxylate. This could be due to enhanced binding of these higher charged excipients and enhanced steric capacity to protein-protein cross-linking.

The maximum possible charge of the oligovalent anion (charge after complete dissociation) seems to have a stronger influence on phase separation than the charge that would be expected at a given pH (incomplete dissociation of the weak acid). This indicates that the phenomenon of "induced charging", i.e. the dissociation of protons from protonated carboxyl groups after binding, affects the actual charge of the oligovalent anion when binding to the protein.

## 3: Ionic strength

Phase separation was reduced by increasing ionic strength in the presence of citrate (4.1.4) and in the presence of mellitate (4.2.3). It was shown in all three parts of the present work that ionic strength adjusted by adding NaCl resulted in reduced attractive protein-protein interactions. The addition of NaCl is assumed to weaken the protein-anion interactions via electrostatic shielding and thereby reduce anion induced attractive protein-protein

interactions. In addition, attractive protein-protein interactions resulting from ion-dipole or dipole-dipole interactions may also be diminished.

#### 4: Concentration of the oligovalent anion

A non-monotonic trend was observed for the width of the miscibility gap as a function of the citrate or mellitate concentration. For very low citrate or mellitate concentrations the width of the miscibility gap was increasing with increasing anion concentration. At higher citrate or mellitate concentrations the width of the miscibility gap was decreasing with increasing anion concentration. The maximal width of the miscibility gap is assumed to be observed at a defined oligovalent anion concentration, where the overall attractive protein-protein interactions are maximal. Therefore, an optimal citrate and mellitate concentration is proposed to exist, at which charge neutralization is reached and repulsive Coulomb interactions between the proteins vanish. The disappearance of LLPS in the presence of higher concentrations of citrate may be mainly caused by concomitantly increasing ionic strength, whereas the disappearance of LSPS in the presence of higher concentrations of mellitate is assumed to be mainly induced by protein charge reversal, resulting from further binding of mellitate to the protein.

The citrate or mellitate concentration, where the maximal width of the miscibility gap was observed, was:

- increasing with increasing distance of pH from pI
- depending on the way of sample preparation, i.e. dialysis or spiking
- depending on the type and (maximum) charge of excipient.

This maximal width of the miscibility gap and therewith the maximum of attractive protein-protein interactions at a specific anion concentration can also be explained with a net charge neutralization of the positively charged protein upon anion binding. Depending on the pH (and thereby the charge of the protein) and the charge of the excipient, different amounts of excipients would be needed to neutralize the charge of the protein.

## 5: Overall protein concentration

In the first part of this work, the influence of the protein concentration on the phase behaviour was not explicitly examined. As the citrate concentrations were adjusted by dialysis and not by a spiking procedure, the protein concentration and the excipient concentration after dialysis was not precisely adjustable.

In contrast, the spiking procedure performed in the second part of this work, opened the possibility to examine the influence of the protein concentration on the phase behaviour in the presence of different mellitate concentrations. At anion concentrations lower than the anion concentration of minimal protein concentration in the supernatant, a dependence of the occurrence of phase separation on the ratio between anion and protein was observed. At anion concentrations higher than the concentration of minimal protein concentration in the supernatant, the protein concentration in the supernatant was observed to depend on the total anion concentration and not on the protein concentration. A theoretical model was applied and the number of mellitate ions required to dissolve the neutral protein-mellitate precipitate  $m$  as well as the equilibrium constant  $K'$  for mellitate binding were calculated. The experimental results indicate that dissolution of individual proteins from the neutral protein-mellitate precipitate occurs upon binding of additional 2.5 – 3 mellitate ions.

## 6: Temperature

The influence of the temperature on phase separation was only observed in the first part of this work in solutions containing 1 mM citrate adjusted by dialysis. The coexistence curve of the antibody in 1 mM citrate pH 7.2 showed the following properties: i) an upper critical solution temperature ii) a critical protein concentration of 93 mg/ml, a critical temperature of 289 K (16 °C) and a width  $w$  (defined by equ (38)) of 26 and iii) an asymmetry with respect to the critical protein concentration. The critical temperature in 1mM citrate buffer was pH-dependent with a higher critical temperature observed at pH 7.4 and pH 8.1 compared to pH 7.2. An upper critical solution temperature transition signifies that clustering or agglomeration of the proteins to form the lower concentrated phase is exothermic.

In part I of this work, the citrate ion was indirectly shown to be binding to the mAb by the comparison of the phase diagram as a function of pH in the absence and in the presence of citrate. In addition, a more direct approach was introduced in the first part of this work to measure weak binding between ions and antibodies. This new approach was yielding a competition constant for citrate of  $82\mu\text{M}$  for a background concentration of 4 mM NaCl.

In part III of the present work, the protein diffusion in solutions containing different buffer salts and non-buffering salts at various pH-values was examined. A model was introduced which relates diffusion coefficients for charged proteins in aqueous solutions to the charge of the protein. The model is taking into account Coulomb interactions between the proteins and between protein and counterions. The model introduced here was well suited to calculate the Debye-Hückel-Henry charge of a protein in solution by using the diffusion coefficient at infinite dilution in the absence of additional salt.

The apparent diameter of the protein at infinite dilution as a function of NaCl concentration could be predicted by the established model. Experimental  $k_D$  values were generally lower than calculated  $k_D$  values probably due to attractive protein-protein interactions not considered by the model. These attractive interactions can therefore be quantitatively estimated by taking the difference between experimental and calculated  $k_D$  values. The diffusion coefficients of the antibody in various buffer systems at pH 6.0 were markedly different. In histidine-hydrochloride buffer, the diffusion coefficients were comparable to those observed in unbuffered NaCl solution. For the antibody in citrate buffer, low  $k_D$  values were observed, probably caused by strong attractive interactions. These were weakened with increasing ionic strength, either by addition of NaCl or additional citrate. The protein diffusion coefficients in succinate buffer were similar to the diffusion coefficients measured for the antibody in citrate buffer, even though  $k_D$  values were less negative. In acetate buffer at pH 6.0, up to a protein concentration of 15 mg/ml, the diffusion coefficient was higher than expected with a concomitant much lower diameter at infinite dilution. A similar observation was made for the protein diffusion coefficient in 2 mM citrate buffer at pH 6.0.

The diffusion behavior of the protein was well described by the introduced model of coupled protein counterion diffusion in the case when the counterions were chloride ions.

However, if the solution contained organic counterions such as acetate and citrate at low ionic strength ( $< 38$  mM), the model failed.

### Conclusion

Summing up all the results, a rationale can be found to explain the phase behaviour and therewith the protein-protein interactions in the protein solution as a function of pH, excipient species and concentration, as well as ionic strengths. This rationale is based on the concept, that the charge of an antibody increases with increasing distance from pI. In addition to the overall net charge, which induces repulsive electrostatic protein-protein interactions, the concept also includes the assumption of an anisotropic charge distribution over the protein surface resulting in attractive protein-protein interactions, which become weaker with increasing ionic strength. Finally, electrostatic binding between oligovalent ions and the protein, resulting in charge neutralization, is completing the concept.

In order to justify the rationale stated above, the monoclonal antibody is considered as a colloidal particle with a non-uniform surface composed of

- positively charged patches
- negatively charged patches
- hydrophobic patches
- hydrophilic patches

The protein-protein interactions and thus the colloidal stability are assumed to be influenced by the

- net charge of the mAb
- dipole moment of the mAb
- number, size and distribution of specific charged and hydrophobic patches

These properties are assumed to be influenced by the

- pH
- ionic strength
- presence and concentration of binding excipients

The concept, which describes the influence of pH, ionic strength and the presence of citrate on the protein-protein interaction potential, is visualized in Figure 38.

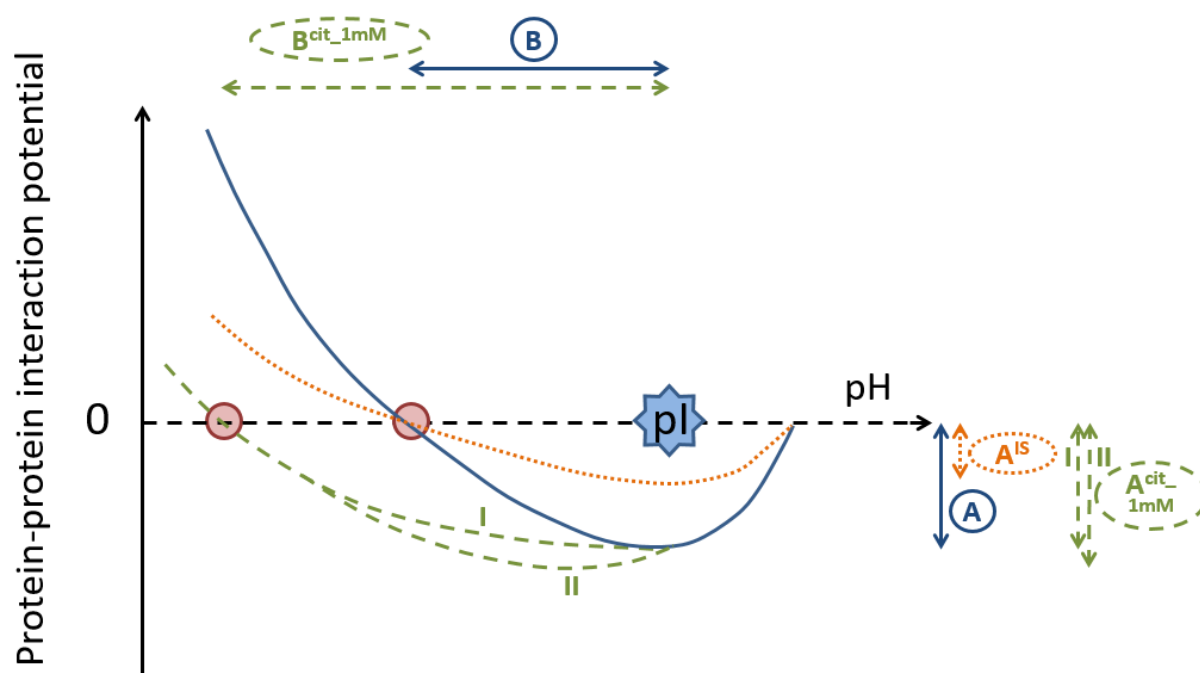


Figure 38: Schematic presentation of the influence of pH, ionic strength and a binding anionic excipient (citrate) on the protein-protein interaction potential. The position of the pI of the mAb is depicted by a blue star. The blue solid line represents the protein-protein interaction potential of the mAb in the absence of any excipients (except counterions) as a function of pH. The two green dashed lines represent two possible protein-protein interaction potentials as a function of pH in the presence of citrate (1 mM adjusted by dialysis). The orange dotted line represents the protein-protein interaction potential at elevated (but moderate) ionic strength (Theory taken from Sule et al., (153)). The extent of maximal attractive net interactions in the absence of citrate is depicted by a blue arrow of size A. Maximal net attraction in the absence of citrate (or other binding excipients) is by theory expected at the pI. In the presence of citrate (1 mM adjusted by dialysis) the size of A (quantifying maximal net attraction) is assumed to either stay constant (case I) or to increase (case II), as depicted by the green dashed arrows of size  $A^{cit_{1mM}}$ . With increasing ionic strength A is assumed to decrease as shown by the shorter orange arrow  $A^{IS}$  (153). The pH at which repulsive balance attractives PPIs (neutral protein-protein interaction potential) is marked by a red circle. The distance between this specific pH and the pI in the absence of any excipients (except counterions) is depicted by the blue arrow of length B. The presence of citrate (1mM adjusted by dialysis) leads to a larger distance between the pH of neutral protein-protein interaction potential and pI as depicted by a longer arrow  $B^{cit_{1mM}}$  compared to B. The size of B at higher ionic strength ( $B^{IS}$ ) is not necessarily equal to the size of B, but it was not more precisely plotted here (insufficient data situation). The sizes A and B are assumed to be protein specific values. The figure is a schematic presentation of the protein-protein interaction potential as a function of pH, ionic strength and presence of citrate.

The sizes A and B in Figure 38 characterize the intrinsic colloidal stability of the mAb independent from most environmental factors (such as pH, ionic strength or presence of

excipients). They could be used to compare different antibodies with respect to their molecule specific protein-protein interaction potential or self-association potential.

The measurement of diffusion was giving a deeper understanding into the effects, which are induced by different excipients and excipient concentrations. The simplified two component model of  $k_D$  in the traditional sense was shown to be unsuitable for the charged mAb at low ionic strengths where at least 3 components with varying concentration need to be taken into account. Therefore, the classical interpretation of low  $k_D$  values representing more attractive PPIs and higher  $k_D$  values representing more repulsive interactions is not valid under these circumstances.

The comparison between measured and calculated diffusion coefficients allows to differentiate between effects which are covered by the theory of coupled protein counterion diffusion (isotropic electrostatic ion-ion interactions) and effects which are not covered by the theory of coupled protein counterion diffusion (charge-dipole, dipole-dipole, v.d. Waals, hydrophobic interactions, non-fundamental forces such as hydration related interactions or patchy interaction). Thereby, the causes of the effects that excipients have on protein diffusion can be elucidated. As the diffusion of the protein and the counterion is coupled, DLS can also reveal information on the counterion diffusion and thereby on the interplay between both, the mAb and the counterion.

Summing up, three different experimental approaches demonstrate an attractive interaction between citrate (representing a negatively charged model excipient) and the antibody used in this work:

- Comparison of phase boundaries as a function of pH in the absence and in the presence of citrate
- Mapping of the ion atmosphere after equilibrium dialysis against a mixture of ions competing for the solvation shell
- Accelerated diffusion of the mAb at infinite dilution in the presence of 2 mM and 5 mM citrate, which would not be expected neither based on a two-component nor on a three-component diffusion model



## Outlook

The knowledge obtained in this work about solution conditions inducing LLPS or LSPS in antibody solutions may enable us to rationally modify the use of ionic excipients and their concentration, to either reduce opalescence or to induce or avoid phase separation. In addition, parameters such as viscosity or aggregation kinetics, which are closely related to the protein-protein interaction potential may be better understood with the knowledge obtained in this work.

The introduced approach to map the ion atmosphere after equilibrium dialysis, and thus measure weak protein-ion interactions, could be used to compare individual formulation excipients with regards to their protein binding affinity. A correlation between binding affinity and the stability and or processability (e.g. long term stability, viscosity or LLPS) of the protein solution could get examined. In addition, investigations of the binding affinity of defined excipients to different mAbs are important.

Comparing individual proteins with regards to their intrinsic tendency to self-association or aggregation, the colloidal interaction has often been measured in a defined formulation buffer at defined pH (46, 49, 57, 64). However, as most proteins have different pIs and the formulation buffer may stabilize one protein, but destabilize the other protein, such a comparison is not advisable. A comparison between individual proteins may be more meaningful by developing a diagram as shown in Figure 38, not schematic but scaled, for each individual protein. A large value of A (as depicted in Figure 38) is related to a protein of a high intrinsic tendency to self-association or aggregation. This could be caused by a strong dipole moment or a pronounced hydrophobicity of the protein. Even though the size of A is the most direct value to characterize the tendency of the protein to self-association or aggregation, this value might be difficult to be measured, as most attractive protein-protein interactions (indicating the size of A in Figure 38) might be limited to a very narrow pH range. Instead, the distance between the pI and the pH, where attractive and repulsive PPIs balance to a certain degree (size of B in Figure 38), may be more easily detectable. The size of B quantifies the pH difference to the pI which is needed to increase repulsive Coulomb PPIs to a certain value balancing out the attractive protein-protein interactions. It is assumed that for proteins with stronger attractions at the pI, a higher  $z_{DHH}$  is needed to

balance the strong attractive interactions by equally stronger repulsive protein-protein interactions. The  $z_{DHH}$  is increased by increasing the distance between pH and pI. For proteins with equal buffer capacity (i.e. pH changes are resulting in equal increase in net charge), the size of B could be directly compared. If proteins with different buffer capacity should be compared, the valence at the specific pH would need to be determined first and, instead of plotting the protein-protein interaction potential (or a related value) against the pH, the protein-protein interaction potential (or a related value) would need to be plotted against the protein net charge. The size of B (pH or charge that is needed to increase the protein-protein interaction potential above zero or above an arbitrarily chosen threshold) may be more easily accessible by experimental approaches than the size of A. The scheme could thus be used to characterize proteins regarding their intrinsic tendency to self-association or aggregation independent from their formulation. It would be important to study whether there exists a correlation between the values of A or B and the stability and / or processability (e.g. long term stability, viscosity, or LLPS) of a protein solution comparing different antibodies.

The comparison of A and  $A^{IS}$  or B and  $B^{IS}$  could be used to elucidate the nature of attractive PPIs. If attractive PPIs were mainly caused by hydrophobic interactions, increasing ionic strength would change the size of A only marginally. The nature of attractive interactions resulting in protein self-association is a commonly discussed issue (50, 194-196). Depending on the nature of molecular interaction, different excipients could be recommended for the formulation of a specific protein solution.

The results of the present study indicate, that there is no direct correlation between the  $k_D$  and the protein-protein interaction potential. However, a potential non-causal correlation between the  $k_D$  and parameters such as viscosity or aggregation rates could be examined in a future study. This correlation might probably only exist in a defined range of e.g. ionic strength or excipient concentration.

The great potential of diffusion measurement could be further used, for example, to understand the different effects of different buffer species on protein stability. The diffusion of proteins in aqueous solutions containing organic buffer systems, which could not be well explained with the established three-component model, needs to be further examined. In

addition to the microscopic diffusion coefficient measurement by DLS, macroscopic diffusion measurements such as Rayleigh interferometry or Schlieren optics could lead to values of the the individual diffusion coefficients  $D_{22}$ ,  $D_{23}$ ,  $D_{32}$  and  $D_{33}$  (94, 103). Likewise, conductivity measurements would be a suitable orthogonal approach. These measurements could underline and extend the knowledge obtained by DLS and could also extend the knowledge of diffusion of proteins at very low ionic strength in organic buffer systems. For the sake of simplicity, the model presented in this thesis only accounts for a three-component system composed of water, the protein and effective counterions. In future research, a model for a four component system should be developed, which would also account for coions.



## 6. REFERENCES

1. Ellwanger K, Reusch U, Fucek I, Knackmuss S, Weichel M, Gantke T, et al. Highly specific and effective targeting of EGFRvIII-positive tumors with TandAb antibodies. *Frontiers in Oncology*. 2017;7(MAY).
2. Rashidi SK, Gargari SLM, Ebrahimizadeh W. Targeting colorectal cancer cell lines using nanobodies; AgSK1 as a potential target. *Iranian Journal of Biotechnology*. 2017;15(2):78-86.
3. Mahaddakar T, Lopus M. From natural products to designer drugs: Development and molecular mechanisms action of novel anti-microtubule breast cancer therapeutics. *Current Topics in Medicinal Chemistry*. 2017;17(22):2559-68.
4. Steeland S, Libert C, Vandembroucke RE. A new venue of TNF targeting. *International Journal of Molecular Sciences*. 2018;19(5).
5. Roberts D, Keeling R, Tracka M, Van Der Walle CF, Uddin S, Warwicker J, et al. The role of electrostatics in protein-protein interactions of a monoclonal antibody. *Molecular Pharmaceutics*. 2014;11(7):2475-89.
6. Fukuda M, Moriyama C, Yamazaki T, Imaeda Y, Koga A. Quantitative Correlation between Viscosity of Concentrated MAb Solutions and Particle Size Parameters Obtained from Small-Angle X-ray Scattering. *Pharmaceutical Research*. 2015;32(12):3803-12.
7. Mason BD, Zhang L, Remmele RL, Zhang J. Opalescence of an IgG2 monoclonal antibody solution as it relates to liquid-liquid phase separation. *Journal of Pharmaceutical Sciences*. 2011;100(11):4587-96.
8. Mason BD, Zhang-Van Enk J, Zhang L, Remmele Jr RL, Zhang J. Liquid-liquid phase separation of a monoclonal antibody and nonmonotonic influence of Hofmeister anions. *Biophysical Journal*. 2010;99(11):3792-800.
9. Nishi H, Miyajima M, Nakagami H, Noda M, Uchiyama S, Fukui K. Phase separation of an IgG1 antibody solution under a low ionic strength condition. *Pharmaceutical Research*. 2010;27(7):1348-60.
10. Raut AS, Kalonia DS. Opalescence in Monoclonal Antibody Solutions and Its Correlation with Intermolecular Interactions in Dilute and Concentrated Solutions. *Journal of Pharmaceutical Sciences*. 2015;104(4):1263-74.
11. Trilisky E, Gillespie R, Osslund TD, Vunnum S. Crystallization and liquid-liquid phase separation of monoclonal antibodies and fc-fusion proteins: Screening results. *Biotechnology Progress*. 2011;27(4):1054-67.
12. Wang Y, Latypov RF, Lomakin A, Meyer JA, Kerwin BA, Vunnum S, et al. Quantitative evaluation of colloidal stability of antibody solutions using PEG-induced liquid-liquid phase separation. *Molecular Pharmaceutics*. 2014;11(5):1391-402.
13. Wang Y, Lomakin A, Latypov RF, Benedek GB. Phase separation in solutions of monoclonal antibodies and the effect of human serum albumin. *Proceedings of the National Academy of Sciences of the United States of America*. 2011;108(40):16606-11.
14. Kayser O, Warzecha H. *Pharmaceutical Biotechnology: Drug Discovery and Clinical Applications*: Wiley; 2012.
15. Leberman R. The Hofmeister series and ionic strength. *FEBS Letters*. 1991;284(2):293-4.
16. Dainiak MB, Muronetz VI, Izumrudov VA, Galaev IY, Mattiasson B. Production of Fab fragments of monoclonal antibodies using polyelectrolyte complexes. *Analytical Biochemistry*. 2000;277(1):58-66.

17. Xu Y, Mazzawi M, Chen K, Sun L, Dubin PL. Protein purification by polyelectrolyte coacervation: Influence of protein charge anisotropy on selectivity. *Biomacromolecules*. 2011;12(5):1512-22.
18. Dammacco F, Sansonno D, Piccoli C, Tucci FA, Racanelli V. The cryoglobulins: An overview. *European Journal of Clinical Investigation*. 2001;31(7):628-38.
19. Nishi H, Miyajima M, Wakiyama N, Kubota K, Hasegawa J, Uchiyama S, et al. Fc domain mediated self-association of an IgG1 monoclonal antibody under a low ionic strength condition. *Journal of Bioscience and Bioengineering*. 2011;112(4):326-32.
20. Broide ML, Berland CR, Pande J, Ogun OO, Benedek GB. Binary-liquid phase separation of lens protein solutions. *Proceedings of the National Academy of Sciences of the United States of America*. 1991;88(13):5660-4.
21. Pande A, Mokhor N, Pande J. Deamidation of Human  $\gamma$ s-Crystallin Increases Attractive Protein Interactions: Implications for Cataract. *Biochemistry*. 2015;54(31):4890-9.
22. Thomson JA, Schurtenberger P, Thurston GM, Benedek GB. Binary liquid phase separation and critical phenomena in a protein/water solution. *Proceedings of the National Academy of Sciences of the United States of America*. 1987;84(20):7079-83.
23. Xia JZ, Donceel K, Clauwaert J. Light scattering by bovine  $\alpha$ -crystallin proteins in solution: Hydrodynamic structure and interparticle interaction. *Biophysical Journal*. 1994;66(3):861-72.
24. Berland CR, Thurston GM, Kondo M, Broide ML, Pande J, Ogun O, et al. Solid-liquid phase boundaries of lens protein solutions. *Proceedings of the National Academy of Sciences of the United States of America*. 1992;89(4):1214-8.
25. Brandon S, Katsonis P, Vekilov PG. Multiple extrema in the intermolecular potential and the phase diagram of protein solutions. *Physical Review E - Statistical, Nonlinear, and Soft Matter Physics*. 2006;73(6).
26. Cheng YC, Lobo RF, Sandler SI, Lenhoff AM. Kinetics and equilibria of lysozyme precipitation and crystallization in concentrated ammonium sulfate solutions. *Biotechnology and Bioengineering*. 2006;94(1):177-88.
27. Gliko O, Neumaier N, Pan W, Haase I, Fischer M, Bacher A, et al. A metastable prerequisite for the growth of lumazine synthase crystals. *Journal of the American Chemical Society*. 2005;127(10):3433-8.
28. Muschol M, Rosenberger F. Liquid-liquid phase separation in supersaturated lysozyme solutions and associated precipitate formation/crystallization. *Journal of Chemical Physics*. 1997;107(6):1953-62.
29. Rosenberger F. Protein crystallization: Specific phenomena and general insights on crystallization kinetics. *Materials Science Forum*1998. p. 241-56.
30. Stradner A, Sedgwick H, Cardinaux F, Poon WCK, Egelhaaf SU, Schurtenberger P. Equilibrium cluster formation in concentrated protein solutions and colloids. *Nature*. 2004;432(7016):492-5.
31. Zhang F, Roosen-Runge F, Sauter A, Roth R, Skoda MWA, Jacobs RMJ, et al. The role of cluster formation and metastable liquid - Liquid phase separation in protein crystallization. *Faraday Discussions*. 2012;159:313-25.
32. Zhang F, Roosen-Runge F, Sauter A, Wolf M, Jacobs RMJ, Schreiber F. Reentrant condensation, liquid-liquid phase separation and crystallization in protein solutions induced by multivalent metal ions. *Pure and Applied Chemistry*. 2014;86(2):191-202.
33. Zhang F, Roth R, Wolf M, Roosen-Runge F, Skoda MWA, Jacobs RMJ, et al. Charge-controlled metastable liquid-liquid phase separation in protein solutions as a universal pathway towards crystallization. *Soft Matter*. 2012;8(5):1313-6.

34. Obermeyer AC, Mills CE, Dong XH, Flores RJ, Olsen BD. Complex coacervation of supercharged proteins with polyelectrolytes. *Soft Matter*. 2016;12(15):3570-81.
35. Hammond PT. Engineering materials layer-by-layer: Challenges and opportunities in multilayer assembly. *AIChE Journal*. 2011;57(11):2928-40.
36. Kataoka K, Harada A, Nagasaki Y. Block copolymer micelles for drug delivery: Design, characterization and biological significance. *Advanced Drug Delivery Reviews*. 2001;47(1):113-31.
37. Xia J, Mattison K, Romano V, Dubin PL, Muhoberac BB. Complexation of trypsin and alcohol dehydrogenase with poly(diallyldimethylammonium chloride). *Biopolymers*. 1997;41(4):359-65.
38. Kokufuta E, Takahashi K. Stoichiometric complexation of bovine trypsin with potassium poly(vinyl alcohol sulphate) and enzymatic activity of the complex. *Polymer*. 1990;31(6):1177-82.
39. Larionova NI, Unksova LY, Mironov VA, Sakharov IY, Kazanskaya NF, Berezin IV. Investigation of complex formation between soluble carboxymethyl ethers of polysaccharides and proteins. *Polymer Science USSR*. 1981;23(8):1999-2006.
40. Signorello L, Pucciarelli S, Bonacucina G, Polzonetti V, Cespi M, Perinelli DR, et al. Quantification, microbial contamination, physico-chemical stability of repackaged bevacizumab stored under different conditions. *Current Pharmaceutical Biotechnology*. 2014;15(2):113-9.
41. Keibel F. Charakterisierung kolloidaler und thermischer Stabilitäten von Antikörpern mittels dynamischer Lichtstreuung. 2009.
42. Paul M, Vieillard V, Jaccoulet E, Astier A. Long-term stability of diluted solutions of the monoclonal antibody rituximab. *International Journal of Pharmaceutics*. 2012;436(1-2):282-90.
43. Radmanovic N, Serno T, Joerg S, Germershaus O. Understanding the freezing of biopharmaceuticals: First-principle modeling of the process and evaluation of its effect on product quality. *Journal of Pharmaceutical Sciences*. 2013;102(8):2495-507.
44. Arzenšek D, Kuzman D, Podgornik R. Colloidal interactions between monoclonal antibodies in aqueous solutions. *Journal of Colloid and Interface Science*. 2012;384(1):207-16.
45. Arzenšek D, Kuzman D, Podgornik R. Hofmeister Effects in Monoclonal Antibody Solution Interactions. *Journal of Physical Chemistry B*. 2015;119(33):10375-89.
46. Chow CK, Allan BW, Chai Q, Atwell S, Lu J. Therapeutic Antibody Engineering to Improve Viscosity and Phase Separation Guided by Crystal Structure. *Molecular Pharmaceutics*. 2016;13(3):915-23.
47. Godfrin PD, Zarraga IE, Zarzar J, Porcar L, Falus P, Wagner NJ, et al. Effect of Hierarchical Cluster Formation on the Viscosity of Concentrated Monoclonal Antibody Formulations Studied by Neutron Scattering. *Journal of Physical Chemistry B*. 2016;120(2):278-91.
48. Kumar V, Dixit N, Zhou L, Fraunhofer W. Impact of short range hydrophobic interactions and long range electrostatic forces on the aggregation kinetics of a monoclonal antibody and a dual-variable domain immunoglobulin at low and high concentrations. *International Journal of Pharmaceutics*. 2011;421(1):82-93.
49. Lehermayr C, Mahler HC, Mäder K, Fischer S. Assessment of net charge and protein-protein interactions of different monoclonal antibodies. *Journal of Pharmaceutical Sciences*. 2011;100(7):2551-62.

50. Menzen T, Friess W. Temperature-ramped studies on the aggregation, unfolding, and interaction of a therapeutic monoclonal antibody. *Journal of Pharmaceutical Sciences*. 2014;103(2):445-55.
51. Neergaard MS, Kalonia DS, Parshad H, Nielsen AD, Møller EH, Van De Weert M. Viscosity of high concentration protein formulations of monoclonal antibodies of the IgG1 and IgG4 subclass - Prediction of viscosity through protein-protein interaction measurements. *European Journal of Pharmaceutical Sciences*. 2013;49(3):400-10.
52. Roberts D, Keeling R, Tracka M, Van Der Walle CF, Uddin S, Warwicker J, et al. Specific ion and buffer effects on protein-protein interactions of a monoclonal antibody. *Molecular Pharmaceutics*. 2015;12(1):179-93.
53. Saito S, Hasegawa J, Kobayashi N, Kishi N, Uchiyama S, Fukui K. Behavior of Monoclonal Antibodies: Relation between the Second Virial Coefficient ( $B_2$ ) at Low Concentrations and Aggregation Propensity and Viscosity at High Concentrations. *Pharmaceutical Research*. 2012;29(2):397-410.
54. Saito S, Hasegawa J, Kobayashi N, Tomitsuka T, Uchiyama S, Fukui K. Effects of ionic strength and sugars on the aggregation propensity of monoclonal antibodies: Influence of colloidal and conformational stabilities. *Pharmaceutical Research*. 2013;30(5):1263-80.
55. Wei JY, Bou-Assaf GM, Houde D, Weiskopf A. Technical Decision-Making with Higher Order Structure Data: Detecting Reversible Concentration-Dependent Self-Association in a Monoclonal Antibody and a Preliminary Investigation to Eliminate It. *Journal of Pharmaceutical Sciences*. 2015;104(11):3984-9.
56. Yadav S, Liu J, Shire SJ, Kalonia DS. Specific interactions in high concentration antibody solutions resulting in high viscosity. *Journal of Pharmaceutical Sciences*. 2010;99(3):1152-68.
57. Yadav S, Shire SJ, Kalonia DS. Factors affecting the viscosity in high concentration solutions of different monoclonal antibodies. *Journal of Pharmaceutical Sciences*. 2010;99(12):4812-29.
58. Yadav S, Shire SJ, Kalonia DS. Viscosity analysis of high concentration bovine serum albumin aqueous solutions. *Pharmaceutical Research*. 2011;28(8):1973-83.
59. Yadav S, Shire SJ, Kalonia DS. Viscosity behavior of high-concentration monoclonal antibody solutions: Correlation with interaction parameter and electroviscous effects. *Journal of Pharmaceutical Sciences*. 2012;101(3):998-1011.
60. Yadav S, Sreedhara A, Kanai S, Liu J, Lien S, Lowman H, et al. Establishing a link between amino acid sequences and self-associating and viscoelastic behavior of two closely related monoclonal antibodies. *Pharmaceutical Research*. 2011;28(7):1750-64.
61. Connolly BD, Petry C, Yadav S, Demeule B, Ciaccio N, Moore JMR, et al. Weak interactions govern the viscosity of concentrated antibody solutions: High-throughput analysis using the diffusion interaction parameter. *Biophysical Journal*. 2012;103(1):69-78.
62. Härtl E, Dixit N, Besheer A, Kalonia D, Winter G. Weak antibody-cyclodextrin interactions determined by quartz crystal microbalance and dynamic/static light scattering. *European Journal of Pharmaceutics and Biopharmaceutics*. 2013;85(3 PART A):781-9.
63. Rubin J, Sharma A, Linden L, Bommarius AS, Behrens SH. Gauging colloidal and thermal stability in human IgG1-sugar solutions through diffusivity measurements. *Journal of Physical Chemistry B*. 2014;118(11):2803-9.
64. Yadav S, Laue TM, Kalonia DS, Singh SN, Shire SJ. The influence of charge distribution on self-association and viscosity behavior of monoclonal antibody solutions. *Molecular Pharmaceutics*. 2012;9(4):791-802.



65. Raut AS, Kalonia DS. Liquid-Liquid Phase Separation in a Dual Variable Domain Immunoglobulin Protein Solution: Effect of Formulation Factors and Protein-Protein Interactions. *Molecular Pharmaceutics*. 2015;12(9):3261-71.
66. Salinas BA, Sathish HA, Bishop SM, Harn N, Carpenter JF, Randolph TW. Understanding and modulating opalescence and viscosity in a monoclonal antibody formulation. *Journal of Pharmaceutical Sciences*. 2010;99(1):82-93.
67. Alford JR, Kendrick BS, Carpenter JF, Randolph TW. High concentration formulations of recombinant human interleukin-1 receptor antagonist: II. aggregation kinetics. *Journal of Pharmaceutical Sciences*. 2008;97(8):3005-21.
68. Cromwell MEM, Hilario E, Jacobson F. Protein aggregation and bioprocessing. *AAPS Journal*. 2006;8(3).
69. Nicoud L, Arosio P, Sozo M, Yates A, Norrant E, Morbidelli M. Kinetic analysis of the multistep aggregation mechanism of monoclonal antibodies. *Journal of Physical Chemistry B*. 2014;118(36):10595-606.
70. Nicoud L, Jagielski J, Pfister D, Lazzari S, Massant J, Lattuada M, et al. Kinetics of Monoclonal Antibody Aggregation from Dilute toward Concentrated Conditions. *Journal of Physical Chemistry B*. 2016;120(13):3267-80.
71. Sahin E, Grillo AO, Perkins MD, Roberts CJ. Comparative effects of pH and ionic strength on protein-protein interactions, unfolding, and aggregation for IgG1 antibodies. *Journal of Pharmaceutical Sciences*. 2010;99(12):4830-48.
72. Zhang-Van Enk J, Mason BD, Yu L, Zhang L, Hamouda W, Huang G, et al. Perturbation of thermal unfolding and aggregation of human IgG1 Fc fragment by hofmeister anions. *Molecular Pharmaceutics*. 2013;10(2):619-30.
73. Zhang J, Liu XY. Effect of protein-protein interactions on protein aggregation kinetics. *Journal of Chemical Physics*. 2003;119(20):10972-6.
74. Thiagarajan G, Semple A, James JK, Cheung JK, Shameem M. A comparison of biophysical characterization techniques in predicting monoclonal antibody stability. *mAbs*. 2016;8(6):1088-97.
75. Le Brun V, Friess W, Schultz-Fademrecht T, Muehlau S, Garidel P. Lysozyme-lysozyme self-interactions as assessed by the osmotic second virial coefficient: Impact for physical protein stabilization. *Biotechnology Journal*. 2009;4(9):1305-19.
76. Möller J, Grobelny S, Schulze J, Bieder S, Steffen A, Erbkamp M, et al. Reentrant liquid-liquid phase separation in protein solutions at elevated hydrostatic pressures. *Physical Review Letters*. 2014;112(2).
77. De Kruif CG, Weinbreck F, De Vries R. Complex coacervation of proteins and anionic polysaccharides. *Current Opinion in Colloid and Interface Science*. 2004;9(5):340-9.
78. Sabliov C, Chen H, Yada R. *Nanotechnology and Functional Foods: Effective Delivery of Bioactive Ingredients*: Wiley; 2015.
79. Bungenberg de Jong HG. Complex systems of biocolloids. I. Survey and classification according to colloid-chemical and electrochemical points of view. *Proceedings of the Section of Sciences*. 1938;41(7):776-87.
80. Kizilay E, MacCarrone S, Foun E, Dinsmore AD, Dubin PL. Cluster formation in polyelectrolyte - Micelle complex coacervation. *Journal of Physical Chemistry B*. 2011;115(22):7256-63.
81. Antonov M, Mazzawi M, Dubin PL. Entering and exiting the protein-polyelectrolyte coacervate phase via nonmonotonic salt dependence of critical conditions. *Biomacromolecules*. 2010;11(1):51-9.

82. Flanagan SE, Malanowski AJ, Kizilay E, Seeman D, Dubin PL, Donato-Capel L, et al. Complex equilibria, speciation, and heteroprotein coacervation of lactoferrin and  $\beta$ -lactoglobulin. *Langmuir*. 2015;31(5):1776-83.
83. Lenormand H, Deschrevel B, Tranchepain F, Vincent JC. Electrostatic interactions between hyaluronan and proteins at pH 4: How do they modulate hyaluronidase activity. *Biopolymers*. 2008;89(12):1088-103.
84. Tavares GM, Croguennec T, Hamon P, Carvalho AF, Bouhallab S. Selective coacervation between lactoferrin and the two isoforms of  $\beta$ -lactoglobulin. *Food Hydrocolloids*. 2015;48:238-47.
85. Ach D, Briançon S, Dugas V, Pelletier J, Broze G, Chevalier Y. Influence of main whey protein components on the mechanism of complex coacervation with Acacia gum. *Colloids and Surfaces A: Physicochemical and Engineering Aspects*. 2015;481:367-74.
86. Cooper CL, Dubin PL, Kayitmazer AB, Turksen S. Polyelectrolyte-protein complexes. *Current Opinion in Colloid and Interface Science*. 2005;10(1-2):52-78.
87. Roosen-Runge F, Zhang F, Schreiber F, Roth R. Ion-activated attractive patches as a mechanism for controlled protein interactions. *Scientific Reports*. 2014;4.
88. Wolf M, Roosen-Runge F, Zhang F, Roth R, Skoda MWA, Jacobs RMJ, et al. Effective interactions in protein-salt solutions approaching liquid-liquid phase separation. *Journal of Molecular Liquids*. 2014.
89. Fesinmeyer RM, Hogan S, Saluja A, Brych SR, Kras E, Narhi LO, et al. Effect of ions on agitation- and temperature-induced aggregation reactions of antibodies. *Pharmaceutical Research*. 2009;26(4):903-13.
90. Wagner M, Reiche K, Blume A, Garidel P. The electrokinetic potential of therapeutic proteins and its modulation: Impact on protein stability. *Colloids and Surfaces A: Physicochemical and Engineering Aspects*. 2012;415:421-30.
91. Zhang L, Tan H, Fesinmeyer RM, Li C, Catrone D, Le D, et al. Antibody solubility behavior in monovalent salt solutions reveals specific anion effects at low ionic strength. *Journal of Pharmaceutical Sciences*. 2012;101(3):965-77.
92. Bai Y, Greenfeld M, Travers KJ, Chu VB, Lipfert J, Doniach S, et al. Quantitative and comprehensive decomposition of the ion atmosphere around nucleic acids. *Journal of the American Chemical Society*. 2007;129(48):14981-8.
93. Lipfert J, Doniach S, Das R, Herschlag D. Understanding nucleic acid-ion interactions. *Annual Review of Biochemistry* 2014. p. 813-41.
94. Cantor CR, Schimmel PR. *Biophysical Chemistry: Part II: Techniques for the Study of Biological Structure and Function*: W. H. Freeman; 1980.
95. Cussler EL. *Diffusion: Mass Transfer in Fluid Systems*: Cambridge University Press; 2009.
96. Harding SE, Johnson P. The concentration-dependence of macromolecular parameters. *Biochemical Journal*. 1985;231(3):543-7.
97. Sukumar M, Doyle BL, Combs JL, Pekar AH. Opalescent appearance of an IgG1 antibody at high concentrations and its relationship to noncovalent association. *Pharm Res*. 2004;21(7):1087-93.
98. Yadav S, Liu J, Scherer TM, Gokarn Y, Demeule B, Kanai S, et al. Assessment and significance of protein-protein interactions during development of protein biopharmaceuticals. *Biophysical Reviews*. 2013;5(2):121-36.
99. Vink H. Mutual diffusion and self-diffusion in the frictional formalism of non-equilibrium thermodynamics. *Journal of the Chemical Society, Faraday Transactions 1: Physical Chemistry in Condensed Phases*. 1985;81(7):1725-30.

100. Yang YW, Yang Z, Zhou ZK, Attwood D, Booth C. Association of triblock copolymers of ethylene oxide and butylene oxide in aqueous solution. A study of BnEmBn copolymers. *Macromolecules*. 1996;29(2):670-80.
101. Teraoka I. *Polymer Solutions: An Introduction to Physical Properties*: Wiley; 2002.
102. Hill SE, Ledward DA, Mitchell JR. *Functional Properties of Food Macromolecules*: Springer US; 1998.
103. Cadman AD, Fleming R, Guy RH. Diffusion of lysozyme chloride in water and aqueous potassium chloride solutions. *Biophysical Journal*. 1981;37(3):569-74.
104. Albright JG, Annunziata O, Miller DG, Paduano L, Pearlstein AJ. Precision measurements of binary and multicomponent diffusion coefficients in protein solutions relevant to crystal growth: Lysozyme chloride in water and aqueous NaCl at pH 4.5 and 25 °C. *Journal of the American Chemical Society*. 1999;121(14):3256-66.
105. Leait DG. The role of supporting electrolytes in protein diffusion. *Journal of Physical Chemistry*. 1989;93(1):474-9.
106. Buzatu D, Annunziata O, Petrescu E, Popa C, Buzatu FD. Dynamic light scattering: A useful optical method to probe common-ion effects in protein-salt aqueous solutions. *Journal of Optoelectronics and Advanced Materials*. 2005;7(6):3161-8.
107. Annunziata O, Buzatu D, Albright JG. Protein diffusion coefficients determined by macroscopic-gradient rayleigh interferometry and dynamic light scattering. *Langmuir*. 2005;21(26):12085-9.
108. Annunziata O, Paduano L, Albright JG. The effect of salt stoichiometry on protein-salt interactions determined by ternary diffusion in aqueous solutions. *Journal of Physical Chemistry B*. 2006;110(32):16139-47.
109. Annunziata O, Paduano L, Albright JG. Multicomponent diffusion of lysozyme in aqueous calcium chloride. The role of common-ion effects and protein-salt preferential interactions. *Journal of Physical Chemistry B*. 2007;111(35):10591-8.
110. Annunziata O, Paduano L, Pearlstein AJ, Miller DG, Albright JG. The effect of salt on protein chemical potential determined by ternary diffusion in aqueous solutions. *Journal of Physical Chemistry B*. 2006;110(3):1405-15.
111. Doherty P, Benedek GB. The effect of electric charge on the diffusion of macromolecules. *The Journal of Chemical Physics*. 1974:5413-20.
112. Bakunin OG. *Turbulence and Diffusion: Scaling Versus Equations*: Springer Berlin Heidelberg; 2008.
113. Filoti DI, Shire SJ, Yadav S, Laue TM. Comparative Study of Analytical Techniques for Determining Protein Charge. *Journal of Pharmaceutical Sciences*. 2015;104(7):2123-31.
114. Friedman MH. *Principles and Models of Biological Transport*: Springer Berlin Heidelberg; 2012.
115. Bennion DN, Newman JS, White RE, Meeting ES. *Proceedings of the Douglas N. Bennion Memorial Symposium: Topics in Electrochemical Engineering*: Electrochemical Society; 1994.
116. Bergemann K, Eckermann C, Garidel P, Grammatikos S, Jacobi A, Kaufmann H, et al. Production and Downstream Processing. *Handbook of Therapeutic Antibodies*. 2008. p. 199-237.
117. Karow AR, Bahrenburg S, Garidel P. Buffer capacity of biologics-from buffer salts to buffering by antibodies. *Biotechnology Progress*. 2013;29(2):480-92.
118. <https://online-shop.eppendorf.de/DE-de/Spitzen-Reaktionsgefasse-und-Platten-44512/Kuevetten-59968/UVette-PF-9817.html>.
119. Lide DR. *CRC Handbook of Chemistry and Physics, 85th Edition*: Taylor & Francis; 2004.

120. Tanford C, Swanson SA, Shore WS. Hydrogen ion equilibria of bovine serum albumin. *Journal of the American Chemical Society*. 1955;77(24):6414-21.
121. Maxwell WR, Partington JR. The dissociation constants of some polybasic acids. *Transactions of the Faraday Society*. 1935;31:922-35.
122. Maxwell WR, Partington JR. The dissociation constants of some polybasic acids. - Part II. *Transactions of the Faraday Society*. 1936;32:775-82.
123. Rudat J. Enzymatische Decarboxylierung von Benzenpolycarbonsäuren [Thesis]. Bonn: Rheinische Friedrich-Wilhelms Universität Bonn; 2006.
124. Maxwell WR, Partington JR. The dissociation constants of some polybasic acids. - Part III. *Transactions of the Faraday Society*. 1937;33:670-8.
125. Waterhouse AL, Sacks GL, Jeffery DW. *Understanding Wine Chemistry*: Wiley; 2016.
126. Cooper A, Chemistry RSo. *Biophysical Chemistry: ROYAL SOCIETY - UK*; 2011.
127. Uversky VN, Permiakov EA. *Methods in Protein Structure and Stability Analysis: Conformational stability, size, shape, and surface of protein molecules*: Nova Biomedical Books; 2007.
128. Ablinger E, Wegscheider S, Keller W, Prassl R, Zimmer A. Effect of protamine on the solubility and deamidation of human growth hormone. *International Journal of Pharmaceutics*. 2012;427(2):209-16.
129. Furuki T, Shimizu T, Chakrabortee S, Yamakawa K, Hatanaka R, Takahashi T, et al. Effects of Group 3 LEA protein model peptides on desiccation-induced protein aggregation. *Biochimica et Biophysica Acta - Proteins and Proteomics*. 2012;1824(7):891-7.
130. Ju ZY, Kilara A. Gelation of pH-Aggregated Whey Protein Isolate Solution Induced by Heat, Protease, Calcium Salt, and Acidulant. *Journal of Agricultural and Food Chemistry*. 1998;46(5):1830-5.
131. Kim KS, Kim SJ, Rhee JS. Effect of acetylation on turbidity of glycinin. *Journal of Agricultural and Food Chemistry*®. 1991;39(9):1578-82.
132. Maji T, Banerjee S, Biswas Y, Mandal TK. Dual-Stimuli-Responsive I -Serine-Based Zwitterionic UCST-Type Polymer with Tunable Thermosensitivity. *Macromolecules*. 2015;48(14):4957-66.
133. Pathak J, Rawat K, Bohidar HB. Is surface patch binding between proteins symmetric about isoelectric pH? *RSC Advances*. 2014;4(47):24710-8.
134. Chi EY, Krishnan S, Randolph TW, Carpenter JF. Physical stability of proteins in aqueous solution: Mechanism and driving forces in nonnative protein aggregation. *Pharmaceutical Research*. 2003;20(9):1325-36.
135. Kitabatake N, Kinekawa Yi. Turbidity measurement of heated egg proteins using a microplate system. *Food Chemistry*. 1995;54(2):201-3.
136. Boström M, Parsons DF, Salis A, Ninham BW, Monduzzi M. Possible origin of the inverse and direct hofmeister series for lysozyme at low and high salt concentrations. *Langmuir*. 2011;27(15):9504-11.
137. Schlesener F. *Colloidal Particles in Critical Fluids*: Cuvillier; 2004.
138. Derjaguin B. On the repulsive forces between charged colloid particles and on the theory of slow coagulation and stability of lyophobic sols. *Transactions of the Faraday Society*. 1940;35:203-15.
139. Verwey EJW. Electrical double layer and stability of emulsions. *Transactions of the Faraday Society*. 1940;35:192-203.
140. Verwey EJW, Overbeek JTG. Long distance forces acting between colloidal particles. *Transactions of the Faraday Society*. 1946;42:B117-B23.

141. Bungenberg de Jong HG, Kruyt HR. Koazervation. (Entmischung in kolloiden Systemen.). *Kolloid-Zeitschrift*. 1929;50(1):39 - 48.
142. Esue O, Xie AX, Kamerzell TJ, Patapoff TW. Thermodynamic and structural characterization of an antibody gel. *mAbs*. 2013;5(2):323-34.
143. McPherson A, Cudney B. Searching for silver bullets: An alternative strategy for crystallizing macromolecules. *Journal of Structural Biology*. 2006;156(3):387-406.
144. McPherson A, Nguyen C, Cudney R, Larson SB. The role of small molecule additives and chemical modification in protein crystallization. *Crystal Growth and Design*. 2011;11(5):1469-74.
145. Liu H, Kumar SK, Sciortino F. Vapor-liquid coexistence of patchy models: Relevance to protein phase behavior. *Journal of Chemical Physics*. 2007;127(8).
146. Lund M. Anisotropic protein-protein interactions due to ion binding. *Colloids and Surfaces B: Biointerfaces*. 2016;137:17-21.
147. Lewus RA, Levy NE, Lenhoff AM, Sandler SI. A comparative study of monoclonal antibodies. 1. phase behavior and protein-protein interactions. *Biotechnology Progress*. 2015;31(1):268-76.
148. Zhang F, Weggler S, Ziller MJ, Ianeselli L, Heck BS, Hildebrandt A, et al. Universality of protein reentrant condensation in solution induced by multivalent metal ions. *Proteins: Structure, Function and Bioinformatics*. 2010;78(16):3450-7.
149. Esue O, Kanai S, Liu J, Patapoff TW, Shire SJ. Carboxylate-dependent gelation of a monoclonal antibody. *Pharmaceutical Research*. 2009;26(11):2478-85.
150. Voorn MJ. Complex Coacervation. I. General theoretical considerations. *Recueil*. 1856;75:317 - 30.
151. Troshin AS, Alexander P, Bacq ZM. Problems of Cell Permeability: International Series of Monographs in Pure and Applied Biology: Modern Trends in Physiological Sciences: Elsevier Science; 2013.
152. Neufeld T, Eisenstein M, Muszkat KA, Fleminger G. A citrate-binding site in calmodulin. *Journal of Molecular Recognition*. 1998;11(1-6):20-4.
153. Sule SV, Cheung JK, Antochshuk V, Bhalla AS, Narasimhan C, Blaisdell S, et al. Solution pH that minimizes self-association of three monoclonal antibodies is strongly dependent on ionic strength. *Molecular Pharmaceutics*. 2012;9(4):744-51.
154. Dumetz AC, Engineering UoDDoC. Protein Interactions and Phase Behavior in Aqueous Solutions: Effects of Salt, Polymer, and Organic Additives: University of Delaware; 2007.
155. Jordan E, Roosen-Runge F, Leibfarth S, Zhang F, Sztucki M, Hildebrandt A, et al. Competing salt effects on phase behavior of protein solutions: Tailoring of protein interaction by the binding of multivalent ions and charge screening. *Journal of Physical Chemistry B*. 2014;118(38):11365-74.
156. Taratuta VG, Holschbach A, Thurston GM, Blankschtein D, Benedek GB. Liquid-liquid phase separation of aqueous lysozyme solutions: Effects of pH and salt identity. *Journal of Physical Chemistry*. 1990;94(5):2140-4.
157. Chemistry NRCCoM. Characterization of Macromolecular Structure: Proceedings of a Conference, April 5-7, 1967: Washington, National Academy of Sciences; 1968.
158. Strobl GR. The Physics of Polymers: Concepts for Understanding Their Structures and Behavior: Springer Berlin Heidelberg; 2013.
159. Galkin O, Chen K, Nagel RL, Hirsch RE, Vekilov PG. Liquid-liquid separation in solutions of normal and sickle cell hemoglobin. *Proceedings of the National Academy of Sciences of the United States of America*. 2002;99(13):8479-83.

160. Quiroz FG, Chilkoti A. Sequence heuristics to encode phase behaviour in intrinsically disordered protein polymers. *Nature Materials*. 2015;14(11):1164-71.
161. Vekilov PG, Feeling-Taylor AR, Petsev DN, Galkin O, Nagel RL, Hirsch RE. Intermolecular interactions, nucleation, and thermodynamics of crystallization of hemoglobin C. *Biophysical Journal*. 2002;83(2):1147-56.
162. Bianchi E, Largo J, Tartaglia P, Zaccarelli E, Sciortino F. Phase diagram of patchy colloids: Towards empty liquids. *Physical Review Letters*. 2006;97(16).
163. Liu H, Kumar SK, Sciortino F, Evans GT. Vapor-liquid coexistence of fluids with attractive patches: An application of Wertheim's theory of association. *Journal of Chemical Physics*. 2009;130(4).
164. Kalikmanov V. *Statistical Physics of Fluids: Basic Concepts and Applications*: Springer Berlin Heidelberg; 2013.
165. Lomakin A, Asherie N, Benedek GB. Monte Carlo study of phase separation in aqueous protein solutions. *Journal of Chemical Physics*. 1996;104(4):1646-56.
166. Sandin S, Öfverstedt LG, Wikström AC, Wrangé Ö, Skoglund U. Structure and flexibility of individual immunoglobulin G molecules in solution. *Structure*. 2004;12(3):409-15.
167. Smit B. Phase diagrams of Lennard-Jones fluids. *The Journal of Chemical Physics*. 1992;96(11):8639-40.
168. Fuoss RM, Sadek H. Mutual interaction of polyelectrolytes. *Science*. 1949;110(2865):552-4.
169. Misra VK, Draper DE. The interpretation of Mg<sup>2+</sup> binding isotherms for nucleic acids using Poisson-Boltzmann theory. *Journal of Molecular Biology*. 1999;294(5):1135-47.
170. Harinarayan C, Skidmore K, Kao Y, Zydney AL, Van Reis R. Small molecule clearance in ultrafiltration/diafiltration in relation to protein interactions: Study of citrate binding to a fab. *Biotechnology and Bioengineering*. 2009;102(6):1718-22.
171. Raibekas AA, Bures EJ, Siska CC, Kohno T, Latypov RF, Kerwin BA. Anion binding and controlled aggregation of human interleukin-1 receptor antagonist. *Biochemistry*. 2005;44(29):9871-9.
172. Kaibara K, Okazaki T, Bohidar HB, Dubin PL. pH-induced coacervation in complexes of bovine serum albumin and cationic polyelectrolytes. *Biomacromolecules*. 2000;1(1):100-7.
173. De Vos WM, Leermakers FAM, De Keizer A, Stuart MAC, Kleijn JM. Field theoretical analysis of driving forces for the uptake of proteins by like-charged polyelectrolyte brushes: Effects of charge regulation and patchiness. *Langmuir*. 2010;26(1):249-59.
174. Sieberz J, Wohlgemuth K, Schembecker G. The influence of impurity proteins on the precipitation of a monoclonal antibody with an anionic polyelectrolyte. *Separation and Purification Technology*. 2015;146:252-60.
175. Cacioppo E, Pusey ML. The solubility of the tetragonal form of hen egg white lysozyme from pH 4.0 to 5.4. *Journal of Crystal Growth*. 1991;114(3):286-92.
176. <http://www.arndt-bruenner.de/mathe/scripts/gleichungssysteme2.htm>.
177. Reiche K, Hartl J, Blume A, Garidel P. Liquid-liquid phase separation of a monoclonal antibody at low ionic strength: Influence of anion charge and concentration. *Biophysical Chemistry*. 2017;220:7-19.
178. Lindon JC. *Encyclopedia of Spectroscopy and Spectrometry*: Elsevier Science; 2010.
179. Sorret LL, DeWinter MA, Schwartz DK, Randolph TW. Challenges in Predicting Protein-Protein Interactions from Measurements of Molecular Diffusivity. *Biophysical Journal*. 2016;111(9):1831-42.

180. Saluja A, Badkar AV, Zeng DL, Nema S, Kalonia DS. Ultrasonic storage modulus as a novel parameter for analyzing protein-protein interactions in high protein concentration solutions: Correlation with static and dynamic light scattering measurements. *Biophysical Journal*. 2007;92(1):234-44.
181. Tang Y, University NDS. *Controlled Delivery of Therapeutic Agents from Polymer-based, in Situ, Gel-forming Systems*: North Dakota State University; 2008.
182. Raj T, Flygare WH. Diffusion studies of bovine serum albumin by quasielastic light scattering. *Biochemistry*. 1974;13(16):3336-40.
183. Wu C, Ying H, Grinnell C, Bryant S, Miller R, Clabbers A, et al. Simultaneous targeting of multiple disease mediators by a dual-variable-domain immunoglobulin. *Nature Biotechnology*. 2007;25(11):1290-7.
184. Cugia F, Monduzzi M, Ninham BW, Salis A. Interplay of ion specificity, pH and buffers: Insights from electrophoretic mobility and pH measurements of lysozyme solutions. *RSC Advances*. 2013;3(17):5882-8.
185. Salis A, Monduzzi M. Not only pH. Specific buffer effects in biological systems. *Current Opinion in Colloid and Interface Science*. 2016;23:1-9.
186. Saluja A, Fesinmeyer RM, Hogan S, Brems DN, Gokarn YR. Diffusion and sedimentation interaction parameters for measuring the second virial coefficient and their utility as predictors of protein aggregation. *Biophysical Journal*. 2010;99(8):2657-65.
187. Finsy R, Moreels E, Bottger A, Lekkerkerker H. Study of the relation between diffusion and sedimentation of charged silica sols by dynamic light scattering, ultracentrifugation, and turbidimetry. *The Journal of Chemical Physics*. 1985;82(8):3812-6.
188. Chari R, Jerath K, Badkar AV, Kalonia DS. Long- and short-range electrostatic interactions affect the rheology of highly concentrated antibody solutions. *Pharmaceutical Research*. 2009;26(12):2607-18.
189. Papp E, Fricsovszky G, Meszena G. Electrochromism of purple membrane. Ionic strength dependence. *Biophysical Journal*. 1986;49(5):1089-100.
190. Paunov VN, Kaler EW, Sandler SI, Petsev DN. A model for hydration interactions between apoferritin molecules in solution. *Journal of Colloid and Interface Science*. 2001;240(2):640-3.
191. Edsall JT, Edelhoch H, Lontie R, Morrison PR. Light scattering in solutions of serum albumin: Effects of charge and ionic strength. *Journal of the American Chemical Society*. 1950;72(10):4641-56.
192. Leaist DG. Soret coefficients of mixed electrolytes. *Journal of Solution Chemistry*. 1990;19(1):1-10.
193. Molisso A, Annunziata O. Composition of coexisting liquid phases determined by Rayleigh interferometry. *Journal of Solution Chemistry*. 2014;43(1):126-34.
194. Esfandiary R, Parupudi A, Casas-Finet J, Gadre D, Sathish H. Mechanism of Reversible Self-Association of a Monoclonal Antibody: Role of Electrostatic and Hydrophobic Interactions. *Journal of Pharmaceutical Sciences*. 2015;104(2):577-86.
195. Geoghegan JC, Fleming R, Damschroder M, Bishop SM, Sathish HA, Esfandiary R. Mitigation of reversible self-association and viscosity in a human IgG1 monoclonal antibody by rational, structure-guided Fv engineering. *mAbs*. 2016;8(5):941-50.
196. Nichols P, Li L, Kumar S, Buck PM, Singh SK, Goswami S, et al. Rational design of viscosity reducing mutants of a monoclonal antibody: Hydrophobic versus electrostatic intermolecular interactions. *mAbs*. 2015;7(1):212-30.





## 7. APPENDICES:

### Appendix 1: Results obtained by isoelectric focussing

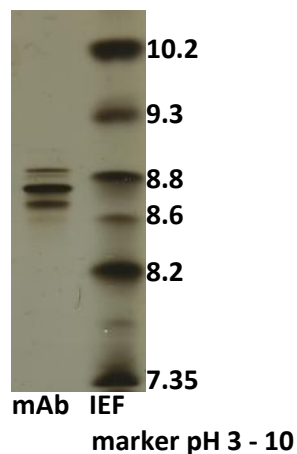


Figure A1: Isoelectric focussing gel obtained by IEF as described in section 3.2.1.8. Five charge variants were observed with pIs between pH 8.6 and pH 8.9. The main peak was observed at ~ pH 8.7. Therefore, the experimental isoelectric point of the protein was defined to be 8.7.

### Appendix 2: pH dependent DSC curves

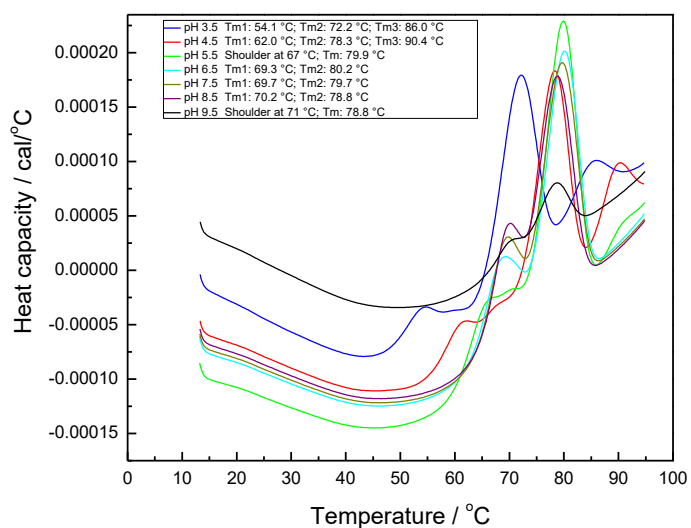


Figure A2: DSC curves of citrate-free antibody solutions between pH 3.5 and pH 9.5,  $c = 2$  mg/mL.



## 8. ACKNOWLEDGEMENTS

I would like to start by thanking Prof. Dr. Alfred Blume for the scientific discussions, the supervision, the competent support and most of all for the humanity and the patience.

Moreover, I am highly grateful to Prof. Dr. Patrick Garidel, for the opportunity to write my Ph.D. thesis with such an interesting subject and for correcting this work.

A special thanks to Dr. Julia Kasper for trust and support.

Many thanks to Christina Beck, Matthias Bollweg, András Pávkovics and Josef Hartl. With all of you it was nice working and the results, you generated were of great value to this work.

A grateful thank to Inge and Eipi who provided technical assistance.

Furthermore, I would like to thank the entire staff of the working groups “Formulation Development” for the pleasant and inspiring working atmosphere in the group. A special thanks to all who have given me support in the lab and those who have ensured mental energy supply in the form of sweets.

Special thanks to all “PraDiDos” who have accompanied me during my PhD thesis for this unforgettable time.

Finally, I would like to thank my family for all their love. My parents and my sister for supporting me throughout my whole life. Steffen for lovingly care for our children and simply for being there. Last but by no means least, Justus and Leonas, you were providing happy distraction to rest my mind outside of my research and you make me realize just how beautiful life can be.



## 9. PUBLICATIONS

1. Niklas Sandler, Katharina Reiche, Jyrki Heinämäki, Jouku Yliruusi, *Effect of Moisture on Powder Flow Properties of Theophylline*, *Pharmaceutics*, 2010. **2**, 275 – 290
2. Michael Wagner, Katharina Reiche, Alfred Blume, Patrick Garidel, *Viscosity measurements of antibody solutions by photon correlation spectroscopy: An indirect approach – limitations and applicability for high-concentration liquid protein solutions*, *Pharmaceutical Development and Technology*, 2013. **18**, 963 – 970
3. Michael Wagner, Katharina Reiche, Alfred Blume, Patrick Garidel, *The electrokinetic potential of therapeutic proteins and its modulation: Impact on protein stability*, *Colloids and Surfaces A: Physicochemical and Engineering Aspects*, 2012. **415**, 421 – 430
4. Katharina Reiche, Josef Hartl, Alfred Blume, Patrick Garidel, *Liquid-liquid phase separation of a monoclonal antibody at low ionic strength: Influence of anion charge and concentration*, *Biophysical chemistry*, 2017. **220**, 7 - 19



## 10. CURRICULUM VITAE

### Personal Data

---

Family Name: Reiche  
First Name: Katharina  
Date of Birth: December 30<sup>th</sup>, 1985  
Place of Birth: Berlin  
Nationality: German

### Work experience

---

01/2016 - today      Project coordinator at Boehringer Ingelheim Pharma GmbH & Co KG  
  
09/2009 – 11/2009      Industrial internship at Boehringer Ingelheim Pharma GmbH & Co. KG

### Education

---

11/2010 – today      Ph.D. student at the Institute of Chemistry of Martin-Luther-Universität Halle-Wittenberg (*Prof. Dr. Alfred Blume*) in cooperation with Boehringer Ingelheim Pharma GmbH & Co. KG  
  
10/2005 – 09/2010      Studies of “Pharmaceutical Sciences”, graduation: master of science, at the Ludwig Maximilian University of Munich

- 04/2010 – 09/2010      Master thesis in the Department Biopharmaceutical Process Science, Pharma Development, Boehringer Ingelheim Pharma GmbH & Co. KG (*Prof. Dr. Wolfgang Friess*)
- 03/2009 – 08/2009      Student research project at the University of Helsinki (*Prof. Dr. Niklas Sandler*)
- 02/2009                  Student research project at the Department of Biophysics, Ludwig Maximilian University Munich (*Prof. Dr. Hermann Gaub*)
- 04/2008 – 08/2008      Bachelor thesis in the Department of Pharmaceutical Technology, at Ludwig Maximilian University of Munich (*Prof. Dr. Wolfgang Friess*)
- 02/2002 – 07/2005      School education at the Ignatz-Taschner Gymnasium, Dachau, Germany (graduation: Abitur)



## **Erklärung:**

Diese Dissertation wurde im Sinne von § 7 der Promotionsordnung vom 13. Juli 2016 von Herrn Prof. Dr. rer. nat. Alfred Blume betreut.

## **Ehrenwörtliche Versicherung**

Hiermit erkläre ich, dass ich die vorliegende Arbeit selbständig verfasst und keine anderen Quellen und Hilfsmittel als die angegebenen verwendet habe. Ich habe die Arbeit an keiner anderen Hochschule vorgelegt und mich zu keinem früheren Zeitpunkt um den Doktorgrad beworben.

Biberach, 28. September 2021.

.....

Katharina Reiche